Dissertation zur Erlangung des Doktorgrades
der Fakultät für Chemie und Pharmazie
der Ludwig–Maximilians–Universität München

Electronic Transport Within the Kubo-Bastin Formalism

Kristina Chadova

aus

Kiew, Ukraine

2017

Contents

List of Publications

The present work is based on the following six publications (listed here in chronological order) reprinted in the chapter 7:

- D. Ködderitzsch, **K. Chadova**, J. Minár, H. Ebert. Impact of finite temperatures and correlations on the anomalous Hall conductivity from *ab initio* theory. New J. Phys., **15**: 053009, 2013.

- H. Ebert, S. Mankovsky, **K. Chadova**, S. Polesya, J. Minár, D. Ködderitzsch. Calculating linear-response functions for finite temperatures on the basis of the alloy analogy model. Phys. Rev. B, **91**: 165132, 2015.

- **K. Chadova**, D.V. Fedorov, C. Herschbach, M. Gradhand, I. Mertig, D. Ködderitzsch, H. Ebert. Separation of the individual contributions to the spin Hall effect in dilute alloys within the first-principles Kubo-Středa approach. Phys. Rev. B, **92**: 045120, 2015.

- **K. Chadova**, S. Wimmer, H. Ebert, D. Ködderitzsch. Tailoring of the extrinsic spin Hall effect in disordered metal alloys. Phys. Rev. B, **92**: 235142, 2015.

- D. Ködderitzsch, **K. Chadova**, H. Ebert. Linear response Kubo-Bastin formalism with application to the anomalous and spin Hall effects: A first-principles approach. Phys. Rev. B, **92**: 184415, 2015.

- **K. Chadova**, S. Mankovsky, J. Minár, H. Ebert. Impact of finite temperatures on the transport properties of Gd from first principles. Phys. Rev. B, **95**: 125109, 2017.

Additional publications (listed here in chronological order):

- D.V. Fedorov, C. Herschbach, A. Johansson, S. Ostanin, I. Mertig, M. Gradhand, **K. Chadova**, D. Ködderitzsch, H. Ebert. Analysis of the giant spin Hall effect in Cu(Bi) alloys. Phys. Rev. B, **88**: 085116, 2013.

- C. Herschbach, D.V. Fedorov, I. Mertig, M. Gradhand, **K. Chadova**, H. Ebert, D. Ködderitzsch. Insight into the skew-scattering mechanism of the spin Hall effect: Potential scattering versus spin-orbit scattering. Phys. Rev. B, **88**: 205102, 2013.

- S. Wimmer, D. Ködderitzsch, **K. Chadova**, H. Ebert. First-principles linear response description of the spin Nernst effect. Phys. Rev. B, **88**: 201108(R), 2013.

- B. Zimmermann, **K. Chadova**, D. Ködderitzsch, S. Blügel, H. Ebert, D.V. Fedorov, N.H. Long, P. Mavropoulos, I. Mertig, Y. Mokrousov, M. Gradhand. Skew scattering in dilute ferromagnetic alloys. Phys. Rev. B, **90**: 220403(R), 2014.

- S. Wimmer, M. Seemann, **K. Chadova**, D. Ködderitzsch, H. Ebert. Spin-orbit-induced longitudinal spin-polarized currents in nonmagnetic solids. Phys. Rev. B, **92**: 041101(R), 2015.

- S. Mankovsky, **K. Chadova**, D. Ködderitzsch, J. Minár, H. Ebert, W. Bensch. Electronic, magnetic, and transport properties of Fe-intercalated $2H$–TaS$_2$ studied by means of the KKR-CPA method. Phys. Rev. B, **92**: 144413, 2015.

- **K. Chadova**, D. Ködderitzsch, J. Minár, H. Ebert, J. Kiss, S. W. D'Souza, L. Wollmann, C. Felser, S. Chadov. Resonant impurity states in chemically disordered half-Heusler Dirac semimetals. Phys. Rev. B, **93**: 195102, 2016.

- S. Wimmer, **K. Chadova**, M. Seemann, D. Ködderitzsch, H. Ebert. Fully relativistic description of spin-orbit torques by means of linear response theory. Phys. Rev. B, **94**: 054415, 2016.

- S. Mankovsky, S. Polesya, **K. Chadova**, H. Ebert, J. B. Staunton, T. Gruenbaum, M. A. W. Schoen, C. H. Back, X. Z. Chen, C. Song. The temperature dependence of FeRh's transport properties. Phys. Rev. B, **95**: 155139, 2017.

- M. Obstbaum, M. Decker, A.K. Greitner, M. Haertinger, T.N.G. Meier, M. Kronseder, **K. Chadova**, S. Wimmer, D. Ködderitzsch, H. Ebert, C.H. Back. Tuning Spin Hall Angles by Alloying. Phys. Rev. Letters, **117**: 167204, 2016.

1. Introduction

Conventional electronics intended to build devices and schemes by manipulating the conducting electrons via charge, nowadays this gradually transforms into what we know as spintronics (SPIN-TRansport electrONICS), i.e., the technology which manipulates one more degree of freedom of the electron - the spin. This concept has evolved as a result of strengthening the technological requirements to the conventional electronic devices - first of all, concerning the reduced energy consumption, especially for the high-frequency operating elements, and also concerning the sensitivity of the devices. In turn, this has increased an interest within the academic community in the effects explicitly involved in the electron charge/spin manipulation, as well as in the materials which provide a large magnitude of these effects. The main theoretical description of these effects was given in the early 1970s [1, 2]. It has become clear that the combination of the material characteristics on different scales (e.g. spin-diffusion lengths, relaxation time, etc.) leads to a variety of spin-transport effects, such as giant magnetoresistance (GMR), anomalous Hall effect (AHE), spin Hall effect (SHE), spin accumulation, spin-transfer torque (STT), anomalous Nernst effect (ANE), spin Nernst effect (SNE), etc. All these phenomena constitute a base of spintronics. At the same time, the practical *ab-initio* numerical models and the technical means for their realistic simulation are still developing. A reliable *ab-initio* description of these effects in realistic models is a necessary step needed in the Material Science in order to predict and understand the particular features of the spin-phenomena in a given material or combined systems. Development of spintronics is intimately connected with the search of new materials which could combine ferromagnetic properties and properties of semiconductors. On the one hand, such materials could be a source of the spin-polarized electrons and, on the other, could be easily integrated with conventional semiconductor components. To create such a hybrid material - semiconductor with ferromagnetic properties appears to be a complex task, as integrating magnetic atoms into the crystal structure of the semiconductor significantly deteriorates its magnetic properties.

Spintronics, as a new field, was recognized in 1988 due to the effect of giant magnetoresistance (GMR) discovered independently by Albert Fert [3] and Peter Grünberg [4]. They found that the mutual magnetic alignment in Fe/Cr multilayers, significantly changes the electrical resistivity of the whole system. The resistivity is maximal when the magnetization directions in ferromagnetic layers are antiparallel, but minimizes for their parallel alignment. The change in electrical resistivity (about 50% at $T = 4.2$ K and $B = 2$ T is due to the change of the electron scattering probability for different spin directions. This discovery has boosted the growth of practical applications. GMR effect was also found in so-called "spin-valve" structures, consisting of two ferromag-

netic layers separated by nonmagnetic conducting spacer [5]. The release of the first spin-valve sensors in hard drive read heads was then announced in 1997 by IBM. Ten years later, the GMR spin-valve was replaced by the related thin-layered structure, the so-called magnetic tunnel junction (MTJ) based on the giant tunneling magnetoresistance (TMR): instead of the conducting nonmagnetic spacer, the electrons tunnel through a thin insulating barrier, which is preferentially passed by electrons with a certain single spin orientation. The TMR signal was shown to be about 100 times larger than that of a spin-valve. Although spintronic devices such as spin valves can be good candidates for the construction of non-volatile memory such as the magnetoresistive random access memory (MRAM) [6] where the read-out process is based on the TMR effect in magnetic tunnel junctions and the writing process is done by exploiting the Oersted field which is generated by a current in order to switch the magnetization. However, it was shown that this process of writing is insufficient in terms of energy, scalability and density. Therefore, to achieve lowpower operation, the switching of the magnetization by the spin polarized currents via spin transfer torque effect (STT) was suggested. Such a STT-MRAM possesses a number of advantages, among which are high speed, very high endurance, non-volatility and, due to current-switching mechanism, it becomes more scalable [7]. However, nowadays the current which is necessary to reorient the magnetization is too high for most commercial applications [8]. Another spin-domain-based memory is the racetrack memory. This type of memory uses magnetic domains to store information in tall columns of a magnetic material arranged perpendicularly on the surface of a silicon substrate [9]. This type of memory would allow for large storage capacity, low energy consumption, and low cost. There is an intensive research going on in this direction to deliver a device for commercially based device.

In spintronic devices a specific current is created by spins pointing in one direction, a so-called spin current. To obtain such a current, it is necessary to order spins in one direction - to polarize them. Also the lifetime of such spins should be long enough for transferring over long distances. The spintronic components can possess memory properties, high-speed switching and at the same time low energy consumption, as the spin flip requires only little energy. In between operations, spintronic devices can be switched off the power supply. But the central problem in spintronic remains, namely the spin coherence time which corresponds to the time of spin-polarized electrons to travel over macroscopic distances without the loss of information. If this time is too short, then the disturbed spin orientation leads to a loss of information carried by every spin. Experiments on spin coherence performed at room temperatures show that in semiconductors (> 100 ns) this time is much longer compared to metals ($\sim 0.1 - 20$ ns) used in spin multilayers. In recent years, a lot of scientific and industrial attention is attracted by diluted magnetic semiconductors (DMS). Despite the fact that the spin coherence time in these materials is higher, the majority of them possess low Curie temperatures which leads to limited applications. This shortcoming can be avoided by the nanostructuring of the semiconductor which increases the solubility of the transition metal impurities up to desired concentrations of $1 - 2\%$ [10, 11]. In an alternative way, the combination of the semiconductor and molecular structures can be used as spintronic components. In the Ref. [12] the logic switch based on changes of the physical

properties of the molecule is discussed. Among the advantages of using such complexes is that due to the larger molecular mass the retention times in memory applications becomes longer. Another benefit is a molecular design and synthesis which allows the self-assembly onto metals and semiconductors for interconnection. For this to be at all possible, it is necessary to ensure that the molecules operate within acceptable temperature margins and switching speeds and, in addition, would need to be supported by negligible parasitic effects within the supporting architecture [12].

Studies held in recent years define a new route in spintronic development known as "Spintronics without magnetism" [13], where no ferromagnetic materials are used. The main idea is the manipulation of the electric current only by spin-orbit coupling. Spin-orbit coupling leads to spin polarization, i.e. allows to sort electrons by their spin: electrons with spin "up" scatter preferentially to the one side of the sample while electrons with spin "down" preferentially to the opposite side with respect to the moving direction. This is the basis of the so-called spin Hall effect. Its mechanism originates from the spin flow excited by the electrical current in perpendicular direction. In turn, it leads to an inhomogeneous spin polarization in the sample due to the asymmetry of electron scattering.

The spin Hall effect can be used for generating of spin polarized electrons which makes it important for spintronic applications. The focus in the present work is put on the theoretical investigation of the anomalous and spin Hall effects which remain central in spintronics.

The main aim of the current work is to study the transport properties (longitudinal and transverse) in metallic systems. In addition, the influence of the effect of the finite temperatures (thermal lattice vibrations and thermal spin fluctuations) is considered. The thesis is organized in the following way: Chapter 2 gives an overview of the main concepts of density functional theory (DFT) as the calculations carried out in the present work are based on DFT formalism. Chapter 3 deals with the Green function formalism as implemented on the basis of the Korringa-Kohn-Rostoker (KKR) or multiple scattering theory (MST) formalism. The subject of Chapter 4 is the alloy-analogy model implemented within the coherent potential approximation (CPA) which allows us to take into account the effect of finite temperatures. Chapter 5 is devoted to the calculation of the transport properties based on the Kubo formalism. In Chapter 6 a detailed analysis of spin-related phenomena such as anomalous and spin Hall effects is provided. Finally, in Chapter 7 the results obtained in the current work are presented by means of corresponding publications.

2. Density functional theory

Calculating the electronic structure of many-body systems is a very complex task with still very high demands to modern computer hardware. The traditional quantum chemical approach to calculate the electronic properties of finite systems like molecules or atomic clusters is usually based on the variational principle. Here, one normally expands a trial wavefunction using a suitable basis set and applies the Rayleigh-Ritz variation procedure in order to find the wavefunction, which minimizes the energy of the whole system. Another method for the calculation of electronic properties, is the so-called Korringa-Kohn-Rostoker Green function (KKR-GF) method, which is very rarely used by quantum chemists. The method has its roots in the calculation of the electronic band structure of solids and has also been applied to electronic systems of finite extend. Within the KKR-GF approach the electrons are separated into two groups. The core electrons, which are tightly bound to the nuclei are treated in an atomic like way. The valence electrons, on the other hand, are able to move freely within the whole system and are just scattered by the partially screened nuclear potentials. Therefore, one can apply the multiple scattering formalism to the valence electrons, giving access to the electronic Green function from which expectation values can be calculated. In order to be able to do calculations for systems containing many atoms it is also necessary to map the many-body electronic problem to a problem of a single electron *seeing* an averaged effective potential. For this the very successful density functional theory (DFT) is used.

The quantum description of electrons in a solid requires the solution of the corresponding many body problem [14] which typically contains 10^{23} particles - both nuclei and electrons. It is out of question to deal with this task directly, and the first approximation is to *freeze* the slow nuclei at fixed positions, by considering only the electron subsystem in an external field. This is the so-called Born-Oppenheimer adiabatic approximation. Therefore the system of interacting particles is moving in a static external potential V_{ext}. The wave function describing the stationary electronic state $\Psi(\mathbf{r}_1, \cdots, \mathbf{r}_N)$ satisfies the Schrödinger equation:

$$
\begin{aligned}
\hat{H}\,\Psi &= \left[\, \sum_i^N \left(-\frac{\hbar^2}{2m}\,\nabla_i^2 + V_{\text{ext}}(\mathbf{r}_i)\right) + \sum_{i<j} U(\mathbf{r}_i, \mathbf{r}_j) \right] \Psi \\
&= [\,\hat{T} + \hat{V} + \hat{U}\,]\,\Psi = E\,\Psi\,,
\end{aligned}
\tag{2.1}
$$

where the first term corresponds to the sum of the one-particle kinetic energies, the second term describes interactions of each particle with the external potential (generated by the nuclei) and the last term contains the repulsive Coulomb interaction

energy between the particles. The kinetic and electron-electron terms are independent of the particular kind of the many-electron system. The system-specific information (which nuclei and at which positions) is hidden entirely in the second term of the above equation.

Due to their interaction, the motion of electrons in condensed media is correlated. At first glance, this leads to the conclusion that it is impossible to describe such a system using the approximation of independent particles. However, we can use a model system of non-interacting particles, where the total energy E and the electron density $n(\mathbf{r})$ match the corresponding functions of the real system, and all interaction effects then are described by an effective external field. This is the essence of density functional theory (DFT). Formally DFT is based on the Hohenberg and Kohn theorems [15] whereby there is a one-to-one correspondence between the ground-state electron density $n_0(\mathbf{r})$ of a many-electron system and the external potential $V_{\text{ext}}(\mathbf{r})$, and thus all ground state properties of the interacting electron gas can be retrieved in a unique way from the electron density $n(\mathbf{r})$ only, i.e. they can be described by introducing certain functionals of the local density. Accordingly, the ground state energy of the ground state density $n_0(\mathbf{r})$ can be written as following:

$$E_0 \; = \; E\left[n_0\right] \; = \; \langle\, \Psi_0\left[n_0\right] |\, \hat{T} \,+\, \hat{V} \,+\, \hat{U} \,|\, \Psi_0\left[n_0\right] \,\rangle\,, \tag{2.2}$$

where the ground state wave function $\Psi_0\left[n_0\right]$ is a unique functional of n_0. The external potential can be represented by means of the density $n(\mathbf{r})$ as following:

$$V\left[n\right] \; = \; \int d^3r \, V_{\text{ext}}(\mathbf{r})\, n(\mathbf{r})\,. \tag{2.3}$$

The ground-state total energy of the system is given by the minimal value of the functional $E\left[n\right]$ which is reached for the ground-state electron density corresponding to $V_{\text{ext}}(\mathbf{r})$.

$$E\left[n\right] \; = \; T\left[n\right] \,+\, U\left[n\right] \,+\, \int d^3r \, V_{\text{ext}}(\mathbf{r})\, n(\mathbf{r})\,. \tag{2.4}$$

The way of minimizing the functional given by Eq. (2.4) was suggested by Kohn and Sham [16]. Hereby, the energy functional for the non-interacting system can be written as follows:

$$E_s\left[n\right] \; = \; \langle\, \Psi_s\left[n\right] |\, \hat{T}_s\left[n\right] \,+\, \hat{V}_{\text{eff}} \,|\, \Psi_s\left[n\right] \,\rangle\,, \tag{2.5}$$

where T_s is the kinetic energy of the non-interacting system and V_{eff} is the effective external potential. In case of $n_s(\mathbf{r}) = n(\mathbf{r})$ V_{eff} is chosen to be as:

$$V_{\text{eff}} \; = \; V_{\text{ext}} \,+\, U \,+\, (T_s - T)\,. \tag{2.6}$$

Then for an arbitrary non-interacting system one can solve the Kohn-Sham equations:

$$\left[-\frac{\hbar^2}{2m}\, \nabla^2 \,+\, V_{\text{eff}}(\mathbf{r}) \right] \phi_i(\mathbf{r}) \; = \; E_i\, \phi_i(\mathbf{r})\,, \tag{2.7}$$

where the electron orbitals $\phi_i(\mathbf{r})$ satisfy the following equation:

$$n(\mathbf{r}) \;=\; n_s(\mathbf{r}) \;=\; \sum_i^N |\phi_i(\mathbf{r})|^2\,. \tag{2.8}$$

The effective single-particle potential can be expressed as follows:

$$V_{\mathrm{eff}} \;=\; V_{\mathrm{ext}} \;+\; V_{\mathrm{ee}} \;+\; V_{\mathrm{xc}} \tag{2.9}$$

$$= V_{\mathrm{ext}} \;+\; e^2 \int d^3r' \, \frac{n(\mathbf{r}')}{|\mathbf{r}' - \mathbf{r}|} \;+\; \frac{\delta E_{\mathrm{xc}}\,[\,n(\mathbf{r})\,]}{\delta n(\mathbf{r})}\,, \tag{2.10}$$

where the first term V_{ext} describes the external potential, the second term V_{ee} corresponds to the electron-electron Coulomb repulsion and the last term V_{xc} is an exchange correlation potential which contains many-electron effects (exchange and correlation).

The Kohn-Sham equations given by Eq. (2.7) has to be solved self-consistently. This means, one starts with an initial guess for the electron density n and computes the corresponding V_{eff} and then by substituting the effective potential into Eq. (2.7) one obtains the functions ϕ_i. Using the calculated set of one-electron wave functions ϕ_i the new electron density can be found (Eq. (2.8)). This procedure repeats until convergence achieved. Therefore, the central issue in applying DFT is the way in which the exchange correlation potential is defined. In case of the homogeneous electron gas the expression for V_{eff} is known, while for the inhomogeneous electron gas further approximations are needed, e.g. such as the widely used local density approximation (LDA).

To treat relativistic effects one has to apply the four-current version of density functional theory [17]. Within this theory the Dirac-Kohn-Sham equations are given as follows [18]:

$$(-i\hbar c\boldsymbol{\alpha} \cdot \boldsymbol{\nabla} \;+\; \beta mc^2 \;+\; V_{\mathrm{eff}} \;+\; e\boldsymbol{\alpha} \cdot \boldsymbol{A}_{\mathrm{eff}}\,)\,\psi_i \;=\; E_i\,\psi_i\,, \tag{2.11}$$

where the functions ψ_i are the four component wavefunctions (spinors), α_i and β are 4×4 Dirac matrices [19]. The four component effective potential is given by $V_{\mathrm{eff}}^{\mu} = (V_{\mathrm{eff}}, -e\boldsymbol{A}_{\mathrm{eff}})$. The effective single particle potential is expressed as:

$$V_{\mathrm{eff}} \;=\; V_{\mathrm{ext}} \;+\; e^2 \int d^3r' \, \frac{n(\mathbf{r}')}{|\mathbf{r}' - \mathbf{r}|} \;+\; \frac{\delta E_{\mathrm{xc}}[\,n(\mathbf{r}), \boldsymbol{j}(\mathbf{r})\,]}{\delta n(\mathbf{r})} \tag{2.12}$$

and the effective vector potential is given by:

$$\boldsymbol{A}_{\mathrm{eff}} \;=\; \boldsymbol{A}_{\mathrm{ext}} \;-\; \frac{e}{c} \int d^3r' \, \frac{\boldsymbol{j}(\mathbf{r}')}{|\mathbf{r}' - \mathbf{r}|} \;+\; \frac{\delta E_{\mathrm{xc}}\,[\,n(\mathbf{r}), \boldsymbol{j}(\mathbf{r})\,]}{\delta \boldsymbol{j}(\mathbf{r})}\,. \tag{2.13}$$

where $\boldsymbol{j}(\mathbf{r})$ is the spatial part of the relativistic four component current $j^{\mu} = (n, \frac{1}{c}\boldsymbol{j})$. Due to the fact, that there is no simple approximation to $E_{\mathrm{xc}}[\,n(\mathbf{r}), \boldsymbol{j}(\mathbf{r})\,]$, the practical application of Eq. (2.11) is quite difficult. However, by means of a Gordon decomposition of the current further approximations can be made. This way, the part of the

Dirac Hamiltonian (Eq. (2.11)) which depends on the effective vector potential can be decomposed into orbital and spin contributions [20, 21]. This leads to the formulation of relativistic spin density functional theory with exchange correlation energy being a functional of n and the spin magnetization $\boldsymbol{m}$, $E_{xc}[n(\mathbf{r}), \boldsymbol{m}(\mathbf{r})]$. Neglecting the orbital current and considering solely spin magnetization density $\boldsymbol{m}$ Eq. (2.11) can be significantly simplified:

$$(-i\hbar c \boldsymbol{\alpha} \cdot \boldsymbol{\nabla} + \beta mc^2 + V_{\text{eff}} + \beta \boldsymbol{\sigma} \cdot \boldsymbol{B}_{\text{eff}})\psi_i = E_i \psi_i, \tag{2.14}$$

where

$$V_{\text{eff}} = V_{\text{ext}} + V_{\text{ee}} + \frac{\delta E_{\text{xc}}[n(\mathbf{r}), \boldsymbol{m}(\mathbf{r})]}{\delta n(\mathbf{r})} + \frac{e}{c} \int d^3 r' \boldsymbol{A}_{ee}(\mathbf{r}') \cdot \frac{\delta \boldsymbol{j}(\mathbf{r}')}{\delta n(\mathbf{r}')} \tag{2.15}$$

and effective magnetic field

$$\boldsymbol{B}_{\text{eff}} = \boldsymbol{B}_{\text{ext}} + \frac{\delta E_{\text{xc}}[n(\mathbf{r}), \boldsymbol{m}(\mathbf{r})]}{\delta \boldsymbol{m}(\mathbf{r})} + \frac{e}{c} \int d^3 r' \boldsymbol{A}_{ee}(\mathbf{r}') \cdot \frac{\delta \boldsymbol{j}(\mathbf{r}')}{\delta \boldsymbol{m}(\mathbf{r}')}. \tag{2.16}$$

Often the last terms that are responsible for magnetic interactions between the electrons in Eq. (2.15) and Eq. (2.16) are neglected [22]. In case of collinear magnetism, the corresponding effective magnetic field is given by $\boldsymbol{B}_{\text{eff}} = B_{\text{eff}}(r)\,\hat{e}_z$ with the magnetization pointing along the z axis. Then one can obtain the following form of the Dirac-Kohn-Sham equations:

$$(-i\hbar c \boldsymbol{\alpha} \cdot \boldsymbol{\nabla} + \beta mc^2 + V_{\text{eff}} + \beta \sigma_z \cdot B_{\text{eff}}) = E_i \psi_i \tag{2.17}$$

with the effective potential

$$V_{\text{eff}} = V_{\text{ext}} + V_{\text{ee}} + \frac{\delta E_{\text{xc}}[n(\mathbf{r}), m(\mathbf{r})]}{\delta n(\mathbf{r})} \tag{2.18}$$

and the effective magnetic field

$$B_{\text{eff}} = B_{\text{ext}} + \frac{\delta E_{\text{xc}}[n(\mathbf{r}), m(\mathbf{r})]}{\delta m(\mathbf{r})}. \tag{2.19}$$

Using spin projected densities $n^+(\mathbf{r})$ and $n^-(\mathbf{r})$ one can express the magnetization density as:

$$n(\mathbf{r}) = n^+(\mathbf{r}) + n^-(\mathbf{r}) \tag{2.20}$$
$$m(\mathbf{r}) = n^+(\mathbf{r}) - n^-(\mathbf{r}). \tag{2.21}$$

In the current work the calculations are based on the Eq. (2.17) with the local density approximation to V_{xc} with the parametrization given by Vosko, Wilk, Nusair [23].

The central problem of the density functional theory is such that there is no simple expression for the exchange correlation energy functional to work with in practice. The simplest and most frequently used approximation for the exchange-correlation energy

functional $E_{\mathrm{xc}}[\,n(\mathbf{r})\,]$ is the local density approximation (LDA), where the corresponding density has a form similar to that for a homogeneous electron gas, but with the density at every point in space replaced by the local value of the charge density $n(\mathbf{r})$. For the treatment of spin polarized systems the local spin density approximation (LSDA) was suggested by Kohn and Sham [16]:

$$E_{\mathrm{xc}}^{\mathrm{LSDA}}\,[\,n^{+}(\mathbf{r}),n^{-}(\mathbf{r})\,] \;=\; \int d^{3}r\,n(\mathbf{r})\,\varepsilon_{\mathrm{xc}}\,[\,n^{+}(\mathbf{r}),n^{-}(\mathbf{r})\,]\;, \qquad (2.22)$$

where $n(\mathbf{r}) \;=\; n^{+}(\mathbf{r}) + n^{-}(\mathbf{r})$. Here $\varepsilon_{\mathrm{xc}}\,[\,n^{+},n^{-}\,]$ is the exchange-correlation energy per electron of a homogeneous system with the densities $n^{+}(\mathbf{r})$ and $n^{-}(\mathbf{r})$ for spins up and down, respectively. Both LDA and LSDA contain no fitting parameters. Furthermore, since the DFT has no small parameter, a purely theoretical analysis of the accuracy of different approximations is almost impossible. Thus, the application of any approximation to the exchange-correlation potential in the real systems may be justified by agreement between the calculated and experimental data.

3. Multiple scattering theory

Multiple scattering theory (MST) was first suggested by Rayleigh in the context of the propagation of heat or electricity through inhomogeneous media [24]. In MST the calculation of the properties of the complex system can be simplified by the decomposition of the system into its constituent parts. Then the problem comes to find solutions for the individual system components. As a result the overall solution of the considered large system can be constructed by assembling solutions of its smaller parts. [25]

MST can be used in the electronic structure calculations of solid materials. In this context it was shown by Korringa [26] that on the basis of MST the eigenvalues and eigenvectors describing electronic states of the translationally invariant system can be calculated. Few years later the same secular equation was derived by Kohn and Rostoker based on the variational formalism [27]. These works provide a basis on which the modern Korringa-Kohn-Rostoker Green function (KKR-GF) method rests. The central role in this method is played by the single-particle Green function (GF). The advantage of the method is that it provides a direct access to the GF of the considered system and as a result the wide spectra of the physical properties can be calculated. Particularly the method avoids difficulties in treating systems with broken translational symmetry (e.g. the presence of impurities or disordered alloys) as it allows for the statistical average of the GF of a statistical ensemble which can be used to calculate average physical properties of the system by means of the coherent potential approximation (CPA) incorporated into the method. Another advantage of equal importance in the KKR-GF method is the possibility to completely separate the lattice-dependent (structural) part leading to structural constants for a particular lattice and a potential-dependent part contained in the t-matrix determined for each potential type of the considered system. Such an approach provides an efficient numerical treatment of complex systems.

3.1. Green function

Green function formalism employed in the KKR methods is based on the multiple scattering theory. The Green function is defined as a resolvent of the operator $\hat{H}$:

$$(E - \hat{H})\,\hat{G} = \hat{1}\,, \qquad (3.1)$$

where $\hat{H}$ is a one-particle Hamiltonian and E-complex scalar. For $E \in \mathbb{R}$ it is associated with the total energy of the system.

Thus, $\hat{G}$ is an analytic function of the complex energy E apart from the poles precisely located at the discrete eigenvalues of $\hat{H}$, corresponding to electron states. A way to avoid such singularities for real energies is to introduce the side limits of $\hat{G}$, namely:

$$\hat{G}^{\pm} = \lim_{\delta \to 0^+} (E - \hat{H} \pm i\delta)^{-1}, \tag{3.2}$$

where the $\hat{G}^+$ is the so-called retarded and $\hat{G}^-$ the advanced Green function, respectively. $G^{+(-)}$ are both analytical in the upper (lower) complex plane. In the following only the retarded Green function will be considered thus the ($\pm$) symbol will be omitted.

Green function can be written in a spectral representation using the corresponding eigenstates $|\psi_i\rangle$ and eigenvalues E_i of $\hat{H}$:

$$\hat{G}^{\pm} = \sum_i \frac{|\psi_i\rangle \langle\psi_i|}{E - E_i \pm i\delta}. \tag{3.3}$$

If the continuous spectrum is considered, then the summation in Eq. (3.3) is replaced by integration. The advanced and retarded Green functions are connected by the important property:

$$\hat{G}^{+\dagger} = \hat{G}^- \tag{3.4}$$

and their difference provides the homogeneous Green function:

$$\tilde{G} = \hat{G}^+ - \hat{G}^- \tag{3.5}$$
$$= 2i \sum_i |\psi_i\rangle\langle\psi_i| \operatorname{Im} \frac{1}{E - E_i + i\delta}$$
$$= 2i \operatorname{Im}\hat{G}^+,$$

which can be used to get the Green function for any complex argument.

$\hat{H}$ can be split into the unperturbed part $\hat{H}_0$ describing a free electron and the perturbation $\hat{V}$:

$$\hat{H} = \hat{H}_0 + \hat{V}. \tag{3.6}$$

The corresponding resolvent of $\hat{H}_0$:

$$(E - \hat{H}_0)\hat{G}_0 = \hat{1}, \tag{3.7}$$

is the free particle Green function $\hat{G}_0$. Using $\hat{G}_0$ one can compute the Green function $\hat{G}$ using Dyson equation:

$$\hat{G} = (E - \hat{H}_0 - \hat{V})^{-1} = \left[(E - \hat{H}_0)(1 - \hat{G}_0\hat{V})\right]^{-1} \tag{3.8}$$
$$= (1 - \hat{G}_0\hat{V})^{-1}\hat{G}_0 \tag{3.9}$$
$$= \hat{G}_0 + \hat{G}_0\hat{V}\hat{G}. \tag{3.10}$$

Obviously,

$$\hat{G} = \hat{G}_0 + \hat{G}_0 \hat{V} \hat{G}_0 + \hat{G}_0 \hat{V} \hat{G}_0 \hat{V} \hat{G}_0 + \ldots \qquad (3.11)$$

This repeated interaction with the potential $\hat{V}$ can be summarized by the so-called scattering operator T:

$$\hat{T} = \hat{V} + \hat{V} \hat{G}_0 \hat{V} + \hat{V} \hat{G}_0 \hat{V} \hat{G}_0 \hat{V} + \ldots \qquad (3.12)$$

$$= \hat{V} + \hat{V} \hat{G}_0 \left(\hat{V} + \hat{V} \hat{G}_0 \hat{V} + \ldots \right) \qquad (3.13)$$

$$= \hat{V} + \hat{V} \hat{G}_0 \hat{T}. \qquad (3.14)$$

Thus, Eq. (3.10) can be written as:

$$\hat{G} = \hat{G}_0 + \hat{G}_0 \hat{T} \hat{G}_0. \qquad (3.15)$$

Comparing the expression given by Eq. (3.10) with the one given by Eq. (3.15) and using Eq. (3.9) one can obtain the following expression (so-called Lippmann-Schwinger equation) for the T-operator:

$$\hat{T} = \hat{V} + \hat{V} \hat{G}_0 \hat{T} \qquad (3.16)$$

$$= \hat{V} + \hat{V} \hat{G} \hat{V} \qquad (3.17)$$

$$= \hat{V} (1 - \hat{G}_0 \hat{V})^{-1}. \qquad (3.18)$$

Therefore the problem to find $\hat{G}$ is reduced to the calculation of the T-operator, which in turn, according to Eq. (3.18), is reduced to finding the inverse of the operator $(1 - \hat{G}_0 \hat{V})$.

3.2. Scattering path operator

As was mentioned previously the MST problem is split into the single potential problems, i.e. the considered system is decomposed into the atomic regions ($\hat{V} = \sum_i v_i$) using for example the muffin-tin construction. In this case, the space is divided into non-overlapping spheres centered at each site. Inside the sphere the potential is assumed to be spherically symmetric and outside each sphere it is set to a constant value. Each atomic region is treated as a single site problem, which will be discussed in more detail in the following sections.

According to Eq. (3.16) the scattering operator $\hat{T}$ can be written as a sum of the individual scattering events v^i as:

$$\hat{T} = \sum_i \hat{T}^i = \sum_i v^i \left(1 + \hat{G}_0 \hat{T} \right), \qquad (3.19)$$

where the operators $\hat{T}^i$ are defined as:

$$\hat{T}^i = v^i + v^i \hat{G}_0 \sum_j \hat{T}^j \tag{3.20}$$

$$= v^i (1 + \hat{G}_0 \sum_j \hat{T}^j) \tag{3.21}$$

$$= v^i (1 + \hat{G}_0 \hat{T}^i + \sum_{j \neq i} \hat{G}_0 \hat{T}^j) \tag{3.22}$$

$$= (1 - v^i \hat{G}_0)^{-1} v^i (1 + \sum_{j \neq i} \hat{G}_0 \hat{T}^j) . \tag{3.23}$$

It is convenient to introduce a corresponding single-site scattering operator t^i:

$$t^i = v^i + v^i \hat{G}_0 t^i = (1 - v^i \hat{G}_0)^{-1} v^i . \tag{3.24}$$

Using the above definition for the t-operator Eq. (3.23) can be re-written as follows:

$$\hat{T}^i = t^i + t^i \hat{G}_0 \sum_{j \neq i} \hat{T}^j . \tag{3.25}$$

Furthermore it is advantageous to introduce the scattering path operator $\hat{\tau}^{ij}$ which was first suggested by Györffy and Stott [28]:

$$\hat{T} = \sum_{i,j} \hat{\tau}^{ij} . \tag{3.26}$$

In contrast to the single site-scattering operator which describes all scattering events at one site including on-site scattering, the scattering path operator takes into account all possible scattering events starting at site i and ending at site j, i.e. describing the transformation of the incoming waves to outgoing waves from all scattering sites:

$$\hat{\tau}^{ij} = t^i \delta_{ij} + t^i \hat{G}_0 t^k \delta kj + \sum_{k \neq i} \sum_{l \neq k} t^i \hat{G}_0 t^k \hat{G}_0 t^l \delta_{lj} + \ldots \tag{3.27}$$

Hereby Eq. (3.15) can be re-written in terms of the scattering path operator:

$$\hat{G} = \hat{G}_0 + \sum_{i,j} \hat{G}_0 \hat{\tau}^{ij} \hat{G}_0 . \tag{3.28}$$

As one can see from the above equation the calculation of the Green function of the system is reduced to the calculation of the scattering path operator, together with the free Green function $\hat{G}_0$.

3.3. Relativistic free electron Green Function

Relativistic free electron Green function in the real space representation is defined as a resolvent of the corresponding Dirac Hamiltonian [29]:

$$\left(E - c\alpha \cdot \mathbf{p} - \beta mc^2\right) G_0(\mathbf{r}, \mathbf{r}', E) = \delta(\mathbf{r} - \mathbf{r}') \mathbf{1}_4 , \tag{3.29}$$

where $\mathbf{p} = -i\hbar\nabla$. The Dirac matrices α_i and β are defined in the following way:

$$\alpha = \begin{pmatrix} 0 & \sigma \\ \sigma & 0 \end{pmatrix}, \quad \beta = \begin{pmatrix} \mathbb{1}_2 & 0 \\ 0 & -\mathbb{1}_2 \end{pmatrix}, \tag{3.30}$$

where σ denotes the 2×2 Pauli matrices. Then, the corresponding solution of Eq. (3.29) is given by:

$$G_0(\mathbf{r}, \mathbf{r}', E) = -\frac{1}{\hbar^2 c^2}\left(c\alpha\cdot\mathbf{p} + \beta mc^2 + E\right)\frac{e^{ipR}}{4\pi\mathbf{R}}, \tag{3.31}$$

where $\mathbf{R} = \mathbf{r} - \mathbf{r}'$. Using the expansion of a plane wave in terms of the complex spherical harmonics [19]:

$$\frac{e^{i\mathbf{pr}}}{4\pi\mathbf{R}} = ip\sum_{l,m} h_l(pr)\, j_l(pr')\, Y_l^m(\hat{\mathbf{r}})\, Y_l^{m*}(\hat{\mathbf{r}}'), \tag{3.32}$$

one obtains an expression for the free-particle Green function in spherical coordinates [30]:

$$G_0(\mathbf{r}, \mathbf{r}', E) = -ip\sum_{\kappa,\mu}\big[\,j_\kappa^\mu(\mathbf{r})\, h_\kappa^{\mu+\times}(\mathbf{r}')\,\Theta(r'-r)$$
$$+\, h_\kappa^{\mu+}(\mathbf{r})\, j_\kappa^{\mu+\times}(\mathbf{r}')\,\Theta(r-r')\,\big] \tag{3.33}$$

with p being a relativistic momentum $p = \sqrt{E^2/c^2 - m^2 c^2}$ [19] and with the bispinors:

$$j_\kappa^\mu(\mathbf{r}) = \sqrt{\frac{E+mc^2}{c^2}}\left(\begin{array}{c} j_l(pr)\,\chi_\kappa^\mu(\hat{\mathbf{r}}) \\ \frac{ipcS_\kappa}{E+mc^2}\, j_{\bar{l}}(pr)\,\chi_{-\kappa}^\mu(\hat{\mathbf{r}}) \end{array}\right), \tag{3.34}$$

$$h_\kappa^{\mu+}(\mathbf{r}) = \sqrt{\frac{E+mc^2}{c^2}}\left(\begin{array}{c} h_l^+(pr)\,\chi_\kappa^\mu(\hat{\mathbf{r}}) \\ \frac{ipcS_\kappa}{E+mc^2}\, h_{\bar{l}}^+(pr)\,\chi_{-\kappa}^\mu(\hat{\mathbf{r}}) \end{array}\right), \tag{3.35}$$

where $j_l(pr)$ and $h_l^+(pr)$ are the spherical Bessel (the incoming regular solution) and Hankel functions (the outgoing irregular solution), respectively, that are solutions to the free electron Schödinger equation in spherical coordinates. Furthermore, $S_\kappa = \operatorname{sgn}\kappa$ and $\bar{l} = l - S_\kappa$ is orbital angular momentum quantum number. The left-hand side solutions of the Dirac equation (row spinors) are marked with the symbol "$\times$":

$$\left(\begin{array}{c} g_\kappa(pr)\,\chi_\kappa^\mu(\hat{\mathbf{r}}) \\ if_\kappa(pr)\,\chi_{-\kappa}^\mu(\hat{\mathbf{r}}) \end{array}\right)^\times = \big(\, g_\kappa(pr)\,\chi_\kappa^\mu(\hat{\mathbf{r}}),\; -if_\kappa(pr)\,\chi_{-\kappa}^\mu(\hat{\mathbf{r}})\,\big)^\dagger. \tag{3.36}$$

For the cases considered here, these are obtained by transposition of the Dirac spinor with complex conjugation applied only to the spin-angular functions. If the free particle Green function is available then one can construct the single-site Green function using the Dyson equation (3.15).

3.4. Dirac equation

In order to compute the Green function of a considered magnetic system it is necessary to solve the single-site Dirac equation in the presence of an external magnetic field. The effective potential $V_{\text{eff}}(r)$ is approximated using the muffin-tin construction, namely the space is divided into non-overlapping (touching) muffin-tin spheres centered at each site i. Such a single site potential v_i is assumed to be spherically symmetric inside each sphere and constant outside. Then the single-site Dirac equation has the form:

$$\big(- i\hbar c\alpha \cdot \nabla + \beta m_e c^2 + V_{\text{eff}}[\,n,m\,](\mathbf{r})$$
$$+ \beta\sigma_z B_{\text{eff}}[\,n,m\,](\mathbf{r})\big)\,\psi_\nu(\mathbf{r}) = E_\nu\,\psi_\nu(\mathbf{r}) \tag{3.37}$$

with

$$B_{\text{eff}}(\mathbf{r}) = B_{\text{ext}}(\mathbf{r}) + B_{xc}(\mathbf{r})$$
$$= B_{\text{ext}}(\mathbf{r}) + \frac{\delta E_{xc}[\,n,m\,]}{\delta m(\mathbf{r})}\,. \tag{3.38}$$

In spherical coordinates Eq. (3.37) can be written as:

$$\big(\hat{H} - E\big)\,\psi_\Lambda(\mathbf{r}) = 0 \tag{3.39}$$

with

$$\hat{H} = i\gamma_5\,\sigma_r\,c\left(\frac{\partial}{\partial r} + \frac{\mathbb{1}_4 - \beta\,\hat{K}_4}{r}\right) + V_{\text{eff}}(r) + \beta\sigma_z\,B_{\text{eff}}(r) + \frac{c^2}{2}(\beta - \mathbb{1}_4)\,, \tag{3.40}$$

where $\hat{K}$ is the spin-orbit operator, $\Lambda = (\kappa,\mu)$ a short-hand notation for the combined spin-orbit and magnetic quantum numbers κ and μ. The Dirac matrices α_i, β are defined in Eq. (3.30) and the matrix γ_5 is defined in the following way:

$$\gamma_5 = \begin{pmatrix} 0 & -\mathbb{1}_2 \\ -\mathbb{1}_2 & 0 \end{pmatrix}\,. \tag{3.41}$$

The Dirac Hamiltonian commutes with the operators σ^2, $\hat{j}^2$ and $\hat{j}_z$, total angular momentum operator j and with the spin-orbit operator $\hat{K} = \beta\,(\mathbb{1}_4 + \hat{l}\cdot\sigma)$. In Eq. (3.40) the following equation for the operator $\sigma_r = \frac{\sigma\cdot\mathbf{r}}{r}$ holds:

$$\sigma_r\,\chi_\Lambda(\hat{r}) = -\chi_{-\Lambda}(\hat{r})\,, \tag{3.42}$$

where $-\Lambda = (-\kappa,\mu)$.

The eigenfunctions of the operators $\sigma^2, \hat{\mathbf{j}}^2, \hat{j}_z$ and $\hat{K}$ are the spin-angular functions defined as [19]:

$$\chi_\Lambda(\hat{r}) = \sum_{m_s} C\left(l\frac{1}{2}j;\,m_l\,,m_s\right) Y_l^{\mu-m_s}(\hat{r})\,\chi_{m_s} \tag{3.43}$$

with the Pauli spin functions:

$$\chi_{+\frac{1}{2}} = \begin{pmatrix} 1 \\ 0 \end{pmatrix} \quad \text{and} \quad \chi_{-\frac{1}{2}} = \begin{pmatrix} 0 \\ 1 \end{pmatrix}, \tag{3.44}$$

Clebsch-Gordan coefficients $C\left(l\frac{1}{2}j; m_l, m_s\right)$ and spherical harmonics $Y_l^{\mu-m_s}$.

The spin-orbit quantum number κ and the magnetic quantum number μ are the eigenvalues of the operators $\hat{K}$ and $\hat{\mathbf{j}}^2$:

$$\hat{K}\,\chi_\Lambda(\hat{r}) = -\kappa\,\chi_\Lambda(\hat{r}), \tag{3.45}$$

$$\hat{j}_z\,\chi_\Lambda(\hat{r}) = \mu\,\chi_\Lambda(\hat{r}), \tag{3.46}$$

where $\hat{j}_z$ is the z-component of the total angular momentum operator $\hat{\mathbf{j}}$:

$$\hat{\mathbf{j}}^2\,\chi_\Lambda(\hat{r}) = j(j+1)\,\chi_\Lambda(\hat{r}). \tag{3.47}$$

Considering $B_{\text{eff}} = 0$ (paramagnetic case) in Eq. (3.40) the following ansatz can be used to solve the Dirac equation of a spherical potential:

$$\psi_\Lambda(\mathbf{r}) = \begin{pmatrix} g_\kappa(r)\,\chi_\Lambda(\hat{r}) \\ if_\kappa(r)\,\chi_{-\Lambda}(\hat{r}) \end{pmatrix}, \tag{3.48}$$

where $g_\kappa(r)$ and $f_\kappa(r)$ are the large and small components of the Dirac bispinor, respectively. In the case of $B_{\text{eff}} \neq 0$ the symmetry of the system is broken in spin space and it is necessary to use an extended ansatz which can be obtained as a superposition of the partial waves with different spin-angular character [31]:

$$\psi_\nu(\mathbf{r}) = \sum_\Lambda \psi_{\Lambda\nu}(\mathbf{r}) = \sum_\Lambda \begin{pmatrix} g_{\kappa\nu}(r)\,\chi_\Lambda(\hat{r}) \\ if_{\kappa\nu}(r)\,\chi_{-\Lambda}(\hat{r}) \end{pmatrix}, \tag{3.49}$$

where linearly independent wave functions are labeled with the index ν. If one substitute this bispinor into Eq. (3.39) one obtains the following expressions for the coupled radial wave functions [32]:

$$\frac{\partial}{\partial r}P_{\Lambda\nu}(r) = -\frac{\kappa}{r}P_{\Lambda\nu}(r) + \frac{1}{c^2}\left[E + c^2 - V_{\text{eff}}(r)\right]Q_{\Lambda\nu}(r)$$
$$+ \frac{B_{\text{eff}}(r)}{c^2}\sum_{\Lambda'}\langle\chi_{-\Lambda}|\,\sigma_z\,|\chi_{-\Lambda'}\rangle\,Q_{\Lambda'\nu}(r), \tag{3.50}$$

$$\frac{\partial}{\partial r}Q_{\Lambda\nu}(r) = \frac{\kappa}{r}Q_{\Lambda\nu}(r) - \left[E - V_{\text{eff}}(r)\right]P_{\Lambda\nu}(r)$$
$$+ B_{\text{eff}}(r)\sum_{\Lambda'}\langle\chi_\Lambda|\,\sigma_z\,|\chi_{\Lambda'}\rangle\,P_{\Lambda'\nu}(r) \tag{3.51}$$

with $P_{\Lambda\nu}(r) = r\,g_{\kappa\nu}(r)$ and $Q_{\Lambda\nu}(r) = cr\,f_{\kappa\nu}(r)$. The spin-angular matrix elements are nonzero only for the following conditions:

$$\langle\chi_\Lambda|\,\sigma_z\,|\chi_{\Lambda'}\rangle = \delta_{\mu\mu'}\begin{cases} -\dfrac{\mu}{\kappa+\frac{1}{2}} & \text{for } \kappa = \kappa' \\ -\sqrt{1 - \dfrac{\mu^2}{(\kappa+\frac{1}{2})^2}} & \text{for } \kappa = -\kappa' - 1 \\ 0 & \text{otherwise}. \end{cases} \tag{3.52}$$

Considering only allowed values for the quantum number κ:

$$\kappa = -l - 1 \qquad \text{if} \qquad j = l + \frac{1}{2}\,, \tag{3.53}$$

$$\kappa = l \qquad \text{if} \qquad j = l - \frac{1}{2} \tag{3.54}$$

a coupling between the wave functions in Eq. (3.50) and Eq. (3.51) is obtained if $\Delta l = l - l' = 0; \pm 2$ with $\Delta\mu = 0$. In practice, only coupling terms with $\Delta l = 0$ are kept as they provide a much larger contribution compared to the terms with $\Delta l = \pm 2$ [31]. However, it was shown that these terms may be important when calculating such quantities as magnetocrystalline anisotropy [33].

3.5. Single-site scattering Green function

The single-site Green function G^n can be expressed in terms of the free particle Green function G_0 via the Dyson equation Eq. (3.15). In order to obtain this expression it is necessary to determine the single-site t-matrices. This can be done by accounting for the matching conditions for the wave functions. Since the space is divided into two regions (with nonzero potential inside the muffin-tin sphere ($r < r_{\mathrm{mt}}$) and with zero potential outside ($r \geq r_{\mathrm{mt}}$)), the corresponding wave functions inside and outside the sphere have to match each other smoothly at the boundary. Therefore, the regular wave function outside the muffin-tin sphere can be expressed as a combination of incoming and outgoing waves (this holds for $r_{\mathrm{mt}} < r < \infty$):

$$Z_\Lambda(\mathbf{r}, E) = \sum_{\Lambda'} j_{\Lambda'}(\mathbf{r}, E)\, t_{\Lambda'\Lambda}^{-1}(E) \, - \, ip\, h_\Lambda^+(\mathbf{r}, E)\,. \tag{3.55}$$

Using this matching conditions, the expression for the t-matrix can be determined [34]. Finally for a single scatterer i the single-site Green function in coordinate representation becomes:

$$
\begin{aligned}
G^i(\mathbf{r}, \mathbf{r}', E) =\,& G_0(\mathbf{r}, \mathbf{r}', E) \\
& + \int\int d^3 r''\, d^3 r'''\, G_0(\mathbf{r}, \mathbf{r}'', E)\, t^i(\mathbf{r}'', \mathbf{r}''', E)\, G_0(\mathbf{r}''', \mathbf{r}', E)
\end{aligned} \tag{3.56}
$$

with the matrix elements of t-matrix given as:

$$t_{\Lambda\Lambda'}^i(E) = \int\int d^3 r\, d^3 r'\, j_\Lambda^\times(\mathbf{r}, E)\, t^i(\mathbf{r}, \mathbf{r}', E)\, j_{\Lambda'}(\mathbf{r}', E)\,. \tag{3.57}$$

Inserting the expression for G_0 (Eq. (3.33)) into Eq. (3.56) leads to the following expression for the single-site Green function:

$$
\begin{aligned}
G^i(\mathbf{r}, \mathbf{r}', E) =\,& \sum_{\Lambda\Lambda'} Z_\Lambda(\mathbf{r}, E)\, t_{\Lambda\Lambda'}^i(E)\, Z_{\Lambda'}^\times(\mathbf{r}', E) \\
& - \sum_\Lambda Z_\Lambda(\mathbf{r}, E)\, J_\Lambda^\times(\mathbf{r}', E)\, \Theta(\mathbf{r}' - \mathbf{r}) \\
& - \sum_\Lambda J_\Lambda(\mathbf{r}, E)\, Z_\Lambda^\times(\mathbf{r}', E)\, \Theta(\mathbf{r} - \mathbf{r}')\,,
\end{aligned} \tag{3.58}
$$

where Z_Λ and J_Λ denote regular and irregular solutions and satisfy the following conditions for $r \geq r_{\text{mt}}$:

$$Z_\Lambda(\mathbf{r}, E) = \sum_{\Lambda'} j_{\Lambda'}(\mathbf{r}, E) \, (t^i)^{-1}_{\Lambda'\Lambda}(E) - ip \, h^+_\Lambda(\mathbf{r}, E) \tag{3.59}$$

$$J_\Lambda(\mathbf{r}, E) = j_\Lambda(\mathbf{r}, E) \,. \tag{3.60}$$

3.6. Multiple-scattering Green function

The multiple scattering Green function describing the whole system with an arbitrary array of scatterers can be constructed in a similar way as performed for the single-site Green function. As a starting point one can use the following Dyson equation:

$$G^{nn} = G^n + G^n \, T^{nn} \, G^n \,, \tag{3.61}$$

where T^{nn} describes the total scattering of the system omitting site n. In real space representation the Green function can be written as follows:

$$\begin{aligned} G(\mathbf{r}, \mathbf{r}', E) = \; & G^n(\mathbf{r}, \mathbf{r}', E) \\ & + \int \int d^3r'' \, d^3r''' \, G^n(\mathbf{r}, \mathbf{r}', E) \, T^{nn}(\mathbf{r}'', \mathbf{r}''', E) \, G^n(\mathbf{r}''', \mathbf{r}', E) \,. \end{aligned} \tag{3.62}$$

According to Eq. (3.26) T^{nn} has a following form:

$$T^{nn}(\mathbf{r}, \mathbf{r}', E) = \sum_{i \neq n} \sum_{j \neq n} \tau^{ij}(\mathbf{r}, \mathbf{r}', E) \,, \tag{3.63}$$

where the multiple scattering path operator τ^{ij} is given in Eq. (3.27):

$$\begin{aligned} \tau^{ij}(\mathbf{r}, \mathbf{r}', E) = \; & \delta_{ij} \, t_i(\mathbf{r}, \mathbf{r}', E) \\ & + \int \int d^3r'' \, d^3r''' \, t_i(\mathbf{r}, \mathbf{r}''', E) \sum_{k \neq i} G_0(\mathbf{r}'', \mathbf{r}''', E) \, \tau^{kj}(\mathbf{r}''', \mathbf{r}', E) \,. \end{aligned} \tag{3.64}$$

As one can see $t_i(\mathbf{r}, \mathbf{r}', E)$ is non-zero only when $\mathbf{r}$ and $\mathbf{r}'$ are located in the same atomic cell i. The same applies to τ^{kj}, namely when $\mathbf{r}$ and $\mathbf{r}'$ belong to the atomic cell k and j, respectively, the provided contribution is non-zero. Furthermore, the free electron Green function can be re-written in terms of cell-centred coordinates:

$$G_0(\mathbf{R}_i + \mathbf{r}_i, \mathbf{R}_j + \mathbf{r}'_j, E) = G^{ij}_0(\mathbf{r}_i, \mathbf{r}'_j, E) = G_0(\mathbf{r}, \mathbf{R}_j - \mathbf{R}_i + \mathbf{r}'_j, E) \,. \tag{3.65}$$

The Hankel functions $h_\Lambda(\mathbf{r}, E)$ are irregular at the atomic positions $\mathbf{R}_i$ and can be expressed in terms of the Bessel functions around all other atomic cells at $\mathbf{R}_j$ [25, 29]. Finally, the free electron Green function acquires the form:

$$G^{ij}_0(\mathbf{r}_i, \mathbf{r}'_j, E) = \sum_{\Lambda\Lambda'} j_\Lambda(\mathbf{r}_i, E) \, G^{ij}_{0,\Lambda\Lambda'}(E) \, j^\times_{\Lambda'}(\mathbf{r}'_j, E) \,. \tag{3.66}$$

The expansion coefficients $G_{0,\Lambda\Lambda'}^{ij}(E)$ known as real-space structure constants depend exclusively on the spatial arrangement of the sites and completely are independent on the individual potentials on these sites V_i. Inserting the expression for the free electron Green function obtained in Eq. (3.66) into the equation for the scattering path operator (Eq. (3.64)) and multiplying from the left with $j_\Lambda^\times(\mathbf{r}_i, E)$ and from the right with $j_{\Lambda'}^\times(\mathbf{r}_j', E)$ followed by further integration over $\mathbf{r}_i$ and $\mathbf{r}_j$, leads to the following matrix equation for $\tau_{\Lambda\Lambda'}^{ij}$:

$$\tau_{\Lambda\Lambda'}^{ij}(E) = \delta_{ij}\, t_{\Lambda\Lambda'}^i(E) + \sum_{k \neq i} \sum_{\Lambda''\Lambda'''} t_{\Lambda\Lambda''}^i(E)\, G_{0,\Lambda''\Lambda'''}^{ik}(E)\, \tau_{\Lambda'''\Lambda'}^{kj}(E) \tag{3.67}$$

with the matrix elements given as:

$$\tau_{\Lambda\Lambda'}^{ij}(E) = \int\int d^3r\, d^3r'\, j_\Lambda^\times(\mathbf{r}_i, E)\, \tau^{ij}(\mathbf{r}_i, \mathbf{r}_j', E)\, j_{\Lambda'}(\mathbf{r}_j', E)\,. \tag{3.68}$$

Furthermore, inserting the expression obtained for the single-site Green function Eq. (3.58) and the expression for the T-matrix Eq. (3.63) into the Dyson equation Eq. (3.62), one obtains an expression for the relativistic multiple scattering Green function:

$$G(\mathbf{r}_i, \mathbf{r}_j', E) = \sum_{\Lambda\Lambda'} Z_\Lambda(\mathbf{r}_i, E)\, \tau_{\Lambda\Lambda'}^{ij}(E)\, Z_{\Lambda'}^\times(\mathbf{r}_j', E)$$
$$- \sum_\Lambda [\, Z_\Lambda(\mathbf{r}_i, E)\, J_\Lambda^\times(\mathbf{r}_i', E)\, \Theta(r' - r)$$
$$+ J_\Lambda(\mathbf{r}_i, E)\, Z_\Lambda^\times(\mathbf{r}_i', E)\Theta(r - r')\,]\,\delta_{ij}\,. \tag{3.69}$$

Comparing the Green function of the entire system given by the above equation with the single site Green function (Eq. (3.58)) one can notice that the main difference is that the single site t-matrix is replaced by the scattering path operator τ^{ij}.

The multiple scattering Green function provides a straightforward way to calculate various physical observables by taking the trace of the Green function and the necessary operator, namely:

$$\langle \hat{O} \rangle = -\frac{1}{\pi} \operatorname{Im} \operatorname{Tr} \hat{O}\,\hat{G}\,. \tag{3.70}$$

Particularly, the density of states $n(E)$, the charge density $\rho(\mathbf{r})$, spin- and orbital magnetic moments can be calculated using the Green function:

$$n(E) = -\frac{1}{\pi} \operatorname{Im} \operatorname{Tr} \int_\Omega d^3r\, G(\mathbf{r}, \mathbf{r}, E)\,, \tag{3.71}$$

$$\rho(\mathbf{r}) = -\frac{1}{\pi} \operatorname{Im} \operatorname{Tr} \int^{E_F} dE\, G(\mathbf{r}, \mathbf{r}, E)\,, \tag{3.72}$$

$$\mu_{\mathrm{spin}} = -\frac{1}{\pi} \operatorname{Im} \operatorname{Tr} \int^{E_F} dE \int_\Omega d^3\beta\, \sigma_z\, G(\mathbf{r}, \mathbf{r}, E)\,, \tag{3.73}$$

$$\mu_{\mathrm{orb}} = -\frac{1}{\pi} \operatorname{Im} \operatorname{Tr} \int^{E_F} dE \int_\Omega d^3 l_z\, G(\mathbf{r}, \mathbf{r}, E)\,. \tag{3.74}$$

As one can see for these quantities only the site-diagonal part of $G(\mathbf{r}_i, \mathbf{r}'_j, E)$ is needed and thus only the scattering path operators τ^{ii} need to be evaluated.

3.7. Coherent potential approximation (CPA)

To compute physical properties of randomly disordered alloys one needs an appropriate treatment of disorder. One of the widely used methods in the calculation of the electronic structure of systems with broken translational symmetry, particularly substitutional alloys, is a single site approach - the coherent potential approximation (CPA) [25]. The main aim is to construct a translationally invariant medium, which reflects the properties of the real material in an averaged way.

In case of disordered systems, the corresponding Hamiltonian can be split into the translationally-invariant potential K and the randomly fluctuating on-site part of the potential [35]:

$$H = K + \sum_i \varepsilon_i \, a_i^\dagger \, a_i \,, \tag{3.75}$$

where $a_i^\dagger$ and a_i are the creation and annihilation operators for electron on site i, respectively. Furthermore, one can introduce an arbitrary effective potential which possesses the symmetry of the empty lattice σ. Taking this into account, the Hamiltonian of the system (Eq. (3.75)) can be re-written in the following manner:

$$H = \underbrace{K + \sum_i \sigma \, a_i^\dagger \, a_i}_{H_0} + \sum_i (\varepsilon_i - \sigma) \, a_i^\dagger \, a_i = H_0 + V \,, \tag{3.76}$$

where the last term is a randomly fluctuating on-site potential $V = \sum_i V_i$ and H_0 is a Hamiltonian of the unperturbed system.

In that case, the averaged Green function can be written as:

$$\langle G(E) \rangle = \langle (E - H)^{-1} \rangle = \langle (E - H_0 - V)^{-1} \rangle \,. \tag{3.77}$$

Introducing the so-called electron self-energy operator $\Sigma(E)$, which remains unknown, however includes all disorder effects, Eq. (3.77) can be modified:

$$\langle G(E) \rangle = \langle (E - H_0 - V)^{-1} \rangle = (E - H_0 - \Sigma(E))^{-1} \,. \tag{3.78}$$

As it can be seen from Eq. (3.78) it is necessary to construct a Green function corresponding to the Hamiltonian $H_0 + \Sigma(E)$ in such a way, that it is equal to the statistically averaged Green function of the original Hamiltonian $H = H_0 + V$.

Using the definition of the unperturbed Green function $G_0(E) = (E - H_0)^{-1}$, Eq. (3.78) can be re-written as:

$$\langle G(E) \rangle = \langle (G_0^{-1} - V)^{-1} \rangle = (G_0^{-1} - \Sigma(E))^{-1} \,. \tag{3.79}$$

The solution of Eq. (3.79) with respect to $\Sigma(E)$, is obtained by sum of the infinite series:

$$\Sigma(E) = \langle V \rangle + \langle V G_0 V \rangle - \langle V \rangle G_0 \langle V \rangle + \langle V G_0 V G_0 V \rangle - \cdots \qquad (3.80)$$

The above solution expressed through the infinite series is an exact solution. To calculate such a sum directly is impossible therefore further approximations are needed. Following the idea discussed in Ref. [36, 37], namely restricting to the terms containing first order in powers of $\langle V \rangle$, for $\forall$ site i, Eq. (3.80) can be written as:

$$\Sigma_i(E) \approx \langle V_i \rangle + \langle V_i G_0 V_i \rangle + \langle V_i G_0 V_i G_0 V_i \rangle + \cdots$$
$$= \left\langle \frac{V_i}{1 - G_0 V_i} \right\rangle = \langle t_i \rangle = 0 \qquad (3.81)$$

with $\langle t_i \rangle$ being a single-site t-matrix. The CPA condition requires that $\Sigma_i = \langle t_i \rangle = 0$. In that case, terms such as $\langle t_i G_0 t_j \rangle$ are also included however the averaging is restricted to an averaging at single site i independently of the surrounding sites.

Altogether, using Eq. (3.81) with $G_0(E) = (E - H_0)^{-1} = (E - K - \sigma)^{-1}$, one needs to determine an effective potential σ. Let's consider a binary disordered alloy such as $A_{1-x}B_x$ where atomic site can be occupied with atom specie A with probability $x_A = x$ or with atom specie B with probability $x_B = 1 - x$ (Fig. (3.1)). In this case to calculate an observable one needs to take into account all possible arrangements of atoms A and B on all possible positions in the solid, namely one needs to calculate the average of all possible configurations. In that case, Eq. (3.81) (taking into account the CPA restriction) is modified in the following way:

$$x \frac{\varepsilon_A - \sigma}{1 - (\varepsilon_A - \sigma) G_0} + (1 - x) \frac{\varepsilon_B - \sigma}{1 - (\varepsilon_B - \sigma) G_0} = 0, \qquad (3.82)$$

where $V_{A,B} = \varepsilon_{A,B} - \sigma$. Equivalently, one can re-write Eq. (3.82) in terms of the scattering path operator [30]:

$$x \tau_A^{ii} + (1 - x) \tau_B^{ii} = \tau_{CPA}^{ii}, \qquad (3.83)$$

where $\tau_{A(B)}^{ii}$ is a scattering path operator of the effective medium with an atom A(B) on site i. This component projected ($\alpha = A, B$) scattering path operator is given as:

$$\tau_\alpha^{ii} = \left[t_\alpha^{-1} - t_{CPA}^{-1} - \tau_{CPA}^{-1} \right]^{-1}. \qquad (3.84)$$

The effective scattering t-matrix t_{CPA} can be determined through the iterative procedure starting from a reasonable guess.

It is necessary to mention as the CPA is a mean field theory, it does not account for any short-range ordering effects that may be of significant importance in case of realistic systems. In order to overcome this shortcoming the cluster generalization of the CPA was suggested - the so-called non-local coherent potential approximation (NLCPA) which was implemented within the multiple-scattering KKR formalism [38–40].
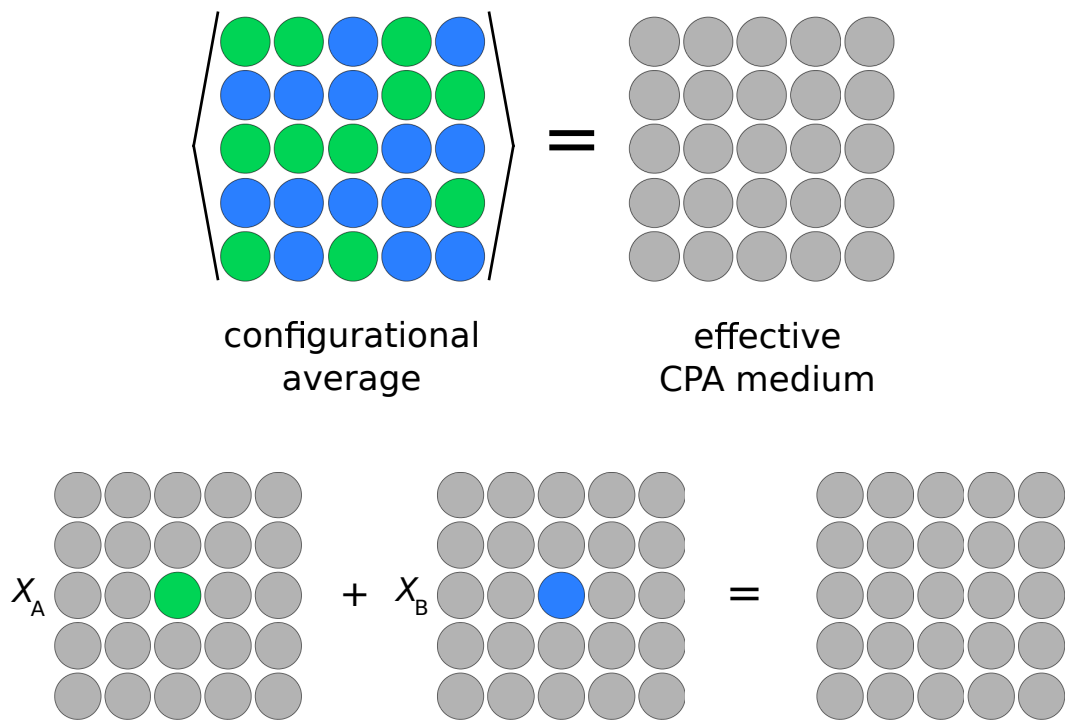
Figure 3.1.: The configurational average of the statistically disordered alloy A_xB_{1-x} is represented by an effective CPA medium (gray spheres).

4. Finite temperature effect

In ideal crystals (i.e., systems with perfect translational symmetry) the electronic states represent the so-called Bloch waves (solutions to the Schrödinger equation for a periodic real-valued potential), which are infinitely spread over the whole space. This reflects a physical property of the conducting electrons - in a perfect metal their mean free path (average distance between the subsequent scattering events) is infinite. In other words, the conductivity of electrons in the Bloch states is infinite and becomes finite only if the translational invariance is broken. In a real solid this can have many reasons: any type of chemical disorder, any local impurity or dislocation, i.e. any randomness, including also the ground-state electron-electron interactions or even a finiteness of the sample – all this leads to a break of translational symmetry. Therefore, the study of the transport properties of a solid first of all means an adequate description of the relevant translational-invariance breaking mechanisms, or in other words - the account of disorder mechanisms, since any translational symmetry break (except of maybe the finiteness of a sample) we call "disorder". When analyzing the relevance of the disorder mechanisms relevant for the transport properties in a particular situation, it is convenient to classify them into static and dynamic (e.g. thermally induced). Altogether here we will consider only four basic of these: chemical (substitutional impurities), structural (various defects), magnetic and electron correlations. The chemical one can be considered as an exclusively static type, whereas the others, despite they can be present at zero-temperature as well, can also be thermally induced. For example, the magnons (thermally induced dynamical magnetic fluctuations) can be "frozen" at zero temperature - this corresponds to a so-called magnetic-glass state. An analogical situation is found for phonons – the amorphous solids with static structural disorder represent a typical frozen-phonon state. On the other hand, both dynamical phonons and magnons can be induced at zero temperature externally - by a mechanical kick or an electromagnetic pulse. In any case, these kinds of disorder show a very pronounced temperature dependence, while chemical disorder is in general temperature independent. Another scattering mechanism leading to finite electrical conductivity is electron-electron scattering. It is temperature dependent, however, its impact on the resistivity is typically insignificant, except for systems with highly localized electrons, where correlations become important. Such systems will not be in our focus.

There is an interplay between various types of disorder that are simultaneously present in a solid. If these have a small amplitude, then the model of serial resistors (each representing a separate source of disorder) can be applied to describe the temperature dependence of the electrical resistivity. Namely, each scattering mechanism is assigned to an individual resistor connected in series, thereby reflecting that the scattering
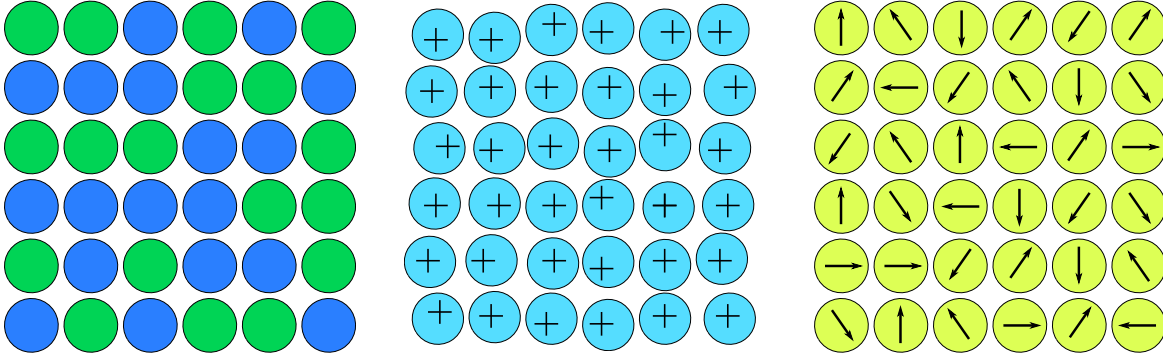
Figure 4.1.: Types of disorder: chemical (left panel), random atomic displacements (middle panel) and magnetic fluctuations (right panel) [41].

events are independent of each other. On the other hand, for a higher degree of disorder, one has to deal with a net of resistors connected in parallel. At any given temperature, different channels are active and contribute to the scattering processes. Further increase of disorder leads to a saturation of the resistivity, indicating that all channels are involved to some extent and the current already uses the most conductive ones. Since in this state translational symmetry breaking induced by different types of disorder are strongly superimposed and interferent there is no rigorous first-principles approach dealing with this situation which has been proposed so far.

In nonmagnetic metals, the scattering mechanism due to phonons can be approximated by the Bloch-Grüneisen formula [42]: within the low temperature regime ($T \ll \Theta_\mathrm{D}$, where Θ_D is the Debye temperature), the resistivity might behave strongly nonlinearly $\rho(T) \sim \beta T^2 + \gamma T^5$; whereas in the high-temperature regime ($T \gg \Theta_\mathrm{D}$) it changes according to $\rho(T) \sim \alpha \cdot T$ (Bloch-Grüneisen law), where α is the electron-phonon coupling constant. Quite often, such a linear behavior is observed in the low temperature regime as well, in particular, for the experimental data and present *ab initio* results [43]. Another scattering mechanism, specific for the magnetic systems, arises due to scattering by spin fluctuations. At zero temperature since all magnetic moments are perfectly aligned, there is no contribution ρ_mag due to that mechanism. For $T > 0$ the magnetic disorder induced by thermal fluctuations results into a corresponding increase of the resistivity. Above the critical temperature (T_C), when the fluctuations of local magnetic moments are saturated, resistivity shows a constant temperature-independent behavior.

These two scattering sources are extremely temperature-dependent. Therefore, a central aspect of this work is to account both scattering mechanisms simultaneously within an arbitrarily wide temperature interval.

4.1. Alloy-analogy model within CPA

Originally the CPA formalism was formulated to describe chemically disordered alloys [44]. Recently it was further modified in order to account for the lattice vibrations [45] and spin fluctuations [46, 47], which broadly extends its application regime. The approach to account for both types of disorder is essentially the same, being based on the same original static alloy model. This becomes possible mainly due to the fact that the dynamical phonons and magnons are much slower compared to the electronic propagation, so that an electron "sees" a static situation at any instant in time. Due to the single-site nature of the CPA, which neglects the inter-site chemical correlations, the same holds here: the direction of the magnetic moment on a given site (or the position of a given atom) is independent on the position of the moment on the other one (or of the other atoms) - i.e., the magnons and phonons are treated as "uncorrelated".

The difference in the description of the lattice vibrations and spin fluctuations lies in the particular construction of the perturbed Green functions (either by atomic displacement or by rotation of the local magnetic moment). In general, the CPA medium Green function is given as an average weighted sum of the corresponding projected Green functions [41]:

$$G(\mathbf{r}, \mathbf{r}', E) = \sum_\alpha x_\alpha \, G_\alpha(\mathbf{r}, \mathbf{r}', E), \quad \sum_\alpha x_\alpha = 1 \,, \tag{4.1}$$

where α corresponds to a particular discrete atomic displacement in case of lattice vibrations, and stands for a particular discrete direction of the local magnetic moment in case of spin fluctuations. The individual projected Green functions $G_\alpha(\mathbf{r}, \mathbf{r}', E)$ are computed in the usual way (see Chapter 2, Section 3.6, Eq. (3.69)) using the spherical solutions Z_α, J_α, with the component-projected τ_α given as follows [41]:

$$\underline{\tau}_\alpha = \left[\underline{t}_\alpha^{-1} - \underline{t}_{\text{CPA}}^{-1} + \underline{\tau}_{\text{CPA}}^{-1} \right]^{-1} \,. \tag{4.2}$$

Dealing with thermal lattice vibrations ($\underline{t}_\alpha = \underline{t}_v$), one needs to compute the matrix $\underline{t}_v$ given by the shifts of the atomic position $\{\Delta\mathbf{R}\}$. This can be done by applying the transformation matrix $\underline{U}$ (the nonrelativistic version of this is given in Ref. [48, 49] and transformed to the relativistic form via a Clebsh-Gordan transformation [19]):

$$\underline{t}_v = \underline{U}(\Delta\mathbf{R}) \, \underline{t} \, \underline{U}(\Delta\mathbf{R})^{-1} \,. \tag{4.3}$$

The thermal distribution of these atomic displacements can be set in several ways. It can be constructed either based on experiment (active vibrational modes can be determined from infrared and Raman spectroscopy) or by performing numerically demanding but straightforward calculations of the phonon modes [50]. However, as it was found out when dealing with transport properties, another much simpler way can be used: to choose the atomic displacements so that they reproduce the thermal root mean square average displacement $\sqrt{\langle u^2 \rangle_T}$ for a particular temperature T. There are different ways to obtain $\sqrt{\langle u^2 \rangle_T}$. In the current work, it is calculated on the basis of the Debye model, using the expression:
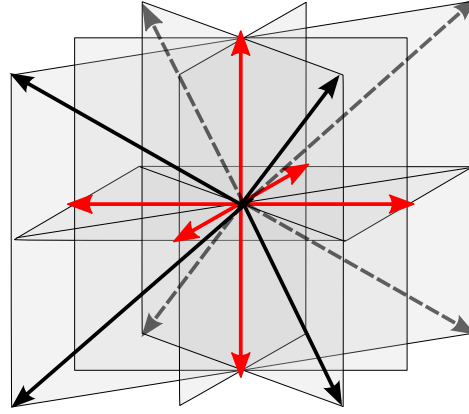
Figure 4.2.: Distribution of atomic displacements (considering 14 directions) conform with the crystal symmetry. As sufficient subset of displacements is marked by red arrows ($N_v = 6$).

$$\langle u^2 \rangle_T \; = \; \frac{3\hbar^2}{m k_{\mathrm{B}} \Theta_{\mathrm{D}}} \left[\frac{\Phi(\Theta_{\mathrm{D}}/T)}{\Theta_{\mathrm{D}}/T} + \frac{1}{4} \right] , \qquad (4.4)$$

where $\Phi(\Theta_{\mathrm{D}}/T)$ is a Debye function, $\hbar$ - Planck constant, k_{B} - Boltzmann constant, Θ_{D} - Debye temperature. The last term is connected with the zero-point vibration energy in the quantum theory of the harmonic oscillator, and can be neglected. The function $\Phi(\Theta_{\mathrm{D}}/T)$ was introduced numerically by Debye and its values are tabulated. On the other hand, the root mean square displacement can be expressed as follows:

$$\langle u^2 \rangle_T \; = \; \sum_{v=1}^{N_v} x_v \, |\, \Delta R_v(T)\,| , \qquad (4.5)$$

where N_v is a number of displacement vectors. For simplicity the probability x_v for the specific atomic shift is chosen as $1/N_v$. In calculations of transport coefficients, it turned out, that the result is not much sensitive to the chosen distribution of atomic displacements. For this reason, it is often enough to take a minimal number of lattice degrees of freedom (in the present work $N_v = 14$). The corresponding distribution of the displacement vectors is shown in Fig. (4.2).

Thermal spin fluctuations ($\underline{t}_\alpha = \underline{t}_f$) perturb the $\underline{t}$ matrix mainly through the rotation of the magnetic moment. This can be taken into account by applying the spin rotation matrix $\underline{R}$ determined by the set of directional vectors $\{\hat{e}\}$:

$$\underline{t}_f \; = \; \underline{R}(\hat{e}) \, \underline{t} \, \underline{R}(\hat{e})^{-1} . \qquad (4.6)$$

In contrast to the phonon case, where the final result is more sensitive to the amplitudes rather than the angular distribution of the atomic shifts, in the magnon case, the angular distribution of the magnetic moments strongly depends on the given temperature, and in turn, becomes critical for the final result. There are different ways to

construct a realistic temperature dependent distribution of the magnetic moments. It might be obtained from first principles calculations. However, this way is numerically very demanding similar to the case of phonon spectra. Alternatively, the distribution of the magnetic moments can be reasonably predefined, e.g. for the ferromagnet one may assume a Gibbs distribution. In this case, the adjusting of the Gibbs parameters can be done using the experimental temperature dependence of magnetization. It turned out that such an approach is often sufficient and results in good agreement with experimental data. The most simple distribution is based on the disordered local moment (DLM) approach with only two degrees of freedom (two directions for the magnetic moments); see Fig. (4.3), top panel. This approach describes the localized magnetic systems in the fully paramagnetic regime reasonably well, whereas in the region $T < T_\mathrm{C}$ strong deviations are observed due to the neglect of the fluctuations along other directions. The corresponding distribution is determined as follows:

$$\frac{1}{N_f} \sum_{f=1}^{N_f} \hat{e}_f \; = \; x_\uparrow \, \hat{z} \; + \; x_\downarrow \, (-\hat{z}) \tag{4.7}$$

with $x_\uparrow + x_\downarrow = 1$, and $N_f = 2$ is the number of orientation vectors $\hat{e}_f$. A much better description is provided by an isotropic spherical spin configuration model (Fig. (4.3), middle panel). In this case, the probability x_f for the orientation vector $\hat{e}_f$ pointing along the specific direction determined by the spherical angles (θ_f, ϕ_f) is given by the following expression:

$$x_f \; = \; \frac{\sin \theta_f \cdot \exp\left[\, w(T) \, \hat{z} \cdot \hat{e}_f / k_\mathrm{B} T \,\right]}{\displaystyle\sum_{f'} \sin \theta_{f'} \cdot \exp\left[\, w(T) \, \hat{z} \cdot \hat{e}_{f'} / k_\mathrm{B} T \,\right]} \, , \tag{4.8}$$

where $w(T)$ denotes a temperature dependent Weiss field-like parameter [51]. As mentioned, in contrast to the DLM spin configuration model, the distribution on a sphere allows to account for the transverse fluctuations, thereby providing a better description of the experimental situation. Another way for the construction of the distribution of the magnetic moments is to orient these along the surface of a cone as shown in Fig. (4.3) (bottom panel). In addition, there are more factors which make the magnetic distribution to deviate from a Gibbs or some other predefined distribution, such as spin-orbit coupling, or various multiple short and long range exchange interactions which can lead to a rather complicated picture of thermal disorder, which does not fit to the single-site CPA representation. In principle, the latter can be accounted for within the non-local CPA formalism [38]. On the other hand, it must be noted that all given magnetic distributions work well for the localized magnetic systems only, since none of the considered models accounts for the longitudinal spin fluctuations (change of the local magnetic moment amplitude) which are essential for itinerant magnets (e.g. Ni), especially in the high temperature region.

The remarkable feature of the alloy analogy model which we apply here, is that, despite the fact that the description of microscopic details of the specific type of disorder could
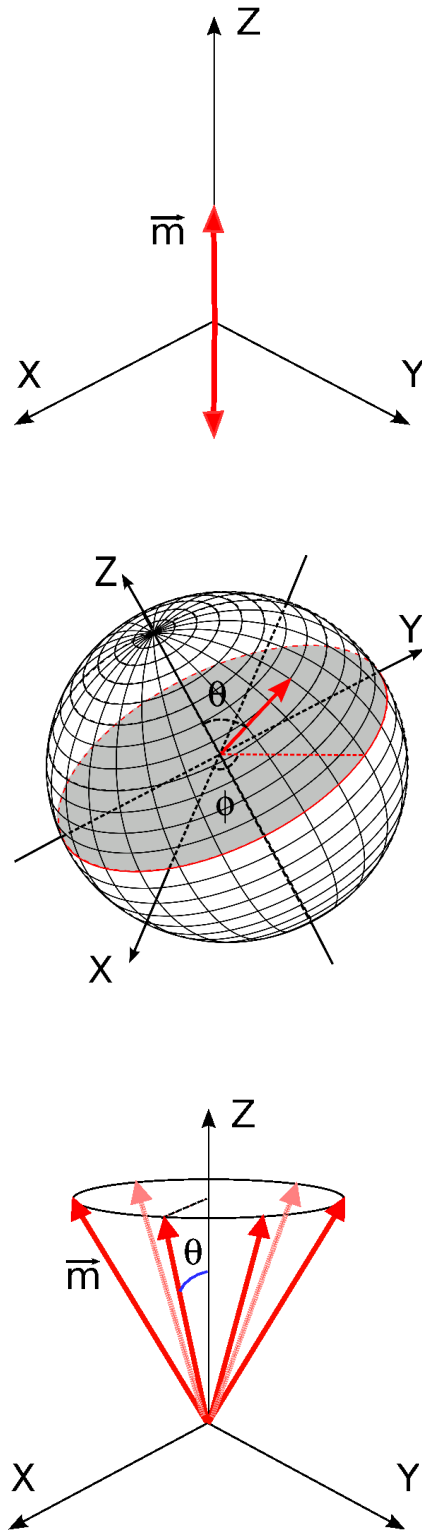
Figure 4.3.: Models of spin configurations: DLM-like distribution of the magnetic moments (top panel), spherical distribution (middle panel), distribution on a cone (bottom panel).

be incomplete, macroscopically it provides a correct description. The main indication of this is the qualitative and quantitative reproduction of the resistivity saturation effect. Thereby, the CPA formalism provides an effective account for various types of disorder. Moreover, it accounts for disorder not just on a level of computing the electrical resistivity, but much more beyond, on the level of the electronic structure, which allows to compute all other properties on the same footing.

5. Electronic transport based on the Kubo formalism

Studying systems in the ground state experimentally, basic information is provided by the linear part of the response to an external perturbation. Linear response can be characterized by a constant coefficient, which in case of electric field due to a perturbation is called conductivity. In anisotropic systems this constant has a tensor structure which is determined by the symmetry of the considered system (as well as by the orientation of the external perturbation). The first general approach to derive linear response coefficients theoretically was suggested by Ryogo Kubo in the 50ies [52]. The suggested formalism is based on the linear response to a small perturbation of a system in the equilibrium which can be expressed in terms of fluctuations of the dynamical variables of the unperturbed system. This linear response formalism is directly applicable to the problem of electrical conduction in solids.

5.1. Kubo equation

To derive the Kubo equation one can start from the system in thermodynamical equilibrium state which can be described by the Hamiltonian $\hat{H}_0$. At some infinitely distant point in time a small perturbation is applied (e.g. infinitely slow switching of the external electric field) and in that case the corresponding time-dependent Hamiltonian of the system has the following form:

$$\hat{H}(t) = \hat{H}_0 + \hat{V}(t) \tag{5.1}$$

with $V(t)$ being a time-dependent perturbation. The system state at any time can be described by the density matrix $\rho(t)$, which satisfies the corresponding von Neumann equation:

$$i\hbar \frac{\partial \rho(t)}{\partial t} = \left[\hat{H}(t), \rho(t) \right], \tag{5.2}$$

where brackets [...] denote the commutator between $\hat{H}(t)$ and $\rho(t)$. The system at $t_0 = 0$ was in the equilibrium state therefore $\left[\hat{H}_0, \rho_0 \right] = 0$, where $\rho_0 = \rho(t_0 = 0)$ - equilibrium density matrix, which is given by:

$$\rho_0 = \frac{e^{-\beta \hat{H}_0}}{\mathrm{Tr}\left\{ e^{-\beta \hat{H}_0} \right\}} \tag{5.3}$$

with $\beta = \frac{1}{k_B T}$, k_B - Boltzmann constant and T - system temperature.

Then the computation of the expectation value of the arbitrary operator $\hat{O}$ involves the equilibrium density matrix:

$$\langle \hat{O} \rangle = \mathrm{Tr} \{ \rho_0 \, \hat{O} \} . \tag{5.4}$$

In case of a time-dependent perturbation, the corresponding expectation value of $\hat{O}$ becomes time-dependent and the calculation of the observable includes time-dependent density matrix $\rho(t)$:

$$\langle \hat{O} \rangle (t) = \mathrm{Tr} \{ \rho(t) \, \hat{O} \} , \tag{5.5}$$

where $\rho(t)$ satisfies Eq. (5.2). This equation can be easily solved if one switches to the interaction representation (Heisenberg picture), namely:

$$\tilde{\rho}(t) = e^{\frac{i}{\hbar} \hat{H}_0 t} \, \rho(t) \, e^{-\frac{i}{\hbar} \hat{H}_0 t} . \tag{5.6}$$

Taking Eq. (5.6) into account, the Hamiltonian of the unperturbed system $\hat{H}_0$ can be completely eliminated from Eq. (5.2):

$$\begin{aligned}
i\hbar \frac{\partial \tilde{\rho}(t)}{\partial t} &= i\hbar \frac{\partial}{\partial t} \left\{ e^{\frac{i}{\hbar} \hat{H}_0 t} \, \rho(t) \, e^{-\frac{i}{\hbar} \hat{H}_0 t} \right\} \\
&= -\hat{H}_0 \, \tilde{\rho}(t) + i\hbar \, e^{\frac{i}{\hbar} \hat{H}_0 t} \frac{\partial \rho(t)}{\partial t} \, e^{-\frac{i}{\hbar} \hat{H}_0 t} + \tilde{\rho}(t) \, \hat{H}_0 \\
&= -\left[\hat{H}_0 \, \tilde{\rho}(t) \right] + e^{\frac{i}{\hbar} \hat{H}_0 t} \left[\hat{H}_0 + \hat{V}(t), \rho(t) \right] e^{-\frac{i}{\hbar} \hat{H}_0 t} \\
&= \left[\tilde{V}(t), \tilde{\rho}(t) \right] ,
\end{aligned} \tag{5.7}$$

where $\tilde{V}(t) = e^{\frac{i}{\hbar} \hat{H}_0 t} \, \hat{V}(t) \, e^{-\frac{i}{\hbar} \hat{H}_0 t}$. The solution of the above equation can be given as integral over time:

$$\tilde{\rho}(t) = \rho_0 - \frac{i}{\hbar} \int_{-\infty}^{t} dt' \left[\tilde{V}(t'), \tilde{\rho}(t') \right] \tag{5.8}$$

with $\rho_0 = \tilde{\rho}(-\infty)$. One can solve Eq. (5.8) iteratively:

$$\begin{aligned}
\tilde{\rho}(t) = \rho_0 &- \frac{i}{\hbar} \int_{-\infty}^{t} dt_1 \left[\tilde{V}(t_1), \rho_0 - \frac{i}{\hbar} \int_{-\infty}^{t_1} dt_2 \left[\tilde{V}(t_2), \right. \right. \\
&\left. \left. \rho_0 - \frac{i}{\hbar} \int_{-\infty}^{t_2} dt_3 \left[\tilde{V}(t_3), \rho_0 - \ldots \right] \right] \right] \\
= \rho_0 &+ \sum_{n=1}^{\infty} \left(-\frac{i}{\hbar} \right)^n \int_{-\infty}^{t} dt_1 \int_{-\infty}^{t_1} dt_2 \ldots \int_{-\infty}^{t_{n-1}} dt_n \\
&\times \left[\tilde{V}(t_1), \left[\tilde{V}(t_2), \left[\ldots, \left[\tilde{V}(t_n), \rho_0 \right] \right] \right] \ldots \right] .
\end{aligned} \tag{5.9}$$

In case of small perturbations ($V(t)$ changes slowly) it is enough to keep only terms of first order in $\tilde{V}(t)$:

$$\tilde{\rho}(t) \approx \rho_0 - \frac{i}{\hbar} \int_{-\infty}^{t} dt' \left[\tilde{V}(t'), \rho_0 \right]. \tag{5.10}$$

Returning back to the Schrödinger picture $\rho(t) = e^{-\frac{i}{\hbar}\hat{H}_0 t} \tilde{\rho}(t) e^{\frac{i}{\hbar}\hat{H}_0 t}$, Eq. (5.10) acquires the form:

$$\rho(t) \approx \rho_0 - \frac{i}{\hbar} \int_{-\infty}^{t} dt' \, e^{-\frac{i}{\hbar}\hat{H}_0 t} \left[\tilde{V}(t'), \rho_0 \right] e^{\frac{i}{\hbar}\hat{H}_0 t}. \tag{5.11}$$

Using the above expression for the time-dependent density operator and taking into account the cyclic permutations under the trace, Eq. (5.5) can be rewritten in a following way:

$$\langle \hat{O} \rangle(t) = \mathrm{Tr}\left\{ \rho_0 \hat{O} \right\} - \frac{i}{\hbar} \int_{-\infty}^{t} dt' \, \mathrm{Tr}\left\{ e^{-\frac{i}{\hbar}\hat{H}_0 t} \left[\tilde{V}(t'), \rho_0 \right] e^{\frac{i}{\hbar}\hat{H}_0 t} \hat{O} \right\}$$

$$= \langle \hat{O} \rangle - \frac{i}{\hbar} \int_{-\infty}^{t} dt' \, \mathrm{Tr}\left\{ \left[\tilde{V}(t'), \rho_0 \right] \underbrace{e^{\frac{i}{\hbar}\hat{H}_0 t} \hat{O} e^{-\frac{i}{\hbar}\hat{H}_0 t}}_{\tilde{O}(t)} \right\}$$

$$= \langle \hat{O} \rangle - \frac{i}{\hbar} \int_{-\infty}^{t} dt' \, \mathrm{Tr}\left\{ \rho_0 \left[\tilde{O}(t), \tilde{V}(t') \right] \right\}$$

$$= \langle \hat{O} \rangle - \frac{i}{\hbar} \int_{-\infty}^{\infty} dt' \, \Theta(t - t') \left\langle \left[\tilde{O}(t), \tilde{V}(t') \right] \right\rangle. \tag{5.12}$$

From the above equation follows, that the time-dependent expectation value of the arbitrary Hermitian operator $\hat{O}$ of the perturbed system can be calculated exclusively in terms of the unperturbed density matrix ρ_0.

In the following, we consider the electrical conductivity as the linear response of the current to an electric field. In this case the time-dependent external electric field is applied at $t = -\infty$ such that $\mathbf{E}(t) = \mathbf{E}_0 e^{-i(\omega + i\delta)t}$ and it increases adiabatically up to its value at $t = 0$. The operator $\hat{O}(t)$ is replaced by the current density operator $\hat{\mathbf{j}}$. However, in the present work we deal as well with the spin Hall effect, therefore $\hat{\mathbf{J}}$ should be used to represent either the charge current or spin current density operator [53]. The corresponding perturbation can be written as $\hat{V}(t) = -\hat{\mathbf{P}} \cdot \mathbf{E}(t)$, where $\hat{\mathbf{P}} = \sum_{i=1}^{N} q_i \hat{\mathbf{r}}_i$ (q_i being the charge and $\hat{\mathbf{r}}_i$ position operator for the i-th point charge) is the polarization of the sample caused by the external electric field. Therefore, for the spatial component

of the current density $\hat{J}_\mu$, Eq. (5.12) can be written as:

$$\langle J_\mu \rangle(t) = \frac{i}{\hbar} \sum_\nu \int\limits_{-\infty}^{\infty} dt' \, \Theta(t - t')$$

$$\left\langle \left[\tilde{J}_\mu(t), \tilde{P}_\nu(t') \right] \right\rangle E_0 e^{-i(\omega + i\delta)t'} \tag{5.13}$$

assuming that $\langle J_\mu \rangle(t = -\infty) = 0$. Making use of the property $\langle [\hat{O}, \hat{V}] \rangle = \mathrm{Tr}\{\rho_0 [\hat{O}, \hat{V}]\} = \mathrm{Tr}\{\rho_0 \hat{O}\hat{V}\} - \mathrm{Tr}\{\rho_0 \hat{V}\hat{O}\}$, the commutator in Eq. (5.13) can be rewritten as:

$$\left\langle \left[\tilde{J}_\mu(t), \tilde{P}_\nu(t') \right] \right\rangle = \mathrm{Tr}\left\{ \rho_0 \left(e^{\frac{i}{\hbar}\hat{H}_0 t} \hat{J}_\mu e^{-\frac{i}{\hbar}\hat{H}_0 t} \, e^{\frac{i}{\hbar}\hat{H}_0 t'} P_\nu e^{-\frac{i}{\hbar}\hat{H}_0 t'} \right.\right.$$

$$\left.\left. - \; e^{\frac{i}{\hbar}\hat{H}_0 t'} P_\nu e^{-\frac{i}{\hbar}\hat{H}_0 t'} e^{\frac{i}{\hbar}\hat{H}_0 t} \hat{J}_\mu e^{-\frac{i}{\hbar}\hat{H}_0 t} \right) \right\}$$

$$= \mathrm{Tr}\left\{ \rho_0 \left(\hat{J}_\mu e^{\frac{i}{\hbar}\hat{H}_0 (t'-t)} P_\nu e^{-\frac{i}{\hbar}\hat{H}_0 (t'-t)} \right.\right.$$

$$\left.\left. - \; e^{\frac{i}{\hbar}\hat{H}_0 (t'-t)} P_\nu e^{-\frac{i}{\hbar}\hat{H}_0 (t'-t)} \hat{J}_\mu \right) \right\}$$

$$= \left\langle \left[J_\mu, \tilde{P}_\nu(t' - t) \right] \right\rangle. \tag{5.14}$$

Furthermore inserting Eq. (5.14) into Eq. (5.13) one obtains the following expression:

$$\langle J_\mu \rangle(t) = \frac{i}{\hbar} \sum_\nu \int\limits_{-\infty}^{\infty} dt' \, \Theta(t - t')$$

$$\left\langle \left[J_\mu, \tilde{P}_\nu(t' - t) \right] \right\rangle E_{0,\nu} \, e^{-i(\omega+i\delta)t} \, e^{-i(\omega+i\delta)(t'-t)}$$

$$= \frac{i}{\hbar} \sum_\nu \int\limits_{-\infty}^{\infty} dt'' \, \Theta(-t'')$$

$$\left\langle \left[J_\mu, \tilde{P}_\nu(t'') \right] \right\rangle e^{-i(\omega+i\delta)t''} \, E_\nu(t). \tag{5.15}$$

Making use of the relation $\langle J_\mu \rangle(t) = \sum_\nu \sigma_{\mu\nu} E_\nu(t)$, one obtains the expression for the conductivity:

$$\sigma_{\mu\nu}(\omega) = \frac{i}{\hbar} \int\limits_{-\infty}^{0} dt \left\langle \left[J_\mu, \tilde{P}_\nu(t) \right] \right\rangle e^{-i(\omega+i\delta)t}. \tag{5.16}$$

The above equation can be modified further by using the Kubo identity for an arbitrary operator [54]:

$$\frac{i}{\hbar} [\hat{O}(t), \rho] = \rho \int\limits_0^\beta d\lambda \, \dot{\hat{O}}(t - i\lambda\hbar), \tag{5.17}$$

Taking into account that $\dot{\mathbf{P}} = V\mathbf{j}$ (V is system volume) and that $\left\langle \left[J_\mu, \tilde{P}_\nu(t) \right] \right\rangle$
$= \mathrm{Tr}\{\rho\left[J_\mu, \tilde{P}_\nu(t) \right]\} = \mathrm{Tr}\{\left[\tilde{P}_\nu(t), \rho \right] J_\mu\}$ the expression for the conductivity tensor takes
the form:

$$
\sigma_{\mu\nu}(\omega) = \int\limits_0^\beta d\lambda \int\limits_{-\infty}^0 dt \left\langle \dot{\tilde{P}}_\nu(t - i\hbar\lambda)\, J_\mu \right\rangle e^{-i(\omega + i\delta)t}
$$

$$
= V \int\limits_0^\beta d\lambda \int\limits_{-\infty}^0 dt \left\langle \tilde{j}_\nu(t - i\hbar\lambda)\, J_\mu \right\rangle e^{-i(\omega + i\delta)t}
$$

$$
= V \int\limits_0^\beta d\lambda \int\limits_0^\infty dt \left\langle j_\nu\, \tilde{J}_\mu(t + i\hbar\lambda) \right\rangle e^{i(\omega + i\delta)t}. \tag{5.18}
$$

Eq. (5.18) represents the Kubo equation [52] for the conductivity tensor and is only re-
stricted to small perturbations. However, to solve this equation is tedious as one has to
take into account many-body effects. Therefore further approximations are necessary.
Assuming a static case $\omega = 0$ and using the independent electron approximation [55],
Eq. (5.18) transforms into:

$$
\sigma_{\mu\nu} = \frac{1}{V} \int\limits_0^\beta d\lambda\, e^{-\lambda(\varepsilon_n - \varepsilon_m)}
$$

$$
\times \int\limits_0^\infty dt \sum_{n,m} \left\langle f(\varepsilon_m)\{1 - f(\varepsilon_n)\} \right.
$$

$$
\left. \times e^{\frac{it}{\hbar}(i\hbar\delta + \varepsilon_n - \varepsilon_m)} \left\langle m|\,\hat{j}_\nu\,|n \right\rangle \left\langle n|\,\hat{J}_\mu\,|m \right\rangle \right\rangle, \tag{5.19}
$$

where $f(\varepsilon) = (e^{\frac{\varepsilon - \mu}{k_B T}} + 1)^{-1}$ is the Fermi-Dirac distribution function with μ denoting
the chemical potential. Integrating over λ leads to $\int\limits_0^\beta d\lambda\, e^{-\lambda(\varepsilon_n - \varepsilon_m)} = \frac{1 - e^{-\beta(\varepsilon_n - \varepsilon_m)}}{\varepsilon_n - \varepsilon_m}$.
The remaining β-dependent part turns into $\frac{1 - e^{-\beta(\varepsilon_n - \varepsilon_m)}}{\varepsilon_n - \varepsilon_m} f(\varepsilon_m)$
$(1 - f(\varepsilon_n)) = \frac{f(\varepsilon_m) - f(\varepsilon_n)}{\varepsilon_n - \varepsilon_m}$. Using the above expressions Eq. (5.19) acquires the follow-
ing form:

$$
\sigma_{\mu\nu} = \frac{1}{V} \sum_{n,m} \frac{f(\varepsilon_m) - f(\varepsilon_n)}{(\varepsilon_n - \varepsilon_m)} \left\langle m|\,\hat{j}_\nu\,|n \right\rangle \left\langle n|\,\hat{J}_\mu\,|m \right\rangle \int\limits_0^\infty dt\, e^{\frac{it}{\hbar}(i\hbar\delta + \varepsilon_n - \varepsilon_m)}
$$

$$
= \frac{i\hbar}{V} \sum_{n,m} \frac{f(\varepsilon_m) - f(\varepsilon_n)}{(\varepsilon_n - \varepsilon_m)(\varepsilon_n - \varepsilon_m + i\hbar\delta)} \left\langle m|\,\hat{j}_\nu\,|n \right\rangle \left\langle n|\,\hat{J}_\mu\,|m \right\rangle. \tag{5.20}
$$

Taking into account that $\lim\limits_{\delta \to 0^+} \frac{1}{(\varepsilon_n - \varepsilon)(\varepsilon_n - \varepsilon + i\delta)} = \lim\limits_{\delta \to 0^+} \frac{d}{d\varepsilon}\left\{ \frac{1}{\varepsilon_n - \varepsilon + i\delta} \right\}$ and $\int\limits_{-\infty}^\infty d\varepsilon$
$(\varepsilon - \hat{H}) = 1$, Eq. (5.20) can be rewritten using the integration over energies in the

following form:

$$\sigma_{\mu\nu} = \frac{i\hbar}{V} \int\limits_{-\infty}^{\infty} d\varepsilon\, f(\varepsilon) \sum_{n,m}$$

$$\left\langle \langle n | \hat{J}_\mu | m \rangle \frac{d}{d\varepsilon} \left(\frac{1}{\varepsilon - \varepsilon_m + i\delta} \right) \langle m | \hat{j}_\nu | n \rangle\, \delta(\varepsilon - \varepsilon_n) \right.$$

$$\left. - \langle m | \hat{j}_\nu | n \rangle\, \delta(\varepsilon - \varepsilon_m) \langle n | \hat{J}_\mu | m \rangle \frac{d}{d\varepsilon} \left\{ \frac{1}{\varepsilon - \varepsilon_n + i\delta} \right\} \right\rangle. \qquad (5.21)$$

Introducing advanced and retarded Green function $G^{\pm}(\varepsilon) = \frac{1}{\varepsilon - \hat{H} \pm i\delta}$, Eq. (5.21) can be rewritten in operator form:

$$\sigma_{\mu\nu} = \frac{i\hbar}{V} \int\limits_{-\infty}^{\infty} d\varepsilon\, f(\varepsilon)\, \mathrm{Tr} \left\langle \hat{J}_\mu \frac{dG^+(\varepsilon)}{d\varepsilon} \hat{j}_\nu\, \delta(\varepsilon - \hat{H}) \right.$$

$$\left. - \hat{J}_\mu\, \delta(\varepsilon - \hat{H})\, \hat{j}_\nu \frac{dG^-(\varepsilon)}{d\varepsilon} \right\rangle. \qquad (5.22)$$

This equation was derived by Bastin [56] and represents the conductivity as a product of Green functions and the current density operators. The computation of the conductivity is numerically very demanding as Eq. (5.22) contains an integration over δ-functions. However, a significant simplification can be achieved by shifting the integration into the complex plane, which is discussed in more detail in the next section.

Furthermore, Eq. (5.22) can be rewritten in terms of the current density operator $\hat{\mathbf{j}}$ in the following way:

$$\sigma_{\mu\nu} = \frac{i\hbar}{V} \int\limits_{-\infty}^{\infty} d\varepsilon\, f(\varepsilon)\, \mathrm{Tr} \left\langle \hat{j}_\mu \frac{dG^+(\varepsilon)}{d\varepsilon} \hat{j}_\nu\, \delta(\varepsilon - \hat{H}) \right.$$

$$\left. - \hat{j}_\mu\, \delta(\varepsilon - \hat{H})\, \hat{j}_\nu \frac{dG^-(\varepsilon)}{d\varepsilon} \right\rangle. \qquad (5.23)$$

Replacing the δ-function in Eq. (5.23) with the following expression and dropping the energy-dependence of the Green function for the sake of brevity:

$$\delta(\varepsilon - \hat{H}) = -\frac{1}{2\pi i} \left[\hat{G}^+ - \hat{G}^- \right] \qquad (5.24)$$

and splitting the expression into two equal parts, one obtains:

$$
\begin{aligned}
\sigma_{\mu\nu} &= -\frac{\hbar}{2\pi V} \int\limits_{-\infty}^{\infty} d\varepsilon\, f(\varepsilon)\, \mathrm{Tr} \left\langle \hat{\jmath}_\mu \frac{dG^+}{d\varepsilon} \hat{\jmath}_\nu \left(G^+ - G^-\right) \right. \\
&\qquad\qquad\qquad\qquad \left. - \hat{\jmath}_\mu \left(G^+ - G^-\right) \hat{\jmath}_\nu \frac{dG^-}{d\varepsilon} \right\rangle \\
&= -\frac{\hbar}{4\pi V} \int\limits_{-\infty}^{\infty} d\varepsilon\, f(\varepsilon)\, \mathrm{Tr} \left\langle \hat{\jmath}_\mu \frac{dG^+}{d\varepsilon} \hat{\jmath}_\nu \left(G^+ - G^-\right) \right. \\
&\qquad\qquad\qquad\qquad \left. - \hat{\jmath}_\mu \left(G^+ - G^-\right) \hat{\jmath}_\nu \frac{dG^-}{d\varepsilon} \right\rangle \\
&\quad -\frac{\hbar}{4\pi V} \int\limits_{-\infty}^{\infty} d\varepsilon\, f(\varepsilon)\, \mathrm{Tr} \left\langle \hat{\jmath}_\mu \frac{dG^+}{d\varepsilon} \hat{\jmath}_\nu \left(G^+ - G^-\right) \right. \\
&\qquad\qquad\qquad\qquad \left. - \hat{\jmath}_\mu \left(G^+ - G^-\right) \hat{\jmath}_\nu \frac{dG^-}{d\varepsilon} \right\rangle .
\end{aligned}
$$

$$(5.25)$$

Leaving the first term in Eq. (5.25) untouched and applying a partial integration on the second term, one arrives at the following expression:

$$
\begin{aligned}
\sigma_{\mu\nu} &= -\frac{\hbar}{4\pi V} \int\limits_{-\infty}^{\infty} d\varepsilon\, f(\varepsilon)\, \mathrm{Tr} \left\langle \hat{\jmath}_\mu \frac{dG^+}{d\varepsilon} \hat{\jmath}_\nu \left(G^+ - G^-\right) \right. \\
&\qquad\qquad\qquad\qquad \left. - \hat{\jmath}_\mu \left(G^+ - G^-\right) \hat{\jmath}_\nu \frac{dG^-}{d\varepsilon} \right\rangle \\
&\quad +\frac{\hbar}{4\pi V} \int\limits_{-\infty}^{\infty} d\varepsilon\, \frac{df(\varepsilon)}{d\varepsilon}\, \mathrm{Tr} \left\langle \hat{\jmath}_\mu G^+ \hat{\jmath}_\nu \left(G^+ - G^-\right) \right. \\
&\qquad\qquad\qquad\qquad \left. - \hat{\jmath}_\mu \left(G^+ - G^-\right) \hat{\jmath}_\nu G^- \right\rangle \\
&\quad +\frac{\hbar}{4\pi V} \int\limits_{-\infty}^{\infty} d\varepsilon\, f(\varepsilon)\, \mathrm{Tr} \left\langle \hat{\jmath}_\mu G^+ \jmath_\nu \left(\frac{dG^+}{d\varepsilon} - \frac{dG^-}{d\varepsilon}\right) \right. \\
&\qquad\qquad\qquad\qquad \left. - \hat{\jmath}_\mu \left(\frac{dG^+}{d\varepsilon} - \frac{dG^-}{d\varepsilon}\right) \jmath_\nu G^- \right\rangle .
\end{aligned}
$$

$$(5.26)$$

If in Eq. (5.26) one keeps the second term unchanged, while one combines the first and

third terms, one obtains the following expression:

$$
\begin{aligned}
\sigma_{\mu\nu} &= -\frac{\hbar}{4\pi V} \int\limits_{-\infty}^{\infty} d\varepsilon \, \frac{df(\varepsilon)}{d\varepsilon} \, \mathrm{Tr} \, \langle \, \hat{j}_\mu \left(G^+ - G^- \right) \hat{j}_\nu \, G^- \\
&\qquad\qquad\qquad\qquad - \hat{j}_\mu \, G^+ \, \hat{j}_\nu \left(G^+ - G^- \right) \rangle \\
&\quad + \frac{\hbar}{4\pi V} \int\limits_{-\infty}^{\infty} d\varepsilon \, f(\varepsilon) \, \mathrm{Tr} \, \Bigg\langle \, \hat{j}_\mu \, \frac{dG^-}{d\varepsilon} \, j_\nu \, G^- - \hat{j}_\mu \, G^- \, j_\nu \, \frac{dG^-}{d\varepsilon} \\
&\qquad\qquad\qquad\qquad + \hat{j}_\mu \, G^+ \, j_\nu \, \frac{dG^+}{d\varepsilon} - \hat{j}_\mu \, \frac{dG^+}{d\varepsilon} \, j_\nu \, G^+ \, \Bigg\rangle \\
&= \sigma_{\mu\nu}^I + \sigma_{\mu\nu}^{II}.
\end{aligned} \tag{5.27}
$$

Considering the term $\sigma_{\mu\nu}^{II}$ and taking into account the part containing G^- only, namely:

$$
\sigma_{\mu\nu}^{II(-)} = \frac{\hbar}{4\pi V} \int\limits_{-\infty}^{\infty} d\varepsilon \, f(\varepsilon) \, \mathrm{Tr} \, \Bigg\langle \, \hat{j}_\mu \, \frac{dG^-}{d\varepsilon} \, j_\nu \, G^- - \hat{j}_\mu \, G^- \, j_\nu \, \frac{dG^-}{d\varepsilon} \, \Bigg\rangle. \tag{5.28}
$$

For brevity the minus superscript is dropped at G^-. Using the identity $v_\mu = \frac{1}{i\hbar} \left[G^{-1}, r_\mu \right]$ and keeping in mind that $j_\mu = -|e| \, v_\mu$, Eq. (5.28) acquires the following form:

$$
\sigma_{\mu\nu}^{II(-)} = -\frac{e}{4\pi i V} \int\limits_{-\infty}^{\infty} d\varepsilon \, f(\varepsilon) \, \mathrm{Tr} \, \Bigg\langle \, \left[G^{-1}, r_\mu \right] \frac{dG}{d\varepsilon} \, j_\nu \, G - \hat{j}_\mu \, G \left[G^{-1}, r_\nu \right] \frac{dG}{d\varepsilon} \, \Bigg\rangle. \tag{5.29}
$$

Application of the identity $\frac{dG(\varepsilon)}{d\varepsilon} = -G^2(\varepsilon)$ allows to rewrite Eq. (5.29) in the following

way:

$$
\sigma_{\mu\nu}^{II(-)} = \frac{e}{4\pi i V} \int_{-\infty}^{\infty} d\varepsilon\, f(\varepsilon)\, \mathrm{Tr} \left\langle\, [\,G^{-1}, r_\mu\,]\, G^2\, j_\nu\, G \;-\; \hat{j}_\mu\, G\, [\,G^{-1}, r_\nu\,]\, G^2\, \right\rangle
$$

$$
= \frac{e}{4\pi i V} \int_{-\infty}^{\infty} d\varepsilon\, f(\varepsilon)\, \mathrm{Tr} \left\langle\, G^{-1}\, r_\mu\, G^2\, j_\nu\, G \;-\; r_\mu\, G\, j_\nu\, G \right.
$$

$$
\left. -\; j_\mu\, r_\nu\, G^2 \;+\; j_\mu\, G\, r_\nu\, G\, \right\rangle
$$

$$
= \frac{e}{4\pi i V} \int_{-\infty}^{\infty} d\varepsilon\, f(\varepsilon)\, \mathrm{Tr} \left\langle\, r_\mu\, G^2\, j_\nu \;-\; r_\mu\, G\, j_\nu\, G \;-\; j_\mu\, r_\nu\, G^2 \;+\; j_\mu\, G\, r_\nu\, G\, \right\rangle
$$

$$
= \frac{e}{4\pi i V} \int_{-\infty}^{\infty} d\varepsilon\, f(\varepsilon)\, \mathrm{Tr} \left\langle\, r_\mu\, G^2\, j_\nu \;-\; r_\nu\, G^2\, j_\mu \;+\; j_\mu\, G\, r_\nu\, G \;-\; r_\mu\, G\, j_\nu\, G \right\rangle
$$

$$
= \frac{e}{4\pi i V} \int_{-\infty}^{\infty} d\varepsilon\, f(\varepsilon)\, \mathrm{Tr} \left\langle\, r_\mu\, G^2\, j_\nu \;-\; r_\nu\, G^2\, j_\mu \right.
$$

$$
\left. -\; \frac{e}{i\hbar} \left\{ [\,G^{-1}, r_\mu\,]\, G\, r_\nu\, G \;-\; r_\mu\, G\, [\,G^{-1}, r_\nu\,]\, G \right\} \right\rangle
$$

$$
= \frac{e}{4\pi i V} \int_{-\infty}^{\infty} d\varepsilon\, f(\varepsilon)\, \mathrm{Tr} \left\langle\, r_\mu\, G^2\, j_\nu \;-\; r_\nu\, G^2\, j_\mu\, \right\rangle. \tag{5.30}
$$

Introducing the superscript "-" at G again, using $\frac{dG(\varepsilon)}{d\varepsilon} = -G^2(\varepsilon)$, and performing partial integration, Eq. (5.30) takes the following form:

$$
\sigma_{\mu\nu}^{II(-)} = -\frac{e}{4\pi i V} \int_{-\infty}^{\infty} d\varepsilon\, f(\varepsilon)\, \mathrm{Tr} \left\langle\, r_\mu\, \frac{dG^-(\varepsilon)}{d\varepsilon}\, j_\nu \;-\; r_\nu\, \frac{dG^-(\varepsilon)}{d\varepsilon}\, j_\mu\, \right\rangle
$$

$$
= \frac{e}{4\pi i V} \int_{-\infty}^{\infty} d\varepsilon\, \frac{f(\varepsilon)}{d\varepsilon}\, \mathrm{Tr} \left\langle\, r_\mu\, G^-\, j_\nu \;-\; r_\nu\, G^-\, j_\mu\, \right\rangle
$$

$$
= \frac{e}{4\pi i V} \int_{-\infty}^{\infty} d\varepsilon\, \frac{f(\varepsilon)}{d\varepsilon}\, \mathrm{Tr} \left\langle\, G^-\, (r_\mu\, j_\nu \;-\; r_\nu\, j_\mu)\, \right\rangle. \tag{5.31}
$$

Following the same algorithm one obtains the same structure for the term which involves G^+. Combination of these two expressions gives the following:

$$
\sigma_{\mu\nu}^{II} = \frac{e}{4\pi i V} \int_{-\infty}^{\infty} d\varepsilon\, \frac{f(\varepsilon)}{d\varepsilon}\, \mathrm{Tr} \left\langle\, (G^+ - G^-)(r_\mu\, j_\nu \;-\; r_\nu\, j_\mu)\, \right\rangle. \tag{5.32}
$$

And eventually the final expression takes the form:

$$
\sigma_{\mu\nu} = -\frac{\hbar}{4\pi V} \int\limits_{-\infty}^{\infty} d\varepsilon \, \frac{df(\varepsilon)}{d\varepsilon} \, \mathrm{Tr} \left\langle \hat{j}_\mu \left(G^+ - G^-\right) \hat{j}_\nu \, G^- - \hat{j}_\mu \, G^+ \, \hat{j}_\nu \left(G^+ - G^-\right) \right\rangle
$$

$$
+ \frac{e}{4\pi i V} \int\limits_{-\infty}^{\infty} d\varepsilon \, \frac{f(\varepsilon)}{d\varepsilon} \, \mathrm{Tr} \left\langle \left(G^+ - G^-\right)(r_\mu \, j_\nu - r_\nu \, j_\mu) \right\rangle. \tag{5.33}
$$

Considering the athermal limit, i.e. $T = 0$ K and taking into account that $\frac{f(\varepsilon)}{d\varepsilon} = -\delta(\varepsilon - \varepsilon_F)$, Eq. (5.33) can be transformed into the expression obtained by Středa [57], namely:

$$
\sigma_{\mu\nu} = \frac{\hbar}{4\pi V} \, \mathrm{Tr} \left\langle \hat{j}_\mu \left(G^+ - G^-\right) \hat{j}_\nu \, G^- - \hat{j}_\mu \, G^+ \, \hat{j}_\nu \left(G^+ - G^-\right) \right\rangle
$$

$$
+ \frac{|e|}{4\pi i V} \, \mathrm{Tr} \left\langle \left(G^+ - G^-\right)(r_\mu \, j_\nu - r_\nu \, j_\mu) \right\rangle. \tag{5.34}
$$

This formula is known as Kubo-Středa equation. The corresponding retarded and advanced Green functions are evaluated at the Fermi energy and providing the so-called Fermi surface contribution. The technical details of the implementation of the Eq. (5.34) within the SPR-KKR code can be found in the work by Lowitzer [53].

5.2. Kubo-Bastin formalism

The calculations of linear response functions considered in the present work were performed on the basis of the Kubo-Středa equation 5.34. It was demonstrated that this formalism provides a coherent description of the AHE [58] and SHE [59] for pure metals, diluted, as well as concentrated alloys, and, in general, leads to good agreement with available experimental data and other theoretical results. However, the mentioned calculations of the conductivity tensor are often performed with a modified version of Eq. (5.34). Namely, the second term (so-called current-orbital term) is neglected due to the small contribution compared to the dominating first term [53].

In general, omitting of the orbital-current term is justified by symmetry reasons (particularly in case of systems with inversion symmetry), as in case of cubic systems this term becomes site diagonal [58, 60, 61]. In addition, following the work by Bastin [56] it was pointed out that the orbital-current term is equivalent to the Fermi sea contribution and therefore can be neglected in metallic systems [60, 61]. The neglect of the current-orbital term definitely simplifies the numerical implementation, however at the same time it imposes a number of restrictions in the range of applications. Recently, first principle calculations based on the Bastin formula implemented within the TB-LMTO (tight-binding linear muffin-tin-orbital) approach have shown, that the Fermi sea term indeed might provide a non-negligible contribution to the anomalous Hall conductivity in the case of uniaxial systems (hexagonal cobalt) and multisublattice

multicomponent systems (Heusler alloys) [62]. Therefore, to consider additionally systems for which the Fermi sea contribution turns out to be noteworthy, such as systems with non-cubic symmetry, semiconductors, isolators (the chemical potential is placed in the energy gap) the formalism on the basis of the Bastin formula [56] was implemented within the fully relativistic spin polarized KKR-GF method [63]. In the following the corresponding Kubo-Bastin expression is derived.

The starting point is an expression for the conductivity tensor derived by Bastin *et.al* [56] on the basis of the Kubo equation [52] obtained as Eq. (5.22), however extended to the case of evaluation of the spin Hall conductivity by introducing a relativistic spin-polarization current-density operator $\hat{J}^\xi$:

$$\sigma_{\mu\nu}^\xi = \frac{i\hbar}{V} \int\limits_{-\infty}^{\infty} d\varepsilon \, f(\varepsilon) \, \mathrm{Tr} \left\langle \hat{J}_\mu^\xi \frac{dG^+(\varepsilon)}{d\varepsilon} \hat{j}_\nu \, \delta(\varepsilon - \hat{H}) - \hat{J}_\mu^\xi \, \delta(\varepsilon - \hat{H}) \, \hat{j}_\nu \frac{dG^-(\varepsilon)}{d\varepsilon} \right\rangle \quad (5.35)$$

with $\mu, \nu \in \{x, y, z\}$ being Cartesian coordinates. The $\xi \in \{x, y, z\}$ denotes the polarization direction of the spin current operator (see appendix A). The calculations performed here are restricted to the case of $\xi = z$. Following the steps performed in the previous section, we arrive at Eq. (5.27) (extended to account for spin Hall conductivity):

$$\sigma_{\mu\nu}^\xi = -\frac{\hbar}{4\pi V} \int\limits_{-\infty}^{\infty} d\varepsilon \frac{df(\varepsilon)}{d\varepsilon} \mathrm{Tr} \left\langle \hat{J}_\mu^\xi \left(G^+ - G^-\right) \hat{j}_\nu \, G^- - \hat{J}_\mu^\xi \, G^+ \, \hat{j}_\nu \left(G^+ - G^-\right) \right\rangle$$

$$+ \frac{\hbar}{4\pi V} \int\limits_{-\infty}^{\infty} d\varepsilon \, f(\varepsilon) \, \mathrm{Tr} \left\langle \hat{J}_\mu^\xi \frac{dG^-}{d\varepsilon} j_\nu \, G^- - \hat{J}_\mu^\xi \, G^- j_\nu \frac{dG^-}{d\varepsilon} \right.$$

$$\left. + \hat{J}_\mu^\xi \, G^+ j_\nu \frac{dG^+}{d\varepsilon} - \hat{J}_\mu^\xi \frac{dG^+}{d\varepsilon} j_\nu \, G^+ \right\rangle. \quad (5.36)$$

The conductivity tensor (Eq. (5.36)) in the limit of $T \to 0$ K, takes the following form:

$$\sigma_{\mu\nu}^\xi = \frac{\hbar}{4\pi V} \mathrm{Tr} \left\langle \hat{J}_\mu^\xi \left(G^+ - G^-\right) \hat{j}_\nu G^- - \hat{J}_\mu^\xi \, G^+ \, \hat{j}_\nu \left(G^+ - G^-\right) \right\rangle$$

$$+ \frac{\hbar}{4\pi V} \int\limits_{-\infty}^{\varepsilon_F} d\varepsilon \, \mathrm{Tr} \left\langle \hat{J}_\mu^\xi \frac{dG^-}{d\varepsilon} j_\nu \, G^- - \hat{J}_\mu^\xi \, G^- j_\nu \frac{dG^-}{d\varepsilon} \right.$$

$$\left. + \hat{J}_\mu^\xi \, G^+ j_\nu \frac{dG^+}{d\varepsilon} - \hat{J}_\mu^\xi \frac{dG^+}{d\varepsilon} j_\nu \, G^+ \right\rangle$$

$$= \sigma_{\mu\nu}^{I\xi} + \sigma_{\mu\nu}^{II\xi}. \quad (5.37)$$

This expression is the central result of the derivation. The first term is evaluated at the Fermi energy ε_F and contains contributions exclusively from the states at the Fermi level and is referred to as Fermi-surface term. The second term is given as an

integration over all occupied states and is called Fermi-sea term. The details of the numerical implementation of the Fermi sea term are discussed in the appendix B.

Furthermore, Eq. (5.37) can be analyzed in terms of symmetry. Let's consider the more general form of the response tensor χ in Eq. (5.37), namely using arbitrary operators $\hat{A}$ and $\hat{B}$, which can denote charge current density operator $\hat{j}$, spin current density operator $\hat{J}$, magnetic torque operator $\hat{T}$ (which is needed for a description of the Gilbert damping [45, 64] or allows to formulate the so-called spin-orbit torque [65]) etc.

$$
\begin{aligned}
\chi_{\mu\nu} = {} & \frac{\hbar}{4\pi V} \operatorname{Tr} \left\langle \hat{A}_\mu \left(G^+ - G^-\right) \hat{B}_\nu \, G^- - \hat{A}_\mu \, G^+ \, \hat{B}_\nu \left(G^+ - G^-\right) \right\rangle \\
& + \frac{\hbar}{4\pi V} \int\limits_{-\infty}^{\varepsilon_F} d\varepsilon \operatorname{Tr} \left\langle \hat{A}_\mu \frac{dG^-}{d\varepsilon} B_\nu \, G^- - \hat{A}_\mu \, G^- B_\nu \frac{dG^-}{d\varepsilon} \right. \\
& \qquad\qquad\qquad\qquad \left. + \hat{A}_\mu \, G^+ B_\nu \frac{dG^+}{d\varepsilon} - \hat{A}_\mu \frac{dG^+}{d\varepsilon} B_\nu \, G^+ \right\rangle \\
= {} & \chi_{\mu\nu}^{I} + \chi_{\mu\nu}^{II} .
\end{aligned}
\tag{5.38}
$$

At the beginning we focus on the symmetry analysis of the Fermi surface term $\chi_{\mu\nu}^{I}$. For this purpose it is enough to consider the symmetry of the subexpression of $\chi_{\mu\nu}^{I}$:

$$
C_{\mu\nu} = \operatorname{Tr} \left\langle \hat{A}_\mu \left(\hat{G}^+ - \hat{G}^-\right) \hat{B}_\nu \, \hat{G}^- - \hat{A}_\mu \, \hat{G}^+ \, \hat{B}_\nu \left(\hat{G}^+ - \hat{G}^-\right) \right\rangle .
\tag{5.39}
$$

Symmetric part of Eq. (5.39):

$$
\begin{aligned}
\frac{1}{2} \left[C_{\mu\nu} + C_{\nu\mu} \right] = {} & + \frac{1}{2} \operatorname{Tr} \left\langle \hat{A}_\mu \left(\hat{G}^+ - \hat{G}^-\right) \hat{B}_\nu \, \hat{G}^- - \hat{A}_\mu \, \hat{G}^+ \, \hat{B}_\nu \left(\hat{G}^+ - \hat{G}^-\right) \right\rangle \\
& + \frac{1}{2} \operatorname{Tr} \left\langle \hat{A}_\nu \left(\hat{G}^+ - \hat{G}^-\right) \hat{B}_\mu \, \hat{G}^- - \hat{A}_\nu \, \hat{G}^+ \, \hat{B}_\mu \left(\hat{G}^+ - \hat{G}^-\right) \right\rangle \\
= {} & + \frac{1}{2} \operatorname{Tr} \left\langle \hat{A}_\mu \left(\hat{G}^+ - \hat{G}^-\right) \hat{B}_\nu \, \hat{G}^- - \hat{A}_\mu \, \hat{G}^+ \, \hat{B}_\nu \left(\hat{G}^+ - \hat{G}^-\right) \right\rangle \\
& + \frac{1}{2} \operatorname{Tr} \left\langle \hat{B}_\mu \, \hat{G}^- \hat{A}_\nu \left(\hat{G}^+ - \hat{G}^-\right) - \hat{B}_\mu \left(\hat{G}^+ - \hat{G}^-\right) \hat{A}_\nu \, \hat{G}^+ \right\rangle \\
= {} & + \frac{1}{2} \operatorname{Tr} \left\langle \hat{A}_\mu \left(\hat{G}^+ - \hat{G}^-\right) \hat{B}_\nu \, \hat{G}^- - \hat{B}_\mu \left(\hat{G}^+ - \hat{G}^-\right) \hat{A}_\nu \, \hat{G}^+ \right\rangle \\
& + \frac{1}{2} \operatorname{Tr} \left\langle \hat{B}_\mu \, \hat{G}^- \hat{A}_\nu \left(\hat{G}^+ - \hat{G}^-\right) - \hat{A}_\mu \, \hat{G}^+ \, \hat{B}_\nu \left(\hat{G}^+ - \hat{G}^-\right) \right\rangle .
\end{aligned}
\tag{5.40}
$$

Only in case when $\hat{\mathbf{A}} = \hat{\mathbf{B}}$ and particularly when $\hat{\mathbf{A}} = \hat{\mathbf{B}} = \hat{\mathbf{j}}$ Eq. (5.40) can be reformulated to a Kubo-Greenwood-like expression [66], which gives access to the symmetric part of the response tensor:

$$
\begin{aligned}
\frac{1}{2} \left[C_{\mu\nu} + C_{\nu\mu} \right] = {} & + \frac{1}{2} \operatorname{Tr} \left\langle \hat{j}_\mu \left(\hat{G}^+ - \hat{G}^-\right) \hat{j}_\nu \, \hat{G}^- - \hat{j}_\mu \left(\hat{G}^+ - \hat{G}^-\right) \hat{j}_\nu \, \hat{G}^+ \right\rangle \\
& + \frac{1}{2} \operatorname{Tr} \left\langle \hat{j}_\mu \, \hat{G}^- \hat{j}_\nu \left(\hat{G}^+ - \hat{G}^-\right) - \hat{j}_\mu \, \hat{G}^+ \, \hat{j}_\nu \left(\hat{G}^+ - \hat{G}^-\right) \right\rangle \\
= {} & - \operatorname{Tr} \left\langle \hat{j}_\mu \left(\hat{G}^+ - \hat{G}^-\right) \hat{j}_\nu \left(\hat{G}^+ - \hat{G}^-\right) \right\rangle \\
= {} & 4 \operatorname{Tr} \left\langle \hat{j}_\mu \operatorname{Im} \hat{G}^+ \hat{j}_\nu \operatorname{Im} \hat{G}^+ \right\rangle .
\end{aligned}
\tag{5.41}
$$

In a similar way the antisymmetric part is obtained:

$$
\begin{aligned}
\frac{1}{2}\left[C_{\mu\nu} - C_{\nu\mu}\right] = &+ \frac{1}{2}\operatorname{Tr}\left\langle \hat{A}_\mu\,(\hat{G}^+ - \hat{G}^-)\,\hat{B}_\nu\,\hat{G}^- - \hat{A}_\mu\,\hat{G}^+\,\hat{B}_\nu\,(\hat{G}^+ - \hat{G}^-)\right\rangle \\
&- \frac{1}{2}\operatorname{Tr}\left\langle \hat{A}_\nu\,(\hat{G}^+ - \hat{G}^-)\,\hat{B}_\mu\,\hat{G}^- - \hat{A}_\nu\,\hat{G}^+\,\hat{B}_\mu\,(\hat{G}^+ - \hat{G}^-)\right\rangle \\
= &+ \frac{1}{2}\operatorname{Tr}\left\langle \hat{A}_\mu\,(\hat{G}^+ - \hat{G}^-)\,\hat{B}_\nu\,\hat{G}^- - \hat{A}_\mu\,\hat{G}^+\,\hat{B}_\nu\,(\hat{G}^+ - \hat{G}^-)\right\rangle \\
&- \frac{1}{2}\operatorname{Tr}\left\langle \hat{B}_\mu\,\hat{G}^-\,\hat{A}_\nu\,(\hat{G}^+ - \hat{G}^-) - \hat{B}_\mu\,(\hat{G}^+ - \hat{G}^-)\,\hat{A}_\nu\,\hat{G}^+\right\rangle \\
= &+ \frac{1}{2}\operatorname{Tr}\left\langle \hat{A}_\mu\,(\hat{G}^+ - \hat{G}^-)\,\hat{B}_\nu\,\hat{G}^- + \hat{B}_\mu\,(\hat{G}^+ - \hat{G}^-)\,\hat{A}_\nu\,\hat{G}^+\right\rangle \\
&- \frac{1}{2}\operatorname{Tr}\left\langle \hat{B}_\mu\,\hat{G}^-\,\hat{A}_\nu\,(\hat{G}^+ - \hat{G}^-) + \hat{A}_\mu\,\hat{G}^+\,\hat{B}_\nu\,(\hat{G}^+ - \hat{G}^-)\right\rangle . \quad (5.42)
\end{aligned}
$$

Only in case of $\hat{\mathbf{A}} = \hat{\mathbf{B}}$ including case when $\hat{\mathbf{A}} = \hat{\mathbf{B}} = \mathbf{j}$ Eq. (5.42) can be modified to the following form:

$$
\begin{aligned}
\frac{1}{2}\left[C_{\mu\nu} - C_{\nu\mu}\right] = &+ \frac{1}{2}\operatorname{Tr}\left\langle \hat{j}_\mu\,(\hat{G}^+ - \hat{G}^-)\,\hat{j}_\nu\,\hat{G}^- + \hat{j}_\mu\,(\hat{G}^+ - \hat{G}^-)\,\hat{j}_\nu\,\hat{G}^+\right\rangle \\
&- \frac{1}{2}\operatorname{Tr}\left\langle \hat{j}_\mu\,\hat{G}^-\,\hat{j}_\nu\,(\hat{G}^+ - \hat{G}^-) + \hat{j}_\mu\,\hat{G}^+\,\hat{j}_\nu\,(\hat{G}^+ - \hat{G}^-)\right\rangle \\
= &+ \frac{1}{2}\operatorname{Tr}\left\langle \hat{j}_\mu\,(\hat{G}^+ - \hat{G}^-)\,\hat{j}_\nu\,(\hat{G}^+ + \hat{G}^-)\right\rangle \\
&- \frac{1}{2}\operatorname{Tr}\left\langle \hat{j}_\mu\,(\hat{G}^+ + \hat{G}^-)\,\hat{j}_\nu\,(\hat{G}^+ - \hat{G}^-)\right\rangle \\
= &+ \frac{1}{2}\operatorname{Tr}\left\langle \left[\hat{j}_\mu\,(\hat{G}^+ - \hat{G}^-)\,\hat{j}_\nu - \hat{j}_\nu\,(\hat{G}^+ - \hat{G}^-)\,\hat{j}_\mu\right](\hat{G}^+ + \hat{G}^-)\right\rangle .
\end{aligned}
$$
$$(5.43)$$

The obtained results show that in case of ideentical operators $\hat{\mathbf{A}} = \hat{\mathbf{B}}$, particularly when the same current density operators are present (the case of anomalous Hall effect), the Fermi surface term provides contributions to the symmetric as well as antisymmetric part of the response tensor. And the Fermi sea term in this case ($\hat{\mathbf{A}} = \hat{\mathbf{B}} = \hat{\mathbf{j}}$) gives access exclusively to the antisymmetric part of the tensor. This can be easily seen from Eq. (5.38), where $\chi_{\mu\nu}^{II} = -\chi_{\nu\mu}^{II}$. In case, when different operators have to be used ($\hat{\mathbf{A}} \neq \hat{\mathbf{B}}$) the simple decomposition into symmetric and antisymmetric part is not possible.

6. Hall effect

The emergence of a transverse voltage (Hall voltage) when a current-carrying conductor is exposed to the external magnetic field is known as the Hall effect. It was discovered by Edwin Hall in 1879 in thin golden films [67] and is referred to in the literature as ordinary Hall effect. In nonmagnetic metals, the effect is caused by electrons drifting in the crossed electrical and magnetic fields. Due to the Lorenz force, the electron trajectory distorts in the direction perpendicular to the current and magnetic field, leading to the charge accumulation at the sample edges, triggering the Hall voltage. Later, it was found that in the ferromagnetic materials the effect is much stronger, however it has a completely different origin and is referred to as the anomalous Hall effect (AHE) [68]. In contrast to the ordinary Hall effect, in the AHE the electron scattering asymmetry occurs due to spin-orbit coupling. Over many years, a considerable amount of theoretical - as well as experimental - studies were required to confirm Hall's inferences. In particular, it was shown that the Hall resistivity ρ_{xy} is proportional to the magnetization M of the sample [69]. This empirical observation has led to the formula describing ρ_{xy} as:

$$\rho_{xy} = R_0 B_z + 4\pi R_s M_z,\tag{6.1}$$

where M_z is the magnetization along the z-axis and B_z is the z component of the magnetic field. In the latter equation the first term describes the ordinary Hall effect, due to the Lorenz force, whereas the second term is responsible for the AHE associated with spin-orbit coupling. In Eq. (6.1) R_0 is the ordinary Hall coefficient, which depends mainly on the density of the carriers while R_s is the anomalous (extraordinary or spontaneous) Hall coefficient, which depends on various material-specific parameters. Using the connection of the resistivity and conductivity tensors for a simple cubic system one obtains:

$$\rho = \sigma^{-1} = \begin{pmatrix} \sigma_{xx} & \sigma_{xy} & 0 \\ -\sigma_{xy} & \sigma_{yy} & 0 \\ 0 & 0 & \sigma_{zz} \end{pmatrix}^{-1}\tag{6.2}$$

$$\approx \begin{pmatrix} \frac{\sigma_{xx}}{\sigma_{xx}^2 + \sigma_{xy}^2} & -\frac{\sigma_{xy}}{\sigma_{xx}^2 + \sigma_{xy}^2} & 0 \\ \frac{\sigma_{xy}}{\sigma_{xx}^2 + \sigma_{xy}^2} & \frac{\sigma_{xx}}{\sigma_{xx}^2 + \sigma_{xy}^2} & 0 \\ 0 & 0 & \frac{1}{\sigma_{zz}} \end{pmatrix},\tag{6.3}$$

together with Eq.(6.1), the corresponding expressions for R_0 and R_s can be derived, taking into account that usually $\sigma_{xy} \ll \sigma_{xx}$:

$$R_0 = \frac{\sigma_{xy}(B_z)}{B_z \left(\sigma_{xx}^2 + \sigma_{xy}^2\right)} \approx \frac{\sigma_{xy}(B_z)}{B_z} \rho_{xx}^2,\tag{6.4}$$

$$R_s \; = \; \frac{\sigma_{xy}(M_z)}{4\pi \, M_z \, (\sigma_{xx}^2 \, + \, \sigma_{xy}^2)} \; \approx \; \frac{\sigma_{xy}(M_z)}{4\pi \, M_z} \, \rho_{xx}^2 \; . \tag{6.5}$$

Although such an empirical treatment, suggested by equation (6.1), was widely used to describe the Hall effect in magnetic systems, it did not provide more insight into its physical nature. Moreover, later with discovery of a non-zero AHE in various magnetically-compensated systems (antiferromagnets and ferrimagnets) it became clear that this empirical form is not generally applicable.

6.1. Anomalous Hall effect

As was already mentioned, the AHE is a key phenomenon among the magnetotransport effects, based on spin-orbit coupling. After being discovered more than hundred years ago, it still remains a subject of intensive debate in the sense of separation of the different contributing mechanisms and determine which one dominates under certain conditions. The disentanglement of these mechanisms experimentally and manipulating them separately is quite a challenging task. Thus a detailed theoretical study is quite desirable in order to investigate different contributions individually. Basically here one has to distinguish between the contributions coming from the electron scattering mechanisms and so-called intrinsic contributions.

An early insight into the intrinsic mechanism has been given by Karplus and Luttinger [70]. They have shown that in the ideal periodic crystal with periodic intrinsic SOC (when the electron's orbital motion is coupled to its intrinsic spin), in addition to normal electron velocity the so-called anomalous velocity arises [71, 72]. If the sum of these anomalous velocities from all occupied electronic states is nonzero it leads to the anomalous Hall conductivity (AHC). It was found that this contribution solely depends on the band structure of the system and does not depend neither on scatterers (impurities, phonons, magnons) [70, 73–77].

Later on, this intrinsic contribution was generalized in terms of an additional phase acquired by the wave function of the quantum object (e.g., the conducting electron) while it propagates through the medium (e.g., crystalline solid). This concept was already known for quite a long time and has been used to interpret various quantum effects (Aaronov-Bohm effect, weak localization, universal oscillations of the conductance, etc.), however systematically it was first introduced by Berry and is referred today as Berry phase. The corresponding medium, in turn, is said to provide the Berry curvature created by the effective potential in which the quantum particle moves. By considering conducting electrons, the phase of the wave function is connected with an electron's spin, which in its simplest form can be described in terms of the Pauli matrices. While propagating, the spin might rotate, which results into a change of the phase of the wave-function. These rotations are described by the part of Hamiltonian, which couples the spin (in a form of a Pauli vector) to the coordinates of the medium. Such coupling can be provided either by exchange or spin-orbit mechanisms. For example,

when magnetization $\mathbf{M}(\mathbf{r}) = M\hat{\mathbf{n}}(\mathbf{r})$ varies as a function of the real space coordinate:

$$H = K - M\left(\hat{\mathbf{n}} \cdot \sigma\right), \tag{6.6}$$

spin couples to the real-space coordinate via exchange mechanism described by the coupling constant M. In case of the spatially uniform medium ($\mathbf{M}$=const) the spin couples to the reciprocal (k-space) coordinate via the spin-orbit parameter α. For example, in the celebrated two-dimensional Rashba model [78, 79] one has:

$$H = K + \alpha\left(\sigma_x k_y - \sigma_y k_x\right) - M\sigma_z, \tag{6.7}$$

where K is the corresponding kinetic term. In both cases the relevant part is described by the scalar product $\hat{\mathbf{n}} \cdot \sigma$, where in the first case the directional unity vector $\hat{\mathbf{n}}$ just points along the magnetization:

$$\hat{\mathbf{n}}(\mathbf{r}) = \frac{1}{M}\begin{pmatrix} M_x(\mathbf{r}) \\ M_y(\mathbf{r}) \\ M_z(\mathbf{r}) \end{pmatrix}, \tag{6.8}$$

and in the second is

$$\hat{\mathbf{n}}(\mathbf{k}) = \frac{1}{\lambda}\begin{pmatrix} \alpha k_y \\ -\alpha k_x \\ -M \end{pmatrix}, \quad \lambda = \left(M^2 + \alpha^2 k_x^2 + \alpha^2 k_y^2\right)^{1/2}, \tag{6.9}$$

so that Eq. (6.7) can be rewritten in a form similar to Eq. (6.6):

$$H = K + \lambda\left(\hat{\mathbf{n}} \cdot \sigma\right). \tag{6.10}$$

Thus, the way in which the electron accumulates the phase depends solely on the geometrical properties of the vector field $\hat{\mathbf{n}}$. In order to see this, we have to go from the global coordinate system into the frame of the spin (so, that the new z-axis corresponds to the spin-quantization axis). In this new reference both Eqs. 6.6 and 6.10 get:

$$H' = T^\dagger H T = T^\dagger K T + \gamma\sigma_z, \tag{6.11}$$

where T is the corresponding rotational matrix: $T^\dagger\left(\hat{\mathbf{n}} \cdot \sigma\right)T = \sigma_z$ and γ is a scalar. Thus, the central quantity is the kinetic term $T^\dagger K T$ modified by the so-called gauge transformation. It is easy to show, that such a gauge transform can be represented in terms of the additional vector-potential $\mathbf{A}$. Indeed, for $K \sim \mathbf{p}^2$: $T^\dagger \mathbf{p}^2 T = \left(\mathbf{p} + \mathbf{A}\right)^2$, where $\mathbf{p}$ is the momentum operator and $\mathbf{A} = T^\dagger \mathbf{p} T$. Since we are working in the space of the Pauli spinors $\varphi = \begin{pmatrix} \varphi^+ \\ \varphi^- \end{pmatrix}$, the gauge transform should be written as

$$T^\dagger K T \sim T^\dagger \begin{pmatrix} \mathbf{p} & 0 \\ 0 & \mathbf{p} \end{pmatrix}^2 T \approx \begin{pmatrix} \mathbf{p} + \mathbf{A}^+ & 0 \\ 0 & \mathbf{p} + \mathbf{A}^- \end{pmatrix}^2. \tag{6.12}$$

The vector-potential transforms into a diagonalized matrix if we assume that vector $\hat{\mathbf{n}}$ varies slowly and the magnetization M (or the exchange-splitting γ-parameter) is large enough in order to prevent spin-flip transitions. This is the so-called adiabatic

condition which is crucial for applying the concept of a Berry phase. Now all the information about the spin rotations described by the unitary operator T, is fully contained in the vector-potential $\mathbf{A}$. By computing its explicit form, one finds that the Pauli components $\mathbf{A}^+$ and $\mathbf{A}^-$ which are related to majority- and minority-spin are of the same form but have an opposite sign: $\mathbf{A}^+ = -\mathbf{A}^-$. In other words, the electrons of opposite spin experience an opposite force. This force can be related to the magnetic field via $\mathbf{B} = \nabla \times \mathbf{A}$, which, however, does not couple to the electron charge. We would obtain the same result also for charge-less spin-$1/2$ particles, as e.g., neutrons. For this reason, the Hall effect produced by the Berry phase mechanism represents nothing else but the spin-Hall effect (this will be discussed in more details in the next chapter). The charge Hall current arises only due to the disbalance of the spin-projected occupations of conducting electrons, given by the Fermi-Dirac functions $f(\epsilon^\pm)$ for the corresponding eigenvalues ϵ^+ and ϵ^-:

$$\mathbf{A} = f(\epsilon^+)\,\mathbf{A}^+ + f(\epsilon^-)\,\mathbf{A}^- = \left(f(\epsilon^+) - f(\epsilon^-)\right)\mathbf{A}^+ . \tag{6.13}$$

The corresponding magnetic flux through the two-dimensional medium (say, in the xy-plane) is defined via the corresponding perpendicular component of the induced magnetic field B_z:

$$\Phi = \int B_z\, dS = \int (\nabla \times \mathbf{A})_z\, dS = \int (\partial_x A_y - \partial_y A_x)\, dS \tag{6.14}$$

$$= \int \left(f(\epsilon^+) - f(\epsilon^-)\right)\left(\partial_x A_y^+ - \partial_y A_x^+\right) dS ,$$

where all quantities are coordinate functions of the corresponding medium. E.g., dS is a real element of the medium ($dS = dxdy$ in the direct and $dS = dk_x dk_y$ in the reciprocal space) and $\partial_{x(y)}$ are the gradients with respect to $x(y)$ coordinates in the direct, and for $k_{x(y)}$ in the reciprocal space. Accordingly, the eigenvalues $\epsilon^\pm$ are also functions of the corresponding spatial coordinates. The relevant part of the Hall conductivity is then defined simply as $\sigma_{xy} = (e^2/\hbar)(\Phi/\Phi_0)$, where $\Phi_0 = \hbar c/e$ is the quantum of the magnetic flux. As it was shown by Bruno and coworkers [80, 81],

$$B_z = \partial_x A_y^+ - \partial_y A_x^+ \sim \hat{\mathbf{n}} \cdot (\partial_x \hat{\mathbf{n}} \times \partial_y \hat{\mathbf{n}}) . \tag{6.15}$$

Assuming a half-metallic situation at zero temperature, i.e., $f(\epsilon^+) = 1$ and $f(\epsilon^-) = 0$, the Hall conductivity can be written as a surface integral

$$\sigma_{xy} = \frac{e^2}{2\hbar} \int B_z\, dxdy = \frac{e^2}{2\hbar} \int \hat{\mathbf{n}} \cdot (\partial_x \hat{\mathbf{n}} \times \partial_y \hat{\mathbf{n}})\, dx\, dy . \tag{6.16}$$

Since $(\partial_x \hat{\mathbf{n}} \times \partial_y \hat{\mathbf{n}})\, dxdy = d\mathbf{\Omega}$ formally represents an oriented element of the spherical surface with a unity radius, given by $\hat{\mathbf{n}} = \hat{\mathbf{n}}(x, y)$, the whole expression in the integral in Eq. (6.16) is equal to the elementary spherical angle $d\Omega = \hat{\mathbf{n}} \cdot d\mathbf{\Omega}$ along $\hat{\mathbf{n}}$. Thus, the integral in Eq. (6.16) reduces simply to a multiple of times t by which the vector $\hat{\mathbf{n}}$ wraps over the sphere while running over the xy-space, i.e. to a purely geometrical characteristic (see, e.g. Ref. [82]):

$$\sigma_{xy} = \frac{e^2}{2\hbar} \cdot 4\pi t . \tag{6.17}$$

This description is applicable only if $\hat{\mathbf{n}}$ varies smoothly, so that its derivatives $\partial_{x(y)}\hat{\mathbf{n}}$ does exist. Considering these simple models one can also easily figure out the quantization conditions of σ_{xy} (i.e., when $t = 0, \pm 1, \pm 2, ..$), by searching for the corresponding distribution of the magnetization field in case of Eq. (6.6), or by fitting the spin-orbit coupling strength α in case of Eq. (6.10). In both cases this will lead to the appearance of the various fascinating vortex textures. In real space an example of such structures are the magnetic skyrmions [83], and in the reciprocal space - the celebrated Weyl points [84, 85]. It is worth to stress, that in Eq. (6.6) the spin-orbit coupling as an active mechanism of the topological AHE was completely neglected. However, it is known to play a crucial role in the formation of the skyrmion structures by causing the Dzyaloshinskii-Moriya interaction [86, 87], which leads to the magnetization canting. Also one can easily show that this nontrivial magnetization distribution might lead to a vanishing total magnetization in the material but still show a non-zero AHE. In the second case, which assumes a constant magnetization, the spin-orbit appears to be the only ingredient necessary for the spin rotations. In this case, the magnetization might also vanish in total, but it is important that the system maintains the local magnetic moments to provide the local exchange splitting, otherwise the charge AHE is fully converted to the spin-Hall effect.

In case of a real solid, the Berry-phase AHE is accounted for within the general Kubo-Bastin formalism (see Chapter 2, Section 5.2), where it corresponds to the $\sigma_{xy}^{\mathrm{II}}$ contribution (so-called Fermi-sea part) obtained via integrating over all occupied states. In addition, if the system has broken translational symmetry due to defects or chemical disorder, usually there is another significant part of the total AHE coming from the scattering effects. These effects concern only the electrons which are strictly conducting, i.e. situated precisely at the Fermi energy, since the possibility of scattering assumes the ability of the electron to be excited, at least infinitesimally. For this reason, in the Kubo-Bastin formalism this contribution is associated with σ_{xy}^{I} (Fermi-surface contribution). Due to the necessary presence of scatterers in the last case and their absence in the former case, these two sources are often referred as extrinsic and intrinsic (due to the properties of the "host" bandstructure) contributions, respectively. The phenomenological description of scattering mechanisms is substantially more complicated than for the Berry-phase contributions (see, e.g. [81]). For this reason, in the following we will consider only their basic empirical features.

One of the relevant scattering mechanisms, known as a skew-scattering, was considered by Smit [73, 74]: an asymmetric scattering, which leads to the change of direction of the electron's trajectory as the electron acquires a temporary orbital component in its otherwise linear motion and is captured into a virtual bound state of the impurity [88]. This is shown schematically in Fig. (6.1) (left panel). The electron is scattered by the attractive scattering center and its linear trajectory is perturbed to introduce a curved segment into its motion [88]. Due to the spin-orbit coupling the probability for the itinerant electron with spin up/down to scatter to the left or to the right of the scattering center becomes different. This, in turn, leads to the asymmetry in the number of the electrons with spin up/down accumulated at the edges of the sample. In the dilute limit (low impurity concentration, $c \ll 1$) at $T = 0$ K the following relation
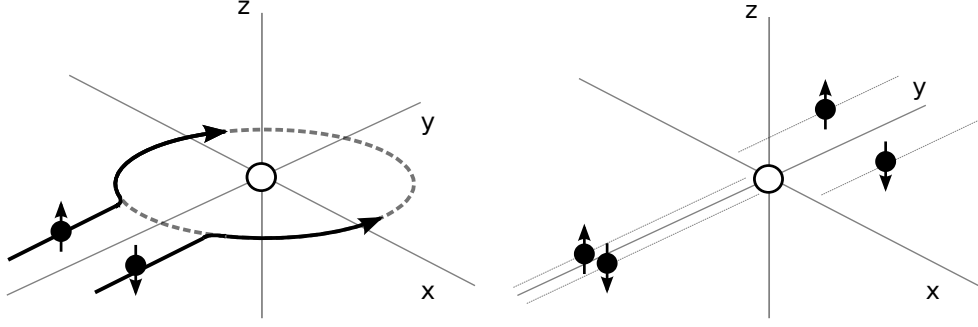
Figure 6.1.: Schematic representation of skew-scattering (left panel) and side-jump scattering (right panel) mechanisms giving rise to the AHE.

is valid for the anomalous Hall coefficient:

$$R_s^{\text{skew}} = a\rho_0 + b\rho_0^2 \tag{6.18}$$

with ρ_0 being a residual resistivity of an alloy, a and b are constants. In the Eq. (6.18) the first term is usually larger compared to the second term, but with increasing impurity concentration in the case of strong scattering, both terms are of the same order of magnitude [89]. However, it was shown that in the concentrated regime this scaling relation is not applicable [90, 91]. Another mechanism is the so-called side-jump, which results in a delay of electron's motion introduced by a scattering process. It was first described by Berger [92, 93]. This mechanism can be interpreted as a side way displacement of the center of mass of an electron's wave packet, depicted in Fig. (6.1) (right panel). The electron's wave packet is distorted as the SOC influences the electron's motion. This contribution does not depend neither on magnitude of the scattering potential nor on its type (impurities, phonons, magnons) and the corresponding anomalous Hall coefficient can be written as:

$$R_s^{\text{sj}} = B\,\rho_{xx}^2\,, \tag{6.19}$$

where B is an empirical coefficient. Based on the work of Smit [74], it was shown that this coefficient has comparable magnitude but opposite sign when compared to the corresponding coefficient related to the intrinsic contribution, but a complete cancellation of both terms does not occur [75]. In other words, the final AHE occurs due to the asymmetric canceling of two large intrinsic (topological) and extrinsic (scattering) contributions.

In contrast to the intrinsic contribution, the last two mechanisms emerge only in the presence of scattering sources, such as impurities (phonons, magnons, etc.) and therefore they have been combined to the so-called - extrinsic (or sometimes also called incoherent) contribution.

There is a large number of theoretical works dedicated to the calculation of the extrinsic contributions to AHE within the different approaches, particularly based on the quantum mechanical Kubo-Středa formula [55, 58, 71, 77] and on the Boltzmann formalism [70, 73, 74, 92–94].

In the present work the calculations of the transport properties are based on the Kubo-Středa equation as well as Kubo-Bastin formula. Such an approach allows not only to study different properties in the dilute limit but in addition to consider a wide concentration range, while the Boltzmann approach is exclusively restricted to the dilute limit.

On the basis of the analysis within the semiclassical picture of the different mechanisms contributing to the AHE in the dilute limit, it was found that the dominant scattering mechanism is the skew-scattering, since its contribution is inversely proportional to the impurity concentration, while the side-jump is completely independent of the impurity amount [71, 95], similar to the intrinsic contribution:

$$\sigma_{xy}^{\mathrm{intr}} \propto c^0 \,, \qquad \sigma_{xy}^{\mathrm{skew}} \propto c^{-1} \,, \qquad \sigma_{xy}^{\mathrm{sj}} \propto c^0 \,. \tag{6.20}$$

Since the measured quantity is the resistivity rather than the conductivity, one expresses Eq. (6.20) as:

$$\rho_{xy}^{\mathrm{intr}} \propto c^2 \,, \qquad \rho_{xy}^{\mathrm{skew}} \propto c \,, \qquad \rho_{xy}^{\mathrm{sj}} \propto c^2 \,. \tag{6.21}$$

Specifically for the dilute regime at $T = 0$ K the separation of different contributions was suggested [95], whereas with increasing the impurity concentration the interplay between different mechanisms increases, making them rather indistinguishable. Thus, the total AHC can be decomposed into three main contributions [95]:

$$\sigma_{xy} = \sigma_{xy}^{\mathrm{skew}} + \sigma_{xy}^{\mathrm{sj}} + \sigma_{xy}^{\mathrm{intr}} \,. \tag{6.22}$$

Since, in the dilute limit the dominant scattering mechanism is skew scattering then according to the scaling relation, suggested in [95] it can be expressed as $\sigma_{xy}^{\mathrm{skew}} = \sigma_{xx} S$, where S is the skewness factor. Taking into account that intrinsic and side-jump contributions are completely independent on the impurity concentration, Eq. (6.22) can be written as follows:

$$\sigma_{xy} = \sigma_{xx} S + \underbrace{\sigma_{xy}^{\mathrm{sj}} + \sigma_{xy}^{\mathrm{intr}}}_{=\mathrm{const}} \,. \tag{6.23}$$

This scheme allows to decompose the total AHC into intrinsic and extrinsic contributions, however it relies on the assumption that the side-jump term is indeed small.

The situation with separation of different contributions becomes even more complicated if finite temperatures get involved due to the emergence of additional sources of scattering, such as scattering by phonons and magnons. The scaling relations introduced for skew-scattering (Eq. (6.18)) and side-jump (Eq. (6.19)) mechanisms are invalid at finite temperatures as the interference between these mechanisms increases with increasing temperature [89]. Nevertheless, there are experimental [96–100] as well as theoretical studies [101–104] aiming to separate different contributions within certain temperature intervals as well as to study the impact of different scattering mechanisms such as phonons [105, 106] and magnons on AHE in general. Whereas most of the theoretical studies consider mainly only one of the mechanisms, in the present work we aimed to study the combined effect using an *ab initio* approach in which we also include the thermal influence.

6.2. Spin Hall effect

Along with anomalous Hall effect lots of experimental and theoretical attention is devoted to the spin Hall effect (SHE). The SHE occurs in nonmagnetic materials when the electrical current flows through the sample with spin-orbit coupling and results in a spin polarization at opposite edges of the sample. The microscopic mechanisms leading to SHE are essentially the same as in case of the AHE. Namely, the electrons with 'spin-up' are scattered in opposite direction with respect to electrons with 'spin-down' due to the presence of the spin-orbit coupling. Based on the fact that both phenomena share the same origin the classification of the contributing mechanisms is identical as in case of the AHE, namely: intrinsic, skew-scattering and side-jump. In contrast to the AHE, the SHE provides an opportunity to generate spin currents avoiding the injection from the ferromagnetic materials making it more attractive in the development of potential spintronic devices. The efficiency of the SHE in various materials is characterized by the so-called spin Hall angle (SHA) α, which describes the conversion of the charge into the spin current. Therefore, materials with large spin Hall angles are indeed highly desirable. In the literature α is defined as the ratio of the transverse conductivity (σ_{xy}^{z}) and the longitudinal conductivity (σ_{xx}) as:

$$\alpha = \frac{\sigma_{xy}^{z}}{\sigma_{xx}} \ . \tag{6.24}$$

Since, the microscopical mechanisms leading to the SHE are the same as those in case of the AHE, the identical decomposition into intrinsic (coherent) and impurity scattering based extrinsic (incoherent) contributions can be made. In turn, the extrinsic contribution splits into skew-scattering and side-jump. This decomposition is done in analogy to the equation valid in case of the AHE:

$$\sigma_{xy}^{z} = \sigma_{xy}^{z(\text{intr})} + \sigma_{xy}^{z(\text{skew})} + \sigma_{xy}^{z(\text{sj})} , \tag{6.25}$$

where $\sigma_{xy}^{z(\text{intr})}$ corresponds to the intrinsic contribution, $\sigma_{xy}^{z(\text{skew})}$ corresponds to skew-scattering and $\sigma_{xy}^{z(\text{sj})}$ gives side-jump contribution. It was shown theoretically [107] that in the superclean regime the dominant scattering mechanism is skew-scattering, which can be expressed as:

$$\sigma_{xy}^{z(\text{skew})} = S \, \sigma_{xx} , \tag{6.26}$$

where S represents the so-called skewness factor.

7. Results

In this chapter the main results of the current work are summarized. The central goal of the present work is to study transverse transport effects, particularly the AHE and SHE and gain broader understanding of the microscopic origin of these phenomena. For that purpose the Kubo-Středa formalism was used which allows to work out a procedure to separate along with commonly accepted contributions (intrinsic, side-jump, skew-sacttering) an additional contribution arising from the side-jump scattering mechanism [108]. This scheme opens a way for further deeper theoretical investigations of the spin Hall effect with a possible elucidation of its dominating mechanisms. Furthermore, the subject of the present work is the development and its subsequent numerical implementation of the general approach which allows to treat many different quantities (AHE, SHE, SOT, Gilbert damping, Edelstein effects, etc.) within an efficient fully relativistic material specific *ab initio* approach [63]. This method is based on the Kubo-Bastin formula for the transport coefficients. The main emphasis is put on the Fermi-sea contribution which appears along with the well-known Fermi-surface contribution and which is important especially in the spin-orbit-induced transverse transport phenomena. The various theoretical and technical aspects of the approach are discussed in detail. The implemented formalism is applicable to pure systems as well as disordered alloys in the full concentration range and treats intrinsic (coherent) and extrinsic (incoherent) contributions within one and the same methodological approach.

Moreover, the investigation of the aforemetioned phenomena is extended to finite temperatures. The alloy-analogy model based on the CPA approach presented in Ref. [47] allowed to study the influence of the combined effect of the thermal lattice vibrations and thermal spin fluctuations as well as their individual effect on the transport properties. The thermally induced lattice vibrations are treated in the present work as randomly distributed uncorrelated atomic displacements. For each site a fixed number of displacement directions are set up with equal statistical weights, and with the amplitude of displacements varying with temperature. Each displacement is treated as a different (pseudo)atomic type that allows to calculate the statistical average within the CPA alloy theory, in full analogy with random alloy systems [47]. The amplitude of displacements for each temperature is taken according to the root-mean-square displacement of the atoms. The later is evaluated in the present work within the Debye model approach. In the case of spin fluctuations the angular distribution of the magnetic moments representing the experimental magnetization was chosen to map the corresponding temperature. From our calculations [47, 109–112] it follows that both scattering channels, connected with the phonon scattering and scattering by spin dis-

order, have similar contributions and in order to obtain reasonable agreement with experimental data, it is necessary to account for a combination of these contributions simultaneously

7.1. Calculating linear-response functions for finite temperatures

The article "Calculating linear-response functions for finite temperatures on the basis of the alloy analogy model" published in The Journal of Physical Review B is reprinted with permission from Phys. Rev. B, 91, 165132 (2015); copyright 2015 American Physical Society.

–

Calculating linear-response functions for finite temperatures on the basis of the alloy analogy model

H. Ebert, S. Mankovsky, K. Chadova, S. Polesya, J. Minár, and D. Ködderitzsch

Department Chemie/Phys. Chemie, Ludwig-Maximilians-Universität München, Butenandtstrasse 5-13, D-81377 München, Germany

A scheme is presented that is based on the alloy analogy model and allows one to account for thermal lattice vibrations as well as spin fluctuations when calculating response quantities in solids. Various models to deal with spin fluctuations are discussed concerning their impact on the resulting temperature-dependent magnetic moment, longitudinal conductivity, and Gilbert damping parameter. It is demonstrated that, by using the Monte Carlo (MC) spin configuration as input, the alloy analogy model is capable of reproducing the results of MC simulations on the average magnetic moment within all spin fluctuation models under discussion. On the other hand, the response quantities are much more sensitive to the spin fluctuation model. Separate calculations accounting for the thermal effect due to either lattice vibrations or spin fluctuations show that they give comparable contributions to the electrical conductivity and Gilbert damping. However, comparison to results accounting for both thermal effects demonstrates violation of Matthiessen's rule, showing the nonadditive effect of lattice vibrations and spin fluctuations. The results obtained for bcc Fe and fcc Ni are compared with the experimental data, showing rather good agreement for the temperature-dependent electrical conductivity and the Gilbert damping parameter.

I. INTRODUCTION

Finite temperature often has a very crucial influence on the response properties of a solid. A prominent example for this is the electrical resistivity of perfect nonmagnetic metals and ordered compounds that take only a nonzero value with a characteristic temperature (T) dependence due to thermal lattice vibrations. While the Holstein transport equation [1,2] provides a sound basis for corresponding calculations, numerical work in this field has been done so far either on a model level or for simplified situations [3–6]. In practice the Boltzmann formalism is often adopted, using the constant-relaxation-time (τ) approximation. This is a very popular approach in particular when dealing with the Seebeck effect, as in this case τ drops out [7,8]. The constant-relaxation-time approximation has also been used extensively when dealing with the Gilbert damping parameter α [9–11]. Within the description of Kambersky [10,12], the conductivity- and resistivitylike intra- and interband contributions to α show a different dependency on τ, leading typically to a minimum for $\alpha(\tau)$ or equivalently for $\alpha(T)$ [10,11,13]. A scheme to deal with the temperature-dependent resistivity that is formally much more satisfying than the constant-relaxation-time approximation is achieved by combining the Boltzmann formalism with a detailed calculation of the phonon properties. As was shown by various authors [14–17], this parameter-free approach leads for nonmagnetic metals in general to a very good agreement with experimental data.

As an alternative to this approach, thermal lattice vibrations have also been accounted for within various studies by quasistatic lattice displacements leading to thermally induced structural disorder in the system. This point of view provides the basis for the use of the alloy analogy, i.e., for the use of techniques to deal with substitutional chemical disorder, also when dealing with temperature-dependent quasistatic random lattice displacements. Examples of this are investigations on the temperature dependence of the resistivity and the Gilbert parameter α based on the scattering matrix approach applied to layered systems [18]. The necessary average over many

configurations of lattice displacements was taken by means of the supercell technique. In contrast to this the configurational average was determined using the coherent potential approximation (CPA) within investigations using a Kubo-Greenwood-like linear expression for α [19]. The same approach to deal with the lattice displacements was also used recently within calculations of angle-resolved photoemission spectra on the basis of the one-step model of photoemission [20].

Another important contribution to the resistivity in the case of magnetically ordered solids is given by thermally induced spin fluctuations [21]. Again, the alloy analogy has been exploited extensively in the past when dealing with the impact of spin fluctuations on various response quantities. The representation of a frozen spin configuration by means of supercell calculations has been applied for calculations of the Gilbert parameter for α [18] as well as for the resistivity or conductivity [18,22,23]. Also, the CPA has been used for calculations of α [24] as well as the resistivity [21,25]. A crucial point in this context is obviously the modeling of the temperature-dependent spin configurations. Concerning this, rather simple models have been used [24], but also quite sophisticated schemes. Here one should mention the transfer of data from Monte Carlo simulations based on exchange parameters calculated in an *ab initio* way [26] as well as work based on the disordered local moment (DLM) method [25,27]. Although the standard DLM does not account for transversal spin components it nevertheless allows representation of the paramagnetic regime with no net magnetization in a rigorous way. Also, for the magnetically ordered regime below the Curie temperature it can be demonstrated that the uncompensated DLM still leads for many situations to good agreement with experimental data on the so-called spin disorder contribution to the resistivity [21,25].

In the following we present technical details and extensions of the so-called alloy analogy scheme which has already been used when dealing with the temperature dependence of response quantities on the basis of Kubo's response formalism [19,24]. Various applications will be presented for the conductivity and Gilbert damping

parameter accounting simultaneously for various types of disorder.

II. THEORETICAL FRAMEWORK

A. Configurational average for linear-response functions

Many important quantities in spintronics can be formulated by making use of the linear-response formalism. Important examples for this are the electrical conductivity [28,29], the spin conductivity [30], and the Gilbert damping parameter [19,31]. Restricting attention here for the sake of brevity to the symmetric part of the corresponding response tensor $\chi_{\mu\nu}$ this can be expressed by a correlation function of the form

$$\chi_{\mu\nu} \propto \mathrm{Tr}\langle \hat{A}_\mu \, \mathrm{Im}G^+ \, \hat{A}_\nu \, \mathrm{Im}G^+ \rangle_c. \tag{1}$$

It should be stressed that this is not a real restriction as the scheme described below has been used successfully when dealing with the impact of finite temperatures on the anomalous Hall conductivity of Ni [32]. In this case the more complex Kubo-Středa or Kubo-Bastin formulation for the full response tensor has to be used [33].

The vector operator $\hat{A}_\mu$ in Eq. (1) stands, for example, in the case of the electrical conductivity $\sigma_{\mu\nu}$ for the current density operator $\hat{j}_\mu$ [29], while in the case of the Gilbert damping parameter $\alpha_{\mu\nu}$ it stands for the torque operator $\hat{T}_\mu$ [9,19]. Within the Kubo-Greenwood-like equation (1) the electronic structure of the investigated system is represented in terms of its retarded Green function $G^+(\mathbf{r},\mathbf{r}',E)$. Within multiple-scattering theory or the Korringa-Kohn-Rostoker (KKR) formalism, $G^+(\mathbf{r},\mathbf{r}',E)$ can be written as [34–36]

$$\begin{aligned} G^+(\vec{r},\vec{r}\,',E) = &\sum_{\Lambda\Lambda'} Z_\Lambda^m(\vec{r},E)\tau_{\Lambda\Lambda'}^{mn}(E)Z_{\Lambda'}^{n\times}(\vec{r}\,',E) \\ &- \delta_{mn}\sum_\Lambda Z_\Lambda^n(\vec{r},E)J_\Lambda^{n\times}(\vec{r}\,',E)\Theta(r_n'-r_n) \\ &+ J_\Lambda^n(\vec{r},E)Z_\Lambda^{n\times}(\vec{r}\,',E)\Theta(r_n-r_n'). \end{aligned} \tag{2}$$

Here $\mathbf{r},\mathbf{r}'$ refer to points within atomic volumes around sites $\mathbf{R}_m,\mathbf{R}_n$, respectively, with $Z_\Lambda^n(\mathbf{r},E) = Z_\Lambda(\mathbf{r}_n,E) = Z_\Lambda(\mathbf{r}-\mathbf{R}_n,E)$ being a function centered at site $\mathbf{R}_n$. Adopting a fully relativistic formulation [35,36] for Eq. (2), one gets in a natural way access to all spin-orbit-induced properties such as, for example, the anomalous and spin Hall conductivity [30,33,37] or the Gilbert damping parameter [19]. In this case, the functions Z_Λ^n and J_Λ^n stand for the regular and irregular solutions, respectively, to the single-site Dirac equation for site n with the associated single-site scattering t matrix $t_{\Lambda\Lambda'}^n$. The corresponding scattering path operator $\tau_{\Lambda\Lambda'}^{nn'}$ accounts for all scattering events connecting the sites n and n'. Using a suitable spinor representation for the basis functions the combined quantum number $\Lambda = (\kappa,\mu)$ stands for the relativistic spin-orbit and magnetic quantum numbers κ and μ, respectively [35,36,38].

As has been demonstrated by various authors [28,29,39] representing the electronic structure in terms of the Green function $G^+(\mathbf{r},\mathbf{r}',E)$ allows chemical disorder in a random alloy to be accounted for by making use of a suitable alloy theory. In this case $\langle\cdots\rangle_c$ stands for the configurational average for a substitutional alloy with reference to the site occupation.
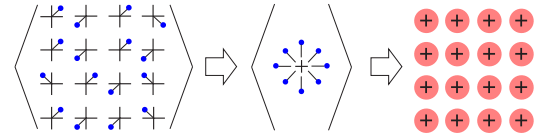
FIG. 1. (Color online) Configurational averaging for thermal lattice displacements: The continuous distribution $P(\Delta\mathbf{R}_n(T))$ for the atomic displacement vectors is replaced by a discrete set of vectors $\Delta\mathbf{R}_v(T)$ occurring with the probability x_v. The configurational average for this discrete set of displacements is made using the CPA, leading to a periodic effective medium.

Corresponding expressions for the conductivity tensor have been worked out by Velický [28] and Butler [29] using the single-site coherent potential approximation which include in particular the so-called vertex corrections.

The CPA can be used to deal with chemical but also with any other type of disorder. In fact, by making use of the different time scales connected with the electronic propagation and spin fluctuations, the alloy analogy is exploited when dealing with finite-temperature magnetism on the basis of the disordered local moment model [27,40]. Obviously, the same approach can be used when dealing with response tensors at finite temperatures. In connection with the conductivity this is often called the adiabatic approximation [41]. Following this philosophy, the CPA has been used recently also when calculating response tensors using Eq. (1) with disorder in the system caused by thermal lattice vibrations [19,32] as well as by spin fluctuations [21,42].

B. Treatment of thermal lattice displacement

A way to account for the impact of the thermal displacement of atoms from their equilibrium positions, i.e., for thermal lattice vibrations, on the electronic structure is to set up a representative displacement configuration for the atoms within an enlarged unit cell (the supercell technique). In this case one has either to use a very large supercell or to take the average over a set of supercells. Alternatively, one may make use of the alloy analogy for the averaging problem. This allows in particular attention to be restricted to the standard unit cell. Neglecting the correlation between the thermal displacements of neighboring atoms from their equilibrium positions the properties of the thermally averaged system can be deduced by making use of the single-site CPA. This basic idea is illustrated by Fig. 1. To make use of this scheme a discrete set of N_v displacement vectors $\Delta\mathbf{R}_v^q(T)$ with probability x_v^q ($v = 1,\ldots,N_v$) is constructed for each basis atom q within the standard unit cell that conforms with the local symmetry and the temperature-dependent root mean square displacement $(\langle u^2\rangle_T)^{1/2}$ according to

$$\sum_{v=1}^{N_v} x_v^q \left|\Delta\mathbf{R}_v^q(T)\right|^2 = \left\langle u_q^2\right\rangle_T. \tag{3}$$

In the general case, the mean square displacement along the direction μ ($\mu = x,y,z$) of the atom i can either be taken from experimental data or represented by the expression based on

the phonon calculations [43]:

$$\langle u_{i,\mu}^2 \rangle_T = \frac{3\hbar}{2M_i} \int_0^\infty d\omega g_{i,\mu}(\omega) \frac{1}{\omega} \coth\frac{\hbar\omega}{2k_B T}, \qquad (4)$$

where $h = 2\pi\hbar$ is the Planck constant, k_B is the Boltzmann constant, and $g_{i,\mu}(\omega)$ is a partial phonon density of states [43]. On the other hand, a rather good estimate for the root mean square displacement can be obtained using Debye's theory. In this case, for systems with one atom per unit cell, Eq. (4) can be reduced to the expression

$$\langle u^2 \rangle_T = \frac{1}{4} \frac{3h^2}{\pi^2 M k_B \Theta_D} \left[\frac{\Phi(\Theta_D/T)}{\Theta_D/T} + \frac{1}{4} \right] \qquad (5)$$

with $\Phi(\Theta_D/T)$ the Debye function and Θ_D the Debye temperature [44]. Ignoring the zero-temperature term $1/4$ and assuming a frozen potential for the atoms, the situation can be dealt with in full analogy to the treatment of disordered alloys on the basis of the CPA. The probability x_v for a specific displacement v may normally be chosen as $1/N_v$. The Debye temperature Θ_D used in Eq. (5) can be either taken from experimental data or calculated by representing it in terms of the elastic constants [45]. In general the latter approach should give more reliable results in the case of multicomponent systems.

To simplify notation we restrict or attention in the following to systems with one atom per unit cell. The index q numbering sites in the unit cell can therefore be dropped, while the index n numbers the lattice sites.

Assuming a rigid displacement of the atomic potential in the spirit of the rigid muffin-tin approximation [46,47] the corresponding single-site t matrix $\underline{t}^{\mathrm{loc}} = \underline{t}^n$ with respect to the local frame of reference connected with the displaced atomic position is unchanged. With respect to the global frame of reference connected with the equilibrium atomic positions $\mathbf{R}_n$, however, the corresponding t matrix $\underline{t}$ is given by the transformation

$$\underline{t} = \underline{U}(\Delta\mathbf{R}) \underline{t}^{\mathrm{loc}} \underline{U}(\Delta\mathbf{R})^{-1}. \qquad (6)$$

The so-called U transformation matrix $\underline{U}(\mathbf{s})$ is given in its nonrelativistic form by [46,47]

$$U_{LL'}(\mathbf{s}) = 4\pi \sum_{L''} i^{l+l''-l'} C_{LL'L''} j_{l''}(|\mathbf{s}|k) Y_{L''}(\hat{s}). \qquad (7)$$

Here $L = (l,m)$ represents the nonrelativistic angular momentum quantum numbers, $j_l(x)$ is a spherical Bessel function, $Y_L(\hat{r})$ is the real spherical harmonics, $C_{LL'L''}$ is a corresponding Gaunt number, and $k = \sqrt{E}$ is the electronic wave vector. We here use atomic Rydberg units for the energy E, which is measured with respect to the so-called muffin-tin zero. The relativistic version of the U matrix is obtained by a standard Clebsch-Gordan transformation [38].

The various displacement vectors $\Delta\mathbf{R}_v(T)$ can be used to determine the properties of a pseudocomponent of a pseudoalloy. Each of the N_v pseudocomponents with $|\Delta\mathbf{R}_v(T)| = \langle u^2 \rangle_T^{1/2}$ is characterized by a corresponding U matrix $\underline{U}_v$ and a t matrix $\underline{t}_v$. As for a substitutional alloy, the site diagonal configurational average can be determined by solving the multicomponent CPA equations within the global frame of
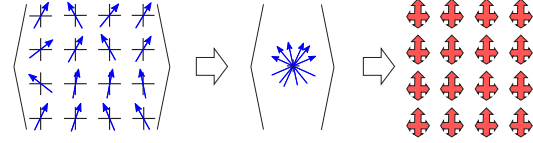
FIG. 2. (Color online) Configurational averaging for thermal spin fluctuations: The continuous distribution $P(\hat{e}_n)$ for the orientation of the magnetic moments is replaced by a discrete set of orientation vectors $\hat{e}_f$ occurring with a probability x_f. The configurational average for this discrete set of orientations is made using the CPA, leading to a periodic effective medium.

reference:

$$\underline{\tau}_{\mathrm{CPA}} = \sum_{v=1}^{N_v} x_v \underline{\tau}_v, \qquad (8)$$

$$\underline{\tau}_v = [(\underline{t}_v)^{-1} - (\underline{t}_{\mathrm{CPA}})^{-1} + (\underline{\tau}_{\mathrm{CPA}})^{-1}]^{-1}, \qquad (9)$$

$$\underline{\tau}_{\mathrm{CPA}} = \frac{1}{\Omega_{\mathrm{BZ}}} \int_{\Omega_{\mathrm{BZ}}} d^3k [(\underline{t}_{\mathrm{CPA}})^{-1} - \underline{G}(\mathbf{k},E)]^{-1}, \qquad (10)$$

where the underline indicates matrices with respect to the combined index Λ. As was pointed out in previous work [42], the cutoff for the angular momentum expansion in these calculations should be taken as $l \geqslant l_{\max} + 1$ with the $l_{\max}$ value used in the calculations for the nondistorted lattice. In all calculations we have used $N_v = 14$: increasing the set of directions for the atomic displacements led to only minor changes of the final results.

The first of these CPA equations represents the requirement for the mean-field CPA medium that embedding of a component v should lead on the average to no additional scattering. Equation (9) gives the scattering path operator for the embedding of the component v into the CPA medium, while Eq. (10) gives the CPA scattering path operator in terms of a Brillouin zone integral with $\underline{G}(\mathbf{k},E)$, the so-called KKR structure constants.

Having solved the CPA equations, the linear-response quantity of interest may be calculated using Eq. (1) as for an ordinary substitutional alloy [28,29]. This implies that one also has to deal with the so-called vertex corrections [28,29] that take into account that one has to deal with a configuration average of the type $\langle \hat{A}_\mu \mathrm{Im}G^+ \hat{A}_\nu \mathrm{Im}G^+ \rangle_c$ which in general will differ from the simpler product $\langle \hat{A}_\mu \mathrm{Im}G^+ \rangle_c \langle \hat{A}_\nu \mathrm{Im}G^+ \rangle_c$.

C. Treatment of thermal spin fluctuations

As for the disorder connected with thermal displacements, the impact of disorder due to thermal spin fluctuations may be accounted for by use of the supercell technique. Alternatively one may again use the alloy analogy and determine the necessary configurational average by means of the CPA as indicated in Fig. 2. As for the thermal displacements in a first step a set of representative orientation vectors $\hat{e}_f$ (with $f = 1, \ldots, N_f$) for the local magnetic moment is introduced (see below). Using the rigid spin approximation the spin-dependent part B_{XC} of the exchange-correlation potential does not change for the local frame of reference fixed to the magnetic moment

when the moment is oriented along an orientation vector $\hat{e}_f$. This implies that the single-site t matrix t_f^{loc} in the local frame is the same for all orientation vectors. With respect to the common global frame that is used to deal with the multiple scattering [see Eq. (10)] the t matrix for a given orientation vector is determined by:

$$\underline{t} = \underline{R}(\hat{e}) \, \underline{t}^{\text{loc}} \, \underline{R}(\hat{e})^{-1}. \tag{11}$$

Here the transformation from the local to the global frame of reference is expressed by the rotation matrices $\underline{R}(\hat{e})$ which are determined by the vectors $\hat{e}$ or corresponding Euler angles [38]. Again the configurational average for the pseudoalloy can be obtained by setting up and solving the CPA equations in analogy to Eqs. (8)–(10).

D. Models of spin disorder

The central problem with the scheme described above is obviously the construction of a realistic and representative set of orientation vectors $\hat{e}_f$ and probabilities x_f for each temperature T to be used in the subsequent calculation of the response quantity using the alloy analogy model. A rather appealing approach is to calculate the exchange-coupling parameters J_{ij} of a system in an *ab initio* way [26,48,49] and to use them in subsequent Monte Carlo (MC) simulations. Figure 3 (top) shows results for the temperature-dependent average reduced magnetic moment of corresponding simulations for bcc Fe obtained for a periodic cell with 4096 atom sites. Note that these results have been obtained using the exchange coupling parameters calculated for the DLM state, modeling the disordered magnetic state above T_C that gave the best agreement with the experimental Curie temperature [27]. The MC calculations for Fe using a classical Heisenberg Hamiltonian have been discussed in [50] in more detail. In the case of Ni the calculations of J_{ij} have been performed for the ferromagnetic (FM) state. The Curie temperature obtained via MC simulations is strongly underestimated, which was also discussed previously by many authors (see, e.g., [51]). The full line gives the value for the reduced magnetic moment of the MC cell $M_{\text{MC}^*}(T) = \langle m_z \rangle_T / m_0$ projected on the z axis, calculated for the last single Monte Carlo step ($\hat{z}$ is the orientation of the total moment, i.e., $\langle \mathbf{m} \rangle_T \| \hat{z}$; the saturated magnetic moment at $T = 0$ K is $m_0 = |\langle \mathbf{m} \rangle_{T=0}|$). This scheme is called MC* in the following. In spite of the rather large number of sites (4096) the curve is rather noisy in particular when approaching the Curie temperature. Nevertheless, the spin configuration of the last MC step was used as an input for subsequent spin-polarized relativistic (SPR) KKR-CPA calculations using the orientation vectors $\hat{e}_f$ with the probability $x_f = 1/N_f$ with $N_f = 4096$. As Fig. 3 (top) shows, the temperature-dependent reduced magnetic moment $M_{\text{KKR(MC}^*)}(T)$ deduced from the electronic structure calculations follows one-to-one the Monte Carlo data $M_{\text{MC}^*}(T)$. This is a very encouraging result for further applications (see below) as it demonstrates that the CPA although being a mean-field method and used here in its single-site formulation is nevertheless capable of reproducing results of MC simulations that go well beyond the mean-field level.

However, using the set of vectors $\hat{e}_f$ of the scheme MC* also for calculations of the Gilbert damping parameters α as a
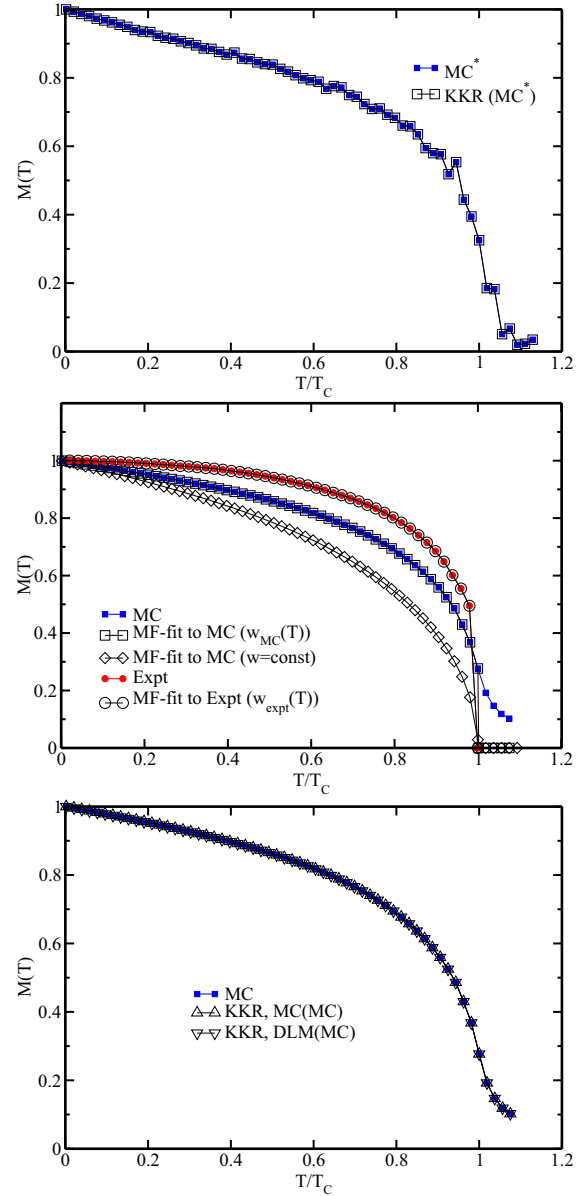
FIG. 3. (Color online) Averaged reduced magnetic moment $M(T) = \langle m_z \rangle_T / |\langle \mathbf{m} \rangle_{T=0}|$ along the z axis as a function of the temperature T. Top: Results of Monte Carlo simulations using the scheme MC* (full squares) compared with results of subsequent KKR calculations (open squares). Middle: Results of Monte Carlo simulations using the scheme MC (full squares) compared with results using a mean-field fit with a constant Weiss field parameter $w_{\text{MC}}(T_C)$ (open diamonds) and a temperature-dependent Weiss field parameter $w_{\text{MC}}(T)$ (open squares). In addition experimental data (full circles) together with a corresponding mean-field fit obtained for a temperature-dependent Weiss field parameter $w_{\text{expt}}(T)$. Bottom: Results of Monte Carlo simulations using the scheme MC (full squares) compared with results of subsequent KKR calculations using the MC scheme (up triangles) and a corresponding DLM (down triangles) spin configuration, respectively.
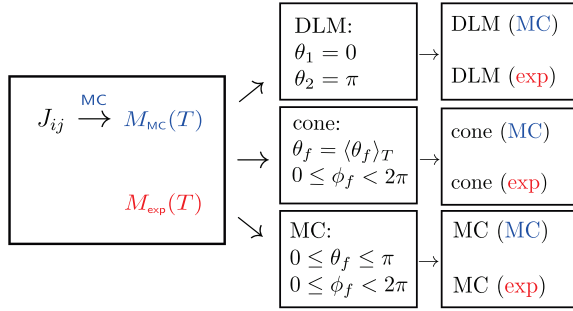
FIG. 4. (Color online) Overview of the different models used to treat spin disorder together with the notation used in the text. The starting point is a temperature-dependent magnetization $M(T)$ either (i) taken from experiment or (ii) obtained from a Monte Carlo simulation that uses exchange-coupling constants from a first-principles electronic structure calculation. Three different models abbreviated as MC, DLM, and cone are then used to obtain a representative distribution of moments [weights and directions $\{x_f, \hat{e}_f(\theta, \phi)\}$] that in turn reproduce $M(T)$. On the right in parentheses the source is given ("MC" or "expt" data) upon which the calculation of response quantities is based.

function of temperature led to extremely noisy and unreliable curves for $\alpha(T)$. For that reason an average has been taken over many MC steps (scheme MC) leading to a much smoother curve for $M_{MC}(T)$ as can be seen from Fig. 3 (middle) with a Curie temperature $T_C^{MC} = 1082$ K. As this enlarged set of vectors $\hat{e}_f$ got too large to be used directly in subsequent SPR-KKR-CPA calculations, a scheme was worked out to get a set of vectors $\hat{e}_f$ and probabilities x_f that is not too large but nevertheless leads to smooth curves for $M(T)$.

The first attempt was to use the Curie temperature T_C^{MC} to deduce a corresponding temperature-independent Weiss field parameter $w(T_C)$ on the basis of the standard mean-field relation

$$w(T_C) = \frac{3k_B T_C}{m_0^2}. \qquad (12)$$

This leads to a reduced magnetic moment curve $M_{MF}(T)$ that shows by construction the same Curie temperature as the MC simulations. For temperatures between $T = 0$ K and T_C, however, the mean-field reduced magnetic moment $M_{MF}(T)$ is well below the MC curve [see Fig. 3 (middle)].

As an alternative to this simple approach we introduced a temperature-dependent Weiss field parameter $w(T)$. This allows us to describe the temperature-dependent magnetic properties using the results obtained beyond the mean-field approximation. At the same time the calculation of the statistical average can be performed by treating the model Hamiltonian in terms of the mean-field theory. For this reason the reduced magnetic moment $M(T)$, being a solution of the equation (see, e.g., [52])

$$M(T) = L\left(\frac{w m_0^2 M(T)}{k_B T}\right), \qquad (13)$$

was fitted to that obtained from MC simulations $M_{MC}(T)$ with the Weiss field parameter $w(T)$ as a fitting parameter, such that

$$\lim_{w \to w(T)} M(T) = M_{MC}(T), \qquad (14)$$

with $L(x)$ the Langevin function.

The corresponding temperature-dependent probability $x(\hat{e})$ for an atomic magnetic moment to be oriented along $\hat{e}$ is proportional to $\exp(w(T)\hat{z} \cdot \hat{e}/k_B T)$ (see, e.g., [52]). To calculate this value we used N_θ and N_ϕ points for a regular grid for the spherical angles θ and ϕ corresponding to the vector $\hat{e}_f$:

$$x_f = \frac{\sin(\theta_f) \exp[w(T)\hat{z} \cdot \hat{e}_f/k_B T]}{\sum_{f'} \sin(\theta_{f'}) \exp[w(T)\hat{z} \cdot \hat{e}_{f'}/k_B T]}. \qquad (15)$$

Figure 5 shows the θ-dependent behavior of $x(\hat{e})$ for three different temperatures. As one notes, the mean-field (MF) fit to the MC results perfectly reproduces these data for all temperatures. This applies of course not only for the angular-resolved distribution of the magnetic moments shown in Fig. 5 but also for the average reduced magnetic moment recalculated using Eq. (13), shown in Fig. 3. Obviously, the MF curve $M_{MF(MC)}(T)$ obtained using the temperature-dependent Weiss field parameter $w(T)$ perfectly reproduces the original $M_{MC}(T)$ curve. The great advantage of this fitting procedure is that it allows the MC data set to be replaced with a large number N_f^{MC} of orientation vectors $\hat{e}_f$ (pointing in principle in any direction) with equal probability $x_f = 1/N_f^{MC}$ [10^6 MC steps have been used to calculate $M_{MC}(T)$ for each T] by a much smaller data set with $N_f = N_\theta N_\phi$ (where $N_\theta = 180$ and $N_\phi = 18$ have been used in all calculations presented here) with x_f given by Eq. (15).

Accordingly, the reduced data set can straightforwardly be used for subsequent electronic structure calculations. Figure 3 (bottom) shows that the calculated temperature-dependent reduced magnetic moment $M_{KKR-MC(MC)}(T)$ agrees perfectly with the reduced magnetic moment $M_{MC}(T)$ given by the underlying MC simulations.

The DLM method has the appealing feature that it combines *ab initio* calculations and thermodynamics in a coherent way. Using a nonrelativistic formulation, it was shown that the corresponding averaging over all orientations of the individual atomic reduced magnetic moments can be mapped onto a binary pseudoalloy with one pseudocomponent having up- and downward orientations of the spin moment with concentrations $x_\uparrow$ and $x_\downarrow$, respectively [25,53]. For a fully relativistic formulation, with spin-orbit coupling included, this simplification cannot be justified any longer and a proper average has to be taken over all orientations [54]. As we do not perform DLM calculations but use here the DLM picture only to represent MC data, this complication is ignored in the following. Having the set of orientation vectors $\hat{e}_f$ determined by MC simulations, the corresponding concentrations $x_\uparrow$ and $x_\downarrow$ can straightforwardly be fixed for each temperature by the requirement

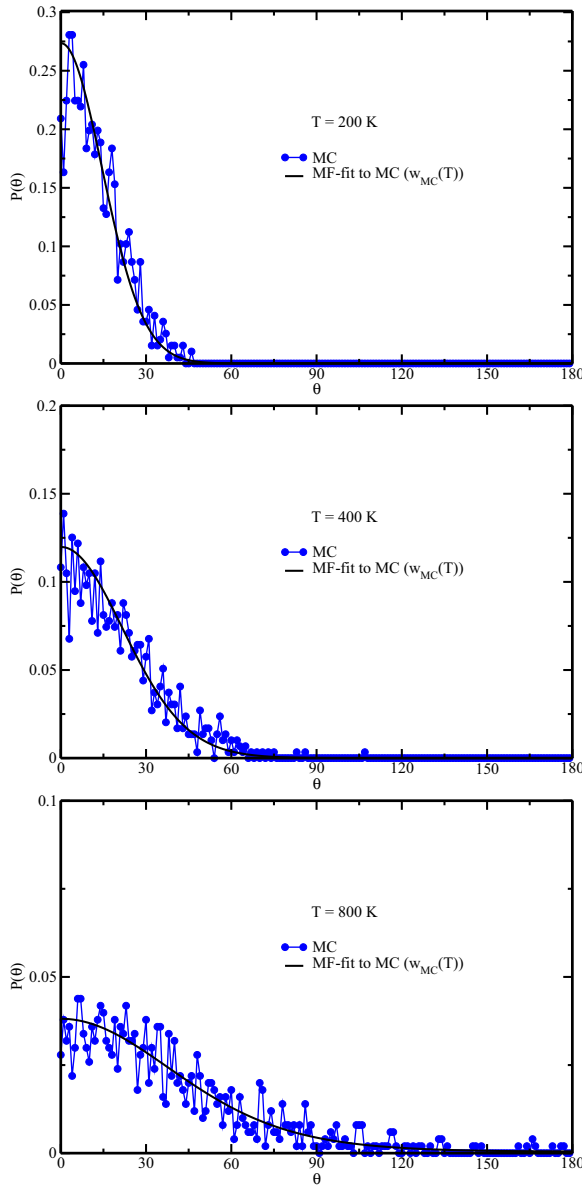$$\frac{1}{N_f}\sum_{f=1}^{N_f} \hat{e}_f = x_\uparrow \hat{z} + x_\downarrow(-\hat{z}), \qquad (16)$$

FIG. 5. (Color online) Angular distribution $P(\theta)$ of the atomic magnetic moment **m** obtained from Monte Carlo simulations (MC) for the temperatures $T = 200$, 400, and 800 K compared with mean-field (MF) data x_f (full line) obtained by fitting using a temperature-dependent Weiss field parameter $w(T)$ [Eq. (13)].

with $x_\uparrow + x_\downarrow = 1$. Using this simple scheme, electronic structure calculations have been performed for a binary alloy having collinear magnetization. The resulting reduced magnetic moment $M_{\text{KKR-DLM(MC)}}(T)$ is shown in Fig. 3 (bottom). Note that again the original MC results are perfectly reproduced. This implies that when calculating the projected reduced magnetic moment M_z that is determined by the averaged Green function $\langle G \rangle$ the transversal magnetization has hardly any impact.

Fig. 3 (middle) gives also experimental data for the $M(T)$ [55]. While the experimental Curie temperature $T_C^{\text{expt}} = 1044$ K [55] is rather well reproduced by the MC simulations $T_C^{\text{MC}} = 1082$ K, note that the MC curve $M_{\text{MC}}(T)$ is well below the experimental curve. In particular, $M_{\text{MC}}(T)$ drops too fast with increasing T in the low-temperature regime and does not show the $T^{3/2}$ behavior. The reason for this is that the MC simulations do not properly account for the low-energy long-ranged spin-wave excitations responsible for the low-temperature magnetization variation. Performing *ab initio* calculations for the spin-wave energies and using these data for the calculation of $M(T)$, much better agreement with experiment can indeed be obtained in the low-temperature regime than with MC simulations [56].

As the fitting scheme sketched above needs only the temperature-reduced magnetic moment $M(T)$ as input it can be applied not only to MC data but also to experimental data. Figure 3 shows that the mean-field fit $M_{\text{MF(expt)}}(T)$ again perfectly fits the experimental reduced magnetic moment curve $M_{\text{expt}}(T)$. Based on this good agreement this corresponding data set $\{\hat{e}_f, x_f\}$ has also been used for the calculation of response tensors (see below).

An additional much simpler scheme to simulate the experimental $M_{\text{expt}}(T)$ curve is to assume that the individual atomic moments are distributed on a cone, i.e., with $N_\theta = 1$ and $N_\phi \gg 1$ [24]. In this case the opening angle $\theta(T)$ of the cone is chosen such as to reproduce $M(T)$. In contrast to the standard DLM picture, this simple scheme already allows transversal components of the magnetization to be taken into account. Corresponding results for response tensor calculations will be shown below.

Finally, it should be stressed here that the various spin configuration models discussed above assume a rigid spin moment, i.e., its magnitude does not change with temperature or with orientation. In contrast to this, Ruban *et al.* [57] use a longitudinal spin fluctuation Hamiltonian with the corresponding parameters derived from *ab initio* calculations. As a consequence, subsequent Monte Carlo simulations based on this Hamiltonian account in particular for longitudinal fluctuations of the spin moments. A similar approach has been used by Drchal *et al.* [58,59], leading to good agreement with the results of Ruban *et al.* However, the scheme used in these calculations does not supply in a straightforward manner the necessary input for temperature-dependent transport calculations. This is different from the work of Staunton *et al.* [60], who performed self-consistent relativistic DLM calculations without the restriction to a collinear spin configuration. This approach in particular accounts in a self-consistent way for longitudinal spin fluctuations.

E. Combined chemical and thermally induced disorder

The various types of disorder discussed above may be combined with each other as well as with chemical, i.e., substitution, disorder. In the most general case a pseudocomponent vft is characterized by its chemical atomic type t, the spin fluctuation f, and the lattice displacement v. Using the rigid muffin-tin and rigid spin approximations, the single-site t matrix t_t^{loc} in the local frame is independent of the orientation vector $\hat{e}_f$ and displacement vector $\Delta \mathbf{R}_v$, and coincides with

$\underline{t}_t$ for the atomic type t. With respect to the common global frame one has accordingly the t matrix

$$\underline{t}_{vft} = \underline{U}(\Delta \mathbf{R}_v) \, \underline{R}(\hat{e}_f) \underline{t}_t \, \underline{R}(\hat{e}_f)^{-1} \underline{U}(\Delta \mathbf{R}_v)^{-1}. \quad (17)$$

With this the corresponding CPA equations are identical to Eqs. (8)–(10) with the index v replaced by the combined index vft. The corresponding pseudoconcentration x_{vft} combines the concentration x_t of the atomic type t with the probabilities for the orientation vector $\hat{e}_f$ and displacement vector $\Delta \mathbf{R}_v$.

III. COMPUTATIONAL DETAILS

The electronic structure of the investigated ferromagnets bcc Fe and fcc Ni, has been calculated self-consistently using the SPR-KKR band structure method [61,62]. For the exchange-correlation potential the parametrization as given by Vosko *et al.* [63] has been used. The angular momentum cutoff of $l_{\max} = 3$ was used in the KKR multiple-scattering expansion. The lattice parameters have been set to the experimental values.

In a second step the exchange-coupling parameters J_{ij} have been calculated using the so-called Lichtenstein formula [26]. Although the self-consistent field (SCF) calculations have been done on a fully relativistic level, the anisotropy of the exchange coupling due to the spin-orbit coupling has been neglected here. Also, the small influence of the magnetocrystalline anisotropy for the subsequent Monte Carlo simulations has been ignored, i.e., these have been based on a classical Heisenberg Hamiltonian. The MC simulations were done in a standard way using the Metropolis algorithm and periodic boundary conditions. The theoretical Curie temperature $T_{\mathrm{C}}^{\mathrm{MC}}$ has been deduced from the maximum of the magnetic susceptibility.

The temperature-dependent spin configuration obtained during a MC simulation has been used to construct a set of orientations $\hat{e}_f$ and probabilities x_f according to the schemes MC* and MC described in Sec. II D to be used within subsequent SPR-KKR-CPA calculations (see above). For the corresponding calculation of the reduced magnetic moment the potential obtained from the SCF calculation for the perfect ferromagnetic state ($T = 0$ K) has been used. The calculation for the electrical conductivity as well as for the Gilbert damping parameter has been performed as described elsewhere [42,64].

IV. RESULTS AND DISCUSSION

A. Temperature-dependent conductivity

Equation (1) has been used together with the various schemes described above to calculate the temperature-dependent longitudinal resistivity $\rho(T)$ of the pure ferromagnets Fe, Co, and Ni. In this case obviously disorder due to thermal displacements of the atoms as well as spin fluctuations contributes to the resistivity.

To give an impression of the impact of the thermal displacements alone Fig. 6 gives the temperature-dependent resistivity $\rho(T)$ of pure Cu ($\Theta_{\mathrm{Debye}} = 315$ K), which is found to be in very good agreement with corresponding experimental data [65]. This implies that the alloy analogy model that ignores any inelastic scattering events should
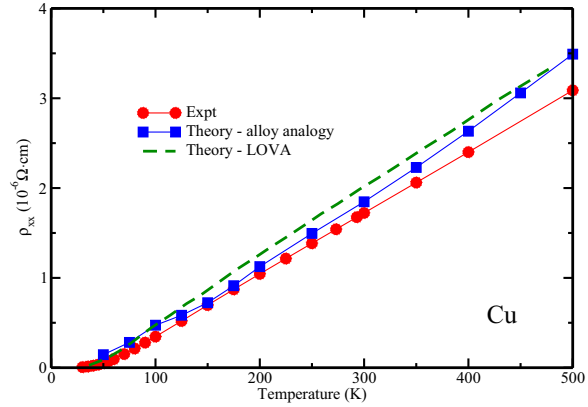
FIG. 6. (Color online) Temperature-dependent longitudinal resistivity of fcc Cu $\rho(T)$ obtained by accounting for thermal vibrations as described in Sec. II B compared with corresponding experimental data [65]. In addition results are shown based on the lowest-order variational approximation (LOVA) to the Boltzmann formalism [15].

in general lead to rather reliable results for the resistivity induced by thermal displacements. Accordingly, comparison with experiment for magnetically ordered systems should allow the most appropriate model for spin fluctuations to be found.

Figure 7 (top) shows theoretical results for $\rho(T)$ of bcc Fe due to thermal displacements $\rho_v(T)$, spin fluctuations described by the scheme MC $\rho_{\mathrm{MC(MC)}}(T)$, as well as the combination of the two influences $[\rho_{v,\mathrm{MC(MC)}}(T)]$. First of all one notes that $\rho_v(T)$ is not influenced within the adopted model by the Curie temperature T_{C} but is determined only by the Debye temperature. $\rho_{\mathrm{MC(MC)}}(T)$, on the other hand, reaches saturation for T_{C} as the spin disorder no longer increases with increasing temperature in the paramagnetic regime. Figure 7 also shows that $\rho_v(T)$ and $\rho_{\mathrm{MC(MC)}}(T)$ are comparable for low temperatures but $\rho_{\mathrm{MC(MC)}}(T)$ exceeds $\rho_v(T)$ more and more for higher temperatures. Most interestingly, however, the resistivity for the combined influence of thermal displacements and spin fluctuations $\rho_{v,\mathrm{MC(MC)}}(T)$ does not coincide with the sum of $\rho_v(T)$ and $\rho_{\mathrm{MC(MC)}}(T)$ but exceeds the sum for low temperatures and lies below the sum when approaching T_{C}.

Figure 7 (bottom) shows the results of three different calculations including the effect of spin fluctuations as functions of the temperature. The curve $\rho_{\mathrm{MC(MC)}}(T)$ is identical with that given in Fig. 7 (top) based on Monte Carlo simulations. The curves $\rho_{\mathrm{DLM(MC)}}(T)$ and $\rho_{\mathrm{cone(MC)}}(T)$ are based on a DLM- and a conelike representation of the MC results, respectively. For all three cases results are given including as well as ignoring the vertex corrections. Note that the vertex corrections play a negligible role for all three spin disorder models. This is fully in line with the experience for the longitudinal resistivity of disordered transition metal alloys: as long as the the states at the Fermi level have dominantly d character the vertex corrections can be neglected in general. On the other hand, if the sp character dominates, inclusion of vertex corrections may alter the result on the order of 10% [66,67].

Comparing the DLM result $\rho_{\mathrm{DLM(MC)}}(T)$ with $\rho_{\mathrm{MC(MC)}}(T)$ one notes in contrast to the results for $M(T)$ shown above
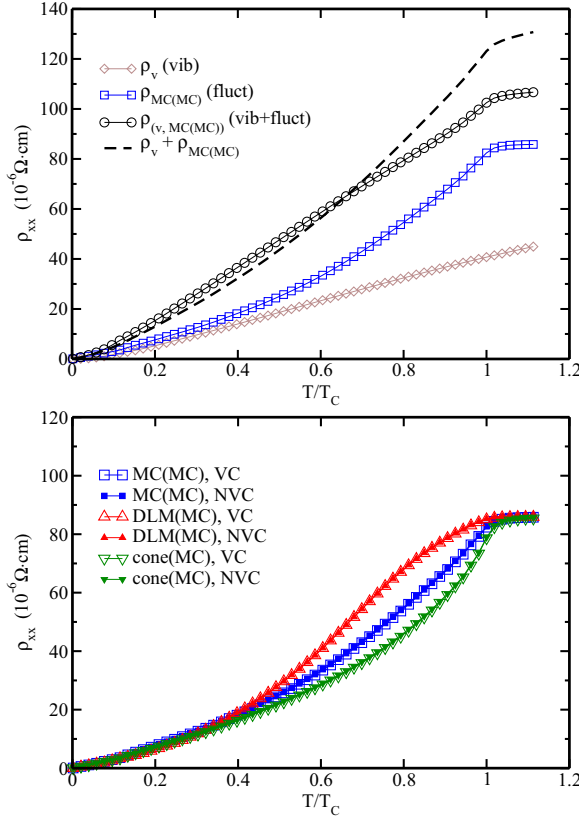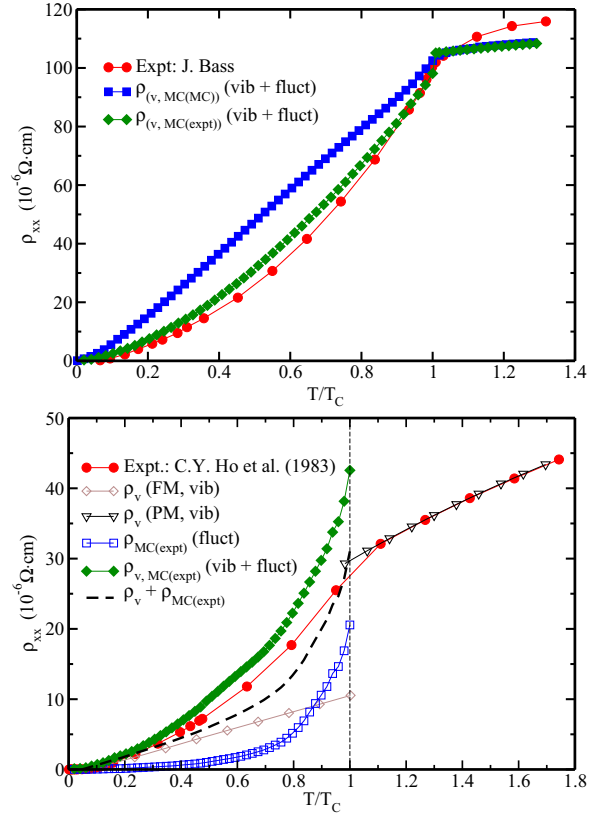
FIG. 7. (Color online) Temperature-dependent longitudinal resistivity of bcc Fe $\rho(T)$ obtained by accounting for thermal vibrations and spin fluctuations as described in Sec. II B. Top: By accounting for vibrations (vib, diamonds), spin fluctuations using the scheme MC (fluct, squares) and both (vib + fluct, circles). The dashed line represents the sum of resistivities contributed by lattice vibrations or spin fluctuations only. Bottom: By accounting for spin fluctuations $\hat{e}_f = \hat{e}(\theta_f, \phi_f)$ using the schemes (see Fig. 4): MC(MC) (squares), DLM(MC) (up triangles), and cone(MC) (down triangles). The full and open symbols represent the results obtained with the vertex corrections included (VC) and excluded (NVC), respectively.

FIG. 8. (Color online) Top: Temperature-dependent longitudinal resistivity of bcc Fe $\rho(T)$ obtained by accounting for thermal vibrations and spin fluctuations using the scheme MC vib + fluct[MC(MC)], squares and a mean-field fit to the experimental temperature magnetic moment M_{expt} {vib + fluct[MC(expt)], diamonds}, compared with experimental data (circles) [65]. Bottom: Corresponding results for fcc Ni. In addition results are shown accounting for thermal displacements (vib) only for the ferromagnetic (FM) and the paramagnetic (PM) regimes. The dashed line represents the sum of resistivities contributed by lattice vibrations or spin fluctuations only. Experimental data have been taken from Ref. [68].

[see Fig. 3 (bottom)] quite an appreciable deviation. This implies that the restricted collinear representation of the spin configuration implied by the DLM model introduces errors for the configurational average that seem in general to be unacceptable. For the Curie temperature and beyond in the paramagnetic regime $\rho_{\text{DLM(MC)}}(T)$ and $\rho_{\text{MC}}(T)$ coincide, as was shown formally before [21].

Comparing finally $\rho_{\text{cone(MC)}}(T)$ based on the conical representation of the MC spin configuration with $\rho_{\text{MC(MC)}}(T)$, one notes that this simplification also leads to quite strong deviations from the more reliable result. Nevertheless, one notes that $\rho_{\text{DLM(MC)}}(T)$ agrees with $\rho_{\text{MC(MC)}}(T)$ for the Curie temperature and also accounts to some extent for the impact of the transversal components of the magnetization.

The theoretical results for bcc Fe ($\Theta_{\text{Debye}} = 420$ K) based on the combined inclusion of the effects of thermal

displacements and spin fluctuations using the MC scheme [$\rho_{\text{v,MC(MC)}}(T)$] are compared in Fig. 8 (top) with experimental data [$\rho_{\text{expt}}(T)$]. For the Curie temperature obviously a very good agreement with experiment is found, while for lower temperatures $\rho_{\text{v,MC(MC)}}(T)$ exceeds $\rho_{\text{expt}}(T)$. This behavior correlates well with that of the temperature-dependent reduced magnetic moment $M(T)$ shown in Fig. 3 (middle). The too rapid decrease of $M_{\text{MC}}(T)$ compared with the experimental results implies an essentially overestimated spin disorder at any temperature, leading in turn to a too large resistivity $\rho_{\text{v,MC(MC)}}(T)$. On the other hand, using the temperature dependence of the experimental reduced magnetic moment $M_{\text{expt}}(T)$ to set up the temperature dependent spin configuration as described above a very satisfying agreement of $\rho_{\text{v,MC(expt)}}(T)$ is found with the experimental resistivity data $\rho_{\text{expt}}(T)$. Note also that above T_C the calculated resistivity increases the saturation,

in contrast to the experimental data, where the continuing increase of $\rho_{\text{expt}}(T)$ can be attributed to the longitudinal spin fluctuations leading to a temperature-dependent distribution of local magnetic moments on Fe atoms [57]. However, this contribution was not taken into account because of the restriction in present calculations of using fixed values for the local reduced magnetic moments.

Figure 8 (bottom) shows corresponding results for the temperature-dependent resistivity of fcc Ni ($\Theta_{\text{Debye}} = 375$ K). For the ferromagnetic regime that the theoretical results are comparable in magnitude when only thermal displacements [$\rho_{\text{v}}(T)$] or only spin fluctuations [$\rho_{\text{MC(expt)}}(T)$] are accounted for. In the latter case the mean-field $w(T)$ has been fitted to the experimental $M(T)$ curve. Taking both into account leads to a resistivity [$\rho_{\text{v,MC(expt)}}(T)$] that is well above the sum of the individual terms $\rho_{\text{v}}(T)$ and $\rho_{\text{MC(expt)}}(T)$. Comparing $\rho_{\text{v,MC(expt)}}(T)$ with experimental data $\rho_{\text{expt}}(T)$, our finding shows that the theoretical results overshoot the experimental ones as one comes closer to the critical temperature. This is a clear indication that the assumption of a rigid spin moment is quite questionable as the resulting contribution to the resistivity due to spin fluctuations as much too small. In fact the simulations of Ruban *et al.* [57] on the basis of a longitudinal spin fluctuation Hamiltonian led on the case of fcc Ni to a strong diminishing of the average local magnetic moment when the critical temperature is approached from below (about 20% compared to the value at $T = 0$ K). For bcc Fe, the change is much smaller (about 3%) justifying in this case the assumption of a rigid spin moment. Taking the extreme point of view that the spin moment vanishes completely above the critical temperature or in the paramagnetic regime only thermal displacements have to be considered as a source for the finite resistivity. Corresponding results are shown in Fig. 8 (bottom) together with corresponding experimental data. The very good agreement between the two obviously suggests that

remaining spin fluctuations above the critical temperature are of minor importance for the resistivity of fcc Ni.

B. Temperature-dependent Gilbert damping parameter

Figure 9 shows results for the Gilbert damping parameter α of bcc Fe obtained using different models for the spin fluctuations. All the curves show the typical conductivitylike behavior for low temperatures and the resistivitylike behavior at high temperatures, reflecting the change from dominating intra- to interband transitions [11]. The curve denoted "expt" is based on a spin configuration obtained from the experimental $M_{\text{expt}}(T)$ data. Using the conical model to fit $M_{\text{expt}}(T)$ as the basis for the calculation of $\alpha(T)$ leads obviously to a rather good agreement with $\alpha_{M(\text{expt})}(T)$. With instead a DLM-like representation of $M_{\text{expt}}(T)$, on the other hand, the transverse spin components are suppressed and noteworthy deviations from $\alpha_{M(\text{expt})}(T)$ are found for the low-temperature regime. Nevertheless, the deviations are less pronounced than in the case of the longitudinal resistivity [see Fig. 7 (bottom)],

FIG. 9. (Color online) Temperature-dependent Gilbert damping parameter $\alpha(T)$ for bcc Fe obtained by accounting for spin fluctuations based on the experimental $M(T)$ dependence and calculated using the schemes MC (circles), DLM (up triangles), and cone (down triangles); as well as the Gilbert damping parameter calculated by accounting for spin fluctuations using the scheme MC and based on the $M(T)$ dependence obtained in MC simulations.

FIG. 10. (Color online) Top: Temperature-dependent Gilbert damping $\alpha(T)$ for bcc Fe, obtained by accounting for thermal vibrations and spin fluctuations accounting for lattice vibrations only (circles) and lattice vibrations and spin fluctuations based on a mean-field fit to the experimental temperature-reduced magnetic moment M_{expt} (diamonds) compared with experimental data (dashed and full lines) [69,70]. Bottom: Corresponding results for fcc Ni. Experimental data have been taken from Ref. [69].

where corresponding results are shown based on $M_{MC}(T)$ as a reference. Obviously, the damping parameter α seems to be less sensitive to the specific spin fluctuation model used than the resistivity. Finally, using the spin configuration deduced from Monte Carlo simulations, i.e., based on $M_{MC}(T)$, quite strong deviations for the resulting $\alpha_{M(MC)}(T)$ from $\alpha_{M(expt)}(T)$ are found. As for the resistivity [see Fig. 7 (bottom)] this seems to reflect the too fast drop of the reduced magnetic moment $M_{MC}(T)$ with temperature in the low-temperature regime compared with the drop in temperature (see Fig. 3). As was found before [19], accounting only for thermal vibrations $\alpha(T)$ [Fig. 7 (bottom)] gives results comparable to the case when only thermal spin fluctuations are allowed. Combing both thermal effects does not lead to a curve that is just the sum of the two $\alpha(T)$ curves. As found for the conductivity [Fig. 7 (top)] obviously the two thermal effects are not simply additive. As Fig. 10 (top) shows, the resulting damping parameter $\alpha(T)$ for bcc Fe that accounts for thermal vibrations as well as spin fluctuations is found to be in reasonable good agreement with experimental data [19].

Figure 10 shows also corresponding results for the Gilbert damping of fcc Ni as a function of temperature. Accounting only for thermal spin fluctuations on the basis of the experimental $M(T)$ curve leads in this case to completely unrealistic results, while accounting only for thermal displacements leads to results already in rather good agreement with experiment. Taking finally both sources of disorder into account, again no simple additive behavior is found but the results are nearly unchanged compared to those based on the thermal displacements alone. This implies that the results for the Gilbert damping parameter of fcc Ni hardly depend on the spin fluctuations but are governed significantly by thermal displacements.

V. SUMMARY

Various schemes based on the alloy analogy that allow inclusion of thermal effects when calculating response properties relevant in spintronics have been presented and discussed. Technical details of implementation within the framework of the spin-polarized relativistic KKR-CPA band structure method have been outlined that allow thermal vibrations as well as spin fluctuations to be dealt with. Various models to represent spin fluctuations have been compared with each other concerning the corresponding results for the temperature dependence of the reduced magnetic moment $M(T)$ as well as response quantities. It was found that response quantities are much more sensitive to the spin fluctuation model than the reduced magnetic moment $M(T)$. Furthermore, it was found that the influence of thermal vibrations and spin fluctuations is not additive when calculating electrical conductivity or the Gilbert damping parameter α. Using experimental data for the reduced magnetic moment $M(T)$ to set up realistic temperature-dependent spin configurations, satisfying agreement for the electrical conductivity as well as the Gilbert damping parameter could be obtained for the elemental ferromagnets bcc Fe and fcc Ni.

[1] T. Holstein, Ann. Phys. (NY) **29**, 410 (1964).

[2] G. D. Mahan, *Many-Particle Physics*, Physics of Solids and Liquids (Springer, New York, 2000).

[3] P. B. Allen, Phys. Rev. B **3**, 305 (1971).

[4] K. Takegahara and S. Wang, J. Phys. F: Met. Phys. **7**, L293 (1977).

[5] G. Grimvall, Phys. Scr. **14**, 63 (1976).

[6] G. D. Mahan and W. Hansch, J. Phys. F: Met. Phys. **13**, L47 (1983).

[7] M. Oshita, S. Yotsuhashi, H. Adachi, and H. Akai, J. Phys. Soc. Jpn. **78**, 024708 (2009).

[8] K. Shirai and K. Yamanaka, J. Appl. Physics **113**, 053705 (2013).

[9] D. Steiauf and M. Fähnle, Phys. Rev. B **72**, 064450 (2005).

[10] V. Kamberský, Phys. Rev. B **76**, 134416 (2007).

[11] K. Gilmore, Y. U. Idzerda, and M. D. Stiles, Phys. Rev. Lett. **99**, 027204 (2007).

[12] V. Kambersky, Czech. J. Phys. **26**, 1366 (1976).

[13] D. Thonig and J. Henk, New J. Phys. **16**, 013032 (2014).

[14] P. B. Allen, T. P. Beaulac, F. S. Khan, W. H. Butler, F. J. Pinski, and J. C. Swihart, Phys. Rev. B **34**, 4331 (1986).

[15] S. Y. Savrasov and D. Y. Savrasov, Phys. Rev. B **54**, 16487 (1996).

[16] B. Xu and M. J. Verstraete, Phys. Rev. B **87**, 134302 (2013).

[17] B. Xu and M. J. Verstraete, Phys. Rev. Lett. **112**, 196603 (2014).

[18] Y. Liu, A. A. Starikov, Z. Yuan, and P. J. Kelly, Phys. Rev. B **84**, 014412 (2011).

[19] H. Ebert, S. Mankovsky, D. Ködderitzsch, and P. J. Kelly, Phys. Rev. Lett. **107**, 066603 (2011).

[20] J. Braun, J. Minár, S. Mankovsky, V. N. Strocov, N. B. Brookes, L. Plucinski, C. M. Schneider, C. S. Fadley, and H. Ebert, Phys. Rev. B **88**, 205409 (2013).

[21] J. Kudrnovský, V. Drchal, I. Turek, S. Khmelevskyi, J. K. Glasbrenner, and K. D. Belashchenko, Phys. Rev. B **86**, 144423 (2012).

[22] J. K. Glasbrenner, K. D. Belashchenko, J. Kudrnovský, V. Drchal, S. Khmelevskyi, and I. Turek, Phys. Rev. B **85**, 214405 (2012).

[23] R. Kováčik, P. Mavropoulos, D. Wortmann, and S. Blügel, Phys. Rev. B **89**, 134417 (2014).

[24] S. Mankovsky, D. Ködderitzsch, and H. Ebert (unpublished).

[25] H. Akai and P. H. Dederichs, Phys. Rev. B **47**, 8739 (1993).

[26] A. I. Liechtenstein, M. I. Katsnelson, V. P. Antropov, and V. A. Gubanov, J. Magn. Magn. Mater. **67**, 65 (1987).

[27] B. L. Gyorffy, A. J. Pindor, J. Staunton, G. M. Stocks, and H. Winter, J. Phys. F: Met. Phys. **15**, 1337 (1985).

[28] B. Velický, Phys. Rev. **184**, 614 (1969).

[29] W. H. Butler, Phys. Rev. B **31**, 3260 (1985).

[30] S. Lowitzer, M. Gradhand, D. Ködderitzsch, D. V. Fedorov, I. Mertig, and H. Ebert, Phys. Rev. Lett. **106**, 056601 (2011).

[31] A. Brataas, Y. Tserkovnyak, and G. E. W. Bauer, Phys. Rev. Lett. **101**, 037207 (2008).

[32] D. Ködderitzsch, K. Chadova, J. Minár, and H. Ebert, New J. Phys. **15**, 053009 (2013).

[33] A. Crépieux and P. Bruno, Phys. Rev. B **64**, 094434 (2001).

[34] J. S. Faulkner and G. M. Stocks, Phys. Rev. B **21**, 3222 (1980).

[35] P. Weinberger, *Electron Scattering Theory for Ordered and Disordered Matter* (Oxford University Press, Oxford, 1990).

[36] H. Ebert, in *Electronic Structure and Physical Properties of Solids*, edited by H. Dreyssé, Lecture Notes in Physics Vol. 535 (Springer, Berlin, 2000), p. 191.

[37] S. Lowitzer, D. Ködderitzsch, and H. Ebert, Phys. Rev. Lett. **105**, 266604 (2010).

[38] M. E. Rose, *Relativistic Electron Theory* (Wiley, New York, 1961).

[39] I. Turek, J. Kudrnovský, V. Drchal, L. Szunyogh, and P. Weinberger, Phys. Rev. B **65**, 125101 (2002).

[40] J. B. Staunton and B. L. Gyorffy, Phys. Rev. Lett. **69**, 371 (1992).

[41] M. Jonson and G. D. Mahan, Phys. Rev. B **42**, 9350 (1990).

[42] S. Mankovsky, D. Ködderitzsch, G. Woltersdorf, and H. Ebert, Phys. Rev. B **87**, 014430 (2013).

[43] H. Böttger, *Principles of the Theory of Lattice Dynamics* (Akademie-Verlag, Berlin, 1983).

[44] E. M. Gololobov, E. L. Mager, Z. V. Mezhevich, and L. K. Pan, Phys. Status Solidi B **119**, K139 (1983).

[45] E. Francisco, M. A. Blanco, and G. Sanjurjo, Phys. Rev. B **63**, 094107 (2001).

[46] N. Papanikolaou, R. Zeller, P. H. Dederichs, and N. Stefanou, Phys. Rev. B **55**, 4157 (1997).

[47] A. Lodder, J. Phys. F: Met. Phys. **6**, 1885 (1976).

[48] L. Udvardi, L. Szunyogh, K. Palotás, and P. Weinberger, Phys. Rev. B **68**, 104436 (2003).

[49] H. Ebert and S. Mankovsky, Phys. Rev. B **79**, 045209 (2009).

[50] S. Mankovsky, S. Polesya, H. Ebert, W. Bensch, O. Mathon, S. Pascarelli, and J. Minár, Phys. Rev. B **88**, 184108 (2013).

[51] M. Pajda, J. Kudrnovský, I. Turek, V. Drchal, and P. Bruno, Phys. Rev. B **64**, 174402 (2001).

[52] S. Tikadzumi, *Physics of Magnetism*, (Willey, Ney York, 1964).

[53] H. Akai, Phys. Rev. Lett. **81**, 3002 (1998).

[54] J. B. Staunton, S. Ostanin, S. S. A. Razee, B. L. Gyorffy, L. Szunyogh, B. Ginatempo, and E. Bruno, Phys. Rev. Lett. **93**, 257204 (2004).

[55] J. Crangle and G. M. Goodman, Proc. R. Soc. London, Ser. A **321**, 477 (1971), http://rspa.royalsocietypublishing.org/content/321/1547/477.full.pdf+html.

[56] S. V. Halilov, H. Eschrig, A. Y. Perlov, and P. M. Oppeneer, Phys. Rev. B **58**, 293 (1998).

[57] A. V. Ruban, S. Khmelevskyi, P. Mohn, and B. Johansson, Phys. Rev. B **75**, 054402 (2007).

[58] V. Drchal, J. Kudrnovský, and I. Turek, EPJ Web Conf. **40**, 11001 (2013).

[59] V. Drchal, J. Kudrnovský, and I. Turek, J. Supercond. Novel Magn. **26**, 1997 (2013).

[60] J. B. Staunton, R. Banerjee, M. dos Santos Dias, A. Deak, and L. Szunyogh, Phys. Rev. B **89**, 054427 (2014).

[61] H. Ebert, D. Ködderitzsch, and J. Minár, Rep. Prog. Phys. **74**, 096501 (2011).

[62] H. Ebert *et al.*, *The Munich SPR-KKR Package*, version 6.3, http://olymp.cup.uni-muenchen.de/ak/ebert/SPRKKR (2012).

[63] S. H. Vosko, L. Wilk, and M. Nusair, Can. J. Phys. **58**, 1200 (1980).

[64] D. Ködderitzsch, S. Lowitzer, J. B. Staunton, and H. Ebert, Phys. Status Solidi B **248**, 2248 (2011).

[65] *Electrical Resistivity of Pure Metals and Alloys*, edited by J. Bass, Landolt-Bornstein, New Series, Group III, Vol. 15, Pt. A (Springer, New York, 1982).

[66] J. Banhart, H. Ebert, P. Weinberger, and J. Voitländer, Phys. Rev. B **50**, 2104 (1994).

[67] I. Turek, J. Kudrnovský, V. Drchal, and P. Weinberger, J. Phys.: Condens. Matter **16**, S5607 (2004).

[68] C. Y. Ho, M. W. Ackerman, K. Y. Wu, T. N. Havill, R. H. Bogaard, R. A. Matula, S. G. Oh, and H. M. James, J. Phys. Chem. Ref. Data **12**, 183 (1983).

[69] S. M. Bhagat and P. Lubitz, Phys. Rev. B **10**, 179 (1974).

[70] B. Heinrich and Z. Frait, Phys. Status Solidi B **16**, 1521 (1966).

7.2. Impact of finite temperatures and correlations on the AHC

The article "Impact of finite temperatures and correlations on the anomalous Hall conductivity from ab initio theory" published in The New Journal of Physics is reprinted with permission from New J. Phys., 15, 053009 (2013); copyright 2013 IOP Publishing.

New Journal of Physics

Impact of finite temperatures and correlations on the anomalous Hall conductivity from *ab initio* theory

Diemo Ködderitzsch[1]**, Kristina Chadova, Ján Minár and Hubert Ebert**

Department Chemie, Physikalische Chemie, Universität München,
Butenandtstraße 5-13, D-81377 München, Germany
E-mail: dkopc@cup.uni-muenchen.de

Abstract.   Finite-temperature effects in the first-principles calculations of electronic transport up to now include almost exclusively only electronic temperatures by means of the Fermi-distribution function neglecting the influence of lattice vibrations. Here, employing the linear response Kubo formalism as implemented in a fully relativistic multiple-scattering Korringa–Kohn–Rostoker Green function method a systematic first-principles study of the anomalous Hall conductivity (AHC) of the 3d-transition metals Fe, Co and Ni is presented. It is shown that the inclusion of both correlations and thermal lattice vibrations is needed to give a material-specific description of the AHC in transition metals. The employed general framework will allow a first-principles description of other transverse transport phenomena treating correlations, finite temperatures and disorder on the same footing, giving valuable insights for experiments.

[1] Author to whom any correspondence should be addressed.

Contents

1. Introduction

The simple experiment by Hall [1] driving a current through a ferromagnet and observing the anomalous Hall effect (AHE) as a transverse voltage has fruitfully spurred the development of experimental and theoretical methods dealing with transport in solids. It now stands as a paradigm for understanding related transverse transport phenomena, such as e.g. the spin Hall-(SHE), anomalous- and spin-Nernst effects that have received intense interest in recent years. They all share a common origin, namely they are obviously spin–orbit-driven *relativistic* effects.

The AHE has for decades eluded theoretical understanding—it took more than 50 years for Karplus and Luttinger [2] to put forward an insight that initiated modern theories of the AHE. They identified the anomalous velocity as an interband matrix element of the current operator that is today the foundation of semiclassical approaches that give a topological formulation of the AHE in terms of the Berry phase of Bloch bands in pure crystals [3, 4]. The latter is used to define the so-called intrinsic contribution to the AHE. Already early on Smit [5, 6] and Berger [7] discussed other extrinsic origins of the AHE, namely skew- and side-jump scattering. There are extrinsic contributions to the AHE that fall in neither category [4]; however, it is now commonly established that we separate the AHE into an intrinsic and a skew-scattering contribution and declare the difference to the total AHE as side-jump scattering [8]. Experiments then rely on a scaling mechanism to extract these contributions from the raw data.

Besides a wealth of model calculations (see the review [8] and references therein) that are tailored to identify general trends but miss the material specific aspect a number of first-principles calculations building on a density-functional theory (DFT) framework have been undertaken recently to compute the anomalous Hall conductivity (AHC) in the transition metals (TMs) [9–12]. Almost all of them rely on the Berry phase formulation for pure crystals and therefore are only able to deal with the intrinsic contribution. Boltzmann transport theory-based formulations have been used in the context of the SHE [13] to compute the skew-scattering contributions in the dilute limit for alloys. Covering the whole concentration range of alloys and including all contributions to the AHE has recently been done [14, 16] on the basis of a Kubo–Středa formulation [17, 18].

The role of correlations in the electronic structure of the 3d-TM has only very recently been addressed in the context of the AHE [10, 11]. Employing the local spin-density approximation (LSDA), or generalized gradient approximation (GGA), gives unfavorable agreement with experiment, and with the AHE being a property of the Fermi surface [9, 19] it became clear that the LSDA/GGA does not supply the proper band structure. This is demonstrated, in particular, for the case of Ni (see also table 1) where the LSDA/GGA strongly overestimates the magnitude of the AHC. Employing the LSDA/GGA+U remedies this problem, by moving down d-bands relative to the Fermi energy (E_F), thereby making the X_2 hole pocket present in LSDA/GGA disappear.

Table 1. Intrinsic AHC σ_{xy} in $(\Omega\,\text{cm})^{-1}$ of the ferromagnetic TMs Fe, Co and Ni from *first-principles* theoretical (present work compared to others) as well as experimental (Exp.) studies. The magnetization has been assumed to be oriented along the [001] direction.

	bcc-Fe	hcp-Co	fcc-Co	fcc-Ni
LSDA, present work	685	325	213	−2062
LSDA + U, present work	703	390	379	−1092
LSDA/GGA	753[a],767[b]	477[a]	249[c]	−2203[a],−2200[d]
	650[e]	481[c]	360[e]	−2410[e]
LSDA + U/GGA+U		643[f]		−960[d],−900[b]
Exp.	1032[g]	813[h]		−646(@RT)[i]
				−1100(5K)[j]

[a] Wang *et al* [9].
[b] Weischenberg *et al* [10].
[c] Roman *et al* [33].
[d] Fuh and Guo [11].
[e] Turek *et al* [16].
[f] Tung *et al* [12].
[g] Dheer [34].
[h] Volkenshtein *et al* [36].
[i] Lavine [35].
[j] Ye *et al* [21].

A further important aspect of the AHE that is addressed in experimental studies but rarely in theoretical considerations is the temperature dependence of the AHE. For the pure 3d-systems, measurements of the AHE are typically done on commercially available specimens or thick layers grown on a substrate [20–22] and the temperature is changed in order to vary the resistivity. The latter makes the discussion of the temperature dependence very delicate when trying to disentangle different mechanisms and contributions to the AHE (inelastic scattering: scattering by phonons/magnons, etc). It is advocated, however, as an *empirical fact* [8, 23] that inelastic scattering processes suppress the skew scattering at higher temperatures with the intrinsic and side-jump (see however the remark above) contributions dominantly prevailing. This then again is used to experimentally analyze the AHE. Recently, model calculations [23] studied the role of inelastic scattering by phonons employing a Kubo formalism and introducing a phenomenological scattering rate γ as the imaginary part of the self-energy. To our knowledge, no first-principles approach has been used so far to deal with the temperature dependence of AHE in 3d-TMs.

In this work, we present a generally applicable formalism and results of a first-principles approach for calculating the AHC of TMs and their alloys. We show that the inclusion of both finite-temperature and correlation effects leads to a unified material-specific description of these systems.

2. Theoretical approach

As the AHE is inherently a relativistic phenomenon, we choose to work within a fully relativistic approach employing the Kohn–Sham–Dirac equation as formulated in spin-polarized DFT

4

employing the Hamiltonian

$$\mathcal{H}_{\mathrm{D}} = -\mathrm{i}\,c\vec{\alpha}\cdot\vec{\nabla} + mc^2\beta + \bar{V}_{\mathrm{KS}}(\vec{r}) + \beta\vec{\Sigma}\cdot\vec{B}_{xc}(\vec{r}) \tag{1}$$

as implemented within the multiple-scattering Korringa–Kohn–Rostoker (KKR) Green function method [24]. Here $\bar{V}_{\mathrm{KS}}$ and $\vec{B}_{xc}$ are the spin-averaged and spin-dependent part of the one-particle potential, respectively, m the electron mass, c the velocity of light and the relativistic matrices $\vec{\alpha}$, β and $\vec{\Sigma}$ have the usual meaning [25–27]. Using the fully relativistic Dirac approach has the important advantage [18] that disorder (see below) can be treated elegantly without recourse to a Pauli approach, which poses difficulties in calculating the vertex corrections (vc). To determine longitudinal and transverse components of the conductivity tensor, a natural starting point is the linear response Kubo framework that can also be used to derive the Berry phase-related semiclassical approach [3, 4, 28]. The Kubo approach has important advantages as compared to the latter. It allows one to straightforwardly include disorder, and is therefore able to describe not only pure systems but also alloys in the full concentration range including intrinsic and extrinsic contributions to the AHE [14, 16]. Further making use of an alloy-analogy model (see below), finite temperatures can be accounted for. It also allows one to include correlations beyond LSDA in the framework of LSDA + U or LSDA+DMFT (dynamical mean field theory) [29, 30]. For cubic and hexagonal systems with the magnetization pointing along the $\hat{e}_z$-direction, the AHE in the Kubo–Středa formalism is given [17, 18] by the off-diagonal tensor element $\sigma_{yx} = -\sigma_{xy}$ of

$$\sigma_{\mu\nu} = \frac{\hbar}{4\pi N\Omega}\mathrm{Trace}\,\langle \hat{j}_\mu(G^+ - G^-)\hat{j}_\nu G^- - \hat{j}_\mu G^+ \hat{j}_\nu(G^+ - G^-)\rangle_{\mathrm{c}}$$

$$+\frac{|e|}{4\pi\mathrm{i}N\Omega}\mathrm{Trace}\,\langle(G^+ - G^-)(\hat{r}_\mu\hat{j}_\nu - \hat{r}_\nu\hat{j}_\mu)\rangle_{\mathrm{c}} \tag{2}$$

with the relativistic current operator $\hat{\vec{j}} = -|e|c\vec{\alpha}$ and the electronic retarded and advanced Green functions $G^\pm$ (calculated at E_{F}) which in the framework of the presented KKR approach are given in a relativistic multiple scattering representation [24]. The angular brackets denote a configurational average that here is carried out using the coherent potential approximation (CPA), which allows one to include vc, which are of utter importance for the *quantitative* determination of both the longitudinal and transversal conductivity in alloys. As has been argued and also shown [8, 14, 16], calculations omitting the vc give the intrinsic AHC. Thereby, subtracting the latter from the AHC obtained from the value including the vc, the extrinsic part can be extracted.

Several sources of electron scattering at finite temperatures will determine the T-dependence of the AHE. We neglect the redistribution of states due to finite temperature in the electronic subsystem as well as electron–magnon interaction that can be treated as spin-disorder scattering in a pseudo-alloy as has been done recently for Pd–Fe alloys [15]. Here, we consider as a dominant effect only thermal lattice vibrations. To include the latter as a source of electron scattering, one could generalize equation (2) to finite temperatures by including the electron–phonon self-energy $\Sigma_{\mathrm{el-ph}}$ when calculating the Green function $G^\pm$. This, however, is computationally very expensive. Therefore, the consideration is restricted to elastic scattering processes by using a quasi-static representation of the thermal displacements of the atoms from their equilibrium positions as has already been used successfully by the authors in the theory of Gilbert damping [31]. Treating each displaced atom as an alloy partner, we introduce an alloy-analogy model to average over a discrete set of displacements that is chosen to reproduce
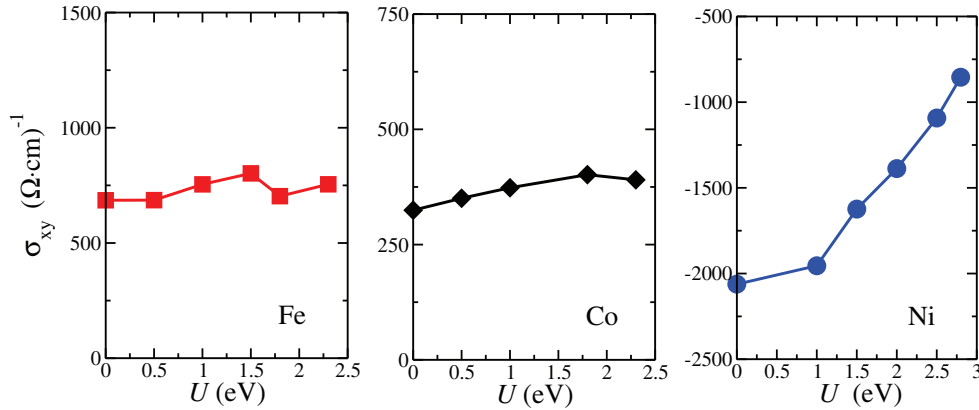
Figure 1. Dependence of the AHC ($T = 0\,\mathrm{K}$) for bcc-Fe (left), hcp-Co (middle) and fcc-Ni (right) as a function of the U-value in the LSDA + U calculation.

the thermal root mean square average displacement $\sqrt{\langle u^2 \rangle_T}$ for a given temperature T. This was chosen according to $\langle u^2 \rangle_T = \frac{3\hbar^2}{mk\Theta_D}[\frac{\Phi(\Theta_D/T)}{\Theta_D/T} + \frac{1}{4}]$ with $\Phi(\Theta_D/T)$ the Debye function, $\hbar$ the reduced Planck constant, k the Boltzmann constant and Θ_D the Debye temperature [32]. Ignoring the zero temperature term and assuming a frozen potential for the atoms, the situation can be dealt with in full analogy to the treatment of disordered alloys using the CPA.

To study the impact of correlations (beyond LSDA), we employed an implementation of the LSDA+DMFT framework into the KKR [30] and obtained the LSDA + U by retaining the static part of the self-energy. Around mean field double counting corrections have been used. The chosen values for U and J are commonly used in the description of 3d-TMs.

3. Results and discussion

We performed LSDA as well as LSDA + U calculations of the AHC of 3d-TMs. The LSDA + U calculations were performed keeping $J = 0.9\,\mathrm{eV}$ fixed and scanning the U-range up to typical values employed for the 3d-TMs. In figure 1 the dependence of the intrinsic AHE at $T = 0\,\mathrm{K}$ for bcc-Fe, hcp-Co and fcc-Ni is shown. Whereas for Fe and Co only small variations of the AHC are observed, a pronounced U-dependence for Ni is seen with the experimentally extracted intrinsic value of $-1100\,\mathrm{S\,cm^{-1}}$ recovered at a U-value of around 2.5 eV (this value is also used in calculation of the T-dependence below). Analysis shows that this is due to a downshift of minority 3d-bands w.r.t. E_F and a vanishing hole pocket at the X_2 point, as has already been recently discussed [11]. In table 1, we show the calculated values for Fe ($U = 1.8\,\mathrm{eV}$), Co (hcp and fcc, $U = 2.3\,\mathrm{eV}$) and Ni ($U = 2.5\,\mathrm{eV}$) in comparison with other calculations as well as experiment. (Note that in our previous calculation [14], we obtained for Ni a value of $-1635\,\mathrm{S\,cm^{-1}}$, which deviates by 20% from the value reported here. This was due to an inappropriate small setting for the muffin-tin radii r_{MT} (i.e. no touching spheres) used in the calculations which employ the atomic-sphere approximation (ASA, r_{ASA}) for the potential construction. The muffin-tin zero in the KKR calculation is obtained by averaging over the area between r_{MT} and r_{ASA}. For Ni it turns out that the AHC is very sensitive to such an inappropriate setting. We checked this issue for Fe and Co and found no such sensitivity, i.e. shrinking r_{MT}

Table 2. Spin- and orbital-magnetic moments in μ_B for the 3d-TMs at $T = 0$ K as calculated in LSDA and LSDA + U (using the U- and J-values mentioned in the text).

	bcc-Fe	hcp-Co	fcc-Co	fcc-Ni
LSDA, spin	2.26	1.60	1.64	0.64
LSDA + U, spin	2.21	1.61	1.66	0.65
LSDA, orbital	0.05	0.08	0.08	0.05
LSDA + U, orbital	0.13	0.12	0.22	0.08
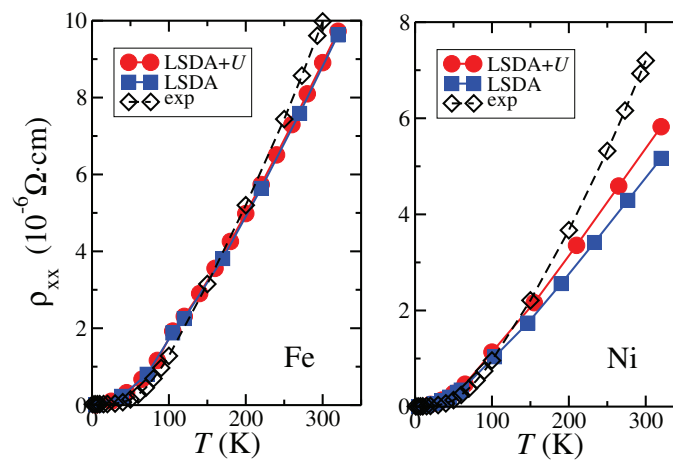
Figure 2. Temperature dependence of the longitudinal resistivity ρ_{xx} of Fe (left) and Ni (right) as calculated in LSDA and LSDA + U compared to experiment [40].

by 5% only changed the AHC values by at most 2%.) In addition, we report the spin- and orbital-magnetic moments of the 3d-TMs calculated in LSDA and LSAD + U in table 2.

Another important aspect is the temperature dependence of the transverse AHC. To assess in a first step the validity of the presented approach to deal with thermal lattice displacements, the longitudinal resistivities were calculated for the 3d-TMs making use of the Kubo–Greenwood expression for the symmetric part of the conductivity tensor [37–39]. The results for ρ_{xx} are shown in figure 2 and compared with experimental data taken from the literature. As can be seen, the agreement is rather good. Therefore, we expect the aforementioned framework to be a reasonable approximation to properly describe electron–phonon scattering and the temperature dependence of the AHE (Note that deviation from the experimental data becomes larger in the high-temperature range. This could be attributed to the effect of spin disorder, which however has been neglected in the current study. In particular, Ni shows a larger deviation which might be due to the fact that it has a smaller Curie temperature resulting in a stronger effect of the spin disorder.)

Early measurements of the AHE in Ni report a value of -646 S cm^{-1} at room temperature [35]. Recent experimental work [21] analyzed this in more detail claiming the AHE to consist of an intrinsic component of about -1100 S cm^{-1} and a sizable skew-scattering contribution at low temperatures, which both diminish at higher temperatures albeit with

7
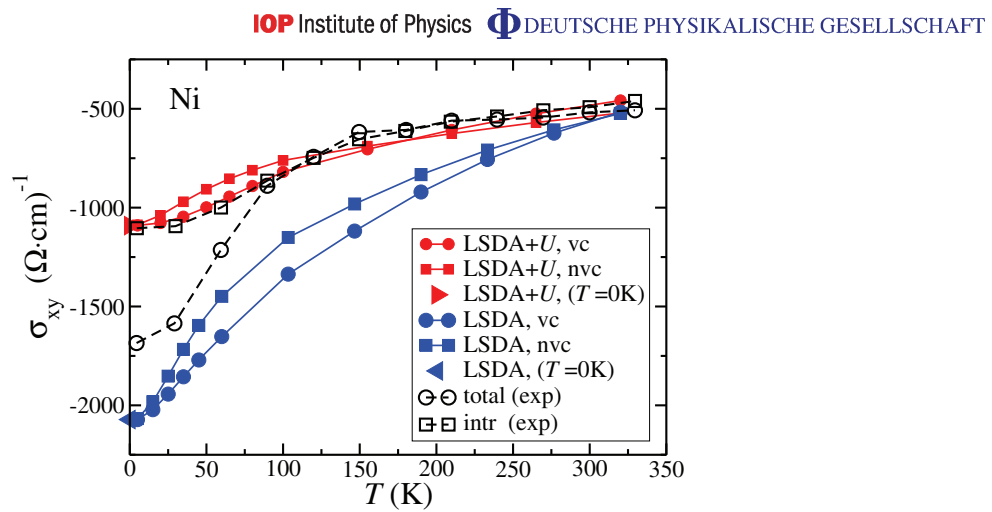
Figure 3. Temperature dependence of the AHC of Ni. Shown are theoretical results obtained by LSDA and LSDA + U both including (vc) and excluding (nvc) vertex corrections and experimental data [21]. Triangle symbols denote the zero temperature intrinsic AHE values for LSDA and LSDA + U, respectively.
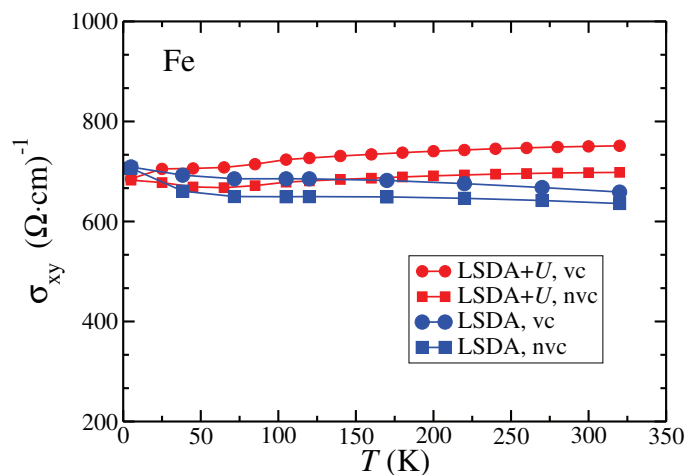
Figure 4. Temperature dependence of the AHC of Fe as calculated in LSDA and LSDA + U.

different rates. In figure 3 the calculated temperature dependence of the AHE in Ni using LSDA and LSDA + U ($U = 2.5$, $J = 0.9$ eV) as well as experimental results [21] are shown. As could be expected from the above, the LSDA result strongly overestimates the magnitude over the whole temperature range, whereas LSDA + U fairly well reproduces the experimental result. This demonstrates that both correlations beyond LSDA as well as temperature-induced thermal vibrations combined need to be taken into account. The vc due to the lattice vibrations have little impact in the low-T regime and are negligible at higher temperatures such that, as seen in experiment, the intrinsic contribution survives. We attribute the deviation from the total AHC in the low-T range to possible impurities that might be present in the sample. In contrast to Ni, the temperature dependence in Fe (see figure 4) is found to be small.

8

IOP Institute of Physics   Φ DEUTSCHE PHYSIKALISCHE GESELLSCHAFT
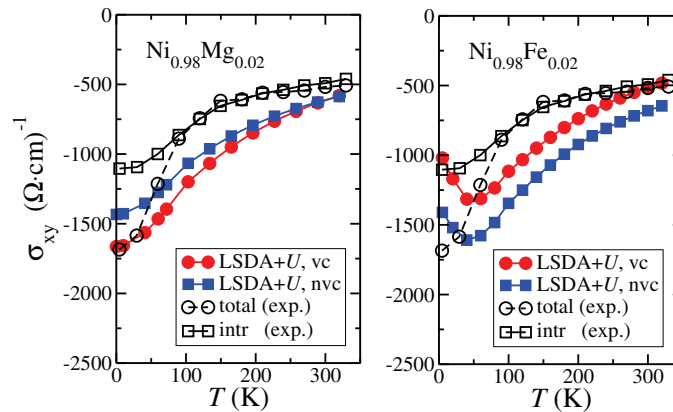
Figure 5. Temperature dependence of the AHC of $Ni_{0.98}Mg_{0.02}$ (left) and $Ni_{0.98}Fe_{0.02}$ (right) as calculated in LSDA $+ U$ compared to experiment [21].

In the context of both the SHE and the AHE [13, 14, 41, 42], it has already been shown that in the dilute/super-clean limit large skew-scattering contributions can arise with the AHC scaling as $\sigma_{xy} \propto \sigma_{xx}$. To demonstrate this and put it in the context of the recent experiment by Ye *et al* [21], we performed calculations for Mg impurities and Fe impurities in Ni, employing the CPA for both the impurities and the thermal lattice vibrations. As can be seen in figure 5, the calculated full AHC (including vc) approaches the experimental curve for higher temperatures. However in the low-temperature regime, larger deviations are visible. Taking the difference between the calculation with vc and that without vc (intrinsic values), one also observes that the impurity-induced extrinsic contribution for Mg shows the same sign as seen in experiment, i.e. it increases the absolute value, whereas for Fe impurities the opposite behavior is seen. This highlights again the fact that the skew-scattering component in an impurity-specific way determines the quantitative low-temperature behavior of the AHC in clean 3d-metals but also that the experimental determination of 'clean' systems is extremely challenging.

In summary, we have used the linear response Kubo formalism as implemented in a fully relativistic multiple-scattering KKR Green function method to study systematically from first principles the AHC of the 3d-TMs Fe, Co and Ni. Going beyond the LSDA in DFT employing the LSDA $+ U$ and including finite temperatures by using a CPA-alloy analogy for the lattice displacements provided the necessary means to allow for a material-specific description of the AHC. Further, the impact of dilute impurities has been analyzed. The presented framework is now ready to be applied to the whole concentration range of correlated TM-alloys. Treating correlations beyond the static limit (LSDA $+ U$) of the LSDA+DMFT combined with a linear response transport formalism is a major issue for future work. Further, the developed method is straightforwardly applicable to a number of related transverse transport phenomena, e.g. the spin Hall- and spincaloric effects such as the anomalous- and spin-Nernst effects [41, 43, 44].

9

References

[1] Hall E H 1881 *Phil. Mag.* **12** 157
[2] Karplus R and Luttinger J M 1954 *Phys. Rev.* **95** 1154
[3] Jungwirth T, Niu Q and MacDonald A H 2002 *Phys. Rev. Lett.* **88** 207208
[4] Sinitsyn N A 2008 *J. Phys.: Condens. Matter* **20** 023201
[5] Smit J 1955 *Physica* **21** 877
[6] Smit J 1958 *Physica* **24** 39
[7] Berger L 1970 *Phys. Rev.* B **2** 4559
[8] Nagaosa N, Sinova J, Onoda S, MacDonald A H and Ong N P 2010 *Rev. Mod. Phys.* **82** 1539
[9] Wang X, Vanderbilt D, Yates J R and Souza I 2007 *Phys. Rev.* B **76** 195109
[10] Weischenberg J, Freimuth F, Sinova J, Blügel S and Mokrousov Y 2011 *Phys. Rev. Lett.* **107** 106601
[11] Fuh H R and Guo G Y 2011 *Phys. Rev.* B **84** 144427
[12] Tung J C, Fuh H R and Guo G Y 2012 *Phys. Rev.* B **86** 024435
[13] Gradhand M, Fedorov D V, Zahn P and Mertig I 2010 *Phys. Rev. Lett.* **104** 186403
[14] Lowitzer S, Ködderitzsch D and Ebert H 2010 *Phys. Rev. Lett.* **105** 266604
[15] Kudrnovský J, Drchal V, Khmelevskyi S and Turek I 2011 *Phys. Rev.* B **84** 214436
[16] Turek I, Kudrnovský J and Drchal V 2012 *Phys. Rev.* B **86** 014405
[17] Středa P 1982 *J. Phys. C: Solid State Phys.* **15** L717
[18] Crépieux A and Bruno P 2001 *Phys. Rev.* B **64** 014416
[19] Haldane F D M 2004 *Phys. Rev. Lett.* **93** 206602
[20] Miyasato T, Abe N, Fujii T, Asamitsu A, Onoda S, Onose Y, Nagaosa N and Tokura Y 2007 *Phys. Rev. Lett.*
99 086602
[21] Ye L, Tian Y, Jin X and Xiao D 2012 *Phys. Rev.* B **85** 220403
[22] Shiomi Y, Onose Y and Tokura Y 2009 *Phys. Rev.* B **79** 100404
[23] Shitade A and Nagaosa N 2012 *J. Phys. Soc. Japan* **81** 083704
[24] Ebert H, Ködderitzsch D and Minár J 2011 *Rep. Prog. Phys.* **74** 096501
[25] Rose M E 1957 *Elementary Theory of Angular Momentum* (New York: Wiley)
[26] Rose M E 1961 *Relativistic Electron Theory* (New York: Wiley)
[27] Eschrig H 1996 *The Fundamentals of Density Functional Theory* (Stuttgart: B G Teubner Verlagsgesellschaft)
[28] Sinitsyn N A, MacDonald A H, Jungwirth T, Dugaev V K and Sinova J 2007 *Phys. Rev.* B **75** 045315
[29] Minár J, Chioncel L, Perlov A, Ebert H, Katsnelson M I and Lichtenstein A I 2005 *Phys. Rev.* B **72** 045125
[30] Minár J 2011 *J. Phys.: Condens. Matter* **23** 253201
[31] Ebert H, Mankovsky S, Ködderitzsch D and Kelly P J 2011 *Phys. Rev. Lett.* **107** 066603
[32] Gololobov E M, Mager E L, Mezhevich Z V and Pan L K 1983 *Phys. Status Solidi* b **119** K139
[33] Roman E, Mokrousov Y and Souza I 2009 *Phys. Rev. Lett.* **103** 097203
[34] Dheer P N 1967 *Phys. Rev.* **156** 637
[35] Lavine J M 1961 *Phys. Rev.* **123** 1273
[36] Volkenshtein N V, Fedorov G V and Shirokovskii V P 1961 *Fiz. Met. Metalloved.* **11** 152
[37] Büttiker M 1986 *Phys. Rev. Lett.* **57** 1761
[38] Banhart J, Bernstein R, Voitländer J and Weinberger P 1991 *Solid State Commun.* **77** 107
[39] Banhart J, Ebert H, Weinberger P and Voitländer J 1994 *Phys. Rev.* B **50** 2104
[40] Ho C Y, Ackerman M W, Wu K Y, Havill T N, Bogaard R H, Matula R A, Oh S G and James H M 1983
J. Phys. Chem. Data **12** 183
[41] Onoda S, Sugimoto N and Nagaosa N 2008 *Phys. Rev.* B **77** 165103
[42] Lowitzer S, Gradhand M, Ködderitzsch D, Fedorov D V, Mertig I and Ebert H 2011 *Phys. Rev. Lett.*
106 056601
[43] Pu Y, Chiba D, Matsukura F, Ohno H and Shi J 2008 *Phys. Rev. Lett.* **101** 117208
[44] Tauber K, Gradhand M, Fedorov D V and Mertig I 2012 *Phys. Rev. Lett.* **109** 026601

7.3. Impact of finite temperatures on the transport properties of Gd

_

Impact of finite temperatures on the transport properties of Gd from first principles

K. Chadova,[1,*] S. Mankovsky,[1] J. Minár,[1,2] and H. Ebert[1]

[1]*Department Chemie, Ludwig-Maximilian-University Munich, Butenandtstrasse 5-13, 81377 Munich, Germany*
[2]*New Technologies-Research Center, University of West Bohemia, Univerzitni 8, 306 14 Pilsen, Czech Republic*

Finite-temperature effects have a pronounced impact on the transport properties of solids. In magnetic systems, besides the scattering of conduction electrons by impurities and phonons, an additional scattering source coming from the magnetic degrees of freedom must be taken into account. A first-principle scheme which treats all these scattering effects on equal footing was recently suggested within the framework of the multiple scattering formalism. Employing the alloy analogy model treated by means of the CPA, thermal lattice vibrations and spin fluctuations are effectively taken into account. In the present work the temperature dependence of the longitudinal resistivity and the anomalous Hall effect in the strongly correlated metal Gd is considered. The comparison with experiments demonstrates that the proposed numerical scheme does provide an adequate description of the electronic transport at finite temperatures.

I. INTRODUCTION

Rare-earth elements may exhibit both ferromagnetic or antiferromagnetic order in certain temperature regimes. Nowadays, it is commonly accepted that Gd, having the hcp structure, possesses a simple ferromagnetic (FM) order up to its Curie temperature T_c. However, in early experimental studies a helical magnetic structure was observed in polycrystalline Gd in the temperature range between 210 and 290 K [1]. Such a helical spin configuration is easily destroyed by a weak magnetic field [1], leading to a collinear magnetic structure in the system. This means that only in the absence of an applied magnetic fields can this type of antiferromagnetism be observed. Recent experiments on single crystals of Gd did not reveal any anomalies in the low-field magnetization curves and confirm that Gd has a normal ferromagnetic structure up to its Curie temperature [2,3]. The Curie temperature determined experimentally was found to be 289 K with a saturated magnetic moment of $7.12\mu_B$ [4]. In another experimental study the Curie temperature was determined to be 293.2 K with an absolute saturation moment of $7.55\mu_B$ [5]. Although Gd behaves like a simple ferromagnet it has nevertheless a rather complex temperature dependence of its magnetization: as the temperature decreases to 230 a spin-reorientation occurs from the magnetization parallel to the c axis to the magnetization tilted by 30° with respect to the c axis, reaching its maximum tilt angle of 60° at around $T = 180$ K [2]. Such a behavior is quite demanding concerning an adequate theoretical description. Therefore, in the present work the direction of the magnetization is taken along the c axis unless it is mentioned otherwise.

It is well established that the magnetism in Gd is dominated by f electrons with a magnetic moment of $7\mu_B$ due to half filling of the highly localized $4f$ states. The observed excessive magnetic moment is attributed to the valence $5d6sp$ band exhibiting spin polarization due to the strong exchange field created by the $4f$ electrons [6], as is extensively discussed in the literature [7–11]. In particular, these discussions concern

the finite-temperature behavior of the magnetic moment of the valence electrons [12] observed experimentally. In earlier discussions it has been suggested to treat these on the basis of the Stoner model [13]. Recent investigations by experiment [9,14,15] as well as theory [10,11,16] based on first-principles calculations clearly demonstrate the finite exchange spitting of valence states above the Curie temperature despite the vanishing total magnetization, which implies a much more complicated picture of interactions than provided by the simple Stoner model.

The rather different origin of the spin magnetic moment for the f and $5d6sp$ electrons leads also to a different dynamical behavior characterized in general by a different magnetization dissipation rate. This would imply separate spin dynamics equations for f and $5d6sp$ spin magnetic moments coupled via the exchange interactions, as was considered in particular in Gilbert damping calculations by Seib and Fähnle [17]. The authors, however, point out that the common equation for all types of spin moments can be used in the limit of slow magnetization dynamics [18], which also allows us to use a common Gilbert damping parameter calculated within the adiabatic approximation.

It is well known that, in magnetic systems, the electrical resistivity is caused by electron scattering by various magnetic inhomogeneities in addition to the electron-phonon scattering as well as scattering by impurities and other structural defects. The latter contribution is responsible for the so-called residual resistivity observed in the zero-temperature limit. The resistivity part due to the phonon mechanism shows usually a T^5 behavior at low temperatures and varies linearly with T above the Debye temperature T_D. This behavior can be described on the *ab initio* level and corresponding studies on transition metals [19] lead in general to good agreement with experimental data. In the present study not only the linear dependence was obtained in the temperature region $T > T_D$ but it was found also well below T_D. A theoretical description of the resistivity caused by thermal spin-fluctuation effects was first given on the basis of the s-d (in rare earth d-f) model Hamiltonian [20–22]. This approach suggests a T^2 dependence in the low-temperature limit and an almost constant resistivity above the Curie temperature. In the intermediate-temperature

———————
*kchpc@cup.uni-muenchen.de

regime the T dependence of the resistivity is expected to be rather complex. Recent *ab initio* calculations of the paramagnetic spin-disorder resistivity for a number of transition metals and their alloys as well as rare-earth metals are based on two alternative approaches: the disordered local moment approach using the coherent-potential approximation (CPA) formalism and averaging the Landauer-Büttiker conductance of a supercell over the random noncollinear spin-disorder configurations, with both leading in general to good agreement with experimental values [10,23]. However, for a quantitative description of the temperature-dependent electrical resistivity from first principles one needs to combine the influence of lattice vibrations and spin fluctuations, which is a nontrivial task. Therefore, certain approximations are required to reach this goal.

During the last years, the anomalous Hall effect (AHE) and its dependence on the temperature attracts also much attention. In the case of Gd, a number of theoretical investigations have been performed to explain the unexpectedly large AHE observed experimentally [24]. Previously, these studies were performed on a model level. An earlier description of the AHE of Gd was based on the uniform electron gas model accounting for spin-orbit coupling effects leading, in turn, to an asymmetry in the scattering process (skew-scattering mechanism) [25]. However, due to the high localization the electrons giving rise to the magnetic moment are unable to participate in conduction; therefore this model is not appropriate to describe the AHE in rare-earth systems. The model developed by Kondo [26] was based on the *s*-*d* (*s*-*f*) interaction leading to a scattering of the conduction electrons by the thermally induced spin moment tilting. In this model the necessary asymmetry is due to the intrinsic spin-orbit coupling of the *f* electrons. Therefore, the Hamiltonian describing the interaction of the conduction and the localized electrons is valid when the orbital angular moment of localized electrons remains unquenched. This is not the case for Gd and therefore it cannot be used to describe the AHE in this metal. Another model which eliminated the above-mentioned constraint was developed by Maranzana [27] and is based on Kondo's model. In this model the skew-scattering mechanism originates from the interaction between the localized spin moment and the orbital momentum of the conduction electron.

Within the discussed models the large AHE in Gd was ascribed solely to the skew-scattering contribution. Another scattering mechanism, the so-called side-jump mechanism, first introduced by Berger [28,29], was accounted within a model suggested by Fert [30]. It was demonstrated, particularly for Gd, that the side-jump contribution is equally important as the skew-scattering mechanism and should be taken into account as well.

In this paper, we discuss the impact of finite temperatures, taking into account thermal lattice vibrations and spin fluctuations, on the transport properties in Gd from first principles by making use of the alloy analogy model [31].

II. COMPUTATIONAL DETAILS

The electronic structure calculations are based on the Korringa–Kohn–Rostoker (KKR) Green's function method [32] implemented in the fully relativistic spin-

polarized Munich SPR-KKR package with angular-momentum cutoff $l_{max} = 4$. A full four-component Dirac formalism is employed to describe the electronic structure within Kohn–Sham–Dirac density functional theory [33]. For *spd* electrons the local density approximation was used with the parametrization given by Vosko *et al.* [34]. To treat the highly correlated $4f$ states the local spin-density approximation $+ U$ (LSDA+U) method was used with the double counting part of the LSDA+U functional evaluated within the so-called atomic limit expression [35]. The temperature effects are treated within the alloy analogy scheme based on the CPA alloy theory [36–38], and assuming a frozen potential for the atoms [31]. For the description of the magnetic spin fluctuations the temperature-dependent magnetization data were taken from experiment [5]. The calculation of the transport properties of Gd is based on the Kubo–Středa formalism, with the corresponding expression for the conductivity given by

$$\sigma_{\mu\nu} = \frac{\hbar}{4\pi N\Omega} \text{Tr}\langle \hat{j}_\mu(G^+ - G^-)\hat{j}_\nu G^- - \hat{j}_\mu G^+ \hat{j}_\nu(G^+ - G^-)\rangle_c$$
$$+ \frac{|e|}{4\pi i N\Omega} \text{Tr}\langle(G^+ - G^-)(\hat{r}_\mu \hat{j}_\nu - \hat{r}_\nu \hat{j}_\mu)\rangle_c, \quad (1)$$

with the relativistic current operator $\hat{\mathbf{j}} = -|e|c\alpha$ and the electronic retarded and advanced Green's functions $G^\pm$ evaluated at the Fermi energy E_F by means of the relativistic multiple scattering or KKR formalism [32]. The angular brackets denote a configurational average which here is carried out using the coherent-potential approximation (CPA) which takes into account the so-called vertex corrections (VCs) [37]. In the last equation, N is the number of sites and Ω is the volume of the unit cell. As was justified by previous work [39] the second term in the Eq. (1) has been omitted.

The Gilbert damping parameter [40,41] was calculated within the linear-response theory using the Kubo–Greenwood-like equation:

$$\alpha_{\mu\nu} = -\frac{\hbar\gamma}{\pi M_s} \text{Tr}\langle \hat{T}_\mu \text{Im} G^+ \hat{T}_\nu \text{Im} G^+ \rangle_c, \quad (2)$$

where M_s is the saturation magnetization, γ is the gyromagnetic ratio, and $\hat{T}_\mu$ is the torque operator [41].

III. RESULTS

A. Electronic structure

The electronic structure of Gd has been calculated by using the experimental lattice parameters $a = 3.629$ Å, $c/a = 1.597$. As was mentioned above, the $4f$ electrons have been treated as the valence electrons with correlations described within the LSDA $+ U$ scheme with the Coulomb parameter $U = 6$ eV and the exchange parameter $J = 0.9$ eV.

The spin magnetic moment obtained in the calculations for $T = 0$ K equals to $7.63\mu_B$ and accordingly is in a good agreement with the experimental saturated magnetic moment of $7.55\mu_B$ per atom [5]. The dominating contribution of $7\mu_B$ is associated with the f electrons, while the excessive spin magnetic moment of $0.63\mu_B$ is a result of the exchange splitting for the $5d6s6p$ electrons due to a strong exchange field produced by the f electrons, as was discussed previously [6,11,12]. The persistence or vanishing of the exchange splitting with
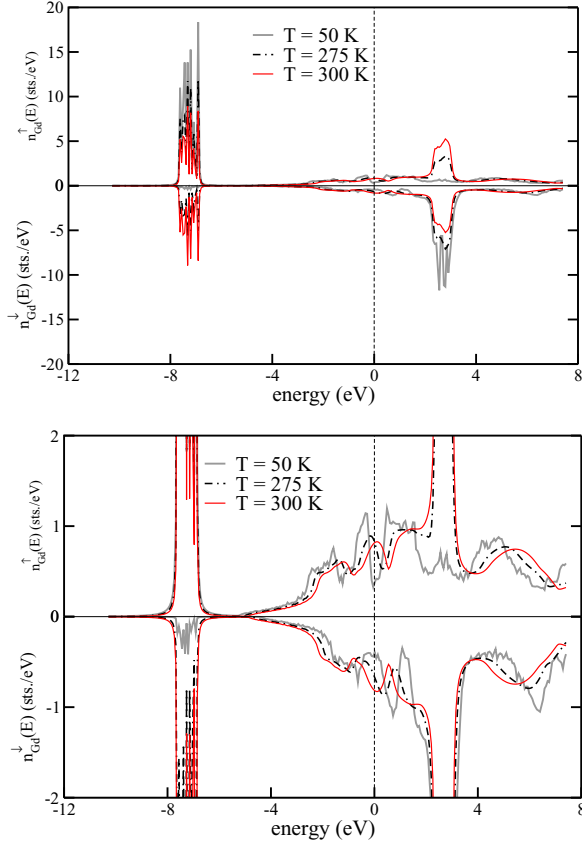
FIG. 1. Spin-resolved DOS of Gd for various temperatures. Bottom panel shows magnified area.
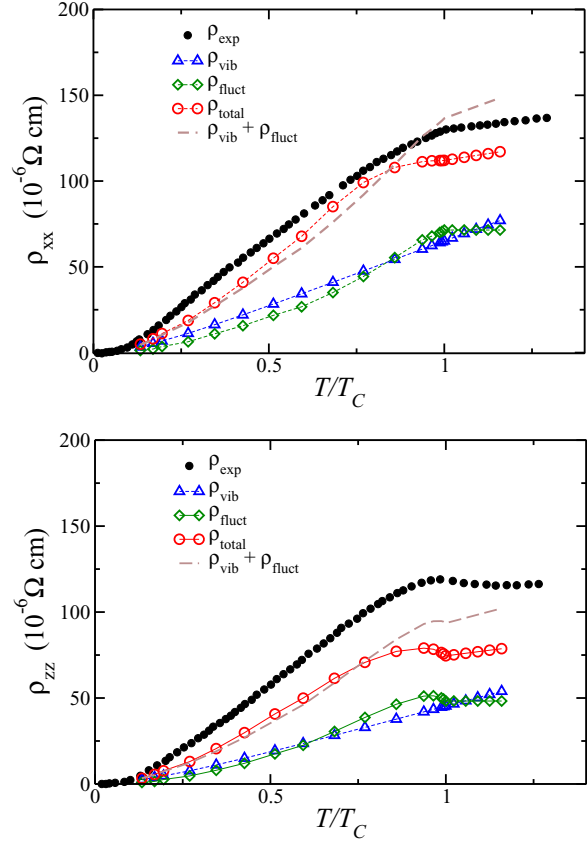

FIG. 2. Temperature-dependent electrical resistivity: (top) in-plane, (bottom) out-of-plane components. Black solid circles show experimental results [5], empty blue triangles show only thermal lattice vibrations, empty green diamonds show only spin fluctuations, empty red circles show total resistivity including both effects simultaneously, and brown dashed line corresponds to the sum of individual contributions.

increasing temperature is a matter of debate both in theory and experiment. Several experimental reports indicate that it collapses approaching the Curie temperature [7], while others demonstrate that the exchange splitting persists even in the paramagnetic state [9,42]. The spin-resolved total density of states (DOS) calculated in the global frame of reference with the quantization axis along the average magnetization at finite temperatures is represented in Fig. 1. Obviously, a temperature increase results in changes of the majority and minority spin DOS due to the spin mixing caused by the thermal spin fluctuations. This leads to the same DOS for both spin directions at $T > T_c$. The energy positions of the f states are almost unchanged in the whole temperature region. However, the exchange splitting of the spin-up and spin-down $5d6s6p$ states (having the main contribution to the DOS at the energies around E_F) decreases (as it depends on the average magnetization of the system) with increasing temperature. In particular, this results in an increase of the DOS at the Fermi level in the paramagnetic state.

B. Electrical resistivity

One of the central transport properties of metallic systems is their electrical resistivity. The experimentally measured

temperature-dependent resistivity of Gd exhibits an anisotropy with different magnitudes along the hexagonal axis (ρ_{zz}) and in the basal plane (ρ_{xx}) [5] (see Fig. 2). Both $\rho(T)$ curves are characterized by an abrupt slope change close to the Curie temperature.

In addition to the total $\rho(T)$ values, we investigated its temperature dependence caused only by lattice vibrations (vib) or only by magnetic fluctuations (fluct), which appear to be of comparable magnitude. From this one has to conclude that these sources of the temperature-dependent resistivity are additive only in the case of weak disorder (low temperatures), which does not hold when approaching the Curie temperature (strong disorder) [43]. In this regime they must be taken into account simultaneously, since only then the overall behavior of the resistivity curves agrees well with experiment. This allows us to conclude that the maximum of the experimental ρ_{zz} (close to the Curie temperature) is not a result of short-range magnetic order as was suggested in earlier literature [5], since the present calculations are based on the single-site CPA. The present
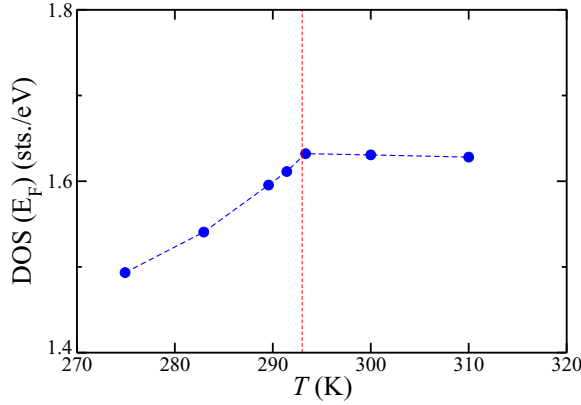
FIG. 3. Total DOS at the Fermi level depending on the temperature.

results suggest its origin as a combination of two competitive mechanisms. On the one hand, thermally induced disorder grows, leading to a resistivity increase and, on the other hand, the effective DOS around E_F relevant for the conductivity increases with increasing $T < T_c$ (Fig. 3), which effectively reduces the resistivity.

While the calculated resistivities agree with the experiment rather well, there is a quantitative underestimation (see Fig. 2). This can have various sources. One could be the so-called "'frozen-potential" approximation used in the present calculations. This approach allows us to account for the most significant contributions to the resistivity, but it neglects the changes in the local magnetic moments with increasing temperature. Nevertheless, as the Gd local magnetic moment is rather robust and does not depend essentially on the temperature, this approximation seems to be well justified. A second reason, which is more crucial for ρ_{zz}, might be the neglect of the anisotropy of the thermal atomic displacements. A third source for discrepancy may be the use of the single-site approximation by the CPA, which neglects the coherent scattering or interference effects which might show up in multiple scattering.

C. Anomalous Hall effect

As was already mentioned, Gd shows a rather large AHE, which is well described within a model that accounts at the same time for skew-scattering and side-jump mechanisms [30]. However, within this model only electron scattering by thermally induced spin fluctuations is discussed, while the contribution from the electron-phonon mechanism is completely neglected. Within the present calculations both contributions are taken into account. The resulting total anomalous Hall resistivity can be seen in Fig. 4 (top panel) in comparison with experimental results (for polycrystalline samples as well as single crystals) and the theoretical result obtained on the basis of model calculations by Fert [30]. One can see that the anomalous Hall resistivity shows a pronounced temperature dependence: the resistivity increases from zero at $T = 0$ K to a maximum value just below the Curie temperature and then drops to zero as the magnetization vanishes with further
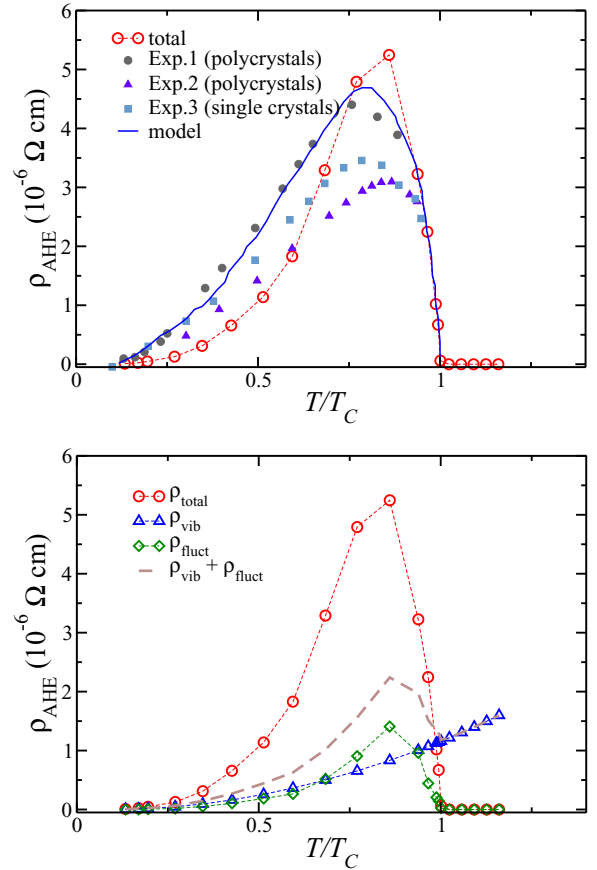
FIG. 4. Anomalous Hall resistivity depending on the temperature: Top panel compares with experimental results (Exp.1 [44], Exp.2 [44], Exp.3 [45,46]) and results from model calculations [30]. Bottom panel shows individual contributions. Empty blue triangles show only thermal lattice vibrations, empty green diamonds show only spin fluctuations, empty red circles show total resistivity including both effects simultaneously, brown dashed line corresponds to the sum of individual contributions.

increasing temperature. Overall there is a qualitative and quantitative agreement of our first-principles results with experiment as well as with the model calculations. In Fig. 4 (bottom panel) the individual contributions arising from the scattering by the lattice vibrations and spin fluctuations are shown. One can see that both mechanisms provide contributions nearly of the same order of magnitude. The qualitative behavior of the total AHR is determined by the scattering due to spin disorder, while the contribution due to lattice vibrations shows, as expected, a monotonic increase with temperature. It is interesting to compare the sum of the individual contributions with the total AHR. From Fig. 4 (bottom panel) one can see that the total AHR significantly exceeds the sum of these contributions. Therefore for the correct description of the total AHR it is necessary to account simultaneously for the combination of scattering due to the thermal lattice vibrations and spin fluctuations.
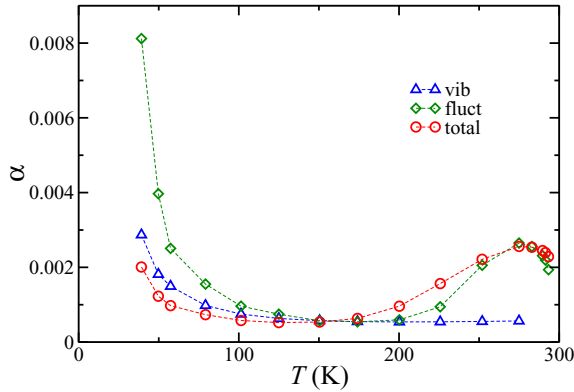
FIG. 5. Gilbert damping parameter in Gd represented as a function of temperature. Empty blue triangles show only thermal lattice vibrations, empty green diamonds show only spin fluctuations, empty red circles show total resistivity including both effects simultaneously.

Comparing the calculated anomalous Hall resistivity with experimental data, one notices that the discrepancy is more pronounced at low temperatures and nearly nonexistent as we approach T_C (see Fig. 4). On one hand, the spread of experimental data is rather large. It would be helpful to have more reliable experimental data to better reveal any systematics in the discrepancies. On the other hand, the discrepancies are connected, of course, to the approximations used in the calculations, which were discussed in the previous section.

D. Gilbert damping

Nowadays, much attention is payed to the ultrafast magnetization dynamics in various materials, including Gd as an important example of rare-earth materials. At the same time, in case of Gd there is a lack of studies, both theoretical and experimental, particularly dealing with the dissipation channels in the slow magnetization dynamics regime. Our work is meant to fill this gap on the theory side.

In the present work, the Gilbert damping parameter for Gd has been calculated in the limit of slow magnetization dynamics [18]. It describes the magnetization dissipation for the whole system, accounting for f-like and $5d6sp$-like spin magnetic moments characterized by their slow simultaneous coherent motion. The corresponding results of calculations of the Gilbert damping as a function of temperature up to the Curie temperature are shown in Fig. 5. The separate contributions due to thermal lattice vibrations and spin fluctuations are shown together with the curve accounting for both sources simultaneously. One can see a monotonic decrease of the Gilbert damping due to electron-phonon scattering with rising temperature. On the other hand, the curve representing the effect of the electron scattering due to thermal spin fluctuations exhibits a decrease in the low-temperature region due to the dominating breathing Fermi-surface dissipation mechanism, while above 150 K the increase of the Gilbert damping is determined by the increase of thermal magnetic disorder leading to magnetization

dynamics due to electron scattering events accompanied by spin-flip electron transitions. However, approaching the Curie temperature, the Gilbert damping reaches a maximum at 275 K with a following decrease up to the Curie temperature. This behavior correlates with the temperature-dependent behavior of the resistivity $\rho_{zz}(T)$ and can be associated with the decrease of probability of spin-flip scattering of transport electrons caused by a modification of the electronic structure discussed above. A similar nonmonotonic behavior has been found for the temperature dependence of the total Gilbert damping.

IV. CONCLUSIONS

In summary, we have studied the transport properties in the highly correlated system Gd from first principles. The electron-electron correlation effects were approximately accounted for by using the LSDA+U approach, resulting in an adequate description of the electronic structure. In turn, it enables a proper physical description of the transport properties. In this contribution we discussed the impact of finite temperatures (including the impact of thermal lattice vibrations and spin fluctuations) on the electrical resistivity as well as on the anomalous Hall resistivity. The applied approach based on the single-site CPA describing thermal lattice vibrations and spin fluctuations allows us to analyze individual contributions to the longitudinal and transverse resistivities arising due to these mechanisms. In both cases it turned out that, in order to obtain reasonable agreement with experimental data, it is necessary to account for a combination of the contributions connected with the phonon scattering and scattering by spin disorder because the simple sum of these contributions, especially for the AHR, significantly deviates from experiment. In the case of the longitudinal resistivity a slight anisotropy was observed which is in agreement with experimental results. For the out-of-plane resistivity a small experimentally detected maximum in the vicinity of the Curie temperature was fully reproduced. The emergence of this maximum according to experimental findings was attributed so far to the magnetic short-range-order effect. However, in the present calculations such an ordering was completely neglected because the distribution of the spin magnetic moments are considered absolutely random. Accordingly, the origin of this maximum is solely due to spin disorder.

In case of the AHR a small anisotropy was observed as well. The calculated temperature-dependent AHR with magnetization pointing along the c axis agrees surprisingly well with the experimental data. The maximum occurred just below the Curie temperature and the further abrupt drop is well reproduced.

K. CHADOVA, S. MANKOVSKY, J. MINÁR, AND H. EBERT

[1] K. P. Belov and A. V. Ped'ko, Sov. Phys. JETP **15**, 62 (1962).

[2] K. Knöpfle and L. M. Sandratskii, Phys. Rev. B **63**, 014411 (2000).

[3] G. Will, R. Nathans, and H. A. Alperin, J. Appl. Phys. **35**, 1045 (1964).

[4] J. F. Elliott, S. Legvold, and F. H. Spedding, Phys. Rev. **91**, 28 (1953).

[5] H. E. Nigh, S. Legvold, and F. H. Spedding, Phys. Rev. **132**, 1092 (1963).

[6] L. W. Roeland, G. J. Cock, F. A. Muller, A. C. Moleman, K. A. McEwen, R. G. Jordan, and D. W. Jones, J. Phys. F: Met. Phys. **5**, L233 (1975).

[7] B. Kim, A. B. Andrews, J. L. Erskine, K. J. Kim, and B. N. Harmon, Phys. Rev. Lett. **68**, 1931 (1992).

[8] E. Weschke, C. Schüssler-Langeheine, R. Meier, A. V. Fedorov, K. Starke, F. Hübinger, and G. Kaindl, Phys. Rev. Lett. **77**, 3415 (1996).

[9] K. Maiti, M. C. Malagoli, A. Dallmeyer, and C. Carbone, Phys. Rev. Lett. **88**, 167205 (2002).

[10] J. K. Glasbrenner, K. D. Belashchenko, J. Kudrnovský, V. Drchal, S. Khmelevskyi, and I. Turek, Phys. Rev. B **85**, 214405 (2012).

[11] L. Oroszlány, A. Deák, E. Simon, S. Khmelevskyi, and L. Szunyogh, Phys. Rev. Lett. **115**, 096402 (2015).

[12] S. Khmelevskyi, I. Turek, and P. Mohn, Phys. Rev. B **70**, 132401 (2004).

[13] M. Donath, B. Gubanka, and F. Passek, Phys. Rev. Lett. **77**, 5138 (1996).

[14] D. Li, J. Pearson, S. D. Bader, D. N. McIlroy, C. Waldfried, and P. A. Dowben, Phys. Rev. B **51**, 13895 (1995).

[15] A. V. Fedorov, T. Valla, F. Liu, P. D. Johnson, M. Weinert, and P. B. Allen, Phys. Rev. B **65**, 212409 (2002).

[16] L. M. Sandratskii, Phys. Rev. B **90**, 184406 (2014).

[17] J. Seib and M. Fähnle, Phys. Rev. B **82**, 064401 (2010).

[18] J. Seib, D. Steiauf, and M. Fähnle, Phys. Rev. B **79**, 064419 (2009).

[19] S. Y. Savrasov and D. Y. Savrasov, Phys. Rev. B **54**, 16487 (1996).

[20] T. Kasuya, Prog. Theor. Phys. **16**, 58 (1956).

[21] T. Kasuya, Prog. Theor. Phys. **22**, 227 (1959).

[22] P. de Gennes and J. Friedel, J. Phys. Chem. Solids **4**, 71 (1958).

[23] J. Kudrnovský, V. Drchal, I. Turek, S. Khmelevskyi, J. K. Glasbrenner, and K. D. Belashchenko, Phys. Rev. B **86**, 144423 (2012).

[24] M. Christen, B. Giovannini, and J. Sierro, Phys. Rev. B **20**, 4624 (1979).

[25] R. Karplus and J. M. Luttinger, Phys. Rev. **95**, 1154 (1954).

[26] J. Kondo, Prog. Theor. Phys. **27**, 772 (1962).

[27] F. E. Maranzana, Phys. Rev. **160**, 421 (1967).

[28] L. Berger, Phys. Rev. B **2**, 4559 (1970).

[29] L. Berger, Phys. Rev. B **5**, 1862 (1972).

[30] R. Asomoza, A. Fert, and R. Reich, J. Less-Common Met. **90**, 177 (1983).

[31] H. Ebert, S. Mankovsky, K. Chadova, S. Polesya, J. Minár, and D. Ködderitzsch, Phys. Rev. B **91**, 165132 (2015).

[32] H. Ebert, D. Ködderitzsch, and J. Minár, Rep. Prog. Phys. **74**, 096501 (2011).

[33] E. Engel and R. M. Dreizler, *Density Functional Theory – An Advanced Course* (Springer, Berlin, 2011).

[34] S. H. Vosko, L. Wilk, and M. Nusair, Can. J. Phys. **58**, 1200 (1980).

[35] M. T. Czyżyk and G. A. Sawatzky, Phys. Rev. B **49**, 14211 (1994).

[36] B. Velický, Phys. Rev. **184**, 614 (1969).

[37] W. H. Butler, Phys. Rev. B **31**, 3260 (1985).

[38] I. Turek, J. Kudrnovský, V. Drchal, L. Szunyogh, and P. Weinberger, Phys. Rev. B **65**, 125101 (2002).

[39] T. Naito, D. S. Hirashima, and H. Kontani, Phys. Rev. B **81**, 195111 (2010).

[40] A. Brataas, Y. Tserkovnyak, and G. E. W. Bauer, Phys. Rev. Lett. **101**, 037207 (2008).

[41] H. Ebert, S. Mankovsky, D. Ködderitzsch, and P. J. Kelly, Phys. Rev. Lett. **107**, 066603 (2011).

[42] D. Li, J. Zhang, P. A. Dowben, and M. Onellion, Phys. Rev. B **45**, 7272 (1992).

[43] J. K. Glasbrenner, B. S. Pujari, and K. D. Belashchenko, Phys. Rev. B **89**, 174408 (2014).

[44] N. Babushkina, Sov. Phys. Solid State **7**, 2450 (1966).

[45] R. S. Lee and S. Legvold, Phys. Rev. **162**, 431 (1967).

[46] N. V. Volkenshtein, I. K. Grigorova, and G. V. Fedorov, Sov. Phys. JETP **23**, 1003 (1966).

7.4. Tailoring of the extrinsic spin Hall effect in disordered metal alloys

The article "Tailoring of the extrinsic spin Hall effect in disordered metal alloys" published in The Journal of Physical Review B is reprinted with permission from Phys. Rev. B, 92, 235142 (2015); copyright 2015 American Physical Society.

Tailoring of the extrinsic spin Hall effect in disordered metal alloys

Kristina Chadova,[*] Sebastian Wimmer, Hubert Ebert, and Diemo Ködderitzsch
Department Chemie, Physikalische Chemie, Universität München, Butenandtstr. 5-13, 81377 München, Germany
(Received 14 April 2015; revised manuscript received 15 September 2015; published 23 December 2015)

We present a first-principles study of the extrinsic spin Hall effect in dilute metallic alloys and show how tailoring the magnitude of the spin Hall conductivity can be achieved by materials design concerning composition and varying the concentration of the alloy partners. An essential ingredient is the relative strength of the spin-orbit coupling of host and impurity partner. This is systematically studied by changing alloy composition and performing model calculations in which the spin-orbit coupling strength is scaled. The calculations reveal that changing the impurity concentration affects the extrinsic contributions, namely skew scattering and side jump, differently. This is put into the context of recent model calculations put forward by Fert and Levy [Phys. Rev. Lett. **106**, 157208 (2011)]. A fully relativistic Kubo-Středa formalism as implemented in the multiple-scattering KKR electronic structure method is used. The calculations were carried out for Pd, Pt, and Cu hosts doped with $4d$ including Ag and Cd and $5d$ impurities including Au and Hg.

I. INTRODUCTION

The scattering of electrons by impurities depends on the spin polarization of the carriers. The resulting asymmetric scattering is caused by spin-orbit coupling (SOC) and leads to a spatial separation of electrons with different spin projections. This effect is known as extrinsic spin Hall effect (SHE). It was first predicted theoretically in 1971 by Dyakonov and Perel [1] but was detected experimentally much later. The idea of creating spin currents in nonmagnetic materials without using ferromagnets or external magnetic fields opens new routes for the construction of spintronic devices. The main characteristic of suitable materials is the so-called spin Hall angle (SHA) α, which represents the ratio of spin to charge conductivity:

$$\alpha = \frac{\sigma_{xy}^z}{\sigma_{xx}}, \tag{1}$$

where σ_{xy}^z represents spin Hall conductivity (skew, side-jump, or total) and σ_{xx} is a longitudinal charge conductivity. Materials with high values of the SHA allow us to generate large spin currents in devices without magnetic components. Recently, large SHAs were predicted theoretically and found experimentally for a number of materials. Particularly for Au wires the measured SHA is $\alpha = 0.1$ [2], for Pt the magnitude of the experimental SHA is $\alpha = 0.08$ [3,4], even higher but negative $\alpha = -0.15$ [5] was obtained experimentally for high resistivity β-Ta, and a gigantic SHA was found in the β-W thin films with a value of $\alpha = 0.3$ [6]. For the above-listed materials the SHE is of intrinsic nature. The intrinsic SHE arises exclusively from the influence of the SOC on the band structure of the material. As such it is difficult to manipulate, and materials design geared towards obtaining a large intrinsic SHE is necessary, i.e., finding a combination of elements that crystallize in an ordered system possessing a significant SHE. One possibility to manipulate the SHE in a given material would be to apply isotropic pressure or uniaxial strain which changes the band structure, lattice parameter, density of states at the Fermi level, etc., which in turn could result in changes

of the intrinsic contribution. The influence of the uniaxial strain on the spin Hall conductivity (SHC) was studied for semiconductors [7]. It was demonstrated that the SHC is rather sensitive to the tensile strain or compression. Alternatively, finite temperatures have an effect on the intrinsic SHE as it was demonstrated from first-principles calculation for $4d$ and $5d$ transition metals, namely for Pd, Au [8], and Pt [9]. In the latter calculations only electronic temperatures were taken into account by introducing a Fermi distribution function. In the case of Pt and Pd there is a decrease in magnitude of the intrinsic contribution with increasing temperature, while in the case of Au the magnitude increases continuously with temperature [8].

On the other hand manipulating the extrinsic contributions to the SHE by alloying is a viable route to obtain large SHAs. This can be done in two major ways: by changing the combination of the host and impurity metals or by changing the concentration of the impurities. Recently, a large SHA was predicted theoretically [10] for Cu doped with Bi impurities with $\alpha = 0.081$, being extrinsic of the skew-scattering type. Later it was confirmed experimentally [11] to be indeed of skew-scattering nature, however with opposite sign $\alpha = -0.24$. A few years later another experiment to measure SHA of Cu doped with Bi impurities was performed by the same experimental group using a different experimental technique [12] which confirmed the sign and the magnitude of the SHA. Other calculations based on Friedel's sum rule for Cu doped with $5d$ impurities took into account both contributions, skew scattering and side jump, and reported large contributions from both mechanisms [13]. The latter approach was refined in subsequent studies in terms of a phase shift model [14], which, however, pointed out that final conclusions can only be reliably drawn from first-principles calculations.

In the following we present first-principles calculations that, in particular, focus on the influence of the SOC strength on the incoherent (extrinsic) contributions to the SHE in dilute disordered alloys: heavy hosts doped with $4d$ and $5d$ impurities (for brevity of notation we include Ag and Cd into $4d$s and Au and Hg into $5d$s) and a light host doped with $5d$ impurities making material specific predictions of systems showing a large SHA. These studies are supplemented by calculations in

———————
[*]kchpc@cup.uni-muenchen.de

which the SOC strength is manipulated to directly expose its influence within a fully relativistic scheme.

II. METHOD

The calculation of the spin Hall conductivity is based on the following linear response expression with spin polarization along the z axis and its current density operator along x due to the electric field along y:

$$\sigma_{xy}^z = \frac{\hbar}{4\pi N\Omega}\text{Tr}\langle \hat{J}_x^z(\hat{G}^+ - \hat{G}^-)\hat{j}_y\hat{G}^- \\ - \hat{J}_x^z\hat{G}^+\hat{j}_y(\hat{G}^+ - \hat{G}^-)\rangle_c, \quad (2)$$

where Ω is the volume of the unit cell and N is a number of sites. In Eq. (2) the relativistic current density operator is given by $\hat{j}_y = -|e|c\alpha_y$. $\hat{J}_x^z = |e|c\alpha_x(\beta\Sigma_z - \frac{\gamma_5\hat{p}_z}{mc})$ is the z component of the relativistic spin-polarization current density operator [15–17] with current density along the x direction. $\alpha_{x,y}$, β, and γ_5 are standard Dirac matrices, and Σ_z is the z component of the vector of the relativistic spin matrices [18,19].

The retarded and advanced Green functions, G^+ and G^-, are evaluated at the Fermi energy. Equation (2) is obtained from the Kubo-Středa equation [20–22] by neglecting a term related to orbital currents. This approximation is justified as this term only gives a small contribution when compared to the extrinsic contributions arising from the first term in the dilute cubic metallic alloy systems considered here (see also Refs. [22–24]). The Green function G is used as given by the fully relativistic multiple-scattering representation supplied by the Kohn-Korringa-Rostoker method [25]. A full four-component Dirac formalism is employed to describe the electronic structure within Kohn-Sham-Dirac density functional theory [26].

The brackets $\langle\ldots\rangle_c$ imply a configurational averaging that, in this work, is carried out in terms of the coherent potential approximation (CPA) combined with transport theory [27]. The vertex corrections (vc) that are essential for describing the extrinsic contributions to the SHC are given by the difference of the configurational averages $\langle\hat{J}_\mu^z G^+\hat{j}_\nu G^-\rangle_c - \langle\hat{J}_\mu^z G^+\rangle_c\langle\hat{j}_\nu G-\rangle_c$ [28]. The averaging procedure for terms in $\langle\hat{J}_\mu^z G^+\hat{j}_\nu G^-\rangle_c$ within the CPA leads to a splitting of the (spin Hall) conductivity into a site-diagonal and a site-off-diagonal term, the latter describing intersite hopping. In line with neglecting the on-site orbital-current related term, the site-diagonal term is also neglected. In the following, the conductivity without vertex corrections is defined as the intrinsic (coherent) part, $\sigma_{xy}^{z(nv)} \equiv \sigma_{xy}^{z(intr)}$, and the part which is solely caused by the vertex corrections, $\sigma_{xy}^{z(vc)} \equiv \sigma_{xy}^{z(extr)} = \sigma_{xy}^z - \sigma_{xy}^{z(intr)}$, is defined to be extrinsic (incoherent). Usually the intrinsic contributions are bound to the existence of well defined energy bands, which for a semiclassical formulation in terms of a Berry phase can be found. For a disordered alloy the denotation "intrinsic contribution" loses its meaning, as there are no well-defined energy bands. The use of "coherent" and "incoherent" is tied to the language of the employed CPA averaging procedure [28,29]. We will, however, use the terms intrinsic and extrinsic in what follows.

We present below a systematic study of the influence of the spin-orbit coupling strength on a model system. As we here use a fully relativistic Dirac approach that encompasses, besides the spin orbit coupling, relativistic effects in all orders beyond $1/c^2$, simple scaling of the velocity of light in a calculation would affect all contributions not only the SOC. Instead a method is used that allows for direct scaling of spin orbit coupling strength (while retaining the other relativistic effects). This is done in a Dirac approach [30] using a modified spin orbit operator that scales the SOC strength for each partial wave while solving for the scattering solutions. Employing
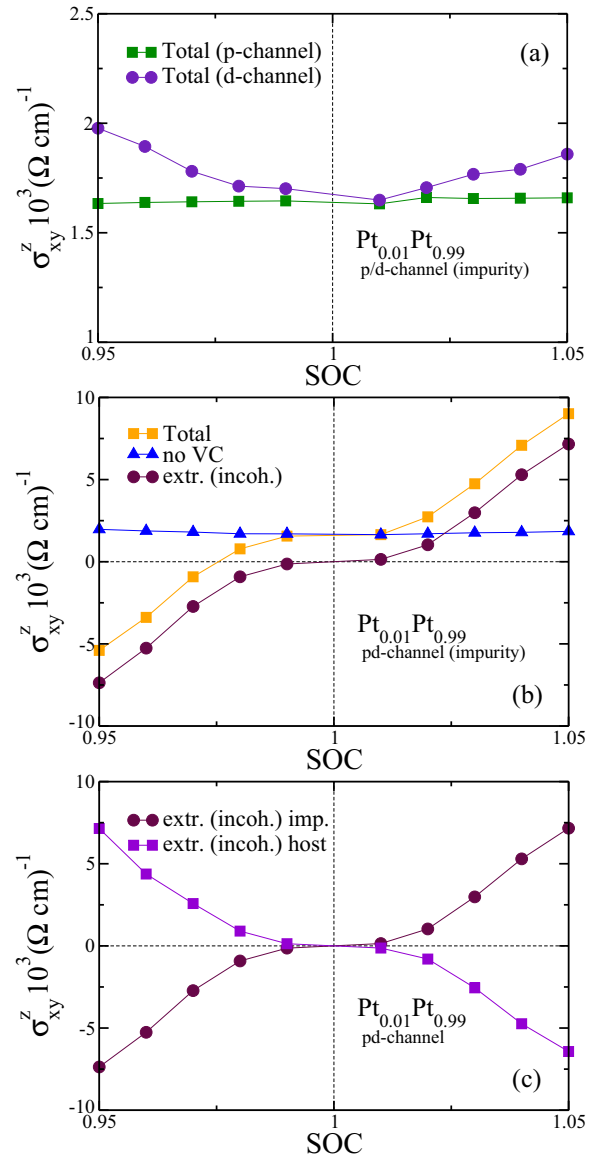

FIG. 1. (Color online) The dependence of the SHC in $Pt_{0.99}Pt_{0.01}$ as a function of the SOC strength: (a) on the impurity with scaling in p and d channel, separately; (b) in p and d channel simultaneously; (c) either on the host or the impurity in p and d channel simultaneously.

this approach also implies that matrix elements of the current operators $\hat{j}_x$ and $\hat{J}_y^z$ involving the Dirac α_μ matrices that couple small and large component have to be transformed [31] to a decoupled form.

III. COMPUTATIONAL DETAILS

The transport calculations were performed using the SPR-KKR Munich package [25] that is based on a fully relativistic Kohn-Sham-Dirac version of density functional theory. The local density approximation was used with the exchange correlation functional as parametrized Vosko-Wilk-Nussair (VWN) [32]. The atomic sphere approximation (ASA) has been used. The angular momentum cutoff was set to $l_{max} = 3$.

Evaluating the SHC using Eq. (2) involved computational demanding Brillouin-zone (BZ) integrations over products of scattering path operators that are constituents of the multiple-scattering representation of the Green functions G^+ and G^-. The calculations were performed for dilute alloys (down to 0.5%) which for lifetime smearing is small. Therefore, the Green functions show a pronounced structure in **k** space, and a large number of **k** points had to be used in the BZ integration: in the order of 10^6–10^7 (in the full BZ). The lattice constants used for the dilute alloys are those of the host elements, namely $a(\text{Cu}) = 3.61$ Å, $a(\text{Pd}) = 3.89$Å, $a(\text{Pt}) = 3.92$Å [33].

IV. RESULTS AND DISCUSSION

A. Manipulation of the spin-orbit coupling in Pt

Since the fundamental source of the SHE is the spin-orbit interaction, it is important to investigate its influence on the extrinsic contribution to the SHE. This could be probed by choosing a fixed host and inserting different impurities, thereby changing the SOC strength. This leads, however, to drastic changes in the host and impurity potential which makes a systematic analysis difficult. For this reason we first discuss the influence of the SOC strength by considering a model approach in which we choose the two alloy partners to be of the same chemical type and scaling the SOC strength on one of the partners. As we are working in a fully relativistic (κ, μ) representation that has no spin-orbit strength parameter, we apply a scheme that allows the direct manipulation of the SOC as mentioned in the previous section.

As a case study we have chosen Pt as an element with strong spin-orbit interaction strength and a large SHE and constructed a model system that consists of a Pt host with 1% of Pt impurity to mimic an alloy behavior. The impurity concentration as well as host and impurity materials were kept fixed. The SOC strength on the impurity (host) was then varied while it remained fixed for the host (impurity). The gradual change of the SOC strength was first applied individually and then simultaneously for the p and d channels. Figure 1(a) shows the total spin Hall conductivity depending on the scaling of

FIG. 2. (Color online) Intrinsic (coherent) part of SHC in: (a) Pd host doped with $4d$ impurities; (b) Pt host doped with $5d$ impurities.
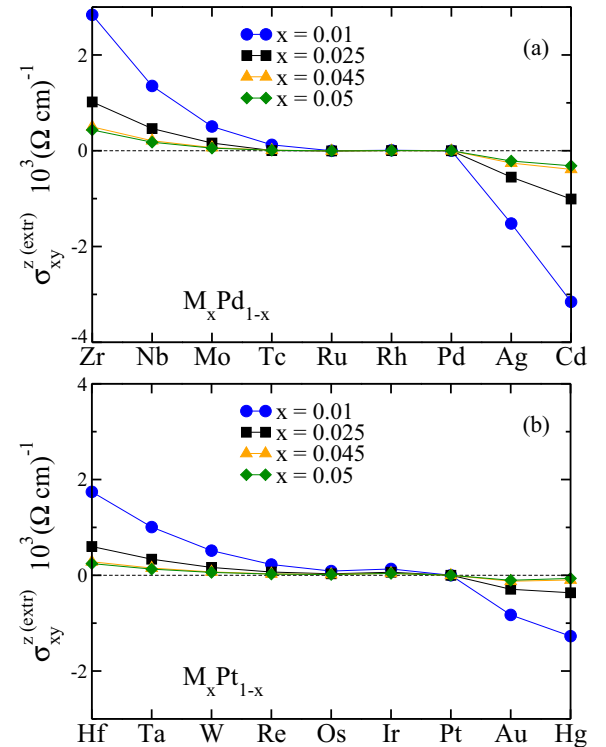

FIG. 3. (Color online) Extrinsic (incoherent) part of SHC in: (a) Pd host doped with $4d$ impurities; (b) Pt host doped with $5d$ impurities.

SOC for the impurity in the p and d channels individually. For this situation no contribution from the extrinsic part of the spin Hall conductivity was observed in either of the channels, i.e., the calculated Hall conductivities with and without vc are the same. In the case of the d channel there is a small dependence of the total SHC on the SOC strength, while for the p channel it shows a rather constant behavior. Figure 1(b) presents a more detailed analysis of the SHC for the SOC scaled on the impurity simultaneously in the p and d channels. As can be seen, the intrinsic part ($\sigma_{xy}^{z(nv)}$) of the SHC is independent of the SOC scaling and is rather small compared to the extrinsic one. The extrinsic contribution on the other hand shows a clear dependence on the SOC strength. The magnitude of the extrinsic conductivity is determined by the SOC strength: the larger the relative difference in SOC between host and impurity element the larger is the contribution. Figure 1(c) shows the dependence of the extrinsic contribution to the SHE on the SOC scaled on the host (impurity), while it is kept fixed on the impurity (host) simultaneously in p and d channels. As can be seen in both cases there is a pronounced dependence of the extrinsic contribution on the SOC. The obtained curves are symmetric. The symmetry of the curves (the magnitude and the sign) can be attributed to the SOC difference for the host and impurity obtained in both cases: either by scaling the SOC in the linear regime on the host by fixing it on the impurity or vise versa. The prime contribution to the extrinsic part of the SHC is due to scattering in both p and d channels, which

is consistent with results obtained recently for the SHE in a copper host doped with $5d$ impurities [34].

B. Pt and Pd hosts doped with $4d$ or $5d$ impurities—case study

In the previous section we used a model to investigate the influence of the SOC on the extrinsic part of the SHE. As a next step we consider real systems based on Pd and Pt host materials doped with $4d$ and $5d$ impurities.

In the following we analyze different contributions to the SHC. The decomposition into intrinsic and extrinsic part is based on the vertex corrections [21,22,35]. The calculations were performed for several impurity concentrations: 1%, 2.5%, 4.5%, and 5%. Figure 2(a) shows the intrinsic contribution of Pd-based and Fig. 2(b) of Pt-based alloy systems.

In case of late impurities for both systems the intrinsic contribution is rather independent of the impurity concentration and shows a constant behavior, while for early ones there is some concentration dependency present.

In contrast to the intrinsic part of the SHC, the extrinsic contribution (Fig. 3) shows a pronounced dependence on the impurity concentration for both systems. Another important characteristic is a sign change that occurs in both systems: For the light impurities (compared to the host element) the sign is positive, while for the heavy ones it becomes negative.

Figure 4 shows the skew-scattering SHA for Pd-based (a) and Pt-based (b) systems. As can be seen for both systems, the skew-scattering SHA strongly depends on the concentration,
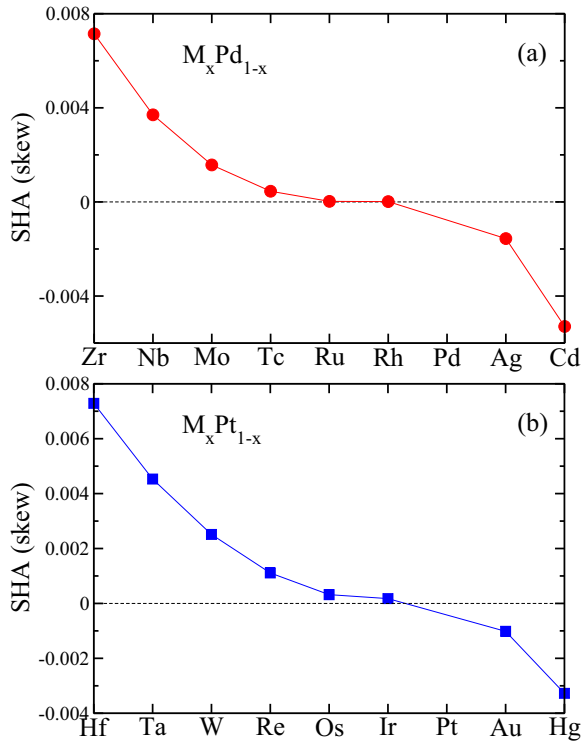

FIG. 4. (Color online) Skew-scattering SHA: (a) Pd host doped with $4d$ impurities; (b) Pt host doped with $5d$ impurities.
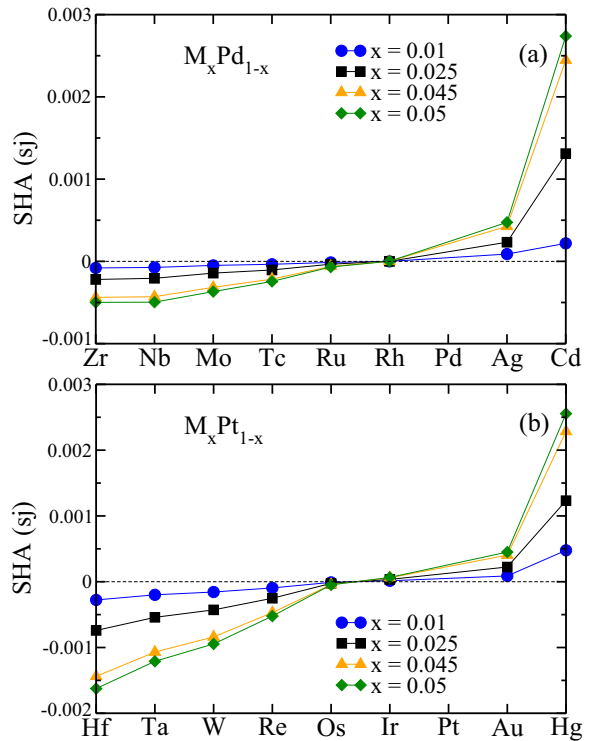

FIG. 5. (Color online) Side-jump SHA: (a) Pd host doped with $4d$ impurities; (b) Pt host doped with $5d$ impurities.
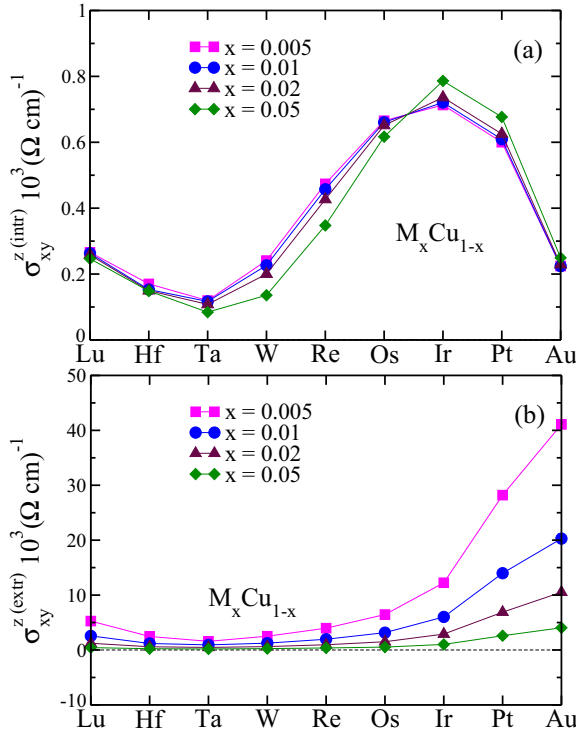
FIG. 6. (Color online) SHC in Cu doped with $5d$ impurities: (a) intrinsic (coherent) contribution; (b) extrinsic (incoherent) contribution.

FIG. 7. (Color online) SHC in Cu doped with $5d$ impurities: (a) skew scattering; (b) side jump.

namely, it is inversely proportional to the concentration in accordance with model [36–38] and other first-principles studies [22,39]. In contrast to the skew-scattering contribution, the side-jump SHA demonstrates strong concentration dependence (Fig. 5).

C. Cu host with $5d$ impurities

Cu has a negligible intrinsic SHE as compared to Pd or Pt hosts. By adding impurities, however, large extrinsic contributions to the SHE can be generated. According to the results of recent model calculations based on resonant scattering [13] for a Cu host doped with $5d$ impurities, large contributions from the skew-scattering and side-jump mechanism to the SHA are obtained [13]. Recently, the skew-scattering contribution was described by first-principles calculations [10,39] and by an extended version of the resonant scattering model of Fert and Levy [34].

In this paper we present both contributions, skew scattering and side jump, based on first-principles calculations.

A decomposition scheme of the conductivity into different contributions is used that is based on the vertex corrections [21,22,35]. Figure 6(a) shows the intrinsic and (b) the extrinsic contribution to the SHC. As can be seen the intrinsic part of the SHC is rather small compared to the extrinsic one, while the latter is inversely proportional to the impurity concentration. For the late $5d$ impurities, the extrinsic contribution is more
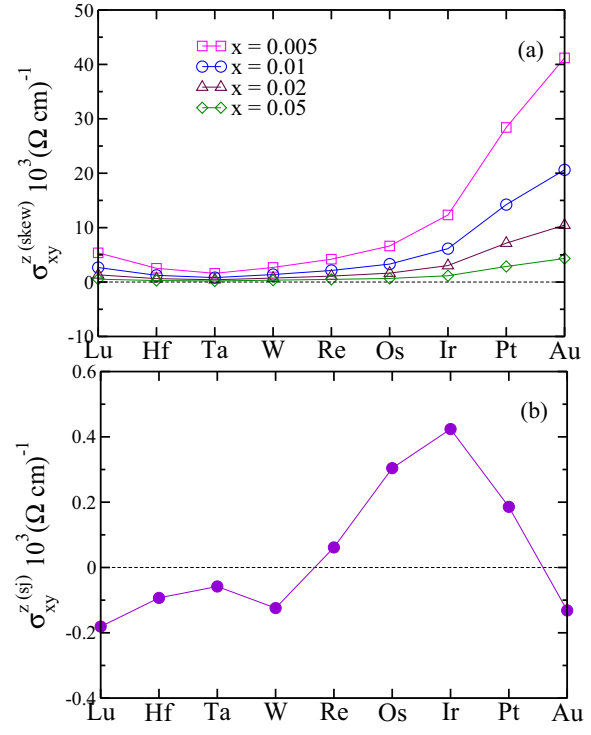
significant due to increasing of the SOC strength of the impurities [40].

The next step in the analysis of the different contributions is the decomposition of the extrinsic part of the SHC into skew-scattering and side-jump contributions. For this purpose, the same decomposition scheme as proposed for the anomalous Hall effect [35] and successfully used to decompose the SHC [22] is applied. Figure 7 shows the skew-scattering (a) and side-jump (b) conductivities for $5d$ impurities in a Cu host with different concentrations. As can be seen, the skew-scattering conductivity depends on the concentration of the impurities: The magnitude is larger for lower impurity concentration. The side-jump conductivity is independent of the impurity amount, and its magnitude is comparable to the intrinsic contribution. In addition, the side-jump conductivity shows a change in sign as a function of the atomic number.

Important for applications in spintronics is the spin Hall angle, as it gives the figure of merit for converting a longitudinal charge current into a transverse spin-polarized current. We performed calculations of the skew-scattering and side-jump contributions to the SHA for Cu with $5d$ impurities (see Fig. 8). The obtained results are compared to calculations based on an analytical model [13] and on the Boltzmann transport formalism [14]. In the Kubo-Středa calculations several concentrations were considered, while in Boltzmann calculations and the analytical model only 1% and 2%, respectively, of impurity concentration was used. Figure 8(a) shows the resulting skew-scattering and side-jump (b) SHA.
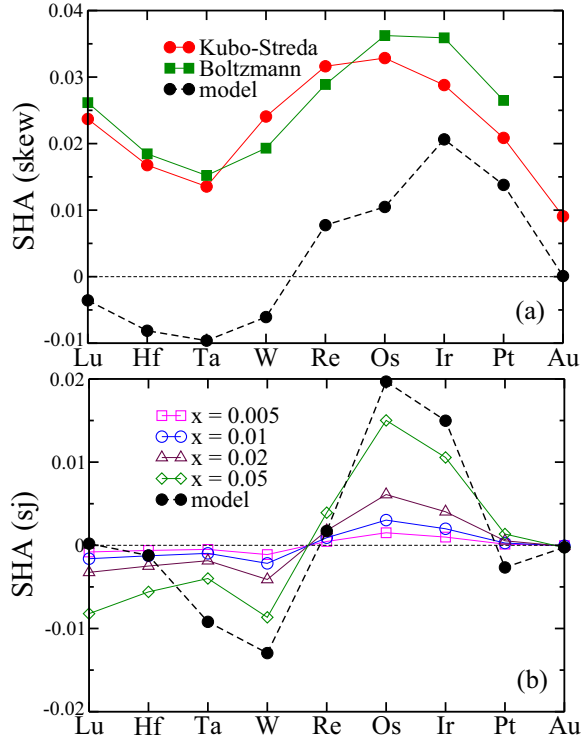
FIG. 8. (Color online) The SHA in Cu doped with $5d$ impurities: (a) skew scattering; (b) side jump. The black curve/full circles indicate results obtained from an analytical model [13] and are normalized in order to compare with other data. In panel (a) the green curve/filled squares are results based on the Boltzmann formalism [14].

The skew-scattering contribution to the SHA is independent of the impurity concentrations, while the side-jump exhibits a pronounced dependence on the concentration (proportional to the concentration [13]). As can be seen, first-principles and analytical model based results agree well [41]. For impurities such as Ta, W, Os, and Ir large values of the side-jump SHA can be obtained by increasing the concentration, as can be seen from Fig. 8(b), which is in an agreement with predictions from calculations based on an analytical model [13]. However, in the case of skew scattering, there is a sign change in the analytical model calculations, while the first principles results give positives values for all impurities.

V. CONCLUSIONS

We have investigated the influence of spin-orbit coupling strength on the extrinsic (incoherent) contribution to the spin Hall conductivity using a model system as well as realistic disordered dilute alloys. The results for the model system are consistent with those obtained for disordered alloys based on Pd and Pt hosts. Namely, a large contribution from the extrinsic contribution to the SHC is observed when the relative difference in the SOC strength of the host and impurity increases. For both sets of systems we observed a sign change in the extrinsic part. The change occurs when the impurity becomes heavier than the host element. Alternatively, to obtain large values of the extrinsic part of the SHC one can change the impurity concentration. By decreasing the concentration the magnitude of the SHC increases, mainly due to the skew-scattering contribution as it is inversely proportional to the impurity concentration in the dilute limit. The side-jump contribution is independent of the impurity concentration and has a small magnitude for all considered systems compared to the dominant skew scattering, thus it does not influence the behavior of the extrinsic part of the SHC. In the dilute limit the side-jump SHC does not depend on the impurity concentration. As, however, the longitudinal conductivity σ_{xx} decreases with increasing concentration, the SHA (sj) does depend on the impurity concentration: For higher concentrations we obtain higher values for the SHA (sj). This is well illustrated for the Cu host doped with $5d$ impurities. The SHA from the skew-scattering contribution is concentration independent. An important observation is that at 5% of the impurity concentration the magnitudes of the side-jump and the skew-scattering SHA become comparable. The magnitude of the side-jump SHC is comparable to the intrinsic part of the SHC. Large values for the side-jump SHA are obtained for Ta, W, Os, and Ir impurities for the concentration 5%. With increasing of the impurity concentration even higher values for the side-jump SHA can be obtained, which is in line with results based on an analytical model [13]. This suggests these are candidates for experimental investigations in order to obtain large SHA values.

[1] M. Dyakonov and V. Perel, Phys. Lett. A **35**, 459 (1971).

[2] T. Seki, Y. Hasegawa, S. Mitani, S. Takahashi, H. Imamura, S. Maekawa, J. Nitta, and K. Takanashi, Nat. Mater. **7**, 125 (2008).

[3] K. Ando, S. Takahashi, K. Harii, K. Sasage, J. Ieda, S. Maekawa, and E. Saitoh, Phys. Rev. Lett. **101**, 036601 (2008).

[4] L. Liu, T. Moriyama, D. C. Ralph, and R. A. Buhrman, Phys. Rev. Lett. **106**, 036601 (2011).

[5] L. Liu, C.-F. Pai, Y. Li, H. W. Tseng, D. C. Ralph, and R. A. Buhrman, Science **336**, 555 (2012).

[6] C. F. Pai, L. Liu, Y. Li, H. W. Tseng, D. C. Ralph, and R. A. Buhrman, Appl. Phys. Lett. **101**, 122404 (2012).

[7] G. Y. Guo, Y. Yao, and Q. Niu, Phys. Rev. Lett. **94**, 226601 (2005).

[8] G. Y. Guo, J. Appl. Phys. **105**, 07C701 (2009).

[9] G. Y. Guo, S. Murakami, T.-W. Chen, and N. Nagaosa, Phys. Rev. Lett. **100**, 096401 (2008).

[10] M. Gradhand, D. V. Fedorov, P. Zahn, and I. Mertig, Phys. Rev. B **81**, 245109 (2010).

[11] Y. Niimi, Y. Kawanishi, D. H. Wei, C. Deranlot, H. X. Yang, M. Chshiev, T. Valet, A. Fert, and Y. Otani, Phys. Rev. Lett. **109**, 156602 (2012).

[12] Y. Niimi, H. Suzuki, Y. Kawanishi, Y. Omori, T. Valet, A. Fert, and Y. Otani, Phys. Rev. B **89**, 054401 (2014).

[13] A. Fert and P. M. Levy, Phys. Rev. Lett. **106**, 157208 (2011).

[14] A. Johansson, C. Herschbach, D. V. Fedorov, M. Gradhand, and I. Mertig, J. Phys.: Condens. Matter **26**, 274207 (2014).

[15] A. Vernes, B. L. Györffy, and P. Weinberger, Phys. Rev. B **76**, 012408 (2007).

[16] V. Bargmann and E. P. Wigner, Proc. Natl. Acad. Sci. USA **34**, 211 (1948).

[17] S. Lowitzer, D. Ködderitzsch, and H. Ebert, Phys. Rev. B **82**, 140402(R) (2010).

[18] M. E. Rose, *Relativistic Electron Theory* (Wiley, New York, 1961).

[19] M. E. Rose, *Elementary Theory of Angular Momentum* (Wiley, New York, 1957).

[20] P. Středa, J. Phys. C **15**, L717 (1982).

[21] A. Crépieux and P. Bruno, Phys. Rev. B **64**, 014416 (2001).

[22] S. Lowitzer, M. Gradhand, D. Ködderitzsch, D. V. Fedorov, I. Mertig, and H. Ebert, Phys. Rev. Lett. **106**, 056601 (2011).

[23] T. Naito, D. S. Hirashima, and H. Kontani, Phys. Rev. B **81**, 195111 (2010).

[24] I. Turek, J. Kudrnovský, and V. Drchal, Phys. Rev. B **86**, 014405 (2012).

[25] H. Ebert, D. Ködderitzsch, and J. Minár, Rep. Prog. Phys. **74**, 096501 (2011).

[26] E. Engel and R. M. Dreizler, *Density Functional Theory – An advanced course* (Springer, Berlin, 2011).

[27] W. H. Butler, Phys. Rev. B **31**, 3260 (1985).

[28] S. Lowitzer, D. Ködderitzsch, and H. Ebert, Phys. Rev. Lett. **105**, 266604 (2010).

[29] I. Turek, J. Kudrnovský, and V. Drchal, Phys. Rev. B **89**, 064405 (2014).

[30] H. Ebert, H. Freyer, A. Vernes, and G.-Y. Guo, Phys. Rev. B **53**, 7721 (1996).

[31] G. Y. Guo and H. Ebert, Phys. Rev. B **51**, 12633 (1995).

[32] S. H. Vosko, L. Wilk, and M. Nusair, Can. J. Phys. **58**, 1200 (1980).

[33] C. Kittel, *Introduction to Solid State Physics* (John Wiley and Sons, Inc., New York, 1996).

[34] C. Herschbach, D. V. Fedorov, I. Mertig, M. Gradhand, K. Chadova, H. Ebert, and D. Ködderitzsch, Phys. Rev. B **88**, 205102 (2013).

[35] N. Nagaosa, J. Sinova, S. Onoda, A. H. MacDonald, and N. P. Ong, Rev. Mod. Phys. **82**, 1539 (2010).

[36] J. Smit, Physica **21**, 877 (1955).

[37] J. Smit, Physica **24**, 39 (1958).

[38] N. A. Sinitsyn, J. Phys.: Condens. Matter **20**, 023201 (2008).

[39] M. Gradhand, D. V. Fedorov, P. Zahn, and I. Mertig, Phys. Rev. Lett. **104**, 186403 (2010).

[40] M. Vijayakumar and M. S. Gopinathan, J. Mol. Struct. **361**, 15 (1996).

[41] According to the Erratum [A. Fert and P. M. Levy, Phys. Rev. Lett. **111**, 199904(E) (2013)] to the paper by Fert and Levy [13], despite the several sign errors introduced in the corresponding equations the sign of the skew-scattering contribution to the SHA remains correct.

7.5. Separation of the individual contributions to the spin Hall effect

The article "Separation of the individual contributions to the spin Hall effect" published in The Journal of Physical Review B is reprinted with permission from Phys. Rev. B, 92, 045120 (2015); copyright 2015 American Physical Society.

Separation of the individual contributions to the spin Hall effect in dilute alloys within the first-principles Kubo-Středa approach

Kristina Chadova,[1,*] Dmitry V. Fedorov,[2,3] Christian Herschbach,[2,3] Martin Gradhand,[4] Ingrid Mertig,[2,3] Diemo Ködderitzsch,[1] and Hubert Ebert[1]

[1]*Department of Chemistry, Physical Chemistry, Ludwig-Maximilians University, 81377 Munich, Germany*
[2]*Max Planck Institute of Microstructure Physics, Weinberg 2, 06120 Halle, Germany*
[3]*Institute of Physics, Martin Luther University Halle-Wittenberg, 06099 Halle, Germany*
[4]*H. H. Wills Physics Laboratory, University of Bristol, Bristol BS8 1TL, United Kingdom*

We present a procedure for the separation of the intrinsic, side-jump, and skew-scattering contributions to the spin Hall conductivity within the *ab initio* Kubo-Středa approach. Furthermore, two distinct contributions to the side-jump mechanism, either independent of the vertex corrections or solely caused by them, are quantified as well. This allows for a detailed analysis of individual microscopic contributions to the spin Hall effect. The efficiency of the proposed method is demonstrated by a first-principles study of dilute metallic alloys based on Cu, Au, and Pt hosts.

PACS number(s): 71.15.Rf, 72.25.Ba, 75.76.+j, 85.75.−d

I. INTRODUCTION

A detailed understanding of the spin Hall effect (SHE) [1] is the key issue for its efficient application in spintronic devices. The phenomenon, being connected to the anomalous Hall effect (AHE) [2–4], is a powerful tool for the creation of spin currents in nonmagnetic materials. Three main mechanisms contributing to the AHE as well as the SHE were established [5–7], all caused by spin-orbit coupling (SOC). They are known as the intrinsic mechanism due to the anomalous velocity [2,8], the extrinsic skew-scattering [3] and side-jump [4] mechanisms. In dilute alloys the skew-scattering contribution to the spin Hall conductivity dominates [9–12] since it is inversely proportional to the impurity concentration, while the other two contributions are concentration independent. Moreover, the skew-scattering mechanism is solely caused by the vertex corrections [5,10,12,13]. These features provide the basis for a simple separation of the skew-scattering contribution [10]. On the other hand, the intrinsic mechanism is caused exclusively by the host band structure [2], which makes it accessible by considering the corresponding ideal crystal [14–16]. The side-jump mechanism is much more subtle. Although it is caused by the presence of impurities in a host, the corresponding contribution to the spin Hall conductivity does not depend on their concentration [5]. Furthermore, for uncorrelated short-range disorder it is even independent of the type of impurities [17]. In contrast to the skew scattering, the side-jump mechanism is not only caused by the vertex corrections but has a contribution independent of them [5]. This complicates its coherent description, and quite often different approximations are used. For instance, in Refs. [12,18] the influence of the vertex corrections was neglected for the semiclassical resonant scattering model proposed to describe the side-jump contribution to the spin Hall conductivity. On the other hand, in Ref. [10] only the part caused by the vertex corrections was considered, which together with the skew-scattering contribution can be elegantly separated

from the rest [19]. However, for a complete description and comparison of the different mechanisms contributing to the SHE, it is highly desirable to have a consistent and fully *ab initio* treatment of the side-jump contribution.

II. APPROACH AND RESULTS

In this paper we propose an efficient procedure for the separation of the three main contributions, as well as the two parts related to the side-jump mechanism, schematically illustrated by Fig. 1. Practically, this is realized by means of the first-principles Kubo-Středa approach as implemented within the multiple-scattering Korringa-Kohn-Rostoker Green-function method [10]. Computational details of the method used can be found in the Appendix. Our procedure is based on the commonly accepted decomposition of the total spin Hall conductivity (SHC),

$$\sigma_{xy}^{z} = \sigma_{xy}^{z\,\text{intr}} + \sigma_{xy}^{z\text{sj}} + \sigma_{xy}^{z\text{skew}}, \tag{1}$$

into its intrinsic (intr), side-jump (sj), and skew-scattering (skew) contributions [5–7]. In addition, for the side-jump contribution we perform the decomposition

$$\sigma_{xy}^{z\text{sj}} = \sigma_{xy}^{z\text{sj(nvc)}} + \sigma_{xy}^{z\text{sj(vc)}}, \tag{2}$$

where the first and second terms represent the parts independent of the vertex corrections and solely caused by them,

	Intrinsic	Side jump	Skew scattering
Without vertex corrections	$\sigma_{xy}^{z\,\text{intr}}$	$\sigma_{xy}^{z\,\text{sj(nvc)}}$	—
Caused by vertex corrections	—	$\sigma_{xy}^{z\,\text{sj(vc)}}$	$\sigma_{xy}^{z\,\text{skew}}$

FIG. 1. Schematic representation of the considered individual contributions to the spin Hall effect.

*kchpc@cup.uni-muenchen.de

respectively. Within the present work, we quantify the four distinct contributions from Eqs. (1) and (2) by applying the proposed separation technique to Cu, Au, and Pt hosts with 5*d* impurities.

The so-called *anomalous-distribution* and *intrinsic skew-scattering* contributions, which were additionally singled out in Ref. [5], are assumed to be included in $\sigma_{xy}^{zsj(nvc)}$ and $\sigma_{xy}^{zsj(vc)}$, respectively. For the former one this is quite natural since the anomalous distribution is caused by the longitudinal component of the coordinate shift [20], whose transversal component to an applied electric field is responsible for the side-jump velocity [5]. Moreover, the anomalous-distribution contribution arises without the vertex corrections. By contrast, the intrinsic skew-scattering contribution arises due to the vertex corrections as well as the asymmetric scattering rate [21], similar to its conventional counterpart represented in our analysis by σ_{xy}^{zskew}. However, in comparison to this quantity, the intrinsic skew-scattering contribution is independent of the impurity concentration [5,21], which makes it similar to the side-jump mechanism. Therefore, here we follow Ref. [7] in parsing the mechanisms, where this contribution was formally attributed to the side-jump scattering.

In the dilute limit, σ_{xy}^{zskew} is inversely proportional to the impurity concentration, which also holds for the longitudinal charge conductivity σ_{xx}. This allows one to rewrite Eq. (1) as [10]

$$\sigma_{xy}^z(\sigma_{xx}) = \sigma_{xy}^{zintr} + \sigma_{xy}^{zsj} + \alpha^{skew}\sigma_{xx}, \qquad (3)$$

where $\alpha^{skew} = \sigma_{xy}^{zskew}/\sigma_{xx}$ is the spin Hall angle related to the skew scattering. Then, the separation of the sum of the intrinsic and side-jump contributions from the skew-scattering contribution can be done by extrapolating to the situation of vanishing charge conductivity

$$\sigma_{xy}^{zintr} + \sigma_{xy}^{zsj} = \sigma_{xy}^z(\sigma_{xx} \to 0). \qquad (4)$$

At low impurity concentrations σ_{xy}^z shows a linear behavior as a function of σ_{xx} [10], which is discussed in more detail in the Appendix. Such a typical situation is shown in Fig. 2 by the results obtained for dilute Cu(Au) alloys [22].
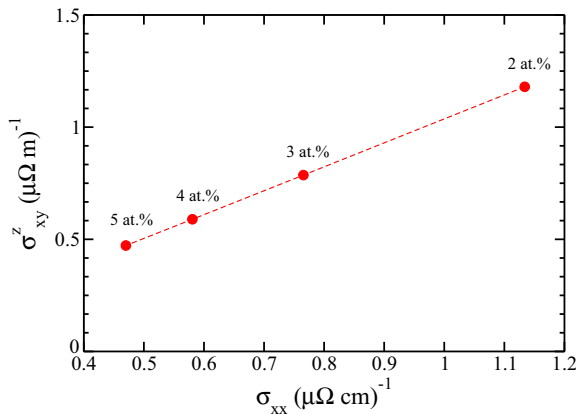

FIG. 2. (Color online) The spin Hall conductivity as a function of the longitudinal charge conductivity is shown for four dilute Cu(Au) alloys labeled by the corresponding impurity concentrations.
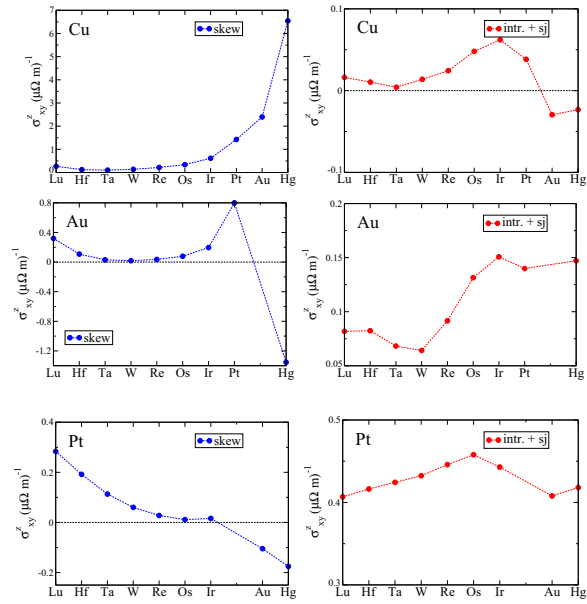

FIG. 3. (Color online) The skew-scattering contribution σ_{xy}^{zskew} (left) at the impurity concentration 1 at. % as well as the sum of the intrinsic and side-jump contributions $\sigma_{xy}^{zintr} + \sigma_{xy}^{zsj}$ (right) are shown as obtained for different dilute alloys based on Cu, Au, and Pt hosts.

Due to the linear behavior of the SHC as a function of the charge conductivity, it is possible to perform an extrapolation using just a few points. This gives us the sum $\sigma_{xy}^{zintr} + \sigma_{xy}^{zsj}$, whose subtraction from the total SHC provides the skew-scattering contribution as well. The corresponding results for Cu, Au, and Pt hosts with different 5*d* impurities are shown in Fig. 3 (left panels). Going from Cu to Pt via Au, the skew-scattering contribution decreases since the difference between impurity and host SOC becomes smaller [13]. On the other hand, the increase of the host SOC enhances the sum shown in the right panels of Fig. 3. In order to demonstrate that this effect is caused by the enhancement of the intrinsic contribution, we need to perform a further separation of the individual contributions σ_{xy}^{zintr} and σ_{xy}^{zsj}.

A possible way to access the intrinsic contribution to the SHC is based on the Berry curvature formalism [15,23]. To obtain this contribution within the used Kubo-Středa approach, we employ a scheme similar to the one proposed and successfully applied to pure metals in case of the AHE [24]. It implies an addition of a small imaginary part $i\epsilon$ to the Fermi energy (E_F), in order to calculate σ_{xy}^z given by Eq. (3) of Ref. [10] via an integration over the Brillouin zone (BZ). Due to this procedure, we avoid the numerical problems caused by a δ-function-like behavior of the integrand at the real energy axis, which is present for pure crystals [24]. Then, the intrinsic contribution to the SHC can be obtained by the extrapolation $\lim_{\epsilon \to 0} \sigma_{xy}^z(E_F + i\epsilon)$. Applying this scheme with the parameters described in the Appendix, we have obtained σ_{xy}^{zintr} as 0.017 $(\mu\Omega\,\text{m})^{-1}$ for Cu, 0.074 $(\mu\Omega\,\text{m})^{-1}$ for Au, and 0.409 $(\mu\Omega\,\text{m})^{-1}$ for Pt. These results are in good agreement with other *ab initio* calculations, which provided

for Au and Pt hosts the values of 0.07–0.08 [25,26] and 0.44 [16] $(\mu\Omega\,\mathrm{m})^{-1}$, respectively. This shows that the Fermi-sea contribution neglected in the used Kubo-Středa formula (see the Appendix) does not exceed 8% of the total intrinsic contribution.

With the intrinsic contribution determined, the separation according to Eq. (1) is achieved. Let us perform now the decomposition of the side-jump contribution following the idea of Eq. (2). As was mentioned above, the skew scattering is solely caused by the vertex corrections. By contrast, the side-jump mechanism is not only provided by them but has also a contribution independent of the vertex corrections. This is transparent within the semiclassical approach, where the side-jump contribution to the spin current density can be written, in analogy to the AHE [5], as

$$j_x^{z\mathrm{sj}} = \sigma_{xy}^{z\mathrm{sj}} E_y = -\frac{|e|}{V}\sum_k g_k S_k^z v_{k,x}^{\mathrm{sj}}. \tag{5}$$

Here, $\mathbf{S}_k$ and $\mathbf{v}_k^{\mathrm{sj}}$ are the spin polarization [13] and the so-called side-jump velocity [20], respectively. According to Ref. [20], $\mathbf{v}_k^{\mathrm{sj}}$ is determined by both the scattering at impurities and the topological properties of the host crystal related to its Berry curvature [23,27]. The nonequilibrium part of the distribution function g_k is proportional to the mean free path [28,29]

$$\mathbf{\Lambda}_k = \mathbf{\Lambda}_k^{\mathrm{out}} + \mathbf{\Lambda}_k^{\mathrm{in}} \tag{6}$$

consisting of the scattering-out and scattering-in terms, where the latter one corresponds to the vertex corrections of the Kubo theory [30]. Thus, Eqs. (5) and (6) support the decomposition of Eq. (2) with $\sigma_{xy}^{z\mathrm{sj(nvc)}}$ and $\sigma_{xy}^{z\mathrm{sj(vc)}}$ describing the parts independent of the vertex corrections and solely caused by them, respectively. Our procedure allows us to obtain these contributions to the side-jump mechanism separately.

Indeed, the part $\sigma_{xy}^{z\mathrm{sj(vc)}}$ was already derived in Ref. [10] via a procedure similar to Eq. (4) but applied to the difference of the SHCs obtained with and without vertex corrections. Here, using the same approach together with our knowledge of the total side-jump contribution, we can obtain its first part as $\sigma_{xy}^{z\mathrm{sj(nvc)}} = \sigma_{xy}^{z\mathrm{sj}} - \sigma_{xy}^{z\mathrm{sj(vc)}}$. Figure 4 shows the two parts of the side-jump contribution to the SHC separately. The most important point is that they are of comparable size. This means it is impossible to neglect one of them, but one has to consider the entire side-jump contribution to the SHC. Another interesting point is related to the magnitude of the side-jump contribution comparing Au and Pt as a host. While for Pt the intrinsic contribution $\sigma_{xy}^{z\mathrm{intr}}$ is about six times larger than for Au, there is no similar enhancement for $\sigma_{xy}^{z\mathrm{sj}}$. In other words, the influence of the Berry curvature on the side-jump mechanism is not as important as the scattering properties caused by impurities.

This finding supports the main assumption of the resonant scattering model proposed by Fert and Levy [12,18] for the estimation of the side-jump contribution to the SHE. Indeed, their approach does not include the influence of the host band structure via the Berry curvature, due to the restriction to systems for which the spherical band approximation can be justified. Taking into account that the vertex corrections are also neglected in the Fert-Levy model, one could assume
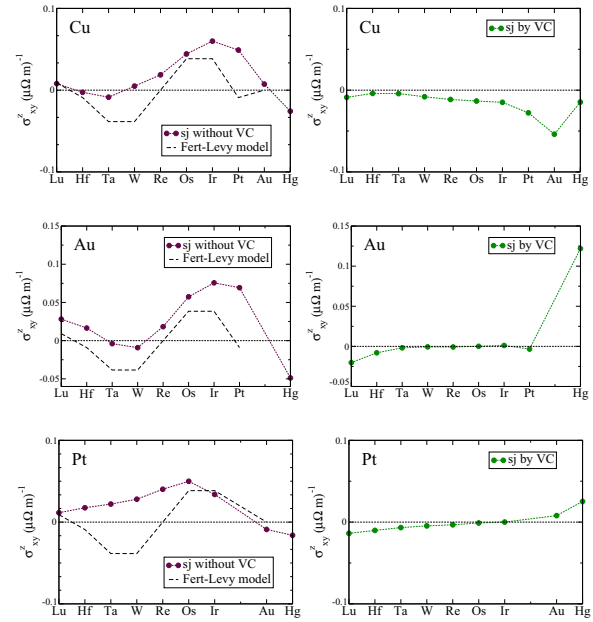

FIG. 4. (Color online) The two parts of the side-jump contribution, $\sigma_{xy}^{z\mathrm{sj(nvc)}}$ (left) and $\sigma_{xy}^{z\mathrm{sj(vc)}}$ (right), are shown for different dilute alloys based on Cu, Au, and Pt hosts. The dashed curves in the left panels are plotted (in arbitrary units) according to Eq. (7) obtained within the Fert-Levy model [12].

that it may describe $\sigma_{xy}^{z\mathrm{sj(nvc)}}$ for hosts with a free-electron-like Fermi surface. For the considered systems, the scattering phase shift of p electron states in the expression derived for this contribution in Ref. [12] has no significant influence on its structure. Therefore, we neglect it and obtain

$$\sigma_{xy}^{z\mathrm{sj(nvc)}} \sim (1 - 4\sin^2\eta_2)\sin 2\eta_2. \tag{7}$$

Here, η_2 is the scattering phase shift corresponding to the impurity d states. Within the resonant scattering model this quantity can be approximated by $\frac{\pi Z_d}{10}$ [12], where Z_d is the number of impurity d electrons which changes from 1 for Lu to 10 for Au impurities. As shown by Fig. 4, for Cu and Au hosts such a model estimation provides reasonable qualitative agreement with the calculated $\sigma_{xy}^{z\mathrm{sj(nvc)}}$. This is not the case for platinum because of its complex Fermi surface [31]. The model-based results also strongly disagree with $\sigma_{xy}^{z\mathrm{sj(vc)}}$. This needs to be kept in mind for comparison of the side-jump contribution obtained within the two different approximations mentioned in the Introduction.

It is important to mention that our results clarify the situation concerning a long-standing question about the magnitude of the side-jump contribution [3,4,7,32,33]. While it is commonly believed that in the dilute limit the skew-scattering mechanism should be dominating [9–12], there was no clear understanding whether the side-jump contribution may ever be significant as well. Various estimations aimed to elucidate this point but based on simple general arguments led to different conclusions. For instance, Crépieux and Bruno stated in Ref. [32] that it is impossible to predict which of the two

extrinsic mechanisms should dominate in the high-disorder regime, while Sushkov *et al.* [33] concluded that the side-jump contribution is generally negligible. Based on our first-principles calculations, we show that the two contributions can be comparable even at impurity concentrations of a few at. %. The same conclusion was obtained by Fert and Levy based on their impurity-specific model consideration [12]. This demonstrates that an adequate description of the electron scattering at impurities is essential, in order to derive a reasonable estimation of the side-jump contribution.

Finally, it is desirable to have a scheme to determine σ_{xy}^{zintr} by considering dilute alloys instead of ideal crystals. In contrast to the latter ones, the aforementioned scheme based on the broadening via a complex energy is not necessary to ensure the convergence using a reasonable number of **k** points [24]. This idea can be realized in the following way. As was discussed above, applying the procedure of Eq. (4) to the total SHC and the difference between the total SHC and its counterpart calculated without the vertex corrections, we obtain $\sigma_{xy}^{zintr} + \sigma_{xy}^{zsj}$ and $\sigma_{xy}^{zsj(vc)}$, respectively. This allows us to separate the resulting sum $\sigma_{xy}^{zintr} + \sigma_{xy}^{zsj(nvc)}$ as $\sigma_{xy}^{zintr} + \sigma_{xy}^{zsj} - \sigma_{xy}^{zsj(vc)}$. Now let us take into account that generally the side-jump contribution depends on the type of impurity atoms solved in the host. By contrast, the intrinsic contribution, entirely provided by the band structure of the related ideal crystal, is impurity independent. Consequently, by an appropriate choice of impurities it should be possible to obtain the case $|\sigma_{xy}^{zintr}| \gg |\sigma_{xy}^{zsj(nvc)}|$, that would provide a good estimation for the intrinsic contribution as the dominant one in the known sum $\sigma_{xy}^{zintr} + \sigma_{xy}^{zsj(nvc)}$. Impurities, which fulfill the required condition, could be recognized by a statistical analysis of results obtained for a large number of different alloys based on the same host. However, one can reduce the computational effort by reasonable predictions of impurities possessing negligible side-jump mechanism. One class of possible candidates is related to light atoms with *s* character of valence electron states. Indeed, the SOC induced by them should be weak because of both the small atomic number and the vanishing atomic orbital moment. From this perspective, Li, Be, Na, and Mg impurities can be taken, in order to estimate the intrinsic contribution.

Following this route, we have performed additional calculations considering the four light impurities in Cu, Au, and Pt hosts. The sum $\sigma_{xy}^{zintr} + \sigma_{xy}^{zsj(nvc)}$ obtained according to the procedure explained above is shown in Fig. 5. Evidently, the chosen impurities provide a good estimate for the intrinsic contribution. By averaging over the four considered alloys for each host, we evaluate σ_{xy}^{zintr} as 0.016 $(\mu\Omega\,\text{m})^{-1}$ for Cu, 0.088 $(\mu\Omega\,\text{m})^{-1}$ for Au, and 0.404 $(\mu\Omega\,\text{m})^{-1}$ for Pt. These values are in good agreement with those obtained by the calculations discussed above, which are shown as horizontal dashed lines in Fig. 5 for comparison. Thus, this way to estimate the intrinsic contribution can be used as a cheaper alternative to the direct but computationally demanding calculations.

III. SUMMARY

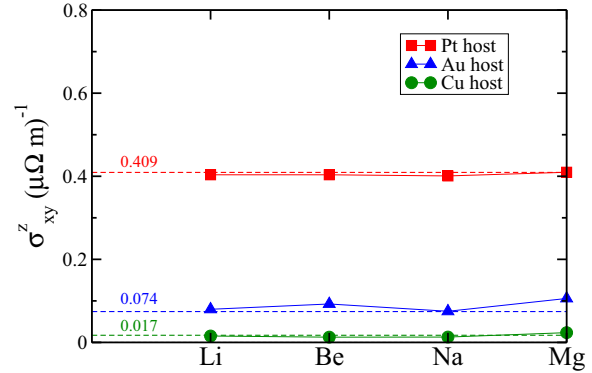We propose an accurate procedure for the separation of the intrinsic, side-jump, and skew-scattering contributions to the

FIG. 5. (Color online) The sum of the intrinsic contribution σ_{xy}^{zintr} and the first part of the side-jump contribution $\sigma_{xy}^{zsj(nvc)}$ calculated for Li, Be, Na, and Mg impurities in Cu (green circles), Au (blue triangles), and Pt (red squares) hosts is shown in comparison to the corresponding intrinsic contribution (dashed lines and numbers) obtained from its straightforward calculations.

spin Hall conductivity within one and the same computational method based on the first-principles Kubo-Středa approach. This is applied to various dilute alloys based on Cu, Au, and Pt hosts, which especially clarifies the influence of the vertex corrections on the side-jump mechanism. The presented scheme opens a way for further deeper theoretical investigations of the spin Hall effect with a possible elucidation of its dominating mechanisms.

ACKNOWLEDGMENTS

APPENDIX: COMPUTATIONAL DETAILS

Based on the Kubo-Středa linear-response theory [32,34], the presented spin Hall conductivity was calculated as a correlation function describing the connection between a spin-current $\hat{\mathbf{J}}$ induced by a charge current $\hat{\mathbf{j}}$:

$$\sigma_{xy}^z = \frac{\hbar}{4\pi N\Omega}\text{Tr}\langle \hat{J}_x^z(\hat{G}^+ - \hat{G}^-)\hat{j}_y\hat{G}^- - \hat{J}_x^z\hat{G}^+\hat{j}_y(\hat{G}^+ - \hat{G}^-)\rangle_c, \quad \text{(A1)}$$

where Ω is the unit-cell volume and N refers to the number of sites. This expression involves the y component of the relativistic current density operator $\hat{j}_y = -|e|c\alpha_y$ and the z component of the relativistic spin-polarization current density operator [24,35,36] with the current density along the x direction: $\hat{J}_x^z = |e|c\alpha_x(\beta\Sigma_z - \frac{\gamma_5\hat{p}_z}{mc})$. Here, α, β, and γ_5 are the standard Dirac matrices and Σ_z refers to the z component of the vector of the relativistic spin

matrices ($\mu = x, y, z$) [37,38]:

$$\alpha_\mu = \begin{pmatrix} 0_2 & \sigma_\mu \\ \sigma_\mu & 0_2 \end{pmatrix}, \quad \beta = \begin{pmatrix} \mathbb{1}_2 & 0_2 \\ 0_2 & -\mathbb{1}_2 \end{pmatrix}, \qquad \text{(A2)}$$

$$\gamma_5 = \begin{pmatrix} 0_2 & -\mathbb{1}_2 \\ -\mathbb{1}_2 & 0_2 \end{pmatrix}, \quad \Sigma_z = \begin{pmatrix} \sigma_z & 0_2 \\ 0_2 & \sigma_z \end{pmatrix} \qquad \text{(A3)}$$

with σ_μ being the Pauli matrices.

Equation (A1) was used for the pure host crystals as well as the alloys considered in our work. To describe the effect of random substitutional disorder for the latter ones, we use the coherent potential approximation (CPA) [30,39]. For this case the brackets $\langle \ldots \rangle_c$ in Eq. (A1) indicate a configurational average treated by means of CPA. The calculation of vertex corrections appearing as a difference between correlated and uncorrelated configurational averages $\langle \hat{J}_x^z \hat{G}^+ \hat{j}_y \hat{G}^- \rangle_c$ and $\langle \hat{J}_x^z \hat{G}^+ \rangle_c \langle \hat{j}_y \hat{G}^- \rangle_c$, respectively, is based on the CPA transport formalism introduced by Butler [30]. Note that the latter slightly differs by the one introduced by Velický [39] and used, e.g., in the TB-LMTO approach [40].

Further note that in Eq. (A1) a term related to the orbital current has been neglected as it was done previously [10,40]. For cubic crystals, which is the case for the systems considered in the presented work, this term has been shown to be small [41]. In the case of the anomalous Hall conductivity, the neglected term is equivalent to the Fermi-sea term [40] present in the Bastin equation [42], which represents a sum over all occupied states and cannot affect a description of skew scattering or side jump but the intrinsic mechanism. It was demonstrated that for cubic systems the Fermi-sea contribution is significantly smaller in comparison to the dominant Fermi-surface contribution [41]. Here, we can estimate the amount of the Fermi-sea contribution by comparing our results obtained for the pure host crystals with those from Refs. [16,25,26] based on the Berry curvature calculations including both contributions. This allows us to conclude that the missing contribution does not exceed 8% of the complete intrinsic contribution to the SHC.

For our first-principles calculations, we either take into account the vertex corrections in Eq. (A1) or completely skip them from the consideration, obtaining either the total SHC σ_{xy}^z or its part called $\sigma_{xy}^{z(\text{nvc})}$, respectively. Their difference gives us the contribution $\sigma_{xy}^{z(\text{vc})}$ which is solely caused by the vertex corrections. The obtained decomposition

$$\sigma_{xy}^z = \sigma_{xy}^{z(\text{nvc})} + \sigma_{xy}^{z(\text{vc})} \qquad \text{(A4)}$$

is extended further as

$$\sigma_{xy}^{z(\text{nvc})} = \sigma_{xy}^{z\text{intr}} + \sigma_{xy}^{z\text{sj(nvc)}} \qquad \text{(A5)}$$

and

$$\sigma_{xy}^{z(\text{vc})} = \sigma_{xy}^{z\text{skew}} + \sigma_{xy}^{z\text{sj(vc)}}. \qquad \text{(A6)}$$

This procedure is schematically represented by Fig. 1 and explained in detail above. The crucial point is the linear behavior of σ_{xy}^z or $\sigma_{xy}^{z(\text{vc})}$ as a function of the longitudinal charge conductivity in the dilute limit, where both $\sigma_{xy}^{z\text{skew}}$ and σ_{xx} are inversely proportional to the impurity concentration. Depending on the magnitude of the intrinsic and side-jump contributions, the well-pronounced linear behavior illustrated by Fig. 2 can be obtained at different concentrations for different alloys. A significant decrease of the impurity concentration would require an enormous increase of the number of **k** points in the Brillouin zone. However, for the considered systems the necessary linear dependence of the SHC as a function of σ_{xx} was achieved with impurity concentrations above 0.5 at. %, which allowed us to use the reasonable number of **k** points mentioned below.

The G^+ and G^- present in Eq. (A1) are the retarded and advanced Green functions evaluated at the Fermi level by means of the relativistic Korringa-Kohn-Rostoker method [43] and obtained as $G^\pm(\mathbf{r}, \mathbf{r}', E) = \lim_{\eta \to 0^+} G(\mathbf{r}, \mathbf{r}', E \pm i\eta)$. The Green function in the real-space multiple-scattering representation is given by (see Ref. [44], and references therein)

$$G(\mathbf{r}, \mathbf{r}', E_F) = \sum_{\Lambda \Lambda'} Z_\Lambda^n(\mathbf{r}, E_F)\, \tau_{\Lambda \Lambda'}^{nm}(E_F)\, Z_{\Lambda'}^{m \times}(\mathbf{r}', E_F)$$

$$- \delta_{nm} \sum_\Lambda \left[Z_\Lambda^n(\mathbf{r}, E_F)\, J_\Lambda^{n \times}(\mathbf{r}', E_F)\Theta(r_n' - r_n) \right.$$

$$\left. + J_\Lambda^n(\mathbf{r}, E_F)\, Z_\Lambda^{n \times}(\mathbf{r}', E_F)\Theta(r_n - r_n') \right] \qquad \text{(A7)}$$

with the four-component site-centered wave functions $Z_\Lambda^n(\mathbf{r}, E_F)$ and $J_\Lambda^n(\mathbf{r}, E_F)$ being regular and irregular solutions to the single-site Dirac equation. Here, $\Lambda = (\kappa, \mu)$ represents the relativistic quantum numbers and τ is the scattering path operator.

The calculations were performed using the atomic sphere approximation for the potential. A wave-function expansion with angular momentum cutoff $l_{\max} = 3$ was used. For the investigated alloys, impurity concentrations in the range 0.5–5 at. % were considered with the corresponding number of **k** points in the BZ as 10^9 to 10^7 to ensure convergence. In case of the pure crystals, a small imaginary part ϵ between 10^{-6} and 10^{-4} Ry was added to the Fermi energy with using about 10^9 **k** points.

[1] M. I. Dyakonov and V. Perel, Phys. Lett. A **35**, 459 (1971); J. E. Hirsch, Phys. Rev. Lett. **83**, 1834 (1999).

[2] R. Karplus and J. M. Luttinger, Phys. Rev. **95**, 1154 (1954); E. Adams and E. Blount, J. Phys. Chem. Solids **10**, 286 (1959).

[3] J. Smit, Physica **21**, 877 (1955); **24**, 39 (1958).

[4] L. Berger, Physica **30**, 1141 (1964); Phys. Rev. B **2**, 4559 (1970); **5**, 1862 (1972).

[5] N. A. Sinitsyn, J. Phys.: Condens. Matter **20**, 023201 (2008).

[6] N. Nagaosa, J. Sinova, S. Onoda, A. H. MacDonald, and N. P. Ong, Rev. Mod. Phys. **82**, 1539 (2010).

[7] J. Sinova, S. O. Valenzuela, J. Wunderlich, C. H. Back, and T. Jungwirth, arXiv:1411.3249.

[8] J. Sinova, D. Culcer, Q. Niu, N. A. Sinitsyn, T. Jungwirth, and A. H. MacDonald, Phys. Rev. Lett. **92**, 126603 (2004).

[9] S. Onoda, N. Sugimoto, and N. Nagaosa, Phys. Rev. Lett. **97**, 126602 (2006).

[10] S. Lowitzer, M. Gradhand, D. Ködderitzsch, D. V. Fedorov, I. Mertig, and H. Ebert, Phys. Rev. Lett. **106**, 056601 (2011).

[11] Y. Niimi, M. Morota, D. H. Wei, C. Deranlot, M. Basletic, A. Hamzic, A. Fert, and Y. Otani, Phys. Rev. Lett. **106**, 126601 (2011).

[12] A. Fert and P. M. Levy, Phys. Rev. Lett. **106**, 157208 (2011).

[13] M. Gradhand, D. V. Fedorov, P. Zahn, and I. Mertig, Phys. Rev. Lett. **104**, 186403 (2010); Phys. Rev. B **81**, 245109 (2010).

[14] Z. Fang, N. Nagaosa, K. S. Takahashi, A. Asamitsu, R. Mathieu, T. Ogasawara, H. Yamada, M. Kawasaki, Y. Tokura, and K. Terakura, Science **302**, 92 (2003).

[15] G. Y. Guo, Y. Yao, and Q. Niu, Phys. Rev. Lett. **94**, 226601 (2005).

[16] G. Y. Guo, S. Murakami, T.-W. Chen, and N. Nagaosa, Phys. Rev. Lett. **100**, 096401 (2008).

[17] J. Weischenberg, F. Freimuth, J. Sinova, S. Blügel, and Y. Mokrousov, Phys. Rev. Lett. **107**, 106601 (2011).

[18] P. M. Levy, Phys. Rev. B **38**, 6779 (1988).

[19] In Ref. [10] the remaining part of the spin Hall conductivity was simply called *intrinsic* contribution, although it is influenced by the side-jump mechanism described without the vertex corrections. Therefore, this one should be distinguished from the conventional intrinsic contribution, represented by $\sigma_{xy}^{z\,\mathrm{intr}}$ in Eq. (1), being a pure feature of the host band structure.

[20] N. A. Sinitsyn, Q. Niu, and A. H. MacDonald, Phys. Rev. B **73**, 075318 (2006).

[21] N. A. Sinitsyn, A. H. MacDonald, T. Jungwirth, V. K. Dugaev, and J. Sinova, Phys. Rev. B **75**, 045315 (2007).

[22] Throughout the paper we use for the SHC the same units and sign as in Ref. [10]. This means the values of σ_{xy}^{z} presented here correspond to the ones of σ_{yx}^{s} considered in Ref. [29]. Their relation to other possible conventions used in literature was exhaustively discussed in Ref. [45].

[23] M. V. Berry, Proc. R. Soc. London A **392**, 45 (1984).

[24] S. Lowitzer, D. Ködderitzsch, and H. Ebert, Phys. Rev. Lett. **105**, 266604 (2010).

[25] Y. Yao and Z. Fang, Phys. Rev. Lett. **95**, 156601 (2005).

[26] G. Y. Guo, J. Appl. Phys. **105**, 07C701 (2009).

[27] M. Gradhand, D. V. Fedorov, F. Pientka, P. Zahn, I. Mertig, and B. L. Györffy, J. Phys.: Condens. Matter **24**, 213202 (2012).

[28] I. Mertig, Rep. Prog. Phys. **62**, 237 (1999).

[29] C. Herschbach, D. V. Fedorov, I. Mertig, M. Gradhand, K. Chadova, H. Ebert, and D. Ködderitzsch, Phys. Rev. B **88**, 205102 (2013).

[30] W. H. Butler, Phys. Rev. B **31**, 3260 (1985).

[31] A. Johansson, C. Herschbach, D. V. Fedorov, M. Gradhand, and I. Mertig, J. Phys.: Condens. Matter **26**, 274207 (2014).

[32] A. Crépieux and P. Bruno, Phys. Rev. B **64**, 014416 (2001).

[33] O. P. Sushkov, A. I. Milstein, M. Mori, and S. Maekawa, Europhys. Lett. **103**, 47003 (2013).

[34] P. Středa, J. Phys. C **15**, L717 (1982).

[35] A. Vernes, B. L. Györffy, and P. Weinberger, Phys. Rev. B **76**, 012408 (2007).

[36] S. Lowitzer, D. Ködderitzsch, and H. Ebert, Phys. Rev. B **82**, 140402(R) (2010).

[37] M. E. Rose, *Elementary Theory of Angular Momentum* (Wiley, New York, 1957).

[38] M. E. Rose, *Relativistic Electron Theory* (Wiley, New York, 1961).

[39] B. Velický, Phys. Rev. **184**, 614 (1969).

[40] I. Turek, J. Kudrnovský, and V. Drchal, Phys. Rev. B **86**, 014405 (2012).

[41] T. Naito, D. S. Hirashima, and H. Kontani, Phys. Rev. B **81**, 195111 (2010).

[42] A. Bastin, C. Lewiner, O. Betbeder-Matibet, and P. Nozieres, J. Phys. Chem. Solids **32**, 1811 (1971).

[43] H. Ebert, in *Electronic Structure and Physical Properties of Solids*, Lecture Notes in Physics Vol. 535, edited by H. Dreyssé (Springer, Berlin, 2000), p. 191.

[44] H. Ebert, D. Ködderitzsch, and J. Minár, Rep. Prog. Phys. **74**, 096501 (2011).

[45] D. V. Fedorov, C. Herschbach, A. Johansson, S. Ostanin, I. Mertig, M. Gradhand, K. Chadova, D. Ködderitzsch, and H. Ebert, Phys. Rev. B **88**, 085116 (2013).

7.6. Linear response Kubo-Bastin formalism

The article "Linear response Kubo-Bastin formalism with application to the anomalous and spin Hall effects: A first-principles approach" published in The Journal of Physical Review B is reprinted with permission from Phys. Rev. B, 92, 184415 (2015); copyright 2015 American Physical Society.

–

Linear response Kubo-Bastin formalism with application to the anomalous and spin Hall effects: A first-principles approach

Diemo Ködderitzsch,[*] Kristina Chadova, and Hubert Ebert

Department Chemie, Physikalische Chemie, Universität München, Butenandtstrasse 5-13, 81377 München, Germany
(Received 22 May 2015; revised manuscript received 19 August 2015; published 17 November 2015)

We present a general first-principles approach to treat various linear response phenomena relevant for spintronics. It is based on a Kubo-Bastin formalism and implemented within the multiple-scattering Korringa-Kohn-Rostoker (KKR) Green's function method with the underlying electronic structure determined by density functional theory. The symmetric (e.g., longitudinal electronic transport) as well as the antisymmetric (e.g., transverse transport) parts of the response tensor are determined, including both the so-called Fermi-sea and the Fermi-surface contributions. To describe spin-orbit-induced phenomena, such as the anomalous and spin Hall effects, a fully relativistic description is employed. Exploiting the adopted Green's function method substitutional disorder in the full concentration range of alloys is treated within the coherent potential approximation, taking full account of occurring vertex corrections in the averaging procedure for the linear response quantities. Extrinsic (scattering related, e.g., side-jump and skew scattering) and intrinsic (band structure–related) contributions to the transport tensors are treated on equal footing. Other phenomena, such as Gilbert damping and spin-orbit torques, are particular cases of the general framework and their determination is briefly addressed. The versatility of the method is demonstrated by presenting results for the anomalous and spin Hall conductivities for elemental transition metals and their alloys.

I. INTRODUCTION

There exist a number of transverse transport phenomena that have attracted a lot of attention in recent years due to their potential application in spintronics and their interesting underlying mechanisms. Among them are the anomalous (AHE) [1] and spin Hall (SHE) [2–4] effects and their spin-caloritronic counterparts [5], the anomalous and spin-Nernst effects [6–8], as well as the newly discovered spin-orbit torque in which a current exerts a torque on the magnetization in a ferromagnet [9–11]. Common to these effects is their relativistic origin, i.e., they are induced by spin-orbit coupling.

Quite generally, mechanisms giving rise to these effects are classified as band structure–related topological intrinsic or scattering-related extrinsic contributions (among the latter are skew and side-jump contributions). Many model calculations exist for these effects, each of which focuses on one or a few underlying mechanisms and typically rely on certain parameters [1,12–14]. Only recently have *ab initio* methods been developed that in most cases start from a density functional theory description of the electronic structure and that are able to provide a material-specific characterization of these phenomena. Several computer codes are now able to determine the intrinsic Berry-phase-associated contributions relying on the existence of well-defined energy bands in ordered systems [15–20]. Disorder in this particular approach can be introduced in a phenomenological way which allows one to include finite lifetime effects and can be used to describe systems with small content of impurities (dilute limit). On the other hand, the Boltzmann approach has been used to deal exclusively with extrinsic skew scattering contributions in the dilute limit. An approach that is capable of treating all the aforementioned linear response phenomena in a general

way, i.e., treating intrinsic and extrinsic contributions on the same footing as well as being able to include disorder away from the dilute limit, is the Kubo linear response formalism in combination with a suitable alloy theory (see below).

The latter is our methodological starting ground in its Kubo-Greenwood (KG) formulation that is well established in describing longitudinal electronic transport, more precisely, giving the symmetric part of the transport tensor that connects a current with the electric field. Only states at the Fermi energy (Fermi surface) contribute to this part of the transport tensor. Many first-principles calculations have been performed employing the KG method implemented within the Korringa-Kohn-Rostoker (KKR) or the linear muffin-tin orbital (LMTO) electronic structure methods, demonstrating the viability to treat disordered systems and giving material-specific results [21–23]. Let us note in passing that already on the KG level the inclusion of vertex corrections (vc) becomes important and is readily incorporated in these approaches.

Going beyond the KG method and capturing the antisymmetric (transverse) parts of the transport tensors is methodologically and computationally much more demanding and only recently first-principles approaches have been devised that are based on the Kubo-Středa and Kubo-Bastin formalism [24–28]. There are several reasons for this: (i) As transverse transport phenomena like the AHE and SHE are manifestly spin-orbit induced, the effect of spin-orbit coupling has to be incorporated appropriately when calculating the electronic structure. (ii) One contribution to the tensor results exclusively from the states at the Fermi level and depends, in particular for pure systems, very sensitively on the topology of the Fermi surface. This implies the use of a huge number of k points needed for the Brillouin-zone integrations. Also, in the dilute limit of disordered alloys the vertex corrections have been shown to be of utter importance [25,29], again leading, together with the fine structure of the electronic states to be

---

sampled, to great computational effort in the evaluation of k-space integrals. (iii) Finally, going beyond KG one either has to include a Fermi-sea term in the Kubo-Bastin formulation or to recast the transport equations into the Kubo-Středa equation. The latter then is often simplified by neglecting an orbital current term or relying on cancellation of terms in inversion symmetric systems, therefore restricting its range of application.

In this paper we present a Kubo-Bastin framework that in its formulation and implementation within relativistic multiple-scattering theory allows one to treat a variety of spin-orbit-induced linear response phenomena including the anomalous and spin Hall effect. It is applicable to pure systems as well as disordered alloys in the full concentration range and treats intrinsic (coherent) and extrinsic (incoherent) contributions within one and the same methodological approach. The application of the scheme to other phenomena (e.g., Gilbert damping, spin-orbit torques) is straightforward and is briefly discussed.

The paper is organized as follows: In Sec. II we formulate a generalized Kubo-Bastin theory within a fully relativistic framework. Based on the given expression we perform a symmetry analysis of the response tensor followed by a particular formulation for the anomalous and spin Hall effects. We then outline the linear response Kubo-Bastin approach within the relativistic KKR method, with more details given in the Appendix. In Sec. III we give technical details concerning the implementation. Finally, in Sec. IV we present results for the AHE and SHE in pure systems as well as disordered alloys. The paper is summarized in Sec. V.

II. THEORY

As we want to discuss, in particular, transverse spin-orbit-induced transport phenomena, we base our approach on the relativistic four-component Dirac formalism when dealing with the underlying electronic structure. This is motivated by the following reasons: (i) no approximation is involved when treating spin-orbit-induced properties, and (ii) it allows one to avoid problems to treat disorder [30] (vertex corrections) which would otherwise occur in a Pauli approach. The corresponding Dirac-Hamiltonian is given as

$$\hat{H}_\mathrm{D} = -i\hbar c\,\boldsymbol{\alpha}\cdot\boldsymbol{\nabla} + (\beta - \mathbb{I}_4)mc^2 + V_\mathrm{KS}(\mathbf{r})\,. \qquad (1)$$

The single-particle potential V_KS appearing in Eq. (1) is determined in the framework of Kohn-Sham-Dirac (KSD) spin-density functional theory (KSD-SDFT) [31,32] and includes an exchange term $\beta\,\boldsymbol{\Sigma}\cdot\mathbf{B}_\mathrm{xc}$. The standard Dirac and spin matrices [31,33,34] α_μ, β, and Σ_μ are given as ($\mu \in \{\mathrm{x,y,z}\}$)

$$\alpha_\mu = \begin{pmatrix} 0_2 & \sigma_\mu \\ \sigma_\mu & 0_2 \end{pmatrix},\ \ \beta = \begin{pmatrix} \mathbb{I}_2 & 0_2 \\ 0_2 & -\mathbb{I}_2 \end{pmatrix},\ \ \Sigma_\mu = \begin{pmatrix} \sigma_\mu & 0_2 \\ 0_2 & \sigma_\mu \end{pmatrix}, \qquad (2)$$

with the σ_μ being the Pauli matrices. The KSD Green's function (GF) is defined as the resolvent of the Dirac-Hamiltonian Eq. (1), $\hat{G}(z) = (z - \hat{H}_\mathrm{D})^{-1}$, with z being a complex energy variable.

A. Generalized Kubo-Bastin formalism

The starting point of our derivation is the Kubo-Bastin [35] like expression for the response tensor χ describing the reaction of the system in the observable represented by an operator $\hat{\mathbf{B}}$ due to the perturbation represented by the operator $\hat{\mathbf{A}}$:

$$\chi_{\mu\nu} = -\frac{\hbar}{2\pi\Omega}\int_{-\infty}^{\infty} f(E)\mathrm{Tr}\left\langle \hat{B}_\mu \frac{d\hat{G}^+}{dE}\hat{A}_\nu(\hat{G}^+ - \hat{G}^-) \right.$$
$$\left. - \hat{B}_\mu(\hat{G}^+ - \hat{G}^-)\hat{A}_\nu\frac{d\hat{G}^-}{dE}\right\rangle dE\,. \qquad (3)$$

Here $\mu,\nu \in \{x,y,z\}$ denote Cartesian coordinates, Ω is the volume of the system, $f(E) = [e^{(E-\mu)/k_\mathrm{B}T} + 1]^{-1}$ denotes the Fermi-Dirac distribution function with the chemical potential μ, the Fermi energy $E_\mathrm{F} = \mu(T = 0\,\mathrm{K})$, $\hat{G}^+$ and $\hat{G}^-$ are the retarded and advanced Green's function operators (for brevity their energy arguments will be suppressed), and $\langle\dots\rangle$ denotes a configurational average. Following a procedure by Crépieux and Bruno [30], when deriving the Kubo-Středa equation we obtain one half of the term (by keeping one half of the term and doing a partial integration on the second half) an expression that lends its hand to further insightful analysis as well as a first-principles implementation:

$$\chi_{\mu\nu} = \chi_{\mu\nu}^I + \chi_{\mu\nu}^{II} \qquad (4)$$

$$\chi_{\mu\nu}^I = -\frac{\hbar}{4\pi\Omega}\int_{-\infty}^{\infty}\frac{df(E)}{dE}\mathrm{Tr}\langle\hat{B}_\mu(\hat{G}^+ - \hat{G}^-)\hat{A}_\nu\hat{G}^-$$
$$- \hat{B}_\mu\hat{G}^+\hat{A}_\nu(\hat{G}^+ - \hat{G}^-)\rangle dE \qquad (5)$$

$$\chi_{\mu\nu}^{II} = +\frac{\hbar}{4\pi\Omega}\int_{-\infty}^{\infty} f(E)\mathrm{Tr}\left\langle\hat{B}_\mu\hat{G}^+\hat{A}_\nu\frac{d\hat{G}^+}{dE} - \hat{B}_\mu\frac{d\hat{G}^+}{dE}\hat{A}_\nu\hat{G}^+\right.$$
$$\left. - \left(\hat{B}_\mu\hat{G}^-\hat{A}_\nu\frac{d\hat{G}^-}{dE} - \hat{B}_\mu\frac{d\hat{G}^-}{dE}\hat{A}_\nu\hat{G}^-\right)\right\rangle dE. \qquad (6)$$

In the limit $T \to 0\,\mathrm{K}$, $f(E)$ becomes a step function and the first term Eq. (5) contributes to χ only in quantities to be evaluated at the Fermi energy E_F, whereas for the second term Eq. (6) the integration is over all occupied states. For this reason in what follows the term $\chi_{\mu\nu}^I$ Eq. (5) will be denoted as Fermi-surface and the term $\chi_{\mu\nu}^{II}$ Eq. (6) as the Fermi-sea term. Note that the last equation is a different but an equivalent form of the original equation by Bastin *et al.* [35].

B. Symmetry analysis

For the particular case of $\hat{\mathbf{A}} = \hat{\mathbf{B}} = \hat{\mathbf{O}}$ the Fermi-sea term is purely antisymmetric, $\chi_{\mu\nu}^{II} = -\chi_{\nu\mu}^{II}$. This can be seen by inspecting the first term in Eq. (6) containing only retarded $(\hat{G}^+)$ as well as the second term in parenthesis containing exclusively advanced $(\hat{G}^-)$ Green's functions. Both terms are antisymmetric, which can be shown by exploiting the property of the trace.

The analysis of the Fermi-surface term can be carried out by considering the symmetry-related subexpression of χ^I, i.e.,

$$C_{\mu\nu} = \mathrm{Tr}\langle\hat{B}_\mu(\hat{G}^+ - \hat{G}^-)\hat{A}_\nu\hat{G}^- - \hat{B}_\mu\hat{G}^+\hat{A}_\nu(\hat{G}^+ - \hat{G}^-)\rangle\,.$$

Extracting the symmetric part for $\hat{\mathbf{A}} = \hat{\mathbf{B}} = \hat{\mathbf{O}}$ leads to

$$\frac{1}{2}[C_{\mu\nu} + C_{\nu\mu}] = -\mathrm{Tr}\langle\hat{O}_\mu(\hat{G}^+ - \hat{G}^-)\hat{O}_\nu(\hat{G}^+ - \hat{G}^-)\rangle$$
$$= 4\mathrm{Tr}\langle\hat{O}_\mu\Im\hat{G}^+\hat{O}_\nu\Im\hat{G}^+\rangle, \qquad (7)$$

a Kubo-Greenwood–like expression, where $\Im\hat{G}^+(E) = \frac{1}{2i}[\hat{G}^+(E) - \hat{G}^-(E)]$. This is frequently used in transport calculations, with $\hat{\mathbf{O}} = \hat{\mathbf{j}}$ being the charge current operator yielding the symmetric (and in particular, the longitudinal) contribution to the conductivity tensor $\sigma_{\mu\nu}$.

Extracting the antisymmetric part for $\hat{\mathbf{A}} = \hat{\mathbf{B}} = \hat{\mathbf{O}}$ gives

$$\frac{1}{2}[C_{\mu\nu} - C_{\nu\mu}] = \frac{1}{2}\mathrm{Tr}\langle[\hat{O}_\mu(\hat{G}^+ - \hat{G}^-)\hat{O}_\nu$$
$$- \hat{O}_\nu(\hat{G}^+ - \hat{G}^-)\hat{O}_\mu](\hat{G}^+ + \hat{G}^-)\rangle$$
$$= 2i\,\mathrm{Tr}\langle[\hat{O}_\mu\Im\hat{G}^+\hat{O}_\nu - \hat{O}_\nu\Im\hat{G}^+\hat{O}_\mu]\Re\hat{G}^+\rangle,$$

where $\Re\hat{G}^+(E) = \frac{1}{2}[\hat{G}^+(E) + \hat{G}^-(E)]$. For the example of a charge-charge current response, this states that the (antisymmetric) anomalous Hall effect results from the Fermi sea as well as the antisymmetric surface contribution. It has been shown that in the latter case the Fermi-sea term can be transformed into a surface term [30,36] and the intrinsic AHE in a (pure) metallic ferromagnet is a topological Fermi-surface property [37].

To highlight the advantages of the presented scheme, let us note in passing that the case $\hat{\mathbf{A}} = \hat{\mathbf{B}} = \hat{\mathbf{T}}$, with $\hat{\mathbf{T}}$ being the magnetic torque operator, allows a formulation of the Gilbert damping [38–40]. Furthermore, the spin-orbit torque, i.e., the torque exerted on the magnetization in a ferromagnet resulting from a charge current [9,41], is obtained by using $\hat{\mathbf{B}} = \mathbf{T}$ and $\hat{\mathbf{A}} = \mathbf{j}$ [42,43].

Finally, we want to point out that further symmetry analysis of the response tensors on grounds of the (magnetic) space group of a bulk system can give additional relations, depending on the particular choice of operators $\hat{\mathbf{A}}$ and $\hat{\mathbf{B}}$ [44,45].

C. Conductivity within Kubo-Bastin linear response formalism

In the chosen relativistic formalism the electric current operator is given by $\hat{\mathbf{j}} = -|e|c\boldsymbol{\alpha}$, with $e > 0$ being the elementary charge. For describing the spin Hall effect, we here employ the relativistic spin (-polarization) current-density operator

$$\hat{\mathbf{J}}^\xi = \left(\beta\Sigma_\xi - \frac{\gamma_5\Pi_\xi}{mc}\right)|e|c\boldsymbol{\alpha}, \qquad (8)$$

inspired by Bargmann and Wigner [46] and already used previously [25,47,48], with the kinetic momentum $\boldsymbol{\Pi} = (\hat{\mathbf{p}} + \frac{|e|}{c}\mathbf{A})\mathbb{1}_4$, the canonical momentum $\hat{\mathbf{p}}$, the vector potential $\mathbf{A}$, and [34]

$$\gamma_5 = \begin{pmatrix} 0_2 & -\mathbb{1}_2 \\ -\mathbb{1}_2 & 0_2 \end{pmatrix}. \qquad (9)$$

For the remainder of the paper we consider the limit $T \to 0$ K of Eqs. (5) and (6) and two particular cases, both of which are characterized by choosing $\hat{\mathbf{A}} = \hat{\mathbf{j}}$ as charge current operator. The (longitudinal) charge and anomalous Hall conductivities are obtained by setting $\hat{\mathbf{B}} = \hat{\mathbf{j}}$. The spin Hall conductivity is obtained by setting $\hat{\mathbf{B}} = \hat{\mathbf{J}}^\xi$, where $\xi \in \{x, y, z\}$ characterizes

the polarization direction of the spin current operator. With this Eqs. (5) and (6) read

$$\sigma_{\mu\nu}^\xi = \sigma_{\mu\nu}^{\xi,I} + \sigma_{\mu\nu}^{\xi,II}, \qquad (10)$$

$$\sigma_{\mu\nu}^{\xi,I} = \frac{\hbar}{4\pi\Omega}\mathrm{Tr}\langle\hat{J}_\mu^\xi(\hat{G}^+ - \hat{G}^-)\hat{j}_\nu\hat{G}^- - \hat{J}_\mu^\xi\hat{G}^+\hat{j}_\nu(\hat{G}^+ - \hat{G}^-)\rangle,$$
$$(11)$$

$$\sigma_{\mu\nu}^{\xi,II} = \frac{\hbar}{4\pi\Omega}\int_{-\infty}^{E_\mathrm{F}}\mathrm{Tr}\left\langle\hat{J}_\mu^\xi\hat{G}^+\hat{j}_\nu\frac{d\hat{G}^+}{dE} - \hat{J}_\mu^\xi\frac{d\hat{G}^+}{dE}\hat{j}_\nu\hat{G}^+\right.$$
$$\left. - \left(\hat{J}_\mu^\xi\hat{G}^-j_\nu\frac{d\hat{G}^-}{dE} - \hat{J}_\mu^\xi\frac{d\hat{G}^-}{dE}\hat{j}_\nu\hat{G}^-\right)\right\rangle dE, \quad (12)$$

where in Eq. (11) the Green's functions are evaluated at the Fermi energy E_F and the energy arguments at the GFs have been omitted throughout. The conductivity tensor $\sigma_{\mu\nu}$ in terms of the charge-charge response is obtained by replacing $\hat{J}_\mu^\xi$ with $\hat{j}_\mu$ in the last expression. For the remainder of the paper we consider the special case $\xi = z$ and, if present, the following particular choice for the exchange field $\mathbf{B}_\mathrm{xc}(\mathbf{r}) = B(r)\hat{\mathbf{e}}_z$ in the Hamiltonian Eq. (1).

Note that in the discussion of longitudinal transport [49] and the AHE one can show that terms involving only retarded or advanced GF, i.e., terms of the type $\langle jG^+jG^+\rangle$ or $\langle jG^-jG^-\rangle$, can be neglected in the weak disorder limit [50], and this is indeed done in actual calculations [51]. In the present work all contributions are taken into account, in particular, because we discuss the full concentration range of alloys.

D. Kubo-Bastin linear response formalism within relativistic multiple-scattering KKR

The formalism presented here is inspired by previous implementations of the (relativistic) Kubo-Greenwood approach [52–56] which go back to a formulation by Butler [21]. These are restricted to the treatment of the symmetric part of the conductivity tensor evaluated at the Fermi energy. Here we report on a very general framework that (i) gives the symmetric as well as antisymmetric contributions by evaluating Fermi sea and surface contributions; (ii) is fully relativistic and therefore captures all important contributions to transverse transport (skew scattering, side jump); (iii) is easily extendable to any other operator pair for dealing with other phenomena like Gilbert damping [38,40,42] and spin-orbit torques; (iv) allows treatment of efficiently disordered systems, avoiding costly supercell approaches; and (v) lends its hand to straightforwardly include finite temperatures effects [57].

The evaluation and first-principles treatment of Eqs. (11) and (12) for solids requires a suitable representation of the GF, which in our chosen formalism will subsequently lead to a product expression containing matrix elements of the current operators with the basis functions and k-space integrals over scattering path operators. Disorder and ensuing vertex corrections in the averaging procedure will be treated by means of the coherent potential approximation (CPA) [21,58].

The real-space representation of the Green's function operator $\hat{G}(z)$ can be very efficiently obtained by using the spin-polarized relativistic version of multiple-scattering theory

[59–63]:

$$G(\mathbf{r},\mathbf{r}',z) = \sum_{\Lambda\Lambda'} Z_\Lambda^n(\mathbf{r},z)\,\tau_{\Lambda\Lambda'}^{nm}(z)\,Z_{\Lambda'}^{m\times}(\mathbf{r}',z)$$

$$- \delta_{nm} \sum_\Lambda \big[Z_\Lambda^n(\mathbf{r},z)\,J_\Lambda^{n\times}(\mathbf{r}',z)\Theta(r_n' - r_n)$$

$$+ J_\Lambda^n(\mathbf{r},z)\,Z_\Lambda^{n\times}(\mathbf{r}',z)\Theta(r_n - r_n')\big]. \quad (13)$$

Here $\mathbf{r},\mathbf{r}'$ refer to atomic sites at $\mathbf{R}_n$ and $\mathbf{R}_m$, respectively, where $Z_\Lambda^n(\mathbf{r},z) = Z_\Lambda(\mathbf{r}_n,z) = Z_\Lambda(\mathbf{r} - \mathbf{R}_n,z)$ as well as $J_\Lambda^n(\mathbf{r},z)$ are basis functions centered at positions $\mathbf{R}_n$. Note that here the basis functions are normalized according to the Oak Ridge–Bristol convention [64]. The four-component wave functions $Z_\Lambda^n(\mathbf{r},z)$ [$J_\Lambda^n(\mathbf{r},z)$] are regular (irregular) solutions to the single-site Dirac equation at complex energy z labeled by the combined quantum numbers Λ [$\Lambda = (\kappa,\mu)$], with κ and μ being the spin-orbit and magnetic quantum numbers [34]. The superscript $\times$ indicates the left-hand side solution of the Dirac equation [60]. The quantity $\tau_{\Lambda\Lambda'}^{nm}(z)$ is the scattering path operator that transfers an electronic wave coming in at site m into a wave going out from site n accounting for all possible intermediate scattering events. The retarded and advanced GF are obtained as the side limits $G^\pm(\mathbf{r},\mathbf{r}',E) = \lim_{\eta\to 0^+} G(\mathbf{r},\mathbf{r}',E \pm i\eta)$.

Inserting the real-space representation Eq. (13) into Eqs. (11) and (12) and cyclic permutation under the trace leads to sums of products of matrix elements evaluated on a given site and scattering path operators τ^{mn}. Pursuing the route of Butler [21] having a subsequent CPA averaging in mind, the conductivity tensor will partition into an on-site term σ^0 involving regular (Z_Λ) as well as irregular solutions (J_Λ) and an off-site term σ^1 containing only regular solutions (both for Fermi sea and surface terms):

$$\sigma_{\mu\nu}^\xi = \sigma_{\mu\nu}^{\xi 0} + \sigma_{\mu\nu}^{\xi 1}$$

$$= \sigma_{\mu\nu}^{\xi 0,I} + \sigma_{\mu\nu}^{\xi 1,I} + \sigma_{\mu\nu}^{\xi 0,II} + \sigma_{\mu\nu}^{\xi 1,II}. \quad (14)$$

Working towards determining the energy derivative of the GF in terms of finite differences (see below) as well as representing the GF above and below the real axis leads to expressions of the form

$$\frac{1}{\Omega}\mathrm{Tr}\big\langle \hat{J}_\mu^\xi \hat{G}(z_a)\hat{j}_\nu \hat{G}(z_b)\big\rangle = \frac{1}{\Omega}\mathrm{Tr}\int_\Omega d^3r\,\hat{J}_\mu^\xi\,\Delta G_\nu(\mathbf{r},\mathbf{r},z_a,z_b)$$

$$= \frac{1}{\Omega_n}\mathrm{Tr}\int_{\Omega_n} d^3r\,\hat{J}_\mu^\xi\,\Delta G_\nu^n(\mathbf{r},\mathbf{r},z_a,z_b),$$

(Ω_n denotes the volume of the unit cell at site n), containing pairs of complex energies z_a and z_b and contributions to ΔG_ν with

$$\Delta G_\nu^n(\mathbf{r},\mathbf{r},z_a,z_b) = \sum_{\alpha\beta} x_\alpha x_\beta \Delta G_\nu^{1,\alpha\beta,n}(\mathbf{r},\mathbf{r},z_a,z_b)$$

$$+ \sum_{k=1}^4 x_\alpha \Delta G_{\nu k}^{0,\alpha,n}(\mathbf{r},\mathbf{r},z_a,z_b), \quad (15)$$

given in Appendix A. The Greek indices (α,β) denote alloy partners and x_α their concentrations. The terms in $\Delta G_{\nu k}^{0,\alpha,n}$ containing irregular solutions J_Λ, $k \in \{1,2,3,4\}$ are associated with the on-site contributions $\sigma^{\xi 0}$ only. The term $\Delta G_{\nu 1}^{1,\alpha\beta,n}$

containing exclusively regular solutions Z_Λ contributes to $\sigma^{\xi 1}$ requiring special treatment when performing the statistical average (done here within the CPA in the case of an alloy). The appearing vertex corrections in this term are important and can, particularly in the dilute limit, give sizable contributions to the transverse conductivities (see Refs. [24,27] and below). As shown by Butler [21], they correspond to the scattering term in Boltzmann transport theory [25,65,66].

The evaluation of Eq. (15) leads to matrix elements of regular functions of the form $M_{\Lambda\Lambda'}^{ab\nu} = \langle Z_\Lambda^\times(z_a)|\hat{O}_\nu|Z_{\Lambda'}(z_b)\rangle_{\Omega_n}$ and matrix elements involving irregular functions whose evaluation is outlined in Appendix B. Let us note that the formalism is very general insofar as other linear response quantities (Gilbert damping, spin-orbit torques, etc.) are easily obtained by the appropriate choice of operators ($\hat{A}$, $\hat{B}$) and adaptation of their matrix elements to be inserted in the final multiple-scattering transport expressions.

The described formalism is applicable to pure systems as well as alloys in the full concentration range. For a pure system with a perfect band structure, the transverse (antisymmetric) component of the response is called intrinsic and is often associated with the existence of the Berry curvature coded in the band structure. An alloy, however, has no well-defined energy bands. Within the formalism presented here, one can separate the full response into coherent and incoherent contributions, with the latter exclusively caused by the vertex corrections. As a manner of speaking, the coherent contributions are here named intrinsic, the incoherent ones are called extrinsic, and the presented formalism captures both of them.

III. IMPLEMENTATION AND COMPUTATIONAL DETAILS

The expressions (11) and (12) as well as the following equations have been implemented into the MUNICH SPR-KKR package [63,67]. A fully relativistic Dirac four-component scheme for the basis functions Z_Λ and J_Λ has been used throughout with an angular momentum cutoff of $\ell_{\max} = 3$. The self-consistent field (SCF) potentials have been obtained within KSD-SDFT employing the Vosko-Wilk-Nussair (VWN) parametrization [68] for the exchange-correlation functional in the local density approximation (LDA). The involved energy integration has been performed on a semicircle in the complex plane using typically 50 energy points and 45^3 ($56^2 \times 30$) for cubic (hcp) system k-points in the BZ. As a shape approximation for the potential, the atomic sphere approximation (ASA) has been used. Experimental lattice constants have been used. Using these SCF potentials, subsequent Kubo-Bastin transport calculations have been performed. For the determination of the Fermi-surface term Eq. (11) in the concentrated regime of alloys approximately 10^5 k points in the BZ turned out to be sufficient due to smearing of the GF in k space for the disordered system. In the dilute limit with the concentration of an alloy partner becoming very small, around 10^6–10^7 k points had to be used to ensure convergence. In contrast to the disordered systems which for the calculations are carried out on the real-energy axis for pure elements, a small imaginary part has been added, $z = E_F + i\eta$, and an extrapolation for $\eta \to 0^+$ has been carried out while ensuring

TABLE I. The AHC σ_{xy} in $(\Omega\,cm)^{-1}$ of the ferromagnetic transition metals bcc-Fe, hcp-Co, and fcc-Ni and the alloys $Fe_{50}Pd_{50}$ and $Ni_{50}Pd_{50}$ from *first-principles* theoretical (present work compared to other) as well as experimental (expt.) studies. The magnetization has been assumed to be oriented along the [001] direction.

	σ_{xy}^0	$\sigma_{xy}^{1,I}$	$\sigma_{xy}^{1,II}$	σ_{xy}	σ_{xy}^{theo}	σ_{xy}^{exp}
Fe	20	687	192	899	750,[d] 878,[e] 796[f]	1032[a]
Co	39	316	169	524	484,[g] 694,[e] 471[f]	813[h]
Ni	–84	–2654	57	–2681	–2500,[e] –2432[f]	–1100[b]
$Fe_{50}Pd_{50}$ (nvc)	–18	314	101	397		
$Fe_{50}Pd_{50}$ (vc)	–18	457	102	541		303[c]
$Ni_{50}Pd_{50}$ (nvc)	–113	–1830	130	–1813		
$Ni_{50}Pd_{50}$ (vc)	–113	–1417	130	–1400		–1293[c]

[a]Reference [69].
[b]Reference [70].
[c]Reference [71].
[d]Intrinsic, BCA, Ref. [16].
[e]Intrinsic, + scattering-independent side-jump, Ref. [72].
[f]Kubo-Bastin, TB-LMTO, Ref. [28].
[g]Intrinsic, BCA, Ref. [73].
[h]Estimated expt. value, Ref. [18].

for every value of η convergence with respect to the k mesh. Values of up to 10^9 k points have been used in this case.

For the treatment of the Fermi-sea contribution, Eq. (12) the energy path has been distorted to a semicircle in the upper (lower) half of the complex plane for the first (second) term containing the retarded (advanced) GF G^+ (G^-) encompassing the valence states. The derivative of the GFs in the complex plane along a direction parallel to the real axis has been obtained by a two-point finite difference formula, $d\hat{G}^\pm(z)/dz \approx \frac{1}{h}[\hat{G}^\pm(z+h/2) - \hat{G}^\pm(z-h/2)]$, with $h \in \mathbb{R}$. A value of $h = 10^{-4}$ Ry turned out to be sufficient because of the smearing of the GF in the complex plane. The latter smoothing of the GF also leads to a fast k-mesh convergence, and it was sufficient to use around 10^3 k points at each energy point, except for the points near and next nearest to the real axis at E_F for which typically 10^6 k points have been used.

Here we restrict the spin current-density operator to z polarization, i.e., only $\hat{\mathbf{J}}^z$ is considered. Other polarization directions and the resulting tensor forms in a fully relativistic approach are discussed elsewhere [45]. Furthermore, as we here consider the SHE in paramagnetic systems without external fields, the vanishing vector potential in Eq. (8) results in a spin-polarization current-density operator with components

$$\hat{J}_\mu^z = \left(\beta\Sigma_z - \frac{\gamma_5\hat{p}_z}{mc}\right)|e|c\alpha_\mu, \quad \mu \in \{x, y\}. \quad (16)$$

More details on the evaluation of matrix elements are given in Appendix B.

IV. RESULTS AND DISCUSSION

In Tables I and II we show the anomalous Hall conductivity (AHC) for various systems as calculated by the Kubo-Bastin approach [Eqs. (11) and (12)] for both pure systems as well as alloys.

TABLE II. The SHC σ_{xy}^z in $(\Omega\,cm)^{-1}$ of the nonmagnetic metals Cu, Pt, and Au and the alloys $Cu_{50}Au_{50}$ and $Au_{50}Pt_{50}$ from *first-principles* theoretical (present work compared to other) studies.

	σ_{xy}^{z0}	$\sigma_{xy}^{z1,I}$	$\sigma_{xy}^{z1,II}$	σ_{xy}^z	$\sigma_{xy}^{z,theo}$
Cu	–17	172	28	184	
Pt	98	4093	133	4324	4400[a]
Au	–16	743	90	817	700,[b] 800[c]
$Cu_{50}Au_{50}$ (nvc)	–20	605	71	656	
$Cu_{50}Au_{50}$ (vc)	–20	872	71	923	
$Au_{50}Pt_{50}$ (nvc)	34	2911	607	3553	
$Au_{50}Pt_{50}$ (vc)	34	2992	607	3634	

[a]Intrinsic, BCA, Ref. [17].
[b]Intrinsic, BCA, Ref. [76].
[c]Intrinsic, BCA, Ref. [77].

Let us first turn to the ferromagnetic systems and the determined values for the anomalous Hall conductivities. Table I shows the total conductivities σ_{xy} and the various contributions to it for the elemental ferromagnets Fe, Co, and Ni as well as for the two alloys $Fe_{50}Pd_{50}$ and $Ni_{50}Pd_{50}$. Discussing the overall numbers, one can state that for the systems considered the Fermi-surface contribution $\sigma_{xy}^{1,I}$ is the dominant one, but also the Fermi-sea term $\sigma_{xy}^{1,II}$ can give a significant contribution. This is seen, in particular, for the systems Fe, Co, and $Fe_{50}Pd_{50}$. Similar observations have been made before [28] in a tight-binding LMTO (TB-LMTO) framework (see the remarks below).

The site-diagonal term σ_{xy}^0 is not significant, contributing only 2%–3% with a maximum of 10%. Note that we here show the sum of both Fermi sea and surface contributions to σ_{xy}^0. Both are numerically delicate, as they contain matrix elements involving the irregular solutions $J_\Lambda^n(\mathbf{r}, z)$ and can become rather large. However, their sum σ_{xy}^0 is small.

The AHC has been calculated recently within a Kubo-Bastin framework implemented in the TB-LMTO electronic structure method [28]. When comparing the results presented here to the latter ones, however, one has to be careful. First, in the TB-LMTO method the coherent potential functions and structure constants depend on the chosen representation. Even though the full conductivity is invariant with respect to the particular choice, some ambiguity in assigning terms contributing to the surface and sea terms arises, as only the sum of the antisymmetric part of the coherent surface term and sea term is invariant. Therefore only the numbers for the total conductivities should be compared. Second, in the LMTO transport approach there appear only intersite hoppings. A term equivalent to the site-diagonal contribution σ^0 appearing in the present work does not exist. Third, the TB-LMTO method employs (configuration independent) effective velocity operators, i.e., the operator matrix elements are nonrandom while here the matrix elements as well as the scattering path operator are configuration dependent.

Turning now to the particular systems, for bcc Fe we find a total AHC that underestimates the experimental value by roughly 10%. On the other hand, this number is comparable to those obtained in calculations of the AHC employing the Berry curvature approach (BCA), including the intrinsic as well as a

KÖDDERITZSCH, CHADOVA, AND EBERT

scattering-independent side-jump term ($\sigma_{xy} = 878\,(\Omega\,\text{cm})^{-1}$, Ref. [72]). Both of these contributions are included in the present formalism (coherent part). Note that calculations using the BCA leaving out the scattering-independent side-jump term give smaller values [15,16] [in the range of $\sigma_{xy} = 750\,(\Omega\,\text{cm})^{-1}$]. For hcp Co the comparison to experiment as well as other theoretical results is less clear-cut, as there is a larger variation. Furthermore, the Fermi-sea term represents a significant contribution to the total AHC, as has been observed in another recent work [28]. For Ni notably all theoretical calculations employing the LDA grossly overestimate the experimental value. This has already been attributed to the deficiencies in properly describing the electronic structure, namely, the correlations are not fully captured by this approximation. Using the LDA $+\,U$ or GGA $+\,U$ approach, AHCs are obtained that are close to experimental values [20,57,72].

For alloys we show results for a particular concentration for $\text{Fe}_{50}\text{Pd}_{50}$ and $\text{Ni}_{50}\text{Pd}_{50}$ in Table I. Results for calculations including the vertex corrections (vc) as well as excluding them (nvc) are given. As can be seen the vc contribute substantially in the Fermi-surface term. On the other hand the Fermi-sea term does not contain any incoherent contribution, i.e. the vc do not occur in this case. This is in accord with the findings in Ref. [28], where it was analytically shown that for the AHE treated within the TB-LMTO CPA the vc are vanishing in the Fermi sea. Note, however, that this proof relied on a particular formulation of the CPA equations within the TB-LMTO formalism.

In Fig. 1 we show the AHC for $\text{Fe}_x\text{Pd}_{1-x}$ as a function of concentration. Overall the concentration dependence as well as the sign change is in good agreement to experiment. For all concentrations the dominant contribution to the AHC is given by the site-off diagonal Fermi-surface term ($\sigma_{xy}^{1,I}$). By analyzing the contribution dependence in more detail one observes
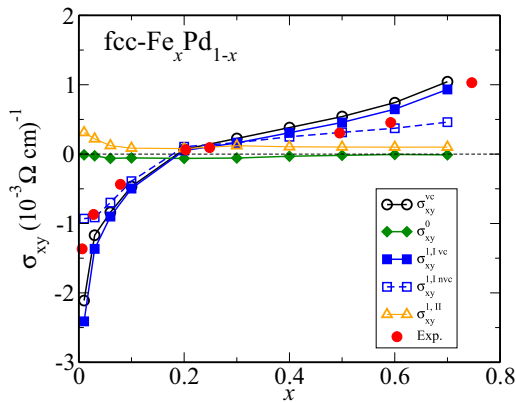

FIG. 1. (Color online) The AHC of fcc-$\text{Fe}_x\text{Pd}_{1-x}$ as a function of concentration x determined within the Kubo-Bastin formalism. The total AHC (σ_{xy}^{vc}) and different contributions to it are shown: the on-site term (σ_{xy}^{0}), the off-site Fermi-surface term, including vertex corrections ($\sigma_{xy}^{1,I,\text{vc}}$) and the off-site Ferm-sea contribution ($\sigma_{xy}^{1,II}$). Additionally, the off-site term omitting the vc ($\sigma_{xy}^{1,I,\text{nvc}}$) is shown for comparison. Experimental data [71] for σ_{xy} (full circles) determined at $T = 4.2$ K is also displayed.

that the incoherent contributions (vc) play a minor role in the middle of the concentration range but become very important at small concentrations. This dominance of extrinsic effects at small concentrations lends credibility to the Boltzmann formalism that is applicable to alloys in the dilute limit and captures the skew-scattering contribution [74]. Note that the formalism presented here gives all contributions to the AHC and allows one to extract intrinsic (coherent) as well as extrinsic (incoherent) contributions (e.g., skew scattering and side jump), as has been done before in the Kubo-Středa approach [24–26]. The site-diagonal term σ_{xy}^{0} gives only a minor contribution to the AHC over the whole concentration range and shows almost negligible variation. The Fermi-sea term $\sigma_{xy}^{1,II}$ follows the same trend, even though it is somewhat larger and shows stronger variation for vanishing concentration ($x \to 0$). One exception to the former statements is the range in which the total AHC changes sign ($x \approx 0.2$). There the site-diagonal as well as the Fermi-sea term gain larger relative weight that is, however, due to the fact that the Fermi-surface term approaches zero.

Let us turn now to the discussion of paramagnetic systems and the spin Hall conductivity (SHC). As both the AHE and SHE share the same relativistic origin and underlying mechanisms, observations made for the SHC can be discussed along the lines above for the AHC. In Table II we show the intrinsic SHC for Cu, Pt, and Au as well as the full SHC for the alloys $\text{Cu}_{50}\text{Au}_{50}$ and $\text{Au}_{50}\text{Pt}_{50}$. Overall, again the site-diagonal contribution σ_{xy}^{z0} is very small. The Fermi-sea contribution $\sigma_{xy}^{z1,II}$ is small but non-negligible, and for $\text{Au}_{50}\text{Pt}_{50}$ is largest and constitutes about 15% of the total SHC. For the pure systems Pt and Au, there is fair agreement to other theoretical BCA-based calculations. Let us note here that for Pt and Au the experimental spin Hall angle α_{sH}, i.e., the ratio between the SHC and the longitudinal charge conductivity for pure systems, is discussed rather controversially, with large scatter in the reported data (Pt: $\alpha_{\text{sH}} = 0.37\ldots 12$, Au: $\alpha_{\text{sH}} = 0.8\ldots 11.3$). Therefore we omitted a detailed list of experimental values in Table II and refer the interested reader to a recent compilation of experimental data [75]. Note further that in the case of the SHC for disordered systems the vertex corrections also vanish numerically in the Fermi-sea term, as has been observed for the AHC (see Table II). This can be seen as a result of the particular construction of the vc Eq. (A2), as these are only expressed in terms of scattering path operators τ and are independent of the chosen operators for the matrix elements.

In Fig. 2 we show the concentration-dependent SHC of the alloy $\text{Cu}_x\text{Au}_{1-x}$. For this system the total SHC is essentially given by the Fermi-surface term $\sigma_{xy}^{z1,I}$, with the site-diagonal and Fermi-sea term giving almost negligible contribution and having the largest relative contribution in the middle of the concentration range. The large diverging scattering contributions for $x \to 0$ and $x \to 1$ are of incoherent (extrinsic) origin, an observation already made for other dilute alloys [25]. A comment concerning both AHC and SHC in dilute alloys seems in due place here: together with the divergence of the SHC at the boundaries, also the longitudinal conductivities will diverge such that the ratio $\sigma_{xy}^{(z)}/\sigma_{xx}$, namely, the anomalous or spin Hall angle, that is usually determined in experiment, will have a finite value. Furthermore, as the intrinsic contribution
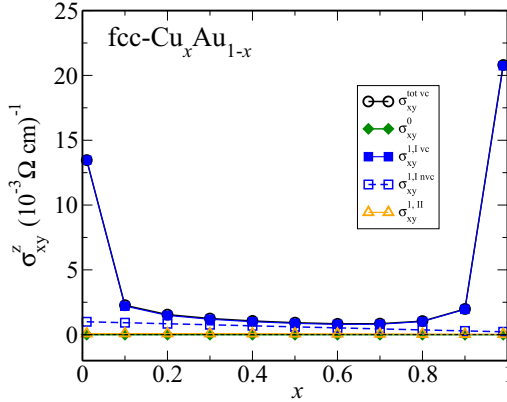
FIG. 2. (Color online) The SHC of Cu_xAu_{1-x} as a function of concentration x determined within the Kubo-Bastin formalism. The total SHC and different contributions (notation: see text and Fig. 1 caption) to it are displayed.

to the AHC/SHC for a perfect crystal (no disorder) is finite, its contribution to the Hall angle at $T = 0$ K will vanish. At finite temperature, however, induced scattering by lattice vibrations or impurities will lead to a finite σ_{xx} and indeed, experimental data for the AHE in metallic systems is often obtained by varying temperature or by doping.

V. SUMMARY

We presented a general linear response Kubo-Bastin approach and a subsequent implementation within a first-principles multiple-scattering Green's function method. The so-called Fermi-surface and Fermi-sea contributions are both treated on equal footing, employing a fully relativistic formulation spin-orbit-induced phenomena, particularly transverse transport quantities as the anomalous and spin Hall effect are properly described. The derived transport expression gives all elements of the (conductivity) tensor, namely, the symmetric and, in particular, antisymmetric components. Furthermore, the approach is not only able to deal with pure systems, but, using the CPA, substitutionally disordered alloys of any concentration can be treated, thereby avoiding inferior approximations as the virtual crystal approximation (VCA) and/or large supercells. The described method is able to capture both intrinsic as well as extrinsic (e.g., side-jump and skew-scattering) contributions to the transport tensors consistently within one and the same formulation. Vertex corrections (within the CPA) are fully taken into account. We presented applications for the AHE and SHE and discussed the various contributions to the (spin) transport tensors for pure systems as well as a number of transition-metal alloys.

As the derived expression within the KKR(-CPA) factorizes into matrix elements of the chosen operators and products of scattering path operators, the method can be straightforwardly adapted to deal with a number of linear response quantities by simply replacing the matrix elements. This concerns, e.g., the Gilbert damping [38] or spin-orbit torques. Spin-caloritronic quantities (e.g., spin and anomalous Nernst effects) will be accessible with minor effort within the presented Kubo-Bastin approach.

Finally, we want to point out that finite-temperature effects can be easily taken into account, as has already been done in Kubo-Greenwood–like formulations for longitudinal transport and Gilbert damping [38,78] using an alloy analogy model for lattice vibrations and spin fluctuations.

APPENDIX A: KKR-CPA TRANSPORT FORMALISM FOR THE KUBO-BASTIN FORMULATION

Starting from Eqs. (11) and (12) and due to the employed contour integration and the required energy derivative of the GF, matrix elements have to be calculated for pairs of complex energies. Note that in former approaches using the Kubo-Greenwood formulation for disordered alloys, calculations were performed on the real axis (symmetric surface term only). This very much simplified the expressions and implementation, as on the real axis the wave functions (Z_Λ and J_Λ) become real and one can neglect the second term in Eq. (13) containing the irregular solutions [see also Eq. (7)]. Furthermore, phase relations have been used to relate wave functions with energy $z = (\lim_{\eta \to 0^+} E_F + i\eta)$ to those with $z = \lim_{\eta \to 0^+}(E_F - i\eta)$, leading to transformation relations between matrix elements for the $\langle jG^+jG^+ \rangle$, $\langle jG^+jG^- \rangle$, $\langle jG^-jG^+ \rangle$, and $\langle jG^-jG^- \rangle$ terms in Eq. (11). Away from the real axis (i.e., when evaluating the Fermi-sea contribution and distorting the integration path for the energy into the complex plane) these are not applicable anymore for arbitrary operator pairs. For the τ matrix the following relation is, however, valid,

$$\tau_{\Lambda\Lambda'}^{nm}(z^*) = (-)^{l+l'}\left[\tau_{\Lambda'\Lambda}^{mn}(z)\right]^*, \tag{A1}$$

and can therefore be exploited. In what follows we work along the solution of the transport equation and notation introduced by Butler [21] and, however, extend it to the Kubo-Bastin formalism. For reasons of simplified notation, we here present only the case of having one atom per unit cell; the indices n and m therefore are numbering the unit cells in the crystal. With this the contributions to ΔG_ν^n Eq. (15) read as

$$\Delta G_\nu^{1,\alpha\beta,n}(\mathbf{r},\mathbf{r},z_a,z_b) = \sum_{\Lambda_1\Lambda_2\Lambda_3\Lambda_4} Z_{\Lambda_1}^{\alpha n}(\mathbf{r},z_a)\, j_{\nu\Lambda_2\Lambda_3}^{A\beta n}(r_{ws},z_a,z_b)Z_{\Lambda_4}^{\alpha n\times}(\mathbf{r},z_b)$$

$$\times \sum_{\Lambda_5\Lambda_6\Lambda_7\Lambda_8} \tilde{D}_{\Lambda_8\Lambda_4}^\alpha(z_b)D_{\Lambda_1\Lambda_5}^\alpha(z_a)\tilde{D}_{\Lambda_6\Lambda_2}^\beta(z_a)D_{\Lambda_3\Lambda_7}^\beta(z_b)\breve{\chi}_{\Lambda_5\Lambda_6\Lambda_7\Lambda_8}(z_a,z_b),$$

$$\Delta G_{\nu 1}^{0,\alpha,n}(\mathbf{r},\mathbf{r},z_a,z_b) = \sum_{\Lambda_1\Lambda_2\Lambda_3\Lambda_4} Z_{\Lambda_1}^{\alpha n}(\mathbf{r},z_a)\, j_{\nu\Lambda_2\Lambda_3}^{A\beta n}(r_{ws},z_a,z_b)Z_{\Lambda_4}^{\alpha n\times}(\mathbf{r},z_b)$$

$$\times \sum_{\Lambda_5\Lambda_6} D_{\Lambda_1\Lambda_5}^{\alpha}(z_a)\tilde{D}_{\Lambda_6\Lambda_4}^{\alpha}(z_a)\quad \bar{\tau}_{\Lambda_5\Lambda_2}^{nn}(z_a)\,\bar{\tau}_{\Lambda_3\Lambda_6}^{nn}(z_b),$$

$$\Delta G_{\nu 2}^{0,\alpha,n}(\mathbf{r},\mathbf{r},z_a,z_b) = -\sum_{\Lambda_1\Lambda_3\Lambda_4}\bar{\tau}_{\Lambda_3\Lambda_4}^{nn\alpha}(z_b)\left[J_{\Lambda_1}^{\alpha n}(\mathbf{r},z_a)\,Z_{\Lambda_4}^{\alpha n\times}(\mathbf{r},z_b)\,j_{\nu\Lambda_1\Lambda_3}^{A\alpha n}(r,z_a,z_b) + Z_{\Lambda_1}^{\alpha n}(\mathbf{r},z_a)\,Z_{\Lambda_4}^{\alpha n\times}(\mathbf{r},z_b)\,\bar{j}_{\nu\Lambda_1\Lambda_3}^{B\alpha n}(r,z_a,z_b)\right],$$

$$\Delta G_{\nu 3}^{0,\alpha,n}(\mathbf{r},\mathbf{r},z_a,z_b) = -\sum_{\Lambda_1\Lambda_2\Lambda_3}\bar{\tau}_{\Lambda_1\Lambda_2}^{nn\alpha}(z_a)\left[Z_{\Lambda_1}^{\alpha n}(\mathbf{r},z_a)\,J_{\Lambda_3}^{\alpha n\times}(\mathbf{r},z_b)\,j_{\nu\Lambda_2\Lambda_3}^{An}(r,z_a,z_b) + Z_{\Lambda_1}^{\alpha n}(\mathbf{r},z_a)\,Z_{\Lambda_3}^{\alpha n\times}(\mathbf{r},z_b)\,\bar{j}_{\nu\Lambda_2\Lambda_3}^{C\alpha n}(r,z_a,z_b)\right],$$

$$\Delta G_{\nu 4}^{0,\alpha,n}(\mathbf{r},\mathbf{r},z_a,z_b) = \sum_{\Lambda_1\Lambda_3}\left[J_{\Lambda_1}^{\alpha n}(\mathbf{r},z_a)\,J_{\Lambda_3}^{\alpha n\times}(\mathbf{r},z_b)\,j_{\nu\Lambda_1\Lambda_3}^{A\alpha n}(r,z_a,z_b) + Z_{\Lambda_1}^{\alpha n}(\mathbf{r},z_a)\,Z_{\Lambda_3}^{\alpha n\times}(\mathbf{r},z_b)\,\bar{j}_{\nu\Lambda_1\Lambda_3}^{D\alpha n}(r,z_a,z_b)\right],$$

with $\bar{\tau}$ denoting the CPA averaged τ matrix and the Greek indices α,β signify the atom type which occupies an atomic site n,m. In the last expression the auxiliary r-dependent quantities containing the charge current operator,

$$j_{\nu\Lambda_1\Lambda_2}^{A\alpha n}(r,z_a,z_b) = \int_0^r d^3r'\, Z_{\Lambda_1}^{\alpha n\times}(\mathbf{r}',z_a)\,\hat{j}_\nu\, Z_{\Lambda_2}^{\alpha n}(\mathbf{r}',z_b),$$

$$j_{\nu\Lambda_1\Lambda_2}^{B\alpha n}(r,z_a,z_b) = \int_0^r d^3r'\, J_{\Lambda_1}^{\alpha n\times}(\mathbf{r}',z_a)\,\hat{j}_\nu\, Z_{\Lambda_2}^{\alpha n}(\mathbf{r}',z_b),$$

$$j_{\nu\Lambda_1\Lambda_2}^{C\alpha n}(r,z_a,z_b) = \int_0^r d^3r'\, Z_{\Lambda_1}^{\alpha n\times}(\mathbf{r}',z_a)\,\hat{j}_\nu\, J_{\Lambda_2}^{\alpha n}(\mathbf{r}',z_b),$$

$$j_{\nu\Lambda_1\Lambda_2}^{D\alpha n}(r,z_a,z_b) = \int_0^r d^3r'\, J_{\Lambda_1}^{\alpha n\times}(\mathbf{r}',z_a)\,\hat{j}_\nu\, J_{\Lambda_2}^{\alpha n}(\mathbf{r}',z_b),$$

$$\bar{j}_{\nu\Lambda_1\Lambda_2}^{X\alpha n}(r,z_a,z_b) = j_{\nu\Lambda_1\Lambda_2}^{X\alpha n}(r_{ws},z_a,z_b) - j_{\nu\Lambda_1\Lambda_2}^{X\alpha n}(r,z_a,z_b),$$

$$\text{for}\quad X = A,B,C,D$$

have been used, where r_{ws} denotes the Wigner-Seitz (or ASA) radius. The following standard definitions [21,64] for the auxiliary matrices $D^\alpha,\tilde{D}^\alpha,x^\alpha,\Delta m^\alpha$, and $\tau^{nn\alpha}$ are employed:

$$D^\alpha = 1 + \bar{\tau}^{00}x^\alpha,\quad \tilde{D}^\alpha = 1 + x^\alpha\bar{\tau}^{00},$$

$$x^\alpha = [1 - \Delta m^\alpha\,\bar{\tau}^{00}]^{-1}\,\Delta m^\alpha,$$

$$\Delta m^\alpha = \bar{m} - m^\alpha,\quad \tau^{nn\alpha} = D^\alpha\bar{\tau}^{00} = \bar{\tau}^{00}\tilde{D}^\alpha,$$

where $\bar{m} = \bar{t}^{-1}$, with $\bar{t}$ being the CPA average of the single-site t matrices t^α and $m^\alpha = [t^\alpha]^{-1}$. In the solution of the transport equations the quantity

$$\tilde{\chi}_{\Lambda_1\Lambda_2\Lambda_3\Lambda_4} = \tilde{\chi}_{K_1K_2} = \{[1 - \chi\,w]^{-1}\chi\}_{K_1K_2},\quad \text{(A2)}$$

where the combined indices $K_1 = (\Lambda_1\Lambda_4), K_2 = (\Lambda_2\Lambda_3)$ play a crucial role as they contain the vertex corrections. The auxiliary quantity χ is given by

$$\chi_{K_1K_2} = \chi_{\Lambda_1\Lambda_2\Lambda_3\Lambda_4}(z_a,z_b)$$

$$= \sum_{m,m\neq n} \bar{\tau}_{\Lambda_1\Lambda_2}^{nm}(z_a)\,\bar{\tau}_{\Lambda_3\Lambda_4}^{mn}(z_b)$$

$$= \left[\frac{1}{\Omega_{BZ}}\int_{\Omega_{BZ}}\bar{\tau}_{\Lambda_1\Lambda_2}(\mathbf{k},z_a)\bar{\tau}_{\Lambda_3\Lambda_4}(\mathbf{k},z_b)\,d^3k\right]$$

$$- \bar{\tau}_{\Lambda_1\Lambda_2}^{nn}(z_a)\,\bar{\tau}_{\Lambda_3\Lambda_4}^{nn}(z_b),\quad \text{(A3)}$$

and is obtained via an integral over the BZ and results from the assumed periodicity of the CPA medium after a Fourier transformation. The determination of the four index quantity χ and the inversion Eq. (A2) are computationally very demanding, in particular, when many k points are needed and with growing system size (number of atoms per unit cell). A scheme to exploit symmetry when dealing with the BZ integral Eq. (A3) has been worked out previously [79]. This allows us to restrict $\chi_{K_1K_2}$ to its nonzero elements and to integrate only over the irreducible part of the BZ. The interaction term w is given as

$$w_{\Lambda_1\Lambda_2\Lambda_3\Lambda_4}(z_a,z_b) = w_{K_1K_2}(z_a,z_b)$$

$$= \sum_\alpha c_\alpha x_{\Lambda_1\Lambda_2}^\alpha(z_a)x_{\Lambda_3\Lambda_4}^\alpha(z_b),$$

where c_α in the last expression denotes the concentration of the alloy partner α (denoted as x_α in the main text).

Setting w to zero in Eq. (A2) amounts to neglecting the vertex corrections. Further note, however, that the formalism is equally well applicable to pure systems. In that case $\chi = \tilde{\chi}$ because $w = 0$.

APPENDIX B: MATRIX ELEMENTS

The regular and irregular solutions of Eq. (1) are expanded into four spinors of the form [80,81]

$$Z_\Lambda(\mathbf{r}) = \sum_{\Lambda'}\begin{pmatrix} g_{\Lambda'\Lambda}(r)\chi_{\Lambda'}(\hat{\mathbf{r}}) \\ if_{\Lambda'\Lambda}(r)\chi_{-\Lambda'}(\hat{\mathbf{r}}) \end{pmatrix},\quad \text{(B1)}$$

where g and f are the radial functions of the large and small components, respectively, and χ_Λ are the usual spin-angular functions [34], being linear combinations of products of complex spherical harmonics Y_l^m and the spin functions $\chi_{m_s}, m_s \in \{-\frac{1}{2},+\frac{1}{2}\}$. The quantum number Λ in the latter expression is used to label the states which can have mixed spin-angular character. We use the notation $-\Lambda = (-\kappa,\mu)$.

Both, the AHE and SHE in the linear response framework originate from a perturbation given by the charge current. Within the relativistic framework used here the current operator is represented by $\hat{\mathbf{j}} = -|e|c\boldsymbol{\alpha}$. Therefore, matrix elements of the Dirac α_μ have to be evaluated. Note, when calculating these matrix elements significant errors can be introduced when using the shape approximation in the form of the ASA.

Here we use a scheme proposed by Shilkova and Shirokovskii [82] that has already been used before to correct for these errors. This can be checked by comparing to yet another form of the matrix elements for α that has been derived before [83] and relies on rewriting the matrix elements using the anticommutator $[\hat{H}_{\mathrm{D}},\boldsymbol{\alpha}]_+$ into an equivalent form containing the momentum operator $\hat{\mathbf{p}}$.

The calculations of matrix elements of the spin-polarization current-density operator Eq. (16) is naturally split into two components. The first component contains products of β,α_μ and Σ_z matrices which can be simplified using

$$\beta\Sigma_z\alpha_\mu = i\varepsilon_{z\mu\nu}\begin{pmatrix} 0 & -\sigma_\nu \\ \sigma_\nu & 0 \end{pmatrix}, \quad \mu \in \{x,y\}, \quad \nu \neq z,\mu,$$
(B2)

where in the last expression ε_{ijk} is the Levi-Civita symbol with the understanding of the mapping $x \to 1$, $y \to 2$, $z \to 3$ for the coordinate directions. By inspection of Eq. (2) it is seen that the matrix elements Eq. (B2) can be easily computed using the existing matrix elements of the current operator containing the α_μ matrices.

The second part involves matrix elements of the operator $\gamma_5\hat{p}_z\alpha_\mu$, i.e.,

$$\gamma_5\hat{p}_z\alpha_\mu = -\frac{\hbar}{i}\nabla_z\Sigma_\mu ,$$
(B3)

which are evaluated using the gradient formula of Ref. [33], Eq. (2.57):

$$\begin{aligned}
\nabla_M \phi_l(r) Y_l^m(\hat{\mathbf{r}}) &= \sqrt{\frac{l+1}{2l+3}} \, C(l\,1,l+1;m\,M) \\
&\quad \times Y_{l+1}^{m+M}(\hat{r})\left[\frac{d\phi_l(r)}{dr} - \frac{l}{r}\phi_l(r)\right] \\
&\quad - \sqrt{\frac{l}{2l-1}} \, C(l\,1,l-1;m\,M) \\
&\quad \times Y_{l-1}^{m+M}(\hat{r})\left[\frac{d\phi_l(r)}{dr} + \frac{l+1}{r}\phi_l(r)\right],
\end{aligned}$$

with $M \in \{-1,0,1\}$ denoting a spherical coordinate, ϕ_l a radial function, Y_l^m a complex spherical harmonic, and $C(j_1j_2j;m_1m_2)$ being a Clebsch-Gordan coefficient. (For phase conventions and definitions employed, see Ref. [33].) To use the latter formula the vector operator components Eq. (B3) have to be transformed from Cartesian coordinates {x,y,z} into spherical coordinates $\{-1,0,1\}$ using $A_{\pm 1} = \mp\frac{1}{\sqrt{2}}(A_x \pm i\,A_y), A_0 = A_z$, both for the momentum operator and the relativistic Pauli-spin operator Σ_μ.

[1] N. Nagaosa, J. Sinova, S. Onoda, A. H. MacDonald, and N. P. Ong, Rev. Mod. Phys. **82**, 1539 (2010).

[2] M. I. Dyakonov and V. I. Perel, Phys. Lett. A **35**, 459 (1971).

[3] J. E. Hirsch, Phys. Rev. Lett. **83**, 1834 (1999).

[4] J. Sinova, D. Culcer, Q. Niu, N. A. Sinitsyn, T. Jungwirth, and A. H. MacDonald, Phys. Rev. Lett. **92**, 126603 (2004).

[5] G. E. Bauer, A. H. MacDonald, and S. Maekawa, Solid State Commun. **150**, 459 (2010).

[6] Z. Ma, Solid State Commun. **150**, 510 (2010).

[7] K. Tauber, M. Gradhand, D. V. Fedorov, and I. Mertig, Phys. Rev. Lett. **109**, 026601 (2012).

[8] S. Wimmer, D. Ködderitzsch, K. Chadova, and H. Ebert, Phys. Rev. B **88**, 201108 (2013).

[9] A. Manchon and S. Zhang, Phys. Rev. B **78**, 212405 (2008).

[10] I. O. Miron, K. Garello, G. Gaudin, P. J. Zermatten, M. V. Costache, S. Auffret, S. Bandiera, B. Rodmacq, A. Schuhl, and P. Gambardella, Nature **476**, 189 (2011).

[11] C. O. Avci, K. Garello, I. M. Miron, G. Gaudin, S. Auffret, O. Boulle, and P. Gambardella, Appl. Phys. Lett. **100**, 212404 (2012).

[12] N. A. Sinitsyn, J. Phys.: Condens. Mattter **20**, 023201 (2008).

[13] H. Kontani, T. Tanaka, and K. Yamada, Phys. Rev. B **75**, 184416 (2007).

[14] A. Fert and P. M. Levy, Phys. Rev. Lett. **106**, 157208 (2011).

[15] Y. Yao, L. Kleinman, A. H. MacDonald, J. Sinova, T. Jungwirth, D.-S. Wang, E. Wang, and Q. Niu, Phys. Rev. Lett. **92**, 037204 (2004).

[16] X. Wang, J. R. Yates, I. Souza, and D. Vanderbilt, Phys. Rev. B **74**, 195118 (2006).

[17] G. Y. Guo, S. Murakami, T.-W. Chen, and N. Nagaosa, Phys. Rev. Lett. **100**, 096401 (2008).

[18] E. Roman, Y. Mokrousov, and I. Souza, Phys. Rev. Lett. **103**, 097203 (2009).

[19] F. Freimuth, S. Blügel, and Y. Mokrousov, Phys. Rev. Lett. **105**, 246602 (2010).

[20] H.-R. Fuh and G.-Y. Guo, Phys. Rev. B **84**, 144427 (2011).

[21] W. H. Butler, Phys. Rev. B **31**, 3260 (1985).

[22] J. Banhart, H. Ebert, and J. Voitländer, Phys. Status Solidi B **139**, K19 (1987).

[23] I. Turek, J. Kudrnovský, V. Drchal, L. Szunyogh, and P. Weinberger, Phys. Rev. B **65**, 125101 (2002).

[24] S. Lowitzer, D. Ködderitzsch, and H. Ebert, Phys. Rev. Lett. **105**, 266604 (2010).

[25] S. Lowitzer, M. Gradhand, D. Ködderitzsch, D. V. Fedorov, I. Mertig, and H. Ebert, Phys. Rev. Lett. **106**, 056601 (2011).

[26] D. Ködderitzsch, S. Lowitzer, J. B. Staunton, and H. Ebert, Phys. Status Solidi B **248**, 2248 (2011).

[27] I. Turek, J. Kudrnovský, and V. Drchal, Phys. Rev. B **86**, 014405 (2012).

[28] I. Turek, J. Kudrnovský, and V. Drchal, Phys. Rev. B **89**, 064405 (2014).

[29] M. Gradhand, D. V. Fedorov, P. Zahn, and I. Mertig, Phys. Rev. Lett. **104**, 186403 (2010).

[30] A. Crépieux and P. Bruno, Phys. Rev. B **64**, 094434 (2001).

[31] H. Eschrig, *The Fundamentals of Density Functional Theory* (B G Teubner Verlagsgesellschaft, Stuttgart, Leipzig, 1996).

[32] E. Engel and R. M. Dreizler, *Density Functional Theory – An Advanced Course* (Springer, Berlin, 2011).

[33] M. E. Rose, *Elementary Theory of Angular Momentum* (Wiley, New York, 1957).

[34] M. E. Rose, *Relativistic Electron Theory* (Wiley, New York, 1961).

–

KÖDDERITZSCH, CHADOVA, AND EBERT

PHYSICAL REVIEW B **92**, 184415 (2015)

[35] A. Bastin, C. Lewiner, O. Betbeder-Matibet, and P. Nozieres, J. Phys. Chem. Solids **32**, 1811 (1971).

[36] P. Středa, J. Phys. C: Solid State Phys. **15**, L717 (1982).

[37] F. D. M. Haldane, Phys. Rev. Lett. **93**, 206602 (2004).

[38] H. Ebert, S. Mankovsky, D. Ködderitzsch, and P. J. Kelly, Phys. Rev. Lett. **107**, 066603 (2011).

[39] A. Brataas, Y. Tserkovnyak, and G. E. W. Bauer, Phys. Rev. B **84**, 054416 (2011).

[40] S. Mankovsky, D. Ködderitzsch, G. Woltersdorf, and H. Ebert, Phys. Rev. B **87**, 014430 (2013).

[41] A. Manchon and S. Zhang, Phys. Rev. B **79**, 094422 (2009).

[42] F. Freimuth, S. Blügel, and Y. Mokrousov, J. Phys.: Condens. Matter **26**, 104202 (2014).

[43] F. Freimuth, S. Blügel, and Y. Mokrousov, Phys. Rev. B **90**, 174423 (2014).

[44] W. H. Kleiner, Phys. Rev. **142**, 318 (1966).

[45] S. Wimmer, M. Seemann, K. Chadova, D. Ködderitzsch, and H. Ebert, Phys. Rev. B **92**, 041101(R) (2015).

[46] V. Bargmann and E. P. Wigner, Proc. Natl. Acad. Sci. USA **34**, 211 (1948).

[47] A. Vernes, B. L. Györffy, and P. Weinberger, Phys. Rev. B **76**, 012408 (2007).

[48] S. Lowitzer, D. Ködderitzsch, and H. Ebert, Phys. Rev. B **82**, 140402(R) (2010).

[49] Branislav K. Nikolić, Phys. Rev. B **64**, 165303 (2001).

[50] N. A. Sinitsyn, A. H. MacDonald, T. Jungwirth, V. K. Dugaev, and J. Sinova, Phys. Rev. B **75**, 045315 (2007).

[51] T. Naito, D. S. Hirashima, and H. Kontani, Phys. Rev. B **81**, 195111 (2010).

[52] J. Banhart and H. Ebert, Solid State Commun. **94**, 445 (1995).

[53] P. Weinberger, P. M. Levy, J. Banhart, L. Szunyogh, and B. Újfalussy, J. Phys.: Condens. Matter **8**, 7677 (1996).

[54] H. Ebert, A. Vernes, and J. Banhart, Phys. Rev. B **54**, 8479 (1996).

[55] J. Banhart, Phys. Rev. B **53**, 7128 (1996).

[56] L. Dulca, J. Banhart, and G. Czycholl, Phys. Rev. B **61**, 16502 (2000).

[57] D. Ködderitzsch, K. Chadova, J. Minár, and H. Ebert, New J. Phys. **15**, 053009 (2013).

[58] B. Velický, Phys. Rev. **184**, 614 (1969).

[59] X. Wang, X.-G. Zhang, W. H. Butler, G. M. Stocks, and B. N. Harmon, Phys. Rev. B **46**, 9352 (1992).

[60] E. Tamura, Phys. Rev. B **45**, 3271 (1992).

[61] L. Szunyogh, B. Újfalussy, P. Weinberger, and J. Kollar, J. Phys.: Condens. Matter **6**, 3301 (1994).

[62] H. Ebert, Fully relativistic band structure calculations for magnetic solids—Formalism and application, in *Electronic Structure and Physical Properties of Solids*, edited by H. Dreyssé, Lecture Notes in Physics Vol. 535 (Springer, Berlin, 2000), p. 191.

[63] H. Ebert, D. Ködderitzsch, and J. Minár, Rep. Prog. Phys. **74**, 096501 (2011).

[64] J. S. Faulkner and G. M. Stocks, Phys. Rev. B **21**, 3222 (1980).

[65] M. Gradhand, D. V. Fedorov, P. Zahn, and I. Mertig, Phys. Rev. B **81**, 020403 (2010).

[66] M. Gradhand, D. V. Fedorov, P. Zahn, and I. Mertig, Phys. Rev. B **81**, 245109 (2010).

[67] H. Ebert *et al.*, The Munich SPR-KKR package, version 6.3, http://olymp.cup.uni-muenchen.de/ak/ebert/SPRKKR, 2012.

[68] S. H. Vosko, L. Wilk, and N. Nussair, Can. J Phys. **58**, 1200 (1980).

[69] P. N. Dheer, Phys. Rev. **156**, 637 (1967).

[70] L. Ye, Y. Tian, X. Jin, and D. Xiao, Phys. Rev. B **85**, 220403 (2012).

[71] V. A. Matveev and G. V. Fedorov, Fiz. Met. Metalloved **53**, 34 (1982).

[72] J. Weischenberg, F. Freimuth, J. Sinova, S. Blügel, and Y. Mokrousov, Phys. Rev. Lett. **107**, 106601 (2011).

[73] J.-C. Tung, H.-R. Fuh, and G.-Y. Guo, Phys. Rev. B **86**, 024435 (2012).

[74] B. Zimmermann *et al.*, Phys. Rev. B **90**, 220403(R) (2014).

[75] J. Sinova, S. O. Valenzuela, J. Wunderlich, C. H. Back, and T. Jungwirth, arXiv:1411.3249.

[76] Y. Yao and Z. Fang, Phys. Rev. Lett. **95**, 156601 (2005).

[77] G. Y. Guo, J. Appl. Phys. **105**, 07C701 (2009).

[78] H. Ebert, S. Mankovsky, K. Chadova, S. Polesya, J. Minar, and D. Ködderitzsch, Phys. Rev. B **91**, 165132 (2015).

[79] T. Huhne and H. Ebert, Phys. Rev. B **65**, 205125 (2002).

[80] H. Ebert, J. Phys.: Condens. Matter **1**, 9111 (1989).

[81] E. Engel, T. Auth, and R. M. Dreizler, Phys. Rev. B **64**, 235126 (2001).

[82] N. A. Shilkova and V. P. Shirokovskii, Phys. Status Solidi B **149**, 195 (1988).

[83] G. Y. Guo and H. Ebert, Phys. Rev. B **51**, 12633 (1995).

8. Summary

The central focus of the current work has been the theoretical study of the longitudinal and transverse (anomalous and spin Hall effect) transport properties of pure systems as well as disordered alloys including the impact of finite temperatures. The investigations dealt with a number of different issues. One of them was to study the extrinsic spin Hall effect in dilute metallic alloys and to show how to tailor the magnitude of the spin Hall conductivity can be achieved by materials design via the composition and varying the concentration of the alloy partners. The calculations revealed that by decreasing the impurity concentration, the magnitude of the SHC increases mainly due to the skew-scattering contribution as it is inversely proportional to the impurity concentration in the dilute limit. In contrast, the side-jump contribution is independent of the impurity concentration and has a small magnitude for all considered systems compared to the dominant skew scattering, thus it does not influence the behavior of the extrinsic part of the SHC. Furthermore, in order to understand the microscopic origin of the various contributions to the spin Hall effect, a procedure for the separation of the intrinsic, skew-scattering and two distinct side-jump contributions to the spin Hall conductivity within the ab initio Kubo-Středa approach was presented. The efficiency of the proposed method is demonstrated by a first-principles study of dilute metallic alloys based on Cu, Au, and Pt as hosts materials.

Moreover, the impact of finite temperatures on the transport properties has been studied in detail. This is achieved by treating thermal lattice vibrations and spin fluctuations using the alloy analogy model. Within this approach which is based on the adiabatic approximation, the temperature induced atomic displacements are seen as a random, quasistatic and temperature dependent distortion of the lattice with a corresponding distortion of the potential. The resulting temperature induced disorder of the potential is treated using the CPA as it is done for chemical disorder due to alloying. The impact of disorder due to thermal spin fluctuations are accounted for by use of the alloy analogy model with the necessary configurational average by means of the CPA. It was demonstrated that taking into account both thermal lattice vibrations and spin fluctuations significantly improves the agreement of the calculated results with experimental data for longitudinal as well as transverse transport.

Finally, the most important part of the current work is dedicated to the development of the Kubo-Bastin formalism and its further implementation within the multiple-scattering KKR Green function method. The suggested general framework allows us to treat along with anomalous and spin Hall effects, other spin-orbit-induced phenomena such as Gilbert damping and spin-orbit torques. Furthermore, the approach is able to

deal not only with pure systems but also with substitutionally disordered alloys in a wide concentration range. The described method allows us to treat intrinsic as well as extrinsic contributions to the conductivity tensors. In addition, the implemented formalism provides symmetric as well as antisymmetric contributions by calculating Fermi sea and surface contributions which are both treated on equal footing. The versatility of the method is demonstrated by presenting results for the anomalous and spin Hall conductivities for elemental transition metals and their alloys.

A. Matrix elements of the Bargmann-Wigner spin-polarization operator.

According to Vernes et al. [113] the relativistic spin-current density operator $\hat{J}_j^p = |e|c\alpha_j T_p$ can be defined via the four-vector polarization operator $\mathbf{T}$ obtained by Bargmann and Wigner [114], which is given by the following expression:

$$\mathbf{T} = \beta\,\mathbf{\Sigma} - \frac{\gamma_5\,\mathbf{\Pi}}{mc}\,, \tag{A.1}$$

$$T_4 = i\frac{\mathbf{\Sigma}\cdot\mathbf{\Pi}}{mc} \tag{A.2}$$

with the kinetic momentum $\mathbf{\Pi} = \hat{\mathbf{p}} + \frac{|e|}{c}\mathbf{A}$ and the canonical momentum $\hat{\mathbf{p}}$. Then the spin-polarization current-density operator J_j^p for the current along the j-axis and projection on the p-axis ($p \in \{x, y, z\}$) can be written as:

$$\hat{J}_j^p = \left(\beta\,\Sigma_p - \frac{\gamma_5\,\hat{p}_p}{mc}\right)|e|\,c\,\alpha_j\,. \tag{A.3}$$

In order to calculate the corresponding matrix elements of the spin-polarization current-density operator (here the derivation is given in terms of the regular matrix elements Z_Λ), one deals with the matrix elements of the first and second term individually, given by Eq. (A.3):

$$M_{\Lambda\Lambda'}^{jp} = \langle\,Z_\Lambda\,|\,\hat{J}_j^p\,|\,Z_{\Lambda'}\,\rangle = |e|c\,\langle\,Z_\Lambda\,|\,\beta\,\Sigma_p\,\alpha_j\,|\,Z_{\Lambda'}\,\rangle - \frac{|e|}{m}\,\langle\,Z_\Lambda\,|\,\gamma_5\,\hat{p}_p\,\alpha_j\,|\,Z_{\Lambda'}\,\rangle\,. \tag{A.4}$$

In the following derivation the prefactors are omitted for the sake of brevity.

A.1. Contribution of $\beta\,\Sigma_p\,\alpha_j$

Taking into account the commutator relations:

$$[\,\beta\,\Sigma_i, \alpha_j\,]_- = 0 \ \text{ for } \ i \neq j\,, \tag{A.5}$$

$$[\,\beta\,\Sigma_i, \alpha_i\,]_- = 2\gamma_5\,\beta = -2\beta\,\gamma_5 \neq 0 \tag{A.6}$$

and considering the properties of the Pauli-matrices one obtains the following expression with $p, j, k \in \{x, y, z\} = \{1, 2, 3\}$ (latin characters associated with cartesian coordinates) $\forall p, j : p \neq j$:

$$\beta \Sigma_p \alpha_j = i\epsilon_{pjk} \begin{pmatrix} 0 & -\sigma_k \\ \sigma_k & 0 \end{pmatrix}, \tag{A.7}$$

where ϵ is the Levi-Civita symbol and $k \neq p, j$. Using this equation, one can calculate the first part of the spin-polarization current-density operator J_j^p matrix elements (here, the prefactors are omitted):

$$M_{\Lambda\Lambda'}^{jp} = \langle Z_\Lambda | \beta \Sigma_p \alpha_j | Z_{\Lambda'} \rangle \tag{A.8}$$

$$= i\epsilon_{pjk} \int dr^3 \begin{pmatrix} g_\Lambda \chi_\Lambda \\ if_\Lambda \chi_{-\Lambda} \end{pmatrix}^\times \begin{pmatrix} 0 & -\sigma_k \\ \sigma_k & 0 \end{pmatrix} \begin{pmatrix} g_{\Lambda'} \chi_{\Lambda'} \\ if_{\Lambda'} \chi_{-\Lambda'} \end{pmatrix}$$

$$= -\epsilon_{pjk} \left[\int g_\Lambda f_{\Lambda'} \langle \chi_\Lambda | \sigma_k | \chi_{-\Lambda'} \rangle \, dr^3 + \int f_\Lambda g_{\Lambda'} \langle \chi_{-\Lambda} | \sigma_k | \chi_{\Lambda'} \rangle \, dr^3 \right]$$

$$= -\epsilon_{pjk} \left[R_{\Lambda\Lambda'}^1 A_{\Lambda\Lambda'}^{1k} + R_{\Lambda\Lambda'}^2 A_{\Lambda\Lambda'}^{2k} \right]$$

$$= -\epsilon_{pjk} S_{\Lambda\Lambda'}^k \tag{A.9}$$

with the radial $(R_{\Lambda\Lambda'})$ and angular $(A_{\Lambda\Lambda'})$ matrix elements given by:

$$R_{\Lambda\Lambda'}^1 = \int r^2 \, dr \, g_\Lambda f_{\Lambda'}, \tag{A.10}$$

$$R_{\Lambda\Lambda'}^2 = \int r^2 \, dr \, f_\Lambda g_{\Lambda'}, \tag{A.11}$$

$$A_{\Lambda\Lambda'}^{1k} = \langle \chi_\Lambda | \sigma_k | \chi_{-\Lambda'} \rangle, \tag{A.12}$$

$$A_{\Lambda\Lambda'}^{2k} = \langle \chi_{-\Lambda} | \sigma_k | \chi_{\Lambda'} \rangle. \tag{A.13}$$

Taking into account the transformation of the operators from cartesian (x, y, z) to spherical coordinates $(-1, 0, +1)$, namely

$$A_x = \frac{1}{\sqrt{2}} (A_- + A_+), \tag{A.14}$$

$$A_y = \frac{i}{\sqrt{2}} (A_- - A_+), \tag{A.15}$$

$$A_z = A_0, \tag{A.16}$$

$$A_{\pm 1} = \mp \frac{1}{\sqrt{2}} (A_x \pm iA_y). \tag{A.17}$$

Equation (A.8) can be rewritten as follows:

$$\tilde{M}_{\Lambda\Lambda'}^x = \frac{1}{\sqrt{2}} \left[J_{\Lambda\Lambda'}^- + J_{\Lambda\Lambda'}^+ \right], \tag{A.18}$$

$$\tilde{M}_{\Lambda\Lambda'}^y = \frac{i}{\sqrt{2}} \left[J_{\Lambda\Lambda'}^- - J_{\Lambda\Lambda'}^+ \right], \tag{A.19}$$

$$\tilde{M}_{\Lambda\Lambda'}^z = J_{\Lambda\Lambda'}^0 \tag{A.20}$$

with the definition

$$J_{\Lambda\Lambda'}^{\lambda} = R_{\Lambda\Lambda'}^{1} A_{\Lambda\Lambda'}^{1\lambda} + R_{\Lambda\Lambda'}^{2} A_{\Lambda\Lambda'}^{2\lambda} \tag{A.21}$$

with $\lambda \in \{-1, 0, +1\}$.

Furthermore, if one considers the case of $\beta\Sigma_p\alpha_p$ and neglects the fact that two operators do not commute Eq. (A.6), one obtains:

$$\beta\,\Sigma_p\,\alpha_p = \begin{pmatrix} 0 & \mathbb{1}_2 \\ -\mathbb{1}_2 & 0 \end{pmatrix} = \gamma_5\,\beta = -\beta\,\gamma_5 = -\alpha_p\,\beta\,\Sigma_p. \tag{A.22}$$

The corresponding matrix elements are written as:

$$
\begin{aligned}
M_{\Lambda\Lambda'}^{pp} &= \int dr^3 \begin{pmatrix} g_\Lambda\,\chi_\Lambda \\ if_\Lambda\,\chi_{-\Lambda} \end{pmatrix}^{\times} \begin{pmatrix} 0 & \mathbb{1}_2 \\ -\mathbb{1}_2 & 0 \end{pmatrix} \begin{pmatrix} g_{\Lambda'}\,\chi_{\Lambda'} \\ if_{\Lambda'}\,\chi_{-\Lambda'} \end{pmatrix} \\
&= i\left[\int g_\Lambda\,f_{\Lambda'}\,\langle\chi_\Lambda\,|\,\chi_{-\Lambda'}\rangle\,dr^3 + \int f_\Lambda\,g_{\Lambda'}\,\langle\chi_{-\Lambda}\,|\,\chi_{\Lambda'}\rangle\,dr^3\right] \\
&= i\left[R_{\Lambda\Lambda'}^{1}\,\delta_{\Lambda-\Lambda'} + R_{\Lambda\Lambda'}^{2}\,\delta_{-\Lambda\Lambda'}\right] \\
&= i\delta_{\Lambda-\Lambda'}\left[R_{\Lambda\Lambda'}^{1} + R_{\Lambda\Lambda'}^{2}\right]
\end{aligned}
$$

with $\delta_{\Lambda-\Lambda'} = \delta_{-\Lambda\Lambda'}$. However, in the present calculations the spin current density operator is restricted to the z polarization, i.e., only $\hat{\mathbf{J}}^z$ is considered.

A.2. Contribution of $\gamma_5\,\hat{p}_p\,\alpha_j$

Starting from $p_i = \frac{\hbar}{i}\nabla_i$, the second part of the spin-polarization current-density operator given in Eq. (A.4) (omitting the prefactors), can be re-written in the following way:

$$
\begin{aligned}
\gamma_5\,p_p\,\alpha_j &= \frac{\hbar}{i}\nabla_p \begin{pmatrix} 0 & -\mathbb{1}_2 \\ -\mathbb{1}_2 & 0 \end{pmatrix}\begin{pmatrix} 0 & \sigma_j \\ \sigma_j & 0 \end{pmatrix} \\
&= -\frac{\hbar}{i}\nabla_p \underbrace{\begin{pmatrix} \sigma_j & 0 \\ 0 & \sigma_j \end{pmatrix}}_{\Sigma_j} \\
&= -\frac{\hbar}{i}\nabla_p\,\Sigma_j. \tag{A.23}
\end{aligned}
$$

Furthermore using the transformation matrix from spherical to cartesian coordinates

$$
U = \begin{array}{c} x \\ y \\ z \end{array}\begin{pmatrix} \frac{1}{\sqrt{2}} & \frac{1}{\sqrt{2}} & 0 \\ -\frac{i}{\sqrt{2}} & \frac{i}{\sqrt{2}} & 0 \\ 0 & 0 & 1 \end{pmatrix}, \tag{A.24}
$$

A. Matrix elements of the Bargmann-Wigner spin-polarization operator.

Eq. (A.23) takes the following form:

$$\gamma_5 \, p_p \, \alpha_j \;=\; \frac{\hbar}{i} \sum_{\lambda\lambda'} U_{i\lambda} \, U_{j\lambda'} \, \nabla_\lambda \, \gamma_5 \, \alpha_{\lambda'} \;=\; -\frac{\hbar}{i} \sum_{\lambda\lambda'} U_{i\lambda} \, U_{j\lambda'} \, \nabla_\lambda \, \Sigma_{\lambda'} \, . \tag{A.25}$$

First, let's consider the case $p = z$ and $j = x$, i.e. we need to calculate the matrix elements of the operator $\gamma_5 \, p_z \, \alpha_x$, which can be rewritten in spherical coordinates (using Eq. (A.24)) as:

$$\gamma_5 \, p_z \, \alpha_x \;=\; -U_{z0} \, U_{x+} \left(\frac{\hbar}{i} \nabla_0 \right) \Sigma_+ \;-\; U_{z0} \, U_{x-} \left(\frac{\hbar}{i} \nabla_0, \; \right) \Sigma_- \, . \tag{A.26}$$

As one can see from Eq. (A.26) it is necessary to calculate actually two sets of matrix elements, i.e.

$$M^{xz}_{\Lambda\Lambda'} \;=\; M^{0+}_{\Lambda\Lambda'} \;+\; M^{0-}_{\Lambda\Lambda'} \, . \tag{A.27}$$

Hereby, one needs to calculate the matrix elements $M^{0+}_{\Lambda\Lambda'}$ and $M^{0-}_{\Lambda\Lambda'}$ in spherical coordinates and afterwards the transformation to the cartesian coordinates is applied. Therefore:

$$M^{0+}_{\Lambda\Lambda'} \;=\; \langle \, Z^b_\Lambda \, | -\frac{\hbar}{i} \nabla_0 \, \Sigma_+ \, | \, Z^a_{\Lambda'} \, \rangle \;=\; -\int d^3r \, Z^{b\times}_\Lambda \left(\frac{\hbar}{i} \nabla_0 \, \Sigma_+ \right) Z^a_{\Lambda'} \, , \tag{A.28}$$

where a, b indicate different energies. The regular wave functions are given by

$$Z^{b\times}_\Lambda \;=\; (\, g^b_\Lambda \, \chi^\dagger_\Lambda, \; -i f^b_\Lambda \, \chi^\dagger_{-\Lambda} \,) \quad \text{and} \quad Z^a_{\Lambda'} \;=\; \begin{pmatrix} g^a_{\Lambda'} \, \chi_{\Lambda'} \\ i f^a_{\Lambda'} \, \chi_{-\Lambda'} \end{pmatrix} \tag{A.29}$$

with the spin-angular functions:

$$\chi_\Lambda(\hat{r}) \;=\; \sum_{m_s = \pm\frac{1}{2}} C(l \, , \frac{1}{2} j \, ; \mu - m_s, \, m_s) \, Y_l^{\mu - m_s}(\hat{r}) \, \chi_{m_s} \, . \tag{A.30}$$

Inserting Eq. (A.29) into Eq. (A.28), one obtains:

$$\begin{aligned} M^{0+}_{\Lambda\Lambda'} \;&=\; -\langle \, Z^b_\Lambda \, | \frac{\hbar}{i} \nabla_0 \, \Sigma_+ \, | \, Z^a_{\Lambda'} \, \rangle \\ &=\; -\frac{\hbar}{i} \int d^3r \, (\, g^b_\Lambda \, \chi^\dagger_\Lambda \,, \; -i f^b_\Lambda \, \chi^\dagger_{-\Lambda} \,) \begin{pmatrix} \nabla_0 \sigma_+ & 0 \\ 0 & \nabla_0 \sigma_+ \end{pmatrix} \begin{pmatrix} g^a_{\Lambda'} \, \chi_{\Lambda'} \\ i f^a_{\Lambda'} \, \chi_{-\Lambda'} \end{pmatrix} \\ &=\; -\frac{\hbar}{i} \int d^3r \left[g^b_\Lambda \, \chi^\dagger_\Lambda \, \nabla_0 \, \sigma_+ \, g^a_{\Lambda'} \, \chi_{\Lambda'} + f^b_\Lambda \, \chi^\dagger_{-\Lambda} \, \nabla_0 \, \sigma_+ \, f^a_{\Lambda'} \chi_{-\Lambda'} \right] \, . \end{aligned} \tag{A.31}$$

To proceed further with the derivation, it is necessary to make use of following gradient formula [115]:

$$
\begin{aligned}
\nabla_M\,\phi_l(r)\,Y_l^m(\hat{r}) &= \sqrt{\frac{l+1}{2l+3}}\,C(l\,1,\,l+1;m\,M) \\
&\times Y_{l+1}^{m+M}(\hat{r})\left[\frac{d\phi_l(r)}{dr}-\frac{l}{r}\phi_l(r)\right] \\
&- \sqrt{\frac{l}{2l-1}}\,C(l\,1,\,l-1;m\,M) \\
&\times Y_{l-1}^{m+M}(\hat{r})\left[\frac{d\phi_l(r)}{dr}+\frac{l+1}{r}\phi_l(r)\right] \\
&= \sum_{\xi=0}^{1}\sqrt{\frac{l+\xi}{2l+4\xi-1}}C(l\,1,\,l-1+2\xi;m\,M) \\
&\times Y_{l-1+2\xi}^{m+M}(\hat{r})\left[(-)^{1+\xi}\frac{d\phi_l(r)}{dr}-\frac{l+1-\xi}{r}\phi_l(r)\right]\,,
\end{aligned}
\tag{A.32}
$$

where $M\in\{-1,0,+1\}$ denote spherical coordinates. The Clebsch-Gordan coefficients used in the previous equation are in the abbreviated form, namely instead of $C(j_1\,j_2\,j;\,m_1\,m_2\,m)$, $C(j_1\,j_2\,j;\,m_1\,m_2)$ is given with $m=m_1+m_2$. ϕ_l represents a radial function and Y_l^m is a complex spherical harmonic.

Furthermore, applying the gradient formula for $M=\lambda$ and $m=\mu-m_s$ and taking into account that $\langle\chi_{m_s}\,|\,\sigma_+\,|\,\chi_{m_s'}\rangle=\sqrt{2}\,\delta_{m_s,\frac{1}{2}}\,\delta_{m_s',-\frac{1}{2}}$, Eq. (A.31) can be rewritten as following:

$$
\begin{aligned}
M_{\Lambda\Lambda'}^{0+} &= -\frac{\hbar}{i}\sqrt{2}\,\Big\{\int r^2\,dr\,g_\Lambda^b\left[\frac{dg_{\Lambda'}^a}{dr}-\frac{l'}{r}g_{\Lambda'}^a\right]\sqrt{\frac{l'+1}{2l'+3}}\sum_{m_s m_s'}C_\Lambda^{m_s}\,C_{\Lambda'}^{m_s'} \\
&\times C(l'\,1,\,l'+1,\,\mu'-m_s',\,0)\,\delta_{l,l'+1}\delta_{\mu-m_s,\mu'-m_s'+0}\,\delta_{m_s,\frac{1}{2}}\,\delta_{m_s',-\frac{1}{2}} \\
&- \int r^2\,dr\,g_\Lambda^b\left[\frac{dg_{\Lambda'}^a}{dr}+\frac{l'+1}{r}g_{\Lambda'}^a\right]\sqrt{\frac{l'}{2l'-1}}\sum_{m_s m_s'}C_\Lambda^{m_s}\,C_{\Lambda'}^{m_s'} \\
&\times C(l'\,1,\,l'-1,\,\mu'-m_s',\,0)\,\delta_{l,l'-1}\delta_{\mu-m_s,\mu'-m_s'+0}\,\delta_{m_s,\frac{1}{2}}\,\delta_{m_s',-\frac{1}{2}} \\
&+ \int r^2\,dr\,f_\Lambda^b\left[\frac{df_{\Lambda'}^a}{dr}-\frac{\bar{l}'}{r}f_{\Lambda'}^a\right]\sqrt{\frac{\bar{l}'+1}{2\bar{l}'+3}}\sum_{m_s m_s'}C_{-\Lambda}^{m_s}\,C_{-\Lambda'}^{m_s'} \\
&\times C(\bar{l}'1,\,\bar{l}'+1,\,\mu'-m_s',\,0)\,\delta_{\bar{l},\bar{l}'+1}\delta_{\mu-m_s,\mu'-m_s'+0}\,\delta_{m_s,\frac{1}{2}}\,\delta_{m_s',-\frac{1}{2}} \\
&- \int r^2\,dr\,f_\Lambda^b\left[\frac{df_{\Lambda'}^a}{dr}+\frac{\bar{l}'+1}{r}f_{\Lambda'}^a\right]\sqrt{\frac{\bar{l}'}{2\bar{l}'-1}}\sum_{m_s m_s'}C_{-\Lambda}^{m_s}\,C_{-\Lambda'}^{m_s'} \\
&\times C(\bar{l}'1,\,\bar{l}'-1,\,\mu'-m_s',\,0)\,\delta_{\bar{l},\bar{l}'-1}\,\delta_{\mu-m_s,\mu'-m_s'+0}\,\delta_{m_s,\frac{1}{2}}\,\delta_{m_s',-\frac{1}{2}}\,\Big\}\,.
\end{aligned}
\tag{A.33}
$$

A. Matrix elements of the Bargmann-Wigner spin-polarization operator.

For $m_s = \frac{1}{2}$, $m'_s = -\frac{1}{2}$, Eq. (A.33) takes the following form:

$$
\begin{aligned}
M^{0+}_{\Lambda\Lambda'} = -\frac{\hbar}{i} & \left\{ R^1_{\Lambda\Lambda'} \left[g^b_\Lambda, g^a_{\Lambda'} \right] A^{1(0+)}_{\Lambda\Lambda'} - R^2_{\Lambda\Lambda'} \left[g^b_\Lambda, g^a_{\Lambda'} \right] A^{2(0+)}_{\Lambda\Lambda'} \right. \\
& \left. + \bar{R}^1_{\Lambda\Lambda'} \left[f^b_\Lambda, f^a_{\Lambda'} \right] A^{1(0+)}_{-\Lambda,-\Lambda'} - \bar{R}^2_{\Lambda\Lambda'} \left[f^b_\Lambda, f^a_{\Lambda'} \right] A^{2(0+)}_{-\Lambda,-\Lambda'} \right\}
\end{aligned}
\tag{A.34}
$$

with the radial $(R_{\Lambda\Lambda'})$ and angular matrix elements $(A_{\Lambda\Lambda'})$ defined as:

$$
\begin{aligned}
R^1_{\Lambda\Lambda'} \left[g^b_\Lambda, g^a_{\Lambda'} \right] &= \int r^2 \, dr \, g^b_\Lambda \left[\frac{dg^a_{\Lambda'}}{dr} - \frac{l'}{r} g^a_{\Lambda'} \right], \\
R^2_{\Lambda\Lambda'} \left[g^b_\Lambda, g^a_{\Lambda'} \right] &= \int r^2 \, dr \, g^b_\Lambda \left[\frac{dg^a_{\Lambda'}}{dr} + \frac{l'+1}{r} g^a_{\Lambda'} \right], \\
\bar{R}^1_{\Lambda\Lambda'} \left[f^b_\Lambda, f^a_{\Lambda'} \right] &= \int r^2 \, dr \, f^b_\Lambda \left[\frac{df^a_{\Lambda'}}{dr} - \frac{\bar{l}'}{r} f^a_{\Lambda'} \right], \\
\bar{R}^2_{\Lambda\Lambda'} \left[f^b_\Lambda, f^a_{\Lambda'} \right] &= \int r^2 \, dr \, f^b_\Lambda \left[\frac{df^a_{\Lambda'}}{dr} + \frac{\bar{l}'+1}{r} f^a_{\Lambda'} \right],
\end{aligned}
\tag{A.35}
$$

$$
A^{1(0+)}_{\Lambda\Lambda'} = \sqrt{2} \sqrt{\frac{l'+1}{2l'+3}} \, C^{\frac{1}{2}}_\Lambda C^{-\frac{1}{2}}_{\Lambda'} \, C(l'\,1,\, l'+1,\, \mu'+\tfrac{1}{2},\, 0) \, \delta_{l,l'+1} \, \delta_{\mu-\mu',1},
\tag{A.36}
$$

$$
A^{2(0+)}_{\Lambda\Lambda'} = \sqrt{2} \sqrt{\frac{l'}{2l'-1}} \, C^{\frac{1}{2}}_\Lambda C^{-\frac{1}{2}}_{\Lambda'} \, C(l'\,1,\, l'-1,\, \mu'+\tfrac{1}{2},\, 0) \, \delta_{l,l'-1} \, \delta_{\mu-\mu',1}.
\tag{A.37}
$$

After deriving the expressions for all matrix elements, it turns out that all of them have a similar structure. Each of them consists of a set of radial $R_{\Lambda\Lambda'}$ and angular $A_{\Lambda\Lambda'}$ matrix elements. However the latter ones occurred in two polarizations. Therefore it is reasonable to show the corresponding angular matrix elements only.

For the case $M^{0-}_{\Lambda\Lambda'} = -\langle Z^b_\Lambda | \frac{\hbar}{i} \nabla_0 \Sigma_- | Z^a_{\Lambda'} \rangle$ and taking into account that $\langle \chi_{m_s} | \sigma_- | \chi_{m'_s} \rangle = \sqrt{2}\, \delta_{m_s,-\frac{1}{2}} \, \delta_{m'_s,\frac{1}{2}}$ ($m_s = -\frac{1}{2}$, $m'_s = \frac{1}{2}$), the corresponding angular matrix elements are as follows:

$$
A^{1(0-)}_{\Lambda\Lambda'} = \sqrt{2} \sqrt{\frac{l'+1}{2l'+3}} \, C^{-\frac{1}{2}}_\Lambda C^{\frac{1}{2}}_{\Lambda'} \, C(l'\,1,\, l'+1,\, \mu'-\tfrac{1}{2},\, 0) \delta_{l,l'+1} \, \delta_{\mu-\mu',-1},
\tag{A.38}
$$

$$
A^{2(0-)}_{\Lambda\Lambda'} = \sqrt{2} \sqrt{\frac{l'}{2l'-1}} \, C^{-\frac{1}{2}}_\Lambda C^{\frac{1}{2}}_{\Lambda'} \, C(l'\,1,\, l'-1,\, \mu'-\tfrac{1}{2},\, 0) \, \delta_{l,l'-1} \, \delta_{\mu-\mu',-1}.
\tag{A.39}
$$

In case of $M^{00}_{\Lambda\Lambda'} = -\langle Z^b_\Lambda | \frac{\hbar}{i} \nabla_0 \Sigma_0 | Z^a_{\Lambda'} \rangle$ with $\langle \chi_{m_s} | \sigma_0 | \chi_{m'_s} \rangle = 2m'_s \, \delta_{m_s,m'_s}$ ($m_s = m'_s = \frac{1}{2}$, $m_s = m'_s = -\frac{1}{2}$) one has accordingly:

$$A_{\Lambda\Lambda'}^{1(00)} = \sqrt{\frac{l'+1}{2l'+3}} \left\{ C_{\Lambda}^{\frac{1}{2}} C_{\Lambda'}^{\frac{1}{2}} C(l'\,1,\, l'+1,\, \mu'-\frac{1}{2},\, 0) \right.$$
$$\left. - C_{\Lambda}^{-\frac{1}{2}} C_{\Lambda'}^{-\frac{1}{2}} C(l'\,1,\, l'+1,\, \mu'+\frac{1}{2},\, 0) \right\} \delta_{l,l'+1}\, \delta_{\mu-\mu',0}\,, \qquad (A.40)$$

$$A_{\Lambda\Lambda'}^{2(00)} = \sqrt{\frac{l'}{2l'-1}} \left\{ C_{\Lambda}^{\frac{1}{2}} C_{\Lambda'}^{\frac{1}{2}} C(l'\,1,\, l'-1,\, \mu'-\frac{1}{2},\, 0) \right.$$
$$\left. - C_{\Lambda}^{-\frac{1}{2}} C_{\Lambda'}^{-\frac{1}{2}} C(l'\,1,\, l'-1,\, \mu'+\frac{1}{2},\, 0) \right\} \delta_{l,l'-1}\delta_{\mu-\mu',0}\,. \qquad (A.41)$$

For the matrix elements $M_{\Lambda\Lambda'}^{++} = -\langle Z_{\Lambda}^{b} \,|\, \frac{\hbar}{i}\, \nabla_{+}\, \Sigma_{+} \,|\, Z_{\Lambda'}^{a} \rangle$ with $\langle \chi_{m_s} \,|\, \sigma_{+} \,|\, \chi_{m_s'} \rangle = \sqrt{2}\, \delta_{m_s,\frac{1}{2}}$ $\delta_{m_s',-\frac{1}{2}}$ $(m_s = \frac{1}{2},\, m_s' = -\frac{1}{2})$ one writes:

$$A_{\Lambda\Lambda'}^{1(++)} = \sqrt{2} \sqrt{\frac{l'+1}{2l'+3}}\, C_{\Lambda}^{\frac{1}{2}} C_{\Lambda'}^{-\frac{1}{2}} C(l'\,1,\, l'+1,\, \mu'+\frac{1}{2},\, +1)\, \delta_{l,l'+1}\, \delta_{\mu-\mu',2}\,, \qquad (A.42)$$

$$A_{\Lambda\Lambda'}^{2(++)} = \sqrt{2} \sqrt{\frac{l'}{2l'-1}}\, C_{\Lambda}^{\frac{1}{2}} C_{\Lambda'}^{-\frac{1}{2}} C(l'\,1,\, l'-1,\, \mu'+\frac{1}{2},\, +1)\, \delta_{l,l'-1}\, \delta_{\mu-\mu',2}\,. \qquad (A.43)$$

For $M_{\Lambda\Lambda'}^{+-} = -\langle Z_{\Lambda}^{b} \,|\, \frac{\hbar}{i}\, \nabla_{+}\, \Sigma_{-} \,|\, Z_{\Lambda'}^{a} \rangle$ with $\langle \chi_{m_s} \,|\, \sigma_{-} \,|\, \chi_{m_s'} \rangle = \sqrt{2}\, \delta_{m_s,-\frac{1}{2}}\, \delta_{m_s',\frac{1}{2}}$ $(m_s = -\frac{1}{2},$ $m_s' = \frac{1}{2})$ one has:

$$A_{\Lambda\Lambda'}^{1(+-)} = \sqrt{2} \sqrt{\frac{l'+1}{2l'+3}}\, C_{\Lambda}^{-\frac{1}{2}} C_{\Lambda'}^{\frac{1}{2}} C(l'\,1,\, l'+1,\, \mu'-\frac{1}{2},\, +1)\, \delta_{l,l'+1}\, \delta_{\mu-\mu',0}\,, \qquad (A.44)$$

$$A_{\Lambda\Lambda'}^{2(+-)} = \sqrt{2} \sqrt{\frac{l'}{2l'-1}}\, C_{\Lambda}^{-\frac{1}{2}} C_{\Lambda'}^{\frac{1}{2}} C(l'\,1,\, l'-1,\, \mu'-\frac{1}{2},\, +1)\, \delta_{l,l'-1}\, \delta_{\mu-\mu',0}\,. \qquad (A.45)$$

For $M_{\Lambda\Lambda'}^{+0} = -\langle Z_{\Lambda}^{b} \,|\, \frac{\hbar}{i}\, \nabla_{+}\, \Sigma_{0} \,|\, Z_{\Lambda'}^{a} \rangle$ and $\langle \chi_{m_s} \,|\, \sigma_{0} \,|\, \chi_{m_s'} \rangle = 2 m_s'\, \delta_{m_s,m_s'}$ $(m_s = m_s' = \frac{1}{2},$ $m_s = m_s' = -\frac{1}{2})$ one gets:

$$A_{\Lambda\Lambda'}^{1(+0)} = \sqrt{\frac{l'+1}{2l'+3}} \left\{ C_{\Lambda}^{\frac{1}{2}} C_{\Lambda'}^{\frac{1}{2}} C(l'\,1,\, l'+1,\, \mu'-\frac{1}{2},\, +1) \right.$$
$$\left. - C_{\Lambda}^{-\frac{1}{2}} C_{\Lambda'}^{-\frac{1}{2}} C(l'\,1,\, l'+1,\, \mu'+\frac{1}{2},\, +1) \right\} \delta_{l,l'+1}\, \delta_{\mu-\mu',1}\,, \qquad (A.46)$$

A. Matrix elements of the Bargmann-Wigner spin-polarization operator.

$$A_{\Lambda\Lambda'}^{2(+0)} = \sqrt{\frac{l'}{2l'-1}} \{ C_\Lambda^{\frac{1}{2}} C_{\Lambda'}^{\frac{1}{2}} C(l'\,1, l'-1, \mu'-\frac{1}{2}, +1)$$
$$- C_\Lambda^{-\frac{1}{2}} C_{\Lambda'}^{-\frac{1}{2}} C(l'\,1, l'-1, \mu'+\frac{1}{2}, +1) \} \, \delta_{l,l'-1} \, \delta_{\mu-\mu',1} \, . \tag{A.47}$$

For $M_{\Lambda\Lambda'}^{-+} = -\langle Z_\Lambda^b | \frac{\hbar}{i} \nabla_- \Sigma_+ | Z_{\Lambda'}^a \rangle$ operator with $\langle \chi_{m_s} | \sigma_+ | \chi_{m'_s} \rangle = \sqrt{2} \, \delta_{m_s, \frac{1}{2}} \, \delta_{m'_s, -\frac{1}{2}}$ ($m_s = \frac{1}{2}$, $m'_s = -\frac{1}{2}$) one has:

$$A_{\Lambda\Lambda'}^{1(-+)} = \sqrt{2} \sqrt{\frac{l'+1}{2l'+3}} \, C_\Lambda^{\frac{1}{2}} C_{\Lambda'}^{-\frac{1}{2}} C(l'\,1, l'+1, \mu'+\frac{1}{2}, -1) \, \delta_{l,l'+1} \, \delta_{\mu-\mu',0} \, , \tag{A.48}$$

$$A_{\Lambda\Lambda'}^{2(-+)} = \sqrt{2} \sqrt{\frac{l'}{2l'-1}} \, C_\Lambda^{\frac{1}{2}} C_{\Lambda'}^{-\frac{1}{2}} C(l'\,1, l'-1, \mu'+\frac{1}{2}, -1) \, \delta_{l,l'-1} \, \delta_{\mu-\mu',0} \, . \tag{A.49}$$

The case $M_{\Lambda\Lambda'}^{--} = -\langle Z_\Lambda^b | \frac{\hbar}{i} \nabla_- \Sigma_- | Z_{\Lambda'}^a \rangle$ with $\langle \chi_{m_s} | \sigma_- | \chi_{m'_s} \rangle = \sqrt{2} \delta_{m_s, -\frac{1}{2}} \, \delta_{m'_s, \frac{1}{2}}$ ($m_s = -\frac{1}{2}$, $m'_s = \frac{1}{2}$) gives:

$$A_{\Lambda\Lambda'}^{1(--)} = \sqrt{2} \sqrt{\frac{l'+1}{2l'+3}} \, C_\Lambda^{-\frac{1}{2}} C_{\Lambda'}^{\frac{1}{2}} C(l'\,1, l'+1, \mu'-\frac{1}{2}, -1) \, \delta_{l,l'+1} \, \delta_{\mu-\mu',-2} \, , \tag{A.50}$$

$$A_{\Lambda\Lambda'}^{2(--)} = \sqrt{2} \sqrt{\frac{l'}{2l'-1}} \, C_\Lambda^{-\frac{1}{2}} C_{\Lambda'}^{\frac{1}{2}} C(l'\,1, l'-1, \mu'-\frac{1}{2}, -1) \, \delta_{l,l'-1} \, \delta_{\mu-\mu',-2} \tag{A.51}$$

and finally for $M_{\Lambda\Lambda'}^{-0} = -\langle Z_\Lambda^b | \frac{\hbar}{i} \nabla_- \Sigma_0 | Z_{\Lambda'}^a \rangle$ with $\langle \chi_{m_s} | \sigma_0 | \chi_{m'_s} \rangle = 2m'_s \delta_{m_s, m'_s}$ with $m_s = m'_s = \frac{1}{2}$, $m_s = m'_s = -\frac{1}{2}$ the angular matrix elements are as follows:

$$A_{\Lambda\Lambda'}^{1(-0)} = \sqrt{\frac{l'+1}{2l'+3}} \{ C_\Lambda^{\frac{1}{2}} C_{\Lambda'}^{\frac{1}{2}} C(l'\,1, l'+1, \mu'-\frac{1}{2}, -1)$$
$$- C_\Lambda^{-\frac{1}{2}} C_{\Lambda'}^{-\frac{1}{2}} C(l'\,1, l'+1, \mu'+\frac{1}{2}, -1) \} \, \delta_{l,l'+1} \, \delta_{\mu-\mu',-1} \, , \tag{A.52}$$

$$A_{\Lambda\Lambda'}^{2(-0)} = \sqrt{\frac{l'}{2l'-1}} \{ C_\Lambda^{\frac{1}{2}} C_{\Lambda'}^{\frac{1}{2}} C(l'\,1, l'-1, \mu'-\frac{1}{2}, -1)$$
$$- C_\Lambda^{-\frac{1}{2}} C_{\Lambda'}^{-\frac{1}{2}} C(l'\,1, l'-1, \mu'+\frac{1}{2}, -1) \} \, \delta_{l,l'-1} \, \delta_{\mu-\mu',-1} \, . \tag{A.53}$$

For the numerical implementation it is necessary to generalize the obtained expressions for the angular matrix elements. In the following, the generic structures of the corresponding matrix elements are written with n being spin-polarization index and s the current index ($n, s \in \{-1, 0, +1\}$):

$$A_{\Lambda\Lambda'}^{1(ns)} = \sqrt{2} \sqrt{\frac{l'+1}{2l'+3}} \, C_\Lambda^{\frac{s}{2}} C_{\Lambda'}^{-\frac{s}{2}} C(l'\,1, l'+1, \mu'+\frac{s}{2}, n)$$
$$\times \, \delta_{l,l'+1} \, \delta_{\mu-\mu',n+s} \qquad \text{for } s \neq 0 \, , \tag{A.54}$$

$$
\begin{aligned}
A_{\Lambda\Lambda'}^{1(ns)} = \sqrt{\frac{l'+1}{2l'+3}} \, \{ & C_\Lambda^{\frac{1}{2}} \, C_{\Lambda'}^{\frac{1}{2}} \, C(l'\,1,\, l'+1,\, \mu' - \frac{1}{2},\, n) \\
& - C_\Lambda^{-\frac{1}{2}} \, C_{\Lambda'}^{-\frac{1}{2}} \, C(l'\,1,\, l'+1,\, \mu' + \frac{1}{2},\, n) \, \} \\
& \times \delta_{l,l'+1} \, \delta_{\mu-\mu',n+s} \qquad \text{for } s = 0 \,,
\end{aligned}
\tag{A.55}
$$

$$
\begin{aligned}
A_{\Lambda\Lambda'}^{2(ns)} = \sqrt{2} \sqrt{\frac{l'}{2l'-1}} \, C_\Lambda^{\frac{s}{2}} \, C_{\Lambda'}^{-\frac{s}{2}} \, C(l'\,1,\, l'-1,\, \mu' + \frac{s}{2},\, n) \\
\times \, \delta_{l,l'-1} \, \delta_{\mu-\mu',n+s} \qquad \text{for } s \neq 0 \,,
\end{aligned}
\tag{A.56}
$$

$$
\begin{aligned}
A_{\Lambda\Lambda'}^{2(ns)} = \sqrt{\frac{l'}{2l'-1}} \, \{ & C_\Lambda^{\frac{1}{2}} \, C_{\Lambda'}^{\frac{1}{2}} \, C(l'\,1,\, l'-1,\, \mu' - \frac{1}{2},\, n) \\
& - C_\Lambda^{-\frac{1}{2}} \, C_{\Lambda'}^{-\frac{1}{2}} \, C(l'\,1,\, l'-1,\, \mu' + \frac{1}{2},\, n) \, \} \\
& \times \delta_{l,l'-1} \, \delta_{\mu-\mu',n+s} \qquad \text{for } s = 0 \,.
\end{aligned}
\tag{A.57}
$$

B. Technical aspects

As was already mentioned, the implementation of the Kubo-Bastin formalism requires a proper treatment of the Fermi sea term, given by the second term of the Eq. (5.37):

$$
\sigma_{\mu\nu}^{\xi,II} = \frac{\hbar}{4\pi V} \int_{-\infty}^{\varepsilon_F} d\varepsilon \, \mathrm{Tr} \left\langle \hat{J}_{\mu}^{\xi} \frac{dG^+}{d\varepsilon} j_{\nu} G^+ - \hat{J}_{\mu}^{\xi} G^+ j_{\nu} \frac{dG^+}{d\varepsilon} \right.
$$

$$
\left. + \hat{J}_{\mu}^{\xi} G^- j_{\nu} \frac{dG^-}{d\varepsilon} - \hat{J}_{\mu}^{\xi} \frac{dG^-}{d\varepsilon} j_{\nu} G^- \right\rangle . \tag{B.1}
$$

The implementation effort significantly reduces as both terms in Eq. (B.1) contain only products of the either retarded G^+ or advanced G^- Green functions, i.e. there is no cross term involved. However, the central task of the implementation is to treat energy derivatives of the corresponding Green functions. Since G^+ and G^- are analytic functions, the limit $\lim_{\Delta z \to 0} \frac{\hat{G}^{\pm}(z + \Delta z) - \hat{G}^{\pm}(z)}{\Delta z}$ exists with $z = x + iy$ ($z \in \mathbb{C}$). Therefore the Cauchy-Riemann relations are valid for $\hat{G}^{\pm} = u(x,y) \pm iv(x,y)$, i.e. $\frac{\partial u}{\partial x} = \frac{\partial v}{\partial y}$, $\frac{\partial u}{\partial y} = -\frac{\partial v}{\partial x}$ leading to:

$$
\frac{d\hat{G}^{\pm}}{dz} = \frac{\partial u}{\partial x} \pm i\frac{\partial v}{\partial x} = \frac{\partial v}{\partial y} \mp i\frac{\partial u}{\partial y} = \frac{\partial u}{\partial x} \mp i\frac{\partial u}{\partial y} . \tag{B.2}
$$

Or equivalently one has:

$$
\frac{d\hat{G}^{\pm}}{dz} = \frac{d\,\mathrm{Re}\,\hat{G}^{\pm}}{d\,\mathrm{Re}\,z} \pm i\frac{d\,\mathrm{Im}\,\hat{G}^{\pm}}{d\,\mathrm{Re}\,z} . \tag{B.3}
$$

For an sufficient and accurate treatment of the Fermi sea term the energy integration path was distorted to a semicircle in the upper (lower) half of the complex plane for the terms containing the retarded G^+ (advanced G^-) Green functions (Fig. (B.1)). Therefore, the energy derivative of the Green functions is calculated numerically in terms of two point finite difference taken along a straight line segment (h) parallel to real axis:

$$
\frac{d\hat{G}^{\pm}(z)}{dz} = \mathrm{Re}\left[\frac{\hat{G}^{\pm}(z + \frac{h}{2}) - \hat{G}^{\pm}(z - \frac{h}{2})}{h} \right]
$$

$$
\pm i\,\mathrm{Im}\left[\frac{\hat{G}^{\pm}(z + \frac{h}{2}) - \hat{G}^{\pm}(z - \frac{h}{2})}{h} \right]
$$

$$
= \frac{\hat{G}^{\pm}(z + \frac{h}{2}) - \hat{G}^{\pm}(z - \frac{h}{2})}{h} , \tag{B.4}
$$
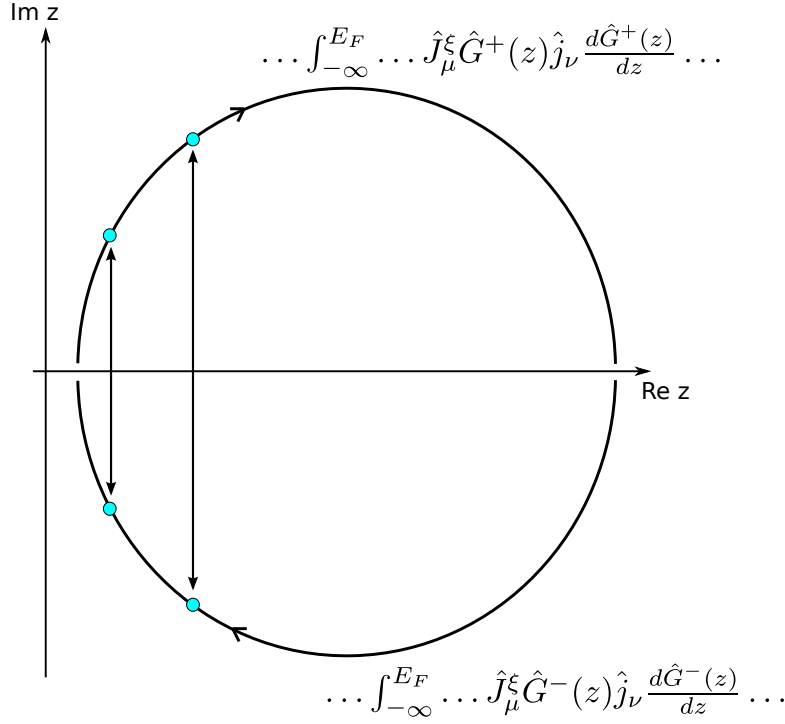
Figure B.1.: The energy contours for the evaluation of the Fermi sea term in case of energy z (upper panel) and energy z^* (lower panel).
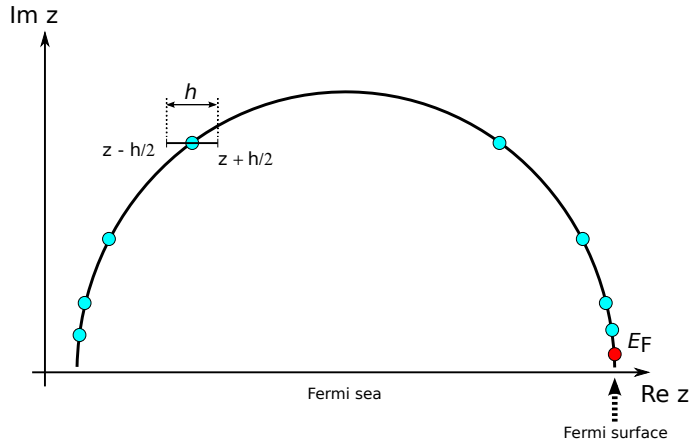

Figure B.2.: Scheme for numerical evaluation of the derivative of the corresponding Green function.

with $h \in \boldsymbol{R}$ and small. The numerical evaluation of the derivative is performed on the semicircle energy path in the complex plane shown in Fig. (B.2).

Further analysis of the Fermi sea term (Eq. (B.1)) leads to the fact that its calculation

can be reduced to the calculation of expressions of the following types:

$$\hat{J}_\mu^\xi \hat{G}^\pm \hat{j}_\nu \frac{d\hat{G}^\pm(z)}{dz} \approx \hat{J}_\mu^\xi \hat{G}^\pm(z)\hat{j}_\nu \left[\frac{\hat{G}^\pm(z+\frac{h}{2}) - \hat{G}^\pm(z-\frac{h}{2})}{h}\right] \qquad (B.5)$$

and:

$$\hat{J}_\mu^\xi \frac{d\hat{G}^\pm(z)}{dz} \hat{j}_\nu \hat{G}^\pm \approx \hat{J}_\mu^\xi \left[\frac{\hat{G}^\pm(z+\frac{h}{2}) - \hat{G}^\pm(z-\frac{h}{2})}{h}\right] \hat{G}^\pm(z)\hat{j}_\nu. \qquad (B.6)$$

Combining equations Eq. (B.5) and Eq. (B.6) and considering only the first part of Eq. (B.1) (containing the product of retarded Green functions $\hat{G}^+$) can be rewritten in the following way:

$$\mathrm{Tr}\left\langle \hat{J}_\mu^\xi \hat{G}^+(z)\hat{j}_\nu \frac{d\hat{G}^+(z)}{dz} - \hat{J}_\mu^\xi \frac{d\hat{G}^+(z)}{dz}\hat{j}_\nu \hat{G}^+(z)\right\rangle$$

$$\approx \frac{1}{h}\mathrm{Tr}\left\langle \hat{J}_\mu^\xi \hat{G}^+(z)\hat{j}_\nu \hat{G}^+(z^+) - \hat{J}_\mu^\xi \hat{G}^+(z)\hat{j}_\nu \hat{G}^+(z^-)\right.$$
$$\left. - \hat{J}_\mu^\xi \hat{G}^+(z)\hat{j}_\nu \hat{G}^+(z) + \hat{J}_\mu^\xi \hat{G}^+(z)\hat{j}_\nu \hat{G}^+(z)\right\rangle$$

$$= \frac{1}{h}\mathrm{Tr}\left\langle \hat{J}_\mu^\xi \hat{G}^+(z)\hat{j}_\nu \hat{G}^+(z^+) - \hat{J}_\mu^\xi \hat{G}^+(z^+)\hat{j}_\nu \hat{G}^+(z)\right.$$
$$\left. - [\hat{J}_\mu^\xi \hat{G}^+(z)\hat{j}_\nu \hat{G}^+(z^-) - \hat{J}_\mu^\xi \hat{G}^+(z^-)\hat{j}_\nu \hat{G}^+(z)]\right\rangle$$

$$= \frac{1}{h}\mathrm{Tr}\left\langle \hat{J}_\mu^\xi \hat{G}^+(z)\hat{j}_\nu \hat{G}^+(z^+) - \hat{j}_\nu \hat{G}^+(z)\hat{J}_\mu^\xi \hat{G}^+(z^+)\right.$$
$$\left. - [\hat{J}_\mu^\xi \hat{G}^+(z)\hat{j}_\nu \hat{G}^+(z^-) - \hat{j}_\nu \hat{G}^+(z)\hat{J}_\mu^\xi \hat{G}^+(z^-)]\right\rangle \qquad (B.7)$$

with $z^\pm = z \pm h/2$. In a same way the second part (containing the product of advanced Green functions $\hat{G}^-$) of Eq. (B.1) is treated. Thereby the calculation of the Fermi sea term is reduced to the calculation of the expressions of the type $\mathrm{Tr}\left\langle \hat{J}_\mu^\xi \hat{G}^+(z)\hat{j}_\nu \hat{G}^+(z^+)\right\rangle$, which also are used in the calculation of the Fermi surface contribution and are already implemented within the Kubo-Středa formalism [53].

C. Numerical tests

The implementation of the Kubo-Bastin equation, particularly of the Fermi sea term, is an important part of the current work. Therefore, to ensure the correctness of the implementation a number of the convergence tests were performed with respect to the few numerical parameters.

According to the work by Butler [116] and in full analogy with the Kubo-Středa equation, the full conductivity tensor $\sigma_{\mu\nu}^{\xi}$ obtained using the Kubo-Bastin formula, can be split into two parts: on-site $\sigma_{\mu\nu}^{\xi 0}$ and off-site $\sigma_{\mu\nu}^{\xi 1}$:

$$
\begin{aligned}
\sigma_{\mu\nu}^{\xi} &= \sigma_{\mu\nu}^{\xi 0} + \sigma_{\mu\nu}^{\xi 1} \\
&= \underbrace{\sigma_{\mu\nu}^{\xi 0,I} + \sigma_{\mu\nu}^{\xi 1,I}}_{\text{Fermi surface}} + \underbrace{\sigma_{\mu\nu}^{\xi 0,II} + \sigma_{\mu\nu}^{\xi 1,II}}_{\text{Fermi sea}} \,,
\end{aligned}
\tag{C.1}
$$

where the on-site terms contain regular (Z_Λ) as well as irregular solutions (J_Λ), whereas the off-site terms consist of regular solutions only. The numerical treatment of the on-site term, both Fermi surface and sea, is a delicate task, as the mentioned irregular solutions can lead to abnormally large values. However, since the full on-site term consists of Fermi sea and surface on-site terms of opposite sign, it eventually acquires rather small values.

In order to determine the optimal settings needed to perform calculations for real system, a number of convergence tests were carried out. For this purpose few testing systems were selected such as disordered alloys as well as pure systems. In the following the results are shown for $Fe_{0.7}Pd_{0.3}$ as an example. At first we checked the convergence of the Fermi sea on-site term depending on the length of the line segment h. This is illustrated in the Fig. (C.1) (top panel) for $Fe_{0.7}Pd_{0.3}$. One can see that there is a slight deviation from the otherwise constant behavior. The converged result is achieved with $h = 10^{-4}$ Ry and therefore, this value is used in the subsequent calculations.

Furthermore the dependence of the Fermi sea $\sigma_{\mu\nu}^{\xi 0II}$ on the number of energy points (NE) sampled on the integration semicircle and on the number of the k-points needed for the Brillouin-zone integrations was investigated. In Fig. (C.1) (bottom panel) the on-site Fermi sea term is shown depending on the number of k-points, plotted for several number of energy points (NE). One can see that $\sigma_{xy}^{\xi 0}$ is rather insensitive to the number of k-points and shows a rather constant behavior already at relatively low numbers. For this reason the adjustable k-mesh was introduced in order to reduce the numerical effort. Namely, the density of k-mesh increases when approaching Fermi energy and the
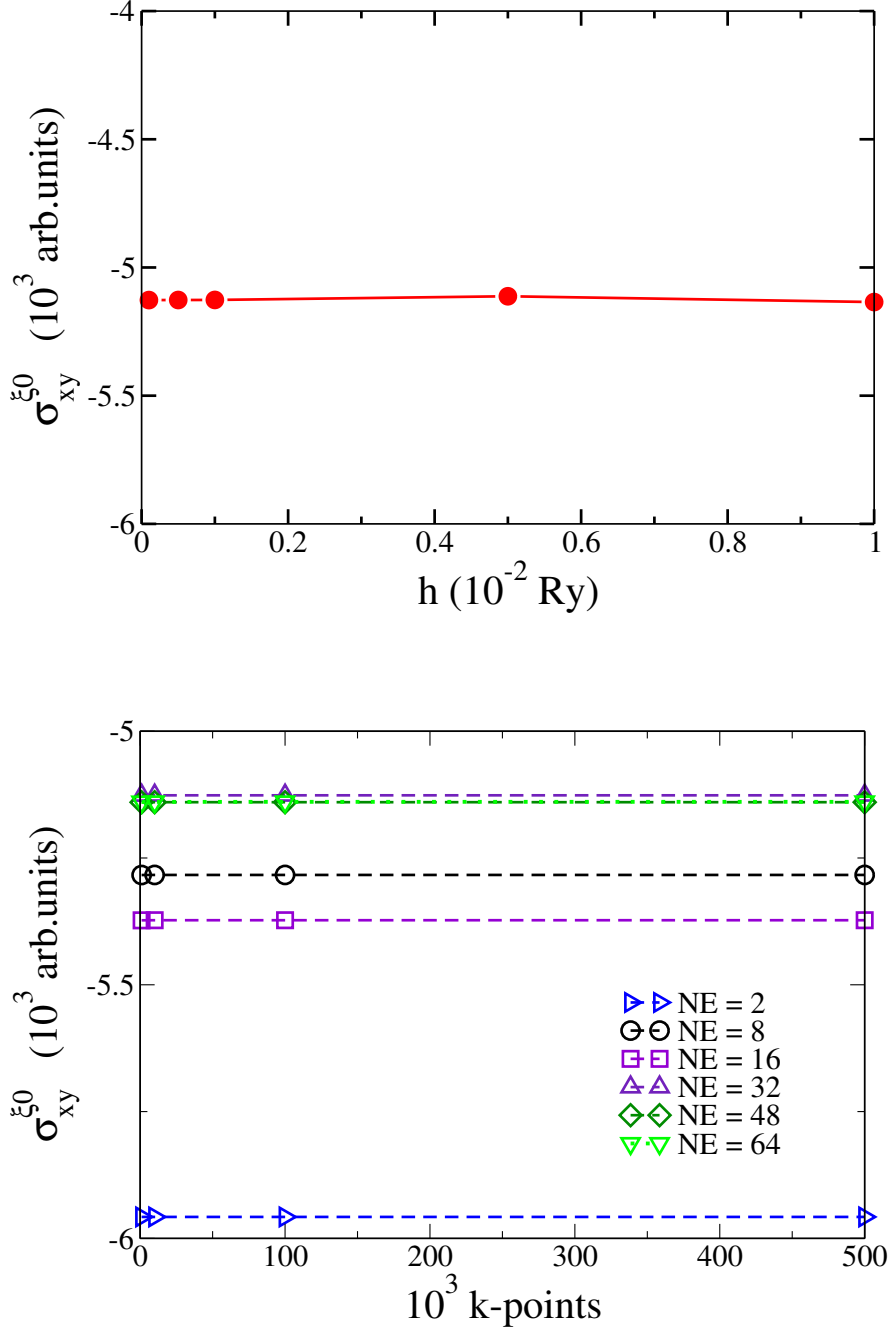
Figure C.1.: On-site Fermi sea term of $Fe_{0.7}Pd_{0.3}$ depending on the parameter h (top panel) and on the number of energy points NE on the contour (excluding E_F) and on the number of k-points (bottom panel).

maximal number is used at the Fermi level (to obtain the Fermi surface contributions). In contrast to the weak k-dependence, $\sigma_{xy}^{\xi 0}$ shows a rather pronounced dependence on the number of energy points on the contour. As one can see, the converged value is obtained already at NE= 32 and therefore is considered sufficient for the subsequent calculations.

D. Acronyms

List of the most important acronyms used in the current work:

- AHC anomalous Hall conductivity

- AHE anomalous Hall effect

- ANE anomalous Nernst effect

- CPA coherent potential approximation

- DFT density functional theory

- GF Green function

- KKR Korringa-Kohn-Rostoker

- NLCPA non-local coherent potential approximation

- SHC spin Hall conductivity

- SHE spin Hall effect

- SNE spin Nernst effect

- SOT spin orbit torque

- STT spin-transfer torque

List of Figures

Bibliography

[1] M. Dyakonov and V. Perel, "Possibility of orientating electron spins with current," JEPT Lett. **13**, 467 (1971).

[2] M. Dyakonov and V. Perel, "Current-induced spin orientation of electrons in semiconductors," Phys. Letters A **35**, 459 (1971).

[3] M. N. Baibich, J. M. Broto, A. Fert, F. N. Van Dau, F. Petroff, P. Etienne, G. Creuzet, A. Friederich, and J. Chazelas, "Giant magnetoresistance of (001)Fe/(001)Cr magnetic superlattices," Phys. Rev. Lett. **61**, 2472 (1988).

[4] G. Binasch, P. Grünberg, F. Saurenbach, and W. Zinn, "Enhanced magnetoresistance in layered magnetic structures with antiferromagnetic interlayer exchange," Phys. Rev. Lett. **39**, 4828 (1989).

[5] B. Dieny, V. S. Speriosu, S. S. P. Parkin, B. A. Gurney, D. R. Wilhoit, and D. Mauri, "Giant magnetoresistive in soft ferromagnetic multilayers," Phys. Rev. B **43**, 1297 (1991).

[6] J. Åkerman, "Toward a universal memory," Science **308**, 508 (2005).

[7] E. Chen, D. Apalkov, Z. Diao, A. Driskill-Smith, D. Druist, D. Lottis, V. Nikitin, X. Tang, S. Watts, S. A. Wolf, et al., "Advances and future prospects of spin-transfer torque random access memory," IEEE Transactions on Magnetics **46**, 1873 (2010).

[8] J. S. Meena, S. M. Sze, U. C. Tseng, and T.-Y. Tseng, "Overview of emerging nonvolatile memory technologies," Nano review **9**, 526 (2014).

[9] S. S. P. Parkin, M. Hayashi, and L. Thomas, "Magnetic domain-wall racetrack memory," Science **320**, 190 (2008).

[10] J. S. Kulkarni, O. Kazakova, D. Erts, M. Morris, M. T. Shaw, and J. D. Holmes, "Structural and magnetic characterization of $ge_{0.99}mn_{0.01}$ nanowire arrays," Chem. Mater. **17**, 3615 (2005).

[11] L. Ottaviano, M. Passacantando, and A. Verna, "Direct structural evidences of Mn dilution in Ge," J. Appl. Physics **100**, 063528 (2006).

[12] K. Galatsis, A. Khitun, R. Ostroumov, K. L. Wang, W. R. Dichtel, E. Plummer, J. Stoddart, J. Zink, J. Lee, Y.-H. Xie, et al., "Alternate state variables for emerging nanoelectronic devices," IEEE Transactions on Nanotechnology **8**, 66 (2009).

[13] D. Awschalom and N. Samarth, "Spintronics without magnetism," Physics **2**, 50 (2009).

[14] J. Hubbard, "Electron correlations in narrow energy bands," Proc. Roy. Soc. A **276**, 238 (1963).

[15] P. Hohenberg and W. Kohn, "Inhomogeneous electron gas," Phys. Rev. **136**, B864 (1964).

[16] W. Kohn and L. Sham, "Self-consistent equations including exchange and correlations effects," Phys. Rev. **140**, A 1133 (1965).

[17] H. Eschrig, G. Seifert, and P. Ziesche, "Current density functional theory of quantum electrodynamics," Solid State Commun. **56**, 777 (1985).

[18] R. Dreizler and E. Gross, *Density Functional Theory* (Springer-Verlag, Heidelberg, 1990).

[19] M. Rose, *Relativistic Electron Theory* (Wiley, New York, 1961).

[20] A. H. MacDonald and S. H. Vosko, "A relativistic density functional formalism," J. Phys. C: Solid State Phys **12**, 2977 (1979).

[21] H. Eschrig, *The Fundamentals of Density Functional Theory* (B G Teubner Verlagsgesellschaft,Stuttgart, Leipzig, 1996).

[22] E. Engel and R. Dreizler, *Density Functional Theory: An Advanced Course* (Springer, Berlin, 2011).

[23] S. Vosko, L. Wilk, and M. Nusair, "Accurate spin-dependent electron liquid correlation energies for local density calculations: a critical analysis," Can. J. Phys. **58**, 1200 (1980).

[24] L. Rayleigh, "On the influence of obstacles arranged in rectangular order upon the properties of a medium," Phil. Mag. **34**, 481 (1892).

[25] A. Gonis and W. H. Butler, *Multiple scattering in solids* (Springer, New York, 2000).

[26] J. Korringa, "On the calculation of the energy of a bloch wave in a metal," Physica **XIII**, 392 (1947).

[27] W. Kohn and N. Rostoker, "Solution of the schrödinger equation in periodic lattices with an application to metallic lithium," Phys. Rev. **94**, 1111 (1954).

[28] B. L. Györffy and M. J. Stott, *Band Structure Spectroscopy of Metals and Alloys* (Academic Press, New York, 1973).

[29] P. Strange, *Relativistic Quantum Mechanics* (Cambridge University Press, Cambridge, 1998).

[30] J. Zabloudil, R. Hammerling, L. Szunyogh, and P. Weinbereger, *Electron scattering in solid matter* (Springer, Berlin, 2005).

[31] R. Feder, F. Rosicky, and B. Ackermann, "Relativistic multiple scattering theory of electrons by ferromagnets," Z. Physik B **52**, 31 (1983).

[32] H. Ebert, *Initio Calculation of the Physical Properties of Solids, Vol. 535 of Lecture Notes in Physics* (Springer, Berlin, 2000).

[33] A. Jenkins and P. Strange, "Relativistic spin-polarized single-site scattering theory," J. Phys.: Cond. Mat. **6**, 3499 (1994).

[34] H. Ebert, *Habilitation thesis* (University of München, 1990).

[35] A. Vedyaev, "Method of coherent potential approximation in the theory of disordered alloys," Theoret. and Math. Phys. **31**, 532 (1977).

[36] J. Korringa, "Dispersion theory for electrons in a random lattice with applications to the electronic structure of alloys," J. Phys. Chem. Sol. **7**, 252 (1958).

[37] J. Beeby, "Electronic structure of alloys," Phys. Rev. **135**, A130 (1964).

[38] D. A. Rowlands, J. B. Staunton, and B. L. Györffy, "Korringa-Kohn-Rostoker nonlocal coherent-potential approximation," Phys. Rev. B **67**, 115109 (2003).

[39] D. Ködderitzsch, H. Ebert, D. Rowlands, and A. Ernst, "Relativistic formulation of the Korringa–Kohn–Rostoker nonlocal coherent-potential approximation," New Journal of Physics **9**, 81 (2007).

[40] D. Rowlands, A. Ernst, B. Györffy, and J. Staunton, "Density functional theory for disordered alloys with short-range order: Systematic inclusion of charge-correlation effects," Phys. Rev. B **73**, 165122 (2006).

[41] H. Ebert, D. Ködderitzsch, and J. Minár, "Calculating condensed matter properties using the KKR-Greens function methodârecent developments and applications," Rep. Prog. Phys. **74**, 096501 (2011).

[42] J. Ziman, *Electrons and Phonons* (Clarendon Press, Oxford, 1960).

[43] S. Y. Savrasov and D. Y. Savrasov, "Electron-phonon interactions and related physical properties of metals from linear-response theory," Phys. Rev. B **54**, 16487 (1996).

[44] P. Soven, "Coherent-potential model of substitutional disordered alloys," Phys. Rev. **156**, 809 (1967).

[45] H. Ebert, S. Mankovsky, D. Ködderitzsch, and P. J. Kelly, "*Ab Initio* calculation of the gilbert damping parameter via the linear response formalism," Phys. Rev. Lett. **107**, 066603 (2011).

[46] J. Staunton and Györffy, "Onsager cavity fields in itinerant-electron paramagnets," Phys. Rev. Lett. **69**, 371 (1992).

[47] H. Ebert, S. Mankovsky, K. Chadova, S. Polesya, J. Minár, and D. Ködderitzsch, "Calculating linear-response functions for finite temperatures on the basis of the alloy analogy model," Phys. Rev. B **91**, 165132 (2015).

[48] N. Papanikolaou, R. Zeller, and N. Dederichs, P.H.and Stefanou, "Lattice distortion in Cu-based dilute alloys: A first-principles study by the KKR Green-function method," Phys. Rev. B **55**, 4157 (1997).

[49] A. Lodder, "Electron-impurity scattering in dilute alloys with lattice distortion. i. general theory," J. Phys. F: Met. Phys. **6**, 1885 (1976).

[50] H. Böttger, *Principles of the Theory of Lattice Dynamics* (Akademie-Verlag, Berlin, 1983).

[51] S. Tikadzumi, *Physics of Magnetism* (Willey, New York, 1964).

[52] R. Kubo, "Statistical-mechanical theory of irreversible processes. I. General theory and simple applications to magnetic and conduction problems," J. Phys. Soc. Japan **12**, 564 (1957).

[53] S. Lowitzer, *Relativistic electronic transport theory - the spin Hall effect and related phenomena* (LMU, 2010).

[54] K. Elk and W. Gasser, *Die Methode der Greenschen Funktionen in der Festkörperphysik* (Akademie-Verlag, Berlin, 1979).

[55] A. Crépieux and P. Bruno, "Theory of the anomalous hall effect from the kubo formula and the dirac equation," Phys. Rev. B **64**, 014416 (2001).

[56] A. Bastin, C. Lewiner, O. Betbeder-Matibet, and P. Nozieres, "Quantum oscillations of the Hall effect of a fermion gas with random impurity scattering," J. Phys. Chem. Sol. **32**, 1811 (1971).

[57] P. Středa, "Theory of quantised Hall conductivity in two dimensions," J. Phys. C: Solid State Phys. **15**, L717 (1982).

[58] S. Lowitzer, D. Ködderitzsch, and H. Ebert, "Coherent description of the intrinsic and extrinsic anomalous hall effect in disordered alloys on an *Ab Initio* level," Phys. Rev. Lett. **105**, 266604 (2010).

[59] S. Lowitzer, M. Gradhand, D. Ködderitzsch, D. Fedorov, I. Mertig, and H. Ebert, "Extrinsic and intrinsic contributions to the spin Hall effect of alloys," Phys. Rev. Lett. **106**, 056601 (2011).

[60] T. Naito, D. S. Hirashima, and H. Kontani, "Tight-binding study of anomalous hall effect in ferromagnetic 3d transition metals," Phys. Rev. B **81**, 195111 (2010).

[61] I. Turek, J. Kudrnovský, and V. Drchal, "*Ab initio* theory of galvanomagnetic phenomena in ferromagnetic metals and disordered alloys," Phys. Rev. B **86**, 014405 (2012).

[62] I. Turek, J. Kudrnovský, and V. Drchal, "Fermi sea term in the relativistic linear muffin-tin-orbital transport theory for random alloys," Phys. Rev. B **89**, 064405 (2014).

[63] D. Ködderitzsch, K. Chadova, and H. Ebert, "Linear response Kubo-Bastin formalism with application to the anomalous and spin Hall effects: A first-principles approach," Phys. Rev. B **92**, 184415 (2015).

[64] S. Mankovsky, D. Ködderitzsch, G. Woltersdorf, and H. Ebert, "First-principles calculation of the Gilbert damping parameter via the linear response formalism with application to magnetic transition metals and alloys," Phys. Rev. B **87**, 014430 (2013).

[65] S. Wimmer, K. Chadova, M. Seemann, Ködderitzsch, and H. Ebert, "Fully relativistic description of spin-orbit torques by means of linear response theory," Phys. Rev. B **94**, 054415 (2016).

[66] D. Greenwood, "The boltzmann equation in the theory of the electrical conduction of metals," Proc. Phys. Soc. **71**, 585 (1958).

[67] E. H. Hall, "On a new action of the magnet on electric currents," Amer. J. Math. **2**, 287 (1879).

[68] E. H. Hall, "On the rotational coefficient in nickel and cobalt," Phil. Mag. **12**, 157 (1881).

[69] A. Kundt ,Wied. Ann. Physik **49**, 257 (1893).

[70] R. Karplus and J. M. Luttinger, "Hall effect in ferromagnetics," Phys. Rev. **95**, 1154 (1954).

[71] N. A. Sinitsyn, "Semiclassical theories of the anomalous hall effect," J. Phys.: Cond. Mat. **20**, 023201 (2008).

[72] D. Xiao, M.-C. Chang, and Q. Niu, "Berry phase effects on electronic properties," Rev. Mod. Phys. **82**, 1959 (2010).

[73] J. Smit, "The spontaneous Hall effect in ferromagnetics I," Physica **21**, 877 (1955).

[74] J. Smit, "The spontaneous Hall effect in ferromagnetics II," Physica **24**, 39 (1958).

[75] J. M. Luttinger, "Theory of the Hall effect in ferromagnetic substances," Phys. Rev. **112**, 739 (1958).

[76] G. Sundaram and Q. Niu, "Wave-packet dynamics in slowly perturbed crystals: Gradient corrections and Berry-phase effects," Phys. Rev. B **59**, 14915 (1999).

[77] N. A. Sinitsyn, A. H. MacDonald, T. Jungwirth, V. K. Dugaev, and J. Sinova, "Anomalous hall effect in a two-dimensional dirac band: The link between the kubo-streda formula and the semiclassical boltzmann equation approach," Phys. Rev. B **75**, 045315 (2007).

[78] E. I. Rashba, "Symmetry of energy bands in crystals of wurtzite type: I. symmetry of bands disregarding spin-orbit interaction," Soviet Physics - Solid State **1**, 368 (1959).

[79] E. I. Rashba and V. I. Sheka, "Symmetry of energy bands in crystals of wurtzite type: Ii. symmetry of bands including spin-orbit interaction," Fiz. Tverd. Tela: Collected Papers **2**, 162 (1959).

[80] P. Bruno, V. K. Dugaev, and M. Taillefumier, "Topological hall effect and berry phase in magnetic nanostructures," Phys. Rev. Lett. **93**, 096806 (2004).

[81] V. K. Dugaev, P. Bruno, M. Taillefumier, B. Canals, and C. Lacroix, "Anomalous hall effect in a two-dimensional electron gas with spin-orbit interaction," Phys. Rev. B **71**, 224423 (2005).

[82] P. Bruno, *The Berry Phase in Magnetism and the Anomalous Hall Effect. Handbook of Magnetism and Advanced Magnetic Materials* (Wiley, 2007), vol. 1: Fundamentals and Theory.

[83] N. S. Kiselev, A. N. Bogdanov, R. Schäfer, and U. K. Rössler, "Chiral skyrmions in thin magnetic films: new objects for magnetic storage technologies?," J. Phys. D: Appl. Phys. **44**, 392001 (2011).

[84] A. A. Burkov and L. Balents, "Weyl semimetal in a topological insulator multilayer," Phys. Rev. Lett. **107**, 127205 (2011).

[85] A. A. Burkov, M. D. Hook, and L. Balents, "Topological nodal semimetals," Phys. Rev. B **84**, 235126 (2011).

[86] I. Dzyaloshinsky, "A thermodynamic theory of weak ferromagnetism of antiferromagnetics," J. Phys. Chem. Sol. **4**, 241 (1958).

[87] T. Moriya, "Anisotropic Superexchange Interaction and Weak Ferromagnetism," Phys. Rev. **120**, 91 (1960).

[88] C. M. Hurd, "Asymmetric scattering of electrons in metals," Contemp. Phys. **16**, 517 (1975).

[89] A. Vedyaev, A. Granovskii, and O. Kotelnikova, *Kinetic properties in the disordered ferromagnetic alloys* (MSU, 1992).

[90] E. Kondorskii, A. Vedyaev, and A. Granovskii, "Theory of the residual anomalous Hall effect in disordered alloys, I," Fiz. Met. Metalov. **40**, 455 (1975).

[91] E. Kondorskii, A. Vedyaev, and A. Granovskii, "Theory of the residual anomalous Hall effect in disordered alloys, II," Fiz. Met. Metalov. **40**, 903 (1975).

[92] L. Berger, "Side-jump mechanism for the Hall effect of ferromagnets," Phys. Rev. B **2**, 4559 (1970).

[93] L. Berger, "Application of the side-jump model to the Hall effect and Nernst effect in ferromagnets," Phys. Rev. B **5**, 1862 (1972).

[94] N. A. Sinitsyn, Q. Niu, and A. H. MacDonald, "Coordinate shift in the semi-classical boltzmann equation and the anomalous hall effect," Phys. Rev. B **73**, 075318 (2006).

[95] N. Nagaosa, J. Sinova, S. Onoda, A. H. MacDonald, and N. P. Ong, "Anomalous Hall effect," Rev. Mod. Phys. **82**, 1539 (2010).

[96] S. N. Kaul, "Anomalous Hall effect in nickel and nickel-rich nickel-copper alloys," Phys. Rev. B **20**, 5122 (1979).

[97] N. Kurbanniyazov, A. V. Cheremushkina, and B. A. Akmuradov, "Hall effect and electrical resistance of Ni, Co, and Ni-Co alloys," Sov. Phys. Journal **16**, 539 (1973).

[98] Y. Tian, L. Ye, and X. Jin, "Proper scaling of the anomalous Hall effect," Phys. Rev. Lett. **103**, 087206 (2009).

[99] L. Ye, Y. Tian, X. Jin, and D. Xiao, "Temperature dependence of the intrinsic anomalous Hall effect in nickel," Phys. Rev. B **85**, 220403 (2012).

[100] D. Hou, Y. Li, D. Wei, D. Tian, L. Wu, and X. Jin, "The anomalous Hall effect in epitaxial face-centered-cubic cobalt films," J. Phys.: Cond. Mat. **24**, 482001 (2012).

[101] A. Shitade and N. Nagaosa, "Anomalous Hall effect in ferromagnetic metals: Role of phonons at finite temperature," J. Phys. Soc. Japan **81**, 083704 (2012).

[102] P. Czaja, F. Freimuth, J. Weischenberg, S. Blügel, and Y. Mokrousov, "Anomalous hall effect in ferromagnets with gaussian disorder," Phys. Rev. B **89**, 014411 (2014).

[103] J. Kondo, "Anomalous Hall effect and magnetoresistance of ferromagnetic metals," Prog. Theor. Phys. **27**, 772 (1962).

[104] F. E. Maranzana, "Contributions to the theory of the anomalous Hall effect in ferro- and antiferromagnetic materials," Phys. Rev. **160**, 421 (1967).

[105] Y. P. Irkhin and V. G. Shavrov, "Theory of the spontaneous Hall effect in ferromagnets," Zh. Eksp. Teor. Fiz. **42**, 1233 (1962).

[106] L. Gurevich and I. Yassievich Fiz. Tverd. Tela **4**, 2854 (1962).

[107] S. Onoda, N. Sugimoto, and N. Nagaosa, "Intrinsic versus extrinsic anomalous Hall effect in ferromagnets," Phys. Rev. Lett. **97**, 126602 (2006).

[108] K. Chadova, D. Fedorov, C. Herschbach, M. Gradhand, I. Mertig, D. Ködderitzsch, and H. Ebert, "Separation of the individual contributions to the spin Hall effect in dilute alloys within the first-principles Kubo-Středa approach," Phys. Rev. B **92**, 045120 (2015).

[109] D. Ködderitzsch, K. Chadova, J. Minár, and H. Ebert, "Impact of finite temperatures and correlations on the anomalous Hall conductivity from *ab initio* theory," New Journal of Physics **15**, 053009 (2013).

[110] S. Mankovsky, S. Polesya, K. Chadova, H. Ebert, J. B. Staunton, T. Gruenbaum, M. A. W. Schoen, C. H. Back, X. Z. Chen, and C. Song, "Temperature-dependent transport properties of FeRh," Phys. Rev. B **95**, 155139 (2017).

[111] K. Chadova, S. Mankovsky, J. Minár, and H. Ebert, "Impact of finite temperatures on the transport properties of Gd from first principles," Phys. Rev. B **95**, 125109 (2017).

[112] S. Mankovsky, K. Chadova, D. Ködderitzsch, J. Minár, and H. Ebert, "Electronic, magnetic, and transport properties of Fe-intercalated 2H-TaS$_2$ studied by means of the KKR-CPA method," Phys. Rev. B **92**, 144413 (2013).

[113] A. Vernes, Györffy, and P. Weinberger, "Spin currents, spin-transfer torque, and spin Hall effects in relativistic quantum mechanics," Phys. Rev. B **76**, 012408 (2007).

[114] V. Bargmann and E. Wigner, "Group theoretical discussion of relativistic wave equations," Proc. Nat. Ac. Sci. US. **34**, 211 (1948).

[115] M. Rose, *Elementary Theory of Angular Momentum* (Wiley,New York, 1957).

[116] W. H. Butler, "Theory of electronic transport in random alloys: Korringa-Kohn-Rostoker coherent-potential approximation," Phys. Rev. B **31**, 3260 (1985).

Acknowledgements

Curriculum Vitae

PERSÖNLICHE ANGABEN

- Name: Kristina Chadova

- Geburtsdatum: 07. Januar 1985

- Geburtsort: Kiew, Ukraine

- Nationalität: ukrainisch

- Familienstand: verheiratet

SCHULBILDUNG

- 1991-2002: Schule in Kiew, Ukraine

STUDIUM

- 2004-2010: Studium der Physik an der Nationalen Technischen Universität, Kiew, Ukraine. Diplomarbeit in theoretischer Festkörperphysik. Titel: "Investigation of the rational construction of the elements in spintronics"

- Juni 2010: Diplomprüfung mit Note 5 (ausgezeichnet).

BERUF

- seit Dezember 2010: wissenschaftlicher Angestellter und Doktorandin im Department Chemie/Lehrbereich Physikalische Chemie an der Ludwig-Maximilians-Universität München